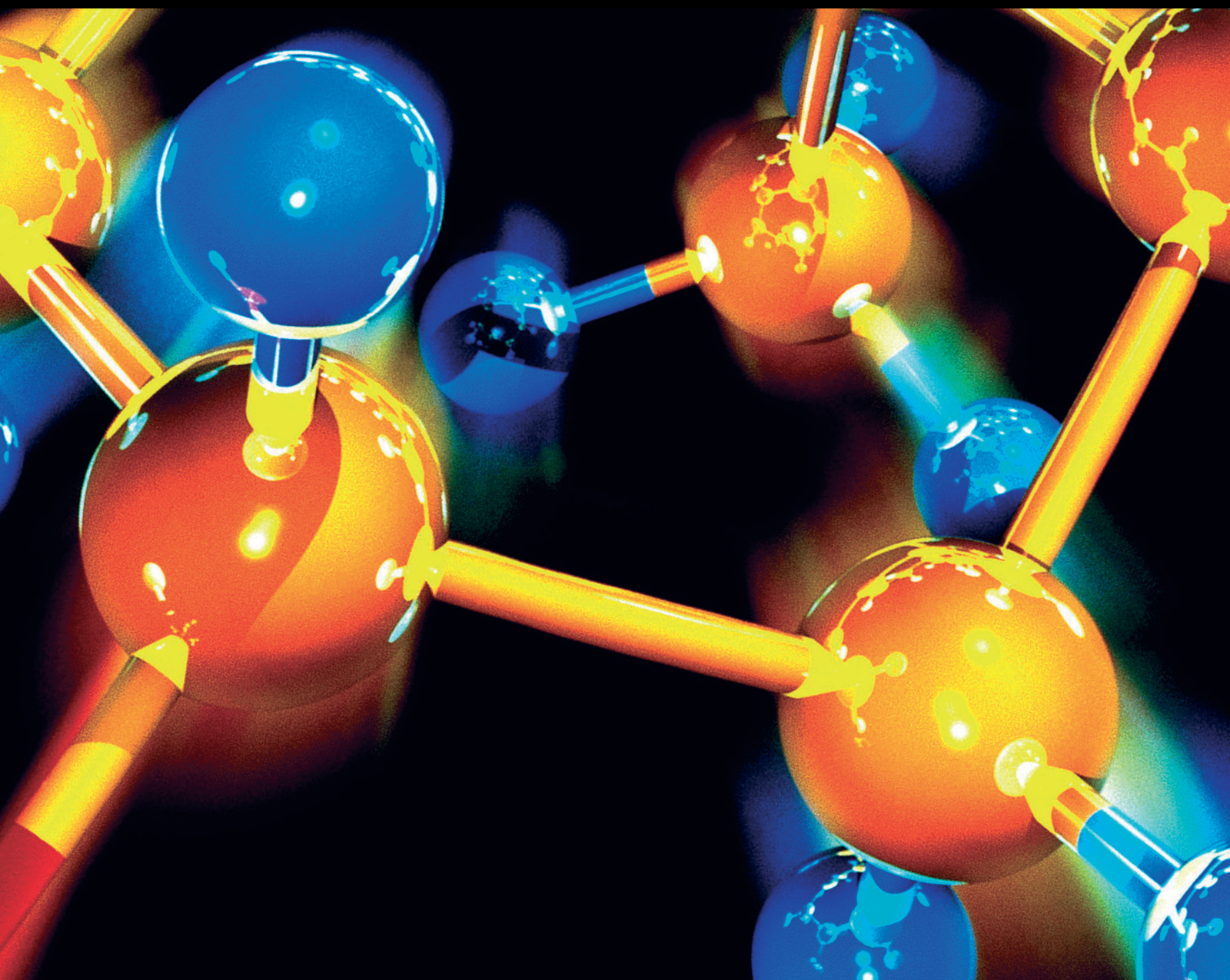


# Mathematical Analysis in Environmental and Biochemical Processes

Lead Guest Editor: Weiguo Li

Guest Editors: Xuncaï Chen and Fenglin Liu





---

# **Mathematical Analysis in Environmental and Biochemical Processes**

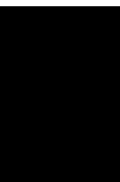
Journal of Chemistry

---

**Mathematical Analysis in  
Environmental and Biochemical  
Processes**

Lead Guest Editor: Weiguo Li

Guest Editors: Xuncaï Chen and Fenglin Liu



---

Copyright © 2022 Hindawi Limited. All rights reserved.


This is a special issue published in "Journal of Chemistry." All articles are open access articles distributed under the Creative Commons Attribution License, which permits unrestricted use, distribution, and reproduction in any medium, provided the original work is properly cited.

# Chief Editor

Kaustubha Mohanty, India

## Associate Editors

Mohammad Al-Ghouti, Qatar


Tingyue Gu , USA


Teodorico C. Ramalho , Brazil

Artur M. S. Silva , Portugal


## Academic Editors

Jinwei Duan, China

Luqman C. Abdullah , Malaysia

Dr Abhilash , India


Amitava Adhikary, USA

Amitava Adhikary , USA

Mozhgan Afshari, Iran

Daryoush Afzali , Iran

Mahmood Ahmed, Pakistan


Islam Al-Akraa , Egypt


Juan D. Alché , Spain

Gomaa A. M. Ali , Egypt

Mohd Sajid Ali , Saudi Arabia

Shafaqat Ali , Pakistan


Patricia E. Allegretti , Argentina

Marco Anni , Italy

Alessandro Arcovito, Italy

Hassan Arida , Saudi Arabia


Umair Ashraf, Pakistan


Narcis Avarvari , France

Davut Avci , Turkey


Chandra Azad , USA

Mohamed Azaroual, France

Rasha Azzam , Egypt


Hassan Azzazy , Egypt

Renal Backov, France

Suresh Kannan Balasingam , Republic of Korea

Sukanta Bar , USA

Florent Barbault , France

Maurizio Barbieri , Italy

James Barker , United Kingdom

Salvatore Barreca , Italy

Jorge Barros-Velázquez , Spain

THANGAGIRI Baskaran , India

Haci Baykara, Ecuador

Michele Benedetti, Italy

Laurent Billon, France

Marek Biziuk, Poland

Jean-Luc Blin , France

Tomislav Bolanca , Croatia

Ankur Bordoloi , India

Cato Brede , Norway


Leonid Breydo , USA


Wybren J. Buma , The Netherlands

J. O. Caceres , Spain

Patrizia Calaminici , Mexico


Claudio Cameselle , Spain


Joaquin Campos , Spain

Dapeng Cao , China

Domenica Capasso , Italy

Stefano Caporali , Italy

Zenilda Cardeal , Brazil

Angela Cardinali , Italy

Stefano Carli , Italy

Maria F. Carvalho , Portugal


Susana Casal , Portugal


David E. Chavez, USA

Riccardo Chelli , Italy

Zhongfang Chen , Puerto Rico

Vladislav Chrastny , Czech Republic


Roberto Comparelli , Italy

Filomena Conforti , Italy

Luca Conti , Italy


Christophe Coquelet, France

Filomena Corbo , Italy


Jose Corchado , Spain

Maria N. D.S. Cordeiro , Portugal

Claudia Crestini, Italy

Gerald Culioli , France

Nguyen Duc Cuong , Vietnam

Stefano D'Errico , Italy


Matthias D'hooghe , Belgium


Samuel B. Dampare, Ghana

Umashankar Das, Canada

Victor David, Romania

Annalisa De Girolamo, Italy


Antonio De Lucas-Consuegra , Spain

Marcone A. L. De Oliveira , Brazil

Paula G. De Pinho , Portugal

Damião De Sousa , Brazil

Francisco Javier Deive , Spain

Tianlong Deng , China

Fatih Deniz , Turkey  
Claudio Di Iaconi, Italy  
Irene Dini , Italy  
Daniele Dondi, Italy  
Yingchao Dong , China  
Dennis Douroumis , United Kingdom  
John Drexler, USA  
Qizhen Du, China  
Yuanyuan Duan , China  
Philippe Dugourd, France  
Frederic Dumur , France  
Grégory Durand , France  
Mehmet E. Duru, Turkey  
Takayuki Ebata , Japan  
Arturo Espinosa Ferao , Spain  
Valdemar Esteves , Portugal  
Cristina Femoni , Italy  
Gang Feng, China  
Dieter Fenske, Germany  
Jorge F. Fernandez-Sanchez , Spain  
Alberto Figoli , Italy  
Elena Forte, Italy  
Sylvain Franger , France  
Emiliano Fratini , Italy  
Franco Frau , Italy  
Bartolo Gabriele , Italy  
Guillaume Galliero , France  
Andrea Gambaro , Italy  
Vijay Kumar Garlapati, India  
James W. Gauld , Canada  
Barbara Gawdzik , Poland  
Pier Luigi Gentili , Italy  
Beatrice Giannetta , Italy  
Dimosthenis L. Giokas , Greece  
Alejandro Giorgetti , Italy  
Alexandre Giuliani , France  
Elena Gomez , Spain  
Yves Grohens, France  
Katharina Grupp, Germany  
Luis F. Guido , Portugal  
Maolin Guo, USA  
Wenshan Guo , Australia  
Leena Gupta , India  
Muhammad J. Habib, USA  
Jae Ryang Hahn, Republic of Korea

Christopher G. Hamaker , USA  
Ashanul Haque , Saudi Arabia  
Yusuke Hara, Japan  
Naoki Haraguchi, Japan  
Serkos A. Haroutounian , Greece  
Rudi Hendra , Indonesia  
Javier Hernandez-Borges , Spain  
Miguel Herrero, Spain  
Mark Hoffmann , USA  
Hanmin Huang, China  
Doina Humelnicu , Romania  
Charlotte Hurel, France  
Nenad Ignjatović , Serbia  
Ales Imramovsky , Czech Republic  
Muhammad Jahangir, Pakistan  
Philippe Jeandet , France  
Sipak Joyasawal, USA  
Sławomir M. Kaczmarek, Poland  
Ewa Kaczorek, Poland  
Mostafa Khajeh, Iran  
Srećko I. Kirin , Croatia  
Anton Kokalj , Slovenia  
Sevgi Kolaylı , Turkey  
Takeshi Kondo , Japan  
Christos Kordulis, Greece  
Ioannis D. Kostas , Greece  
Yiannis Kourkoutas , Greece  
Henryk Kozłowski, Poland  
Yoshihiro Kudo , Japan  
Avvaru Praveen Kumar , Ethiopia  
Dhanaji Lade, USA  
Isabel Lara , Spain  
Jolanta N. Latosinska , Poland  
João Paulo Leal , Portugal  
Woojin Lee, Kazakhstan  
Yuan-Pern Lee , Taiwan  
Matthias Lein , New Zealand  
Huabing Li, China  
Jinan Li , USA  
Kokhwa Lim , Singapore  
Teik-Cheng Lim , Singapore  
Jianqiang Liu , China  
Xi Liu , China  
Xinyong Liu , China  
Zhong-Wen Liu , China

Eulogio J. Llorent-Martínez , Spain  
Pasquale Longo , Italy  
Pablo Lorenzo-Luis , Spain  
Zhang-Hui Lu, China  
Devanand Luthria, USA  
Konstantin V. Luzyanin , United Kingdom  
Basavarajaiah S M, India  
Mari Maeda-Yamamoto , Japan  
Isabel Mafra , Portugal  
Dimitris P. Makris , Greece  
Pedro M. Mancini, Argentina  
Marcelino Maneiro , Spain  
Giuseppe F. Mangiatordi , Italy  
Casimiro Mantell , Spain  
Carlos A Martínez-Huitle , Brazil  
José M. G. Martinho , Portugal  
Andrea Mastinu , Italy  
Cesar Mateo , Spain  
Georgios Matthaiolampakis, USA  
Mehrab Mehrvar, Canada  
Saurabh Mehta , India  
Oinam Romesh Meitei , USA  
Saima Q. Memon , Pakistan  
Morena Miciaccia, Italy  
Maurice Millet , France  
Angelo Minucci, Italy  
Liviu Mitu , Romania  
Hideto Miyabe , Japan  
Ahmad Mohammad Alakraa , Egypt  
Kaustubha Mohanty, India  
Subrata Mondal , India  
José Morillo, Spain  
Giovanni Morrone , Italy  
Ahmed Mourran, Germany  
Nagaraju Mupparapu , USA  
Markus Muschen, USA  
Benjamin Mwashote , USA  
Mallikarjuna N. Nadagouda , USA  
Lutfun Nahar , United Kingdom  
Kamala Kanta Nanda , Peru  
Senthilkumar Nangan, Thailand  
Mu. Naushad , Saudi Arabia  
Gabriel Navarrete-Vazquez , Mexico  
Jean-Marie Nedelec , France  
Sridhar Goud Nerella , USA  
Nagatoshi Nishiwaki , Japan  
Tzortzis Nomikos , Greece  
Beatriz P. P. Oliveira , Portugal  
Leonardo Palmisano , Italy  
Mohamed Afzal Pasha , India  
Dario Pasini , Italy  
Angela Patti , Italy  
Massimiliano F. Peana , Italy  
Andrea Penoni , Italy  
Franc Perdih , Slovenia  
Jose A. Pereira , Portugal  
Pedro Avila Pérez , Mexico  
Maria Grazia Perrone , Italy  
Silvia Persichilli , Italy  
Thijs A. Peters , Norway  
Christophe Petit , France  
Marinos Pitsikalis , Greece  
Rita Rosa Plá, Argentina  
Fabio Polticelli , Italy  
Josefina Pons, Spain  
V. Prakash Reddy , USA  
Thathan Premkumar, Republic of Korea  
Maciej Przybyłek , Poland  
María Quesada-Moreno , Germany  
Maurizio Quinto , Italy  
Franck Rabilloud , France  
C.R. Raj, India  
Sanchayita Rajkhowa , India  
Manzoor Rather , India  
Enrico Ravera , Italy  
Julia Revuelta , Spain  
Muhammad Rizwan , Pakistan  
Manfredi Rizzo , Italy  
Maria P. Robalo , Portugal  
Maria Roca , Spain  
Nicolas Roche , France  
Samuel Rokhum , India  
Roberto Romeo , Italy  
Antonio M. Romerosa-Nievas , Spain  
Arpita Roy , India  
Eloy S. Sanz P rez , Spain  
Nagaraju Sakkani , USA  
Diego Sampedro , Spain  
Shengmin Sang , USA


Vikram Sarpe , USA  
Adrian Saura-Sanmartin , Spain  
St phanie Sayen, France  
Ewa Schab-Balcerzak , Poland  
Hartwig Schulz, Germany  
Gulaim A. Seisenbaeva , Sweden  
Serkan Selli , Turkey  
Murat Senturk , Turkey  
Beatrice Severino , Italy  
Sunil Shah Shah , USA  
Ashutosh Sharma , USA  
Hideaki Shirota , Japan  
Cl udia G. Silva , Portugal  
Ajaya Kumar Singh , India  
Vijay Siripuram, USA  
Ponnurengam Malliappan Sivakumar ,  
Japan  
Tom s Sobrino , Spain  
Raquel G. Soengas , Spain  
Yujiang Song , China  
Olivier Soppera, France  
Radhey Srivastava , USA  
Vivek Srivastava, India  
Theocharis C. Stamatatos , Greece  
Athanasios Stavrakoudis , Greece  
Darren Sun, Singapore  
Arun Suneja , USA  
Kamal Swami , USA  
B.E. Kumara Swamy , India  
Elad Tako , USA  
Shoufeng Tang, China  
Zhenwei Tang , China  
Vijai Kumar Reddy Tangadanchu , USA  
Franco Tassi, Italy  
Alexander Tatarinov, Russia  
Lorena Tavano, Italy  
Tullia Tedeschi, Italy  
Vinod Kumar Tiwari , India  
Augusto C. Tome , Portugal  
Fernanda Tonelli , Brazil  
Naoki Toyooka , Japan  
Andrea Trabocchi , Italy  
Philippe Trens , France  
Ekaterina Tsipis, Russia  
Esteban P. Urriolabeitia , Spain

Toyonobu Usuki , Japan  
Giuseppe Valacchi , Italy  
Ganga Reddy Velma , USA  
Marco Viccaro , Italy  
Jaime Villaverde , Spain  
Marc Visseaux , France  
Balaga Viswanadham , India  
Alessandro Volonterio , Italy  
Zoran Vujcic , Serbia  
Chun-Hua Wang , China  
Leiming Wang , China  
Carmen W ngler , Germany  
Wieslaw Wiczkowski , Poland  
Bryan M. Wong , USA  
Frank Wuest, Canada  
Yang Xu, USA  
Dharmendra Kumar Yadav , Republic of  
Korea  
Maria C. Yebra-Biurrun , Spain  
Dr Nagesh G Yernale, India  
Tomokazu Yoshimura , Japan  
Maryam Yousaf, China  
Sedat Yurdakal , Turkey  
Shin-ichi Yusa , Japan  
Claudio Zaccone , Italy  
Ronen Zangi, Spain  
John CG Zhao , USA  
Zhen Zhao, China  
Antonio Zizzi , Italy  
Mire Zloh , United Kingdom  
Grigoris Zoidis , Greece  
Deniz  AHİN , Turkey



# Contents

## **High-Dose or Low-Dose Aspirin Application in the Initial Phase of Kawasaki Disease: A Meta-Analysis and Systematic Review**

Kun Liu, Lu Wang, and Linxia Gong 



Research Article (8 pages), Article ID 6303653, Volume 2022 (2022)

## **Spray-Dried Griseofulvin-Lactose Matrix for Enhanced Solubility Using a Spray-Drying Biochemical Process**

Tian Lan, Jie Yang, Zhi-jie Yang, and Hong-wen Wu 



Research Article (7 pages), Article ID 8372048, Volume 2022 (2022)

## **Efficacy, Influencing Factors, and Safety of Alteplase Intravenous Thrombolysis in Patients with Acute Ischemic Stroke Combined with Atrial Fibrillation**

Yongyin Zhang, Haoye Cai, Hao Shu, Ruqian He, Xuerong Huang , and Xiaoyi Song 


Research Article (7 pages), Article ID 9909703, Volume 2022 (2022)

## **Changes of Cell Adhesion Molecules and T Cell Subset Populations in Acute Myeloid Leukemia Patients Undergoing Intravenous Administration of Cytarabine Supplemented with Idarubicin**

Jinhua Piao, Didi Wang, Siying Pei , Tangdong Ge, Jing Li, and Pengxia Zhang 



Research Article (7 pages), Article ID 5507328, Volume 2022 (2022)

## **Clinical Observation on the Treatment of Chronic Subjective Dizziness by the Herbal-Scraping Duplex Method Based on Holographic Theory**

Huanwen Luo, Caidan Liu, Ziwei Xiao, and Yana He 

Research Article (8 pages), Article ID 9195636, Volume 2022 (2022)

## **Research Progress in Isolation and Enrichment of Fetal Cells from Maternal Blood**

Ying Tang, Qiaojin Tang, Haiyan Luo, Xuehui Zhang, Qiuyu Chen, Wenyong Tang, Ting Wang, Lihua Yang , and Hongwu Liao 


Review Article (8 pages), Article ID 7131241, Volume 2022 (2022)

## **Mechanism of Baclofen Inhibiting the Proliferation and Metastasis of GBM by Regulating YAP**

Lin Zhu, Juan Lu, Zhijun Bao, and Shiwen Guo 



Research Article (10 pages), Article ID 2753571, Volume 2021 (2021)

## **Screening of Active Components and Key Targets of Radix Codonopsis in the Treatment of Gastric Cancer**

Lijun Tang, Jinhui Chen, Jin Yin, and Mingli Fang 



Research Article (10 pages), Article ID 6056636, Volume 2021 (2021)

## **Study on the Mechanism of *Salvia miltiorrhiza* in the Treatment of Traumatic Bone Defects**

Qian Tan, Yaoxi Liu, Ting Lei, Weihua Ye, Xin Hu, Haibo Mei , and Ge Yang 


Research Article (9 pages), Article ID 8646394, Volume 2021 (2021)

## **SPSS Analysis of Pain Factors in Rotator Cuff Repair**

Yi Zhou, Huali Chen , Jing Wang, Hui Wu, Yuanjie Zeng, Xiaohui Yi, and Yan Zhang 

Research Article (5 pages), Article ID 8491846, Volume 2021 (2021)

**Application of Nanooptics in Photographic Imagery and Medical Imaging**

Yunrun Liu, Na Pang, Yunzhou Cai, Yanqing Yang, Chunyu Zeng, and Yuehong Wang 

Review Article (15 pages), Article ID 2384322, Volume 2021 (2021)


**Chemical Constituents and Pharmacological Activities of Steroid Saponins Isolated from *Rhizoma Paridis***

Fen Liu , Luning Li , Xinchun Tian , Dengtian Zhang , Wenxue Sun , and Shulong Jiang 

Review Article (7 pages), Article ID 1442906, Volume 2021 (2021)

## Research Article

# High-Dose or Low-Dose Aspirin Application in the Initial Phase of Kawasaki Disease: A Meta-Analysis and Systematic Review

Kun Liu, Lu Wang, and Linxia Gong 

Department of Pediatrics,  
Nanjing Integrated Traditional Chinese and Western Medicine Hospital Affiliated with Nanjing University of Chinese Medicine,  
Nanjing, Jiangsu, China

Correspondence should be addressed to Linxia Gong; [gonglx1688@163.com](mailto:gonglx1688@163.com)

Received 24 December 2021; Accepted 27 January 2022; Published 14 October 2022

Academic Editor: Weiguo Li

Copyright © 2022 Kun Liu et al. This is an open access article distributed under the Creative Commons Attribution License, which permits unrestricted use, distribution, and reproduction in any medium, provided the original work is properly cited.

The initial dose of aspirin for Kawasaki disease (KD) is controversial to a great extent. In order to compare the efficacy of high-dose and low-dose aspirin in the treatment of KD, this study included articles containing information on the treatment of KD with aspirin before August 2021, which were collected from public databases. The results of different studies were summarized and weighted by an inverse variance model, and heterogeneity was assessed using the Q-test and  $I^2$ . A meta-analysis of 12258 patients from nine retrospective studies was conducted. In general, no significant differences between high-dose and low-dose groups were found in the incidence of coronary artery abnormality (CAA) (RR = 1.154; 95% CI = 1.027–1.316) and the incidence of intravenous immunoglobulin (RR = 0.926; 95% CI = 0.594–1.441). But high-dose aspirin might be linked to the shortened duration of fever (RR = -0.134; 95% CI = -0.203–0.064) as well as hospitalized stay (RR = -1.263; 95% CI = -1.392–1.122). *Conclusion.* For the treatment of the acute phase of KD, low-dose aspirin plus intravenous immunoglobulin could be as effective as high-dose aspirin in preventing CAA. Nonetheless, high-dose aspirin might be related to reducing fever time and hospitalization time.

## 1. Introduction

Kawasaki disease (KD), also known as mucosal cutaneous lymph node syndrome, is an acute, self-limited vasculitis that predominantly affects children under five years of age [1,2]. Initial symptoms include high fever, inflammation of the skin mucosa, and neck lymphadenopathy. Coronary artery abnormalities (CAA), usually developing in 15% to 25% of all patients during the first two weeks of the disease, are regarded as the most severe complication of KD [3]. At present, KD is considered to be one of the most main causes for acquired heart disease among children in developed countries [4,5].

Although the cause of KD is still unclear, recent studies have observed the dysfunction of innate immune responses in the process of CAA [6]. At the initial stage of the disease, neutrophils infiltrated into the adventitia of the coronary

artery wall from the intima. Inflammation leads to the destruction of the structural integrity of the coronary arteries and laminar flow. Therefore, treatment against inflammation and platelet thrombosis is widely accepted as primary care.

In order to prevent coronary artery complications, the American Heart Association recommended giving 2 g/kg intravenous immunoglobulin (IVIG) plus 80–100 mg/kg/day high-dose aspirin (acetylsalicylic acid, ASA) in the acute stage of KD [7]. Similarly, IVIG (2 g/kg) plus 30–50 mg/kg/day of moderate-dose aspirin was recommended by the Japanese Society of Pediatric Cardiology and Cardiosurgery until the patient had no fever [8]. After that, patients need to receive low-dose aspirin (3–5 mg/kg/day) for 6–8 weeks. The combined application of aspirin and IVIG at a high dose (>30 mg/kg/day) might exert strong anti-inflammatory, anti-platelet, and immunomodulatory functions. It is worth noting that although the therapeutic effect of IVIG is

recognized as the key measure to prevent the formation of CAA in KD, the appropriate dose of aspirin is still widely controversial.

Many studies, including clinical trials and meta-analyses, show that the efficacy of low-dose aspirin (3–5 mg/kg/day) in treating KD is not inferior to that of high-dose aspirin (>30 mg/kg/day) [9,10]. In addition, the adverse effects of high-dose aspirin, including anemia, gastrointestinal bleeding, Reye syndrome, and sensorineural hearing loss, have attracted people's attention for a long time [11].

Hence, the initial dose of aspirin used in the initial stage of KD is a highly controversial subject. It is necessary to conduct a comprehensive meta-analysis by using the latest clinical evidence to comprehensively evaluate and compare the effects of high-dose aspirin and low-dose aspirin in the initial treatment of KD.

## 2. Methods

**2.1. Research Type.** Controlled studies or cohort studies published in China and abroad are the research type; languages are limited to Chinese and English.

**2.2. Study Population.** The study population was based on the subjects who meet KD-related diagnostic criteria and at the stage of initial use of aspirin, regardless of gender.

**2.3. Intervention Measure.** Children in the experimental group were treated with high-dose or low-dose aspirin, while children in the control group were treated with different drugs or different doses of aspirin than those in the experimental group.

**2.4. Inclusion and Exclusion Criteria.** The Population-Intervention-Comparison-Outcome (PICO) strategy was applied for data inclusion. Generally, the stratified patients were children with a clear diagnosis of KD. All qualified studies include IVIG plus aspirin intervention in the treatment of acute KD. The comparison was made between the administration of high-dose (>30 mg/kg/day) aspirin and low-dose (<10 mg/kg/day) aspirin in KD treatment. The observed results included the incidence of CAA, the incidence of IVIG resistance, the duration of fever, and hospitalized stay.

**2.5. Literature Search Strategy.** An extensive literature search was conducted using keywords ['Kawasaki syndrome' OR 'Lymph node syndrome, mucocutaneous' OR 'Kawasaki disease'] AND ['Aspirin' OR 'Acetylsalicylic Acid' OR 'Acid, Acetylsalicylic' OR '2-(Acetyloxy)benzoic Acid' OR 'Acetylsalicylic Acid' OR 'Aloxiiprimum' OR 'Colfarit' OR 'Dispril' OR 'Easprin' OR 'Ecotrin' OR 'Endosprin' OR 'Magnecyl' OR 'Micristin' OR 'Polopirin' OR 'Polopiryryna' OR 'Solprin' OR 'Solupsan' OR 'Zorprin' OR 'Acetylsal'] in [Title/Abstract] to acquire potential qualified studies from public databases of PubMed, Web of Science, Ovid, EMBASE, and Cochrane Library before August 2021. Written language was restricted

to English. The selected paper was composed of two authors (L.K. and W.L.) independently to determine whether a study was suitable for inclusion. A third author (G.L.) joined and reassessed the paper when disagreement occurred. After the differences were resolved, all the papers unanimously supported by the authors were selected for meta-analysis.

**2.6. Data Extraction.** Data from selected papers were collected by two authors (L.K. and G.L.) independently. Information was collected, including publication year, first author's name, the total number of enrolled patients, clinical characteristics, aspirin dose, IVIG dose, quality evaluation of the study (NOS score), and major and minor outcomes of the patients.

**2.7. Quality Evaluation.** All enrolled studies received a methodological evaluation by two authors (L.K. and G.L.), respectively, using Newcastle-Ottawa scale (NOS) scoring system. The assessment was based on criteria of participant enrollment, comparability of different treatments, and outcome measurements. Briefly, studies with more than six stars were regarded as high quality and suitable for further analysis.

**2.8. Statistical Analysis.** After data extraction and evaluation as mentioned above, the relative risk (RR) for dichotomous outcomes and the mean difference (MD) for continuous outcomes were calculated. Statistical analysis was performed using Stata 16.0 statistical software. Results from different studies were pooled and weighted via the inverse variance model. A two-tailed *P* value of less than 0.05 was considered statistically significant. Once the studies were synthesized, the heterogeneity was assessed with the *Q* test and  $I^2$ . Values of  $I^2$  less than 25%, from 25 to 50%, and over 50% represented a low, moderate, and high level of heterogeneity, respectively. In addition, subgroup analysis regarding the different aspirin dosages and sample sizes as well as meta-regression test was subsequently performed to exclude inner bias among studies.

## 3. Results

**3.1. Target Study Enrollment.** The model included in the literature is shown in Figure 1. After eliminating duplicates, a total of 614 studies were selected from databases. After reviewing titles and abstracts, 116 articles of interest were identified. All the 116 papers were read in full to evaluate the suitable meta-analysis paper. Finally, nine retrospective cohort studies (RCS) were selected for further analysis.

**3.2. Demographic and Clinical Characteristics of Enrolled Studies.** The clinical features of all selected studies are summarized in Table 1 [11–19]. According to the recommendations of the American Heart Association and the Japanese Circulation Society, all studies used the same dose of IVIG and different doses of aspirin for treatment. For counting, 12258 involved patients were divided into 2495

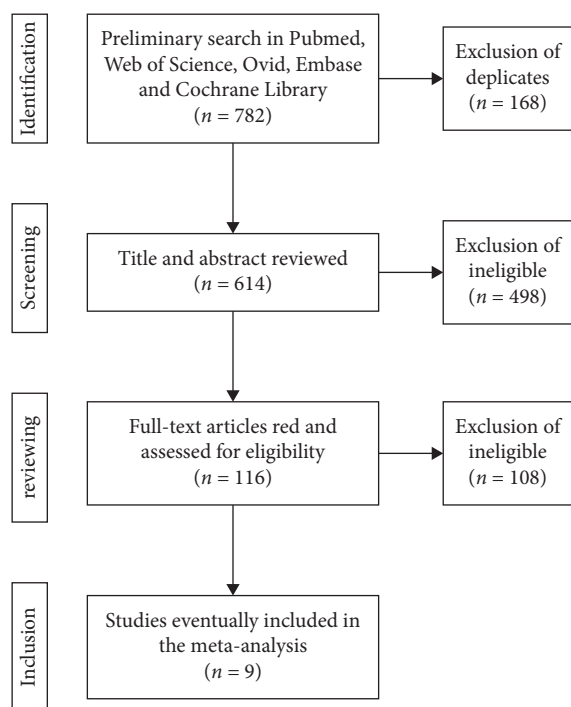


FIGURE 1: Schema flow of search strategy and history to compare the efficacy of high-dose and low-dose aspirin.

patients in the high-dose aspirin group and 9763 patients in the low-dose aspirin group.

Of the nine registered studies, six applied 80 mg/kg as high-dose aspirin treatment, while the other three applied 30 mg/kg. Unanimously, the low-dose aspirin group used a dose of 3–5 mg/kg. Moreover, all studies have reported that the incidence of CAA formation is the main result (Table 2). For secondary outcomes, five studies reported the incidence of IVIG resistance, three studies reported the duration of fever, and three studies reported the length of hospitalized days. Notably, eight out of nine studies received more than six stars in the NOS scoring system, which reflected that they were suitable for further meta-analysis.

**3.3. Incidence of Coronary Artery Abnormality.** All the CAA occurrence data in the studies were imported into the software Stata SE, and the fixed Mantel–Haenszel model was used to compare between the high-dose and low-dose aspirin groups (Figure 2). The level of heterogeneity was considered at a low level with  $I^2=17.6$ , and  $P=0.286$  ( $RR=1.154$  and  $95\%CI=1.027-1.316$ ). The result indicated no significant difference between the two groups in CAA incidence. The publication bias was checked with Egger's test. A  $P$  value of 0.579 showed that no obvious publication bias was observed.

According to different aspirin doses recommended by American and Japanese societies for the initial treatment of KD, North America usually uses a high-dose choice of over 80 mg/kg, while Asia often uses a dose of over 30 mg/kg. Therefore, subgroup analysis was further applied to check if different high-dose strategies affect CAA formation

(Figure 3). In line with general results previously, subgroups using  $\geq 80$  mg/kg or  $\geq 30$  mg/kg aspirin exposed only little difference in CAA incidence.

Subsequently, a meta-regression analysis was conducted to determine whether some factors had a significant influence on heterogeneity. Potential factors including the choice for high-dose aspirin treatment and sample size underwent meta-regression analysis. The results showed that the dose of aspirin has little impact on heterogeneity with  $P$  value = 0.655 and 95% CI =  $-1.052-0.750$ . Similarly, the size of the study might also not have a significant correlation with heterogeneity with  $P$  value = 0.775 and 95% CI between  $-0.759-0.978$ .

**3.4. Incidence of IVIG Resistance.** To date, cases with IVIG resistance reported in five out of nine studies were also input into Stata software for analysis (Figure 4). Surprisingly, the result revealed no significant difference between the two groups in the incidence of IVIG resistance ( $RR=0.926$ ; 95% CI =  $0.594-1.441$ ). However, high heterogeneity ( $I^2=90.2\%$ ;  $P=0.001$ ) implied that inner differences might exist among studies and further investigation is required.

**3.5. Duration of Fever and Length of Hospitalization.** In addition, other secondary outcomes were evaluated, including the duration of fever and the length of hospitalization. In specific, three studies provided information about the duration of moderate heterogeneous fever (Figure 5). Unsurprisingly, compared with the low-dose group, high dose of aspirin is associated with a shorter duration of fever, reflecting the potential beneficial effects of increasing aspirin dose.

In addition, the length of hospital stay was also checked using data from three papers (Figure 6). Inconsistent with the previous report, the application of high-dose aspirin might be a factor cutting the length of stay in the hospital [20]. Nevertheless, the high heterogeneity was not to be neglected.

## 4. Discussion

In the years after KD was first reported, pediatricians soon realized that a small number of patients died suddenly within two to three weeks after the fever began. It was not long until doctors found that CAA was the main cause of the accidental death [21,22]. Nowadays, in developed countries, KD is recognized as the leading cause of acquired heart disease in children [23]. In the 1980s, a series of clinical trials laid the foundation of the standard treatment of KD. The efficiency single shot of high-dose IVIG plus aspirin has been learned and soon established as the standard therapy for preventing the development of CAA in KD [24,25]. Nevertheless, the dose of aspirin has been controversial for a long time, and its specific mechanism is still unclear.

Because of its anti-inflammatory and antithrombotic properties, aspirin has been used for KD treatment long before it was applied as IVIG, but there is little information about its role in preventing CCA. When evidence

TABLE 1: Characteristics of the enrolled studies.

Author	Year	Nation	Study type	Patients number	Age, month, mean (SD)	Gender (male%)	CAA criteria	IVIG dose	NOS score	Interventions
Platt et al.	2019	USA	RCS	260	H: 32.4 (20.4–50.4)* L: 28.8 (18–52.8)	H: 118 (64.4%) L: 142 (57%)	—	2 g/kg	8	H: 75.5 mg/kg/day L: 4.4 mg/kg/day
Dhanrajani et al.	2018	Canada	RCS	249	H: 36 (18–64)* L: 36 (17–56)	H: 127 (58.3%) L: 122 (59%)	—	2 g/kg	7	H: 80–100 mg/kg/day L: 3–5 mg/kg/day
Huang et al.	2017	China	RCS	910	H: 25.8 (19.4) L: 23.7 (11.3)	H: 86 (69%) L: 672 (63%)	Japanese criteria	2 g/kg	8	H: 30–50 mg/kg/day L: 3–5 mg/kg/day
Dallaire et al.	2017	Canada	RCS	1213	H: 40.8 (28.8) L: 38.4 (26.4)	H: 848 (59.4%) L: 365 (58.4%)	Z score	2 g/kg	8	H: 80 mg/kg/day L: 3–5 mg/kg/day
Kim et al.	2016	South Korea	RCS	8456	H: 32.6 (23.8) L: 30.8 (23.5)	H: 7947 (58.3%) L: 509 (57.4%)	Z score	2 g/kg	8	H: >30 mg/kg/day L: 3–5 mg/kg/day
Kuo et al.	2015	Taiwan, China	RCS	851	H: 28.8 (28.8) L: 34.8 (26.4)	H: 305 (65.9%) L: 546 (61.9%)	Japanese criteria	2 g/kg	6	H: >30 mg/kg/day L: 3–5 mg/kg/day
Rahbarimanesht et al.	2014	Iran	RCS	69	—	—	—	2 g/kg	4	H: 80–100 mg/kg/day L: 3–5 mg/kg/day
Lee et al.	2012	South Korea	RCS	180	H: 30.2 (22.3) L: 30.7 (25.1)	H: 129 (55.8%) L: 51 (58.5%)	Japanese criteria	2 g/kg	7	H: 80–100 mg/kg/day L: 3–5 mg/kg/day
Saulsbury	2002	USA	RCS	70	—	—	—	2 g/kg	7	H: 80–100 mg/kg/day L: 3–5 mg/kg/day

Note. \* Studies only provided with medium (IQR) value.

TABLE 2: Comparison between high-dose and low-dose aspirin groups.

Author	High-dose aspirin group					Low-dose aspirin group				
	Dose (mg/kg/day)	CAA (n)	Days of fever	Days in hospital	IVIG resistance (n)	Dose (mg/kg/day)	CAA (n)	Days of fever	Days in hospital	IVIG resistance (n)
Platt et al.	75.5	10	—	3 (1)	—	4.4	10	—	3 (1)	—
Dhanrajani et al.	80–100	6	—	—	11	3–5	2	—	—	28
Huang et al.	30–50	136	—	—	28	3–5	15	—	—	86
Dallaire et al.	80	174	7.8 (3.8)	—	207	3–5	81	7.9 (2.6)	—	100
Kuo et al.	>30	52	—	6.3 (0.2)	31	3–5	84	—	6.7 (0.2)	38
Lee et al.	80–100	3	6.2 (8.3)	—	22	3–5	2	13.3 (13.5)	—	8
Kim et al.	>30	1968	5.7 (2.2)	—	838	3–5	93	6.1 (1.9)	—	86
Rahbarimanesh et al.	80–100	1	—	6.1 (1.3)	—	3–5	2	—	6.36 (2.8)	—
Saulsbury	80–100	0	—	—	—	3–5	0	—	—	—

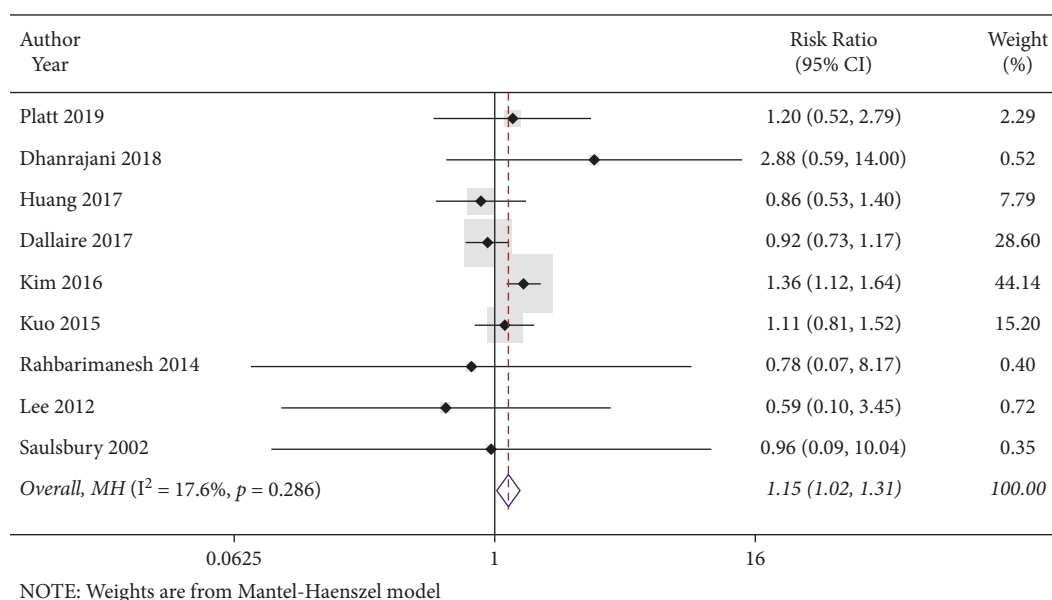


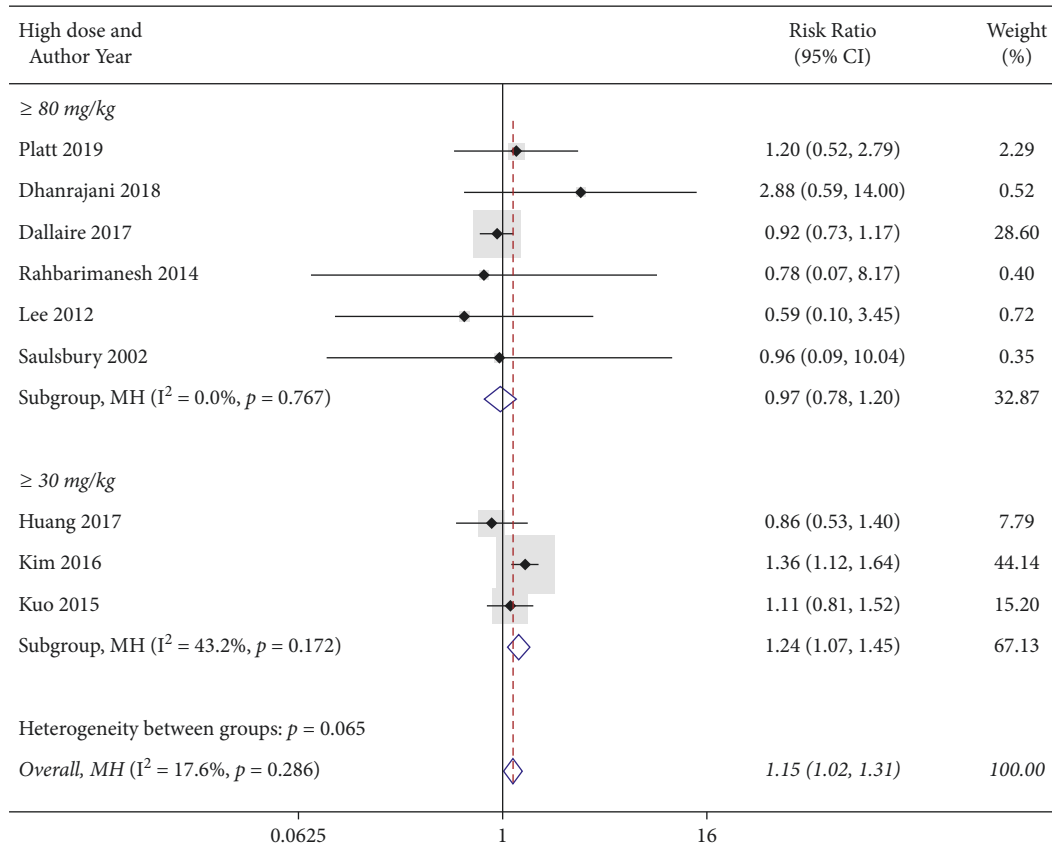
FIGURE 2: The relative risk of coronary artery abnormalities identified in the meta-analysis from nine enrolled studies.

accumulated and the predominant role of IVIG in managing CCA formation was eventually established, high-dose aspirin was applied concomitantly and hence added to the standard protocol of KD treatment. Nonetheless, unlike the appropriate dose of IVIG, which has been clarified and accepted unanimously, the optimal dose of aspirin in KD treatment has been debated for a long time. Recent studies proposed that the usage of low-dose aspirin (3–5 mg/kg per day) was not inferior to the higher-dose mentioned above. One study has proposed that the incidence of growing CAA changes little when aspirin was applied in high dose, low dose, and no aspirin at all.

According to these previous reports, the meta-analysis of our study demonstrated that there is no obvious correlation between aspirin dose and the incidence of CAA with minimal heterogeneity. Additionally, the quality and results of the selected cohort were evaluated by NOS score, meta-regression test, and sensitivity analysis. Factors including publication bias, sample size, dosage selection of

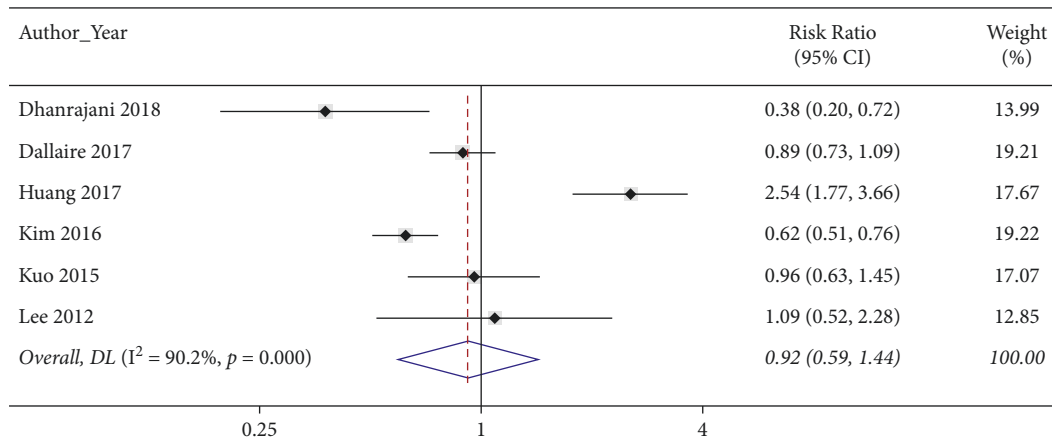
the high-dose group, or discordant results from individual studies might have no significant impact on the overall conclusion. Although the etiology of KD and KD-related arteritis is still not clear, several factors have been noticed as candidate genes in KD. For example, the activation of immune cells (neutrophil and T cell) and multiple cytokines (TNF- $\alpha$ , IL-6, and IL-10) have been reported to be involved in the pathogenesis of KD and artery injury [26,27]. Unfortunately, the pharmaceutical mechanism of aspirin in CAA formation remains obscure, and well-designed randomized clinical trials would be needed in the future.

Generally, IVIG resistance occurs in 10% of patients, who have a significantly high risk of CAA and other adverse effects [28]. Therefore, the incidence rate of IVIG would be crucial for the outcome of KD patients. Surprisingly, our result showed that there was no preference in the risk of IVIG resistance. However, the high heterogeneity in the analysis was not to be overlooked. In fact, two retrospective



NOTE: Weights and between-subgroup heterogeneity test are from Mantel-Haenszel model

FIGURE 3: Subgroup analysis based on different dosages of aspirin in high-dose groups.



NOTE: Weights are from random-effects model

FIGURE 4: The relative risk of IVIG resistance identified in the meta-analysis from nine enrolled studies.

studies (Dhanrajani 2018 [13] and Kim 2016 [16]) with a large sample size concluded that high-dose aspirin was positively linked to reducing the risk of IVIG resistance. Besides, another meta-analysis also carried out a similar conclusion, indicating the complex nature of the subject [29]. Last but not least, a high-dose aspirin was related to a shorter fever time and shorter hospital stay of KD patients, which may be due to the anti-inflammatory property of aspirin.

**4.1. Limitations.** Based on the meta-analysis, our study has several limitations. Firstly, despite the study aimed to include as many qualified studies as possible, few studies were missing or disputably discarded. Secondly, as all the enrolled papers were retrospective studies, more randomized clinical trials should be added to the analysis to minimize the intrinsic differences between studies. Finally, most studies contained only records of short-term follow-up. The long-term effect of aspirin as the treatment for KD is still unclear.



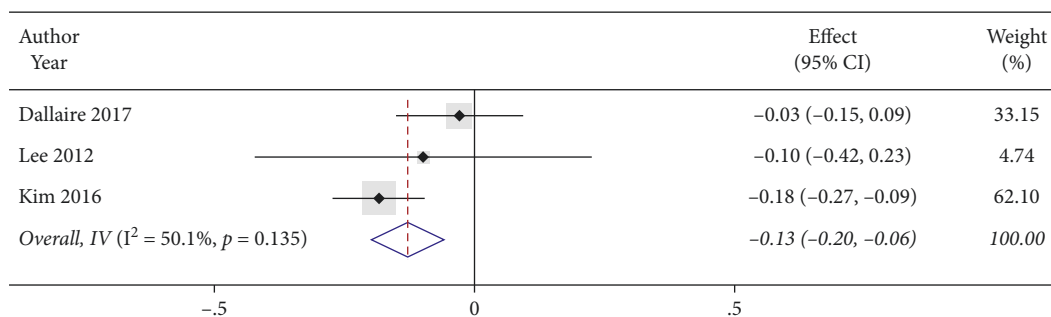


FIGURE 5: The relative risk of duration of fever identified in the meta-analysis from three enrolled studies.

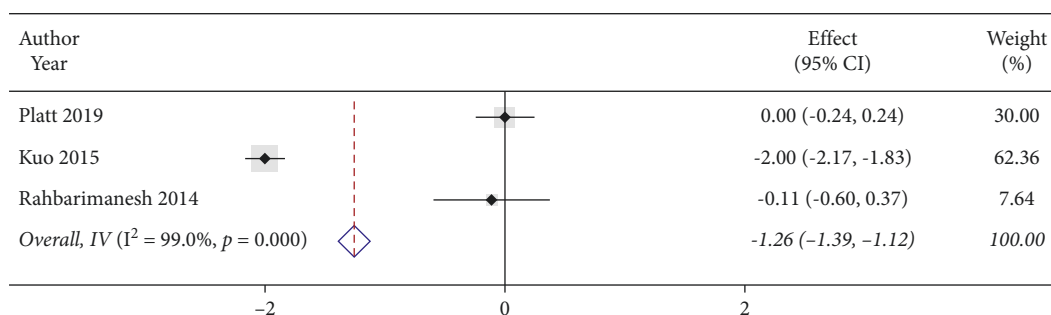


FIGURE 6: The relative risk of the length of hospitalized days identified in the meta-analysis from three enrolled studies.

## 5. Conclusion

To conclude, the meta-analysis of our study clearly indicated that the dose of aspirin poses no obvious effects on preventing CAA as well as IVIG resistance in KD patients. However, high-dose aspirin might be linked to a shorter febrile and total hospital stay, compared to patients with low-dose aspirin.

## Data Availability

All data applied in this study are included in the published form of the article. Request for more information about datasets would be welcome by contacting the corresponding author.

## Conflicts of Interest

The authors declare that they have no conflicts of interest.

## Authors' Contributions

K. L. and L. W. collected data and performed analysis and interpretation of the data. L. G. designed the study. K. L. wrote the draft of the manuscript. L. G. helped in revising the manuscript.

## References

- [1] T. Kawasaki, "[Acute febrile mucocutaneous syndrome with lymphoid involvement with specific desquamation of the fingers and toes in children]," *Arerugi*, vol. 16, no. 3, pp. 178–222, 1967.
- [2] S. T. Shulman and A. H. Rowley, "Kawasaki disease: insights into pathogenesis and approaches to treatment," *Nature Reviews Rheumatology*, vol. 11, no. 8, pp. 475–482, 2015.
- [3] M. B. F. Son and J. W. Newburger, "Kawasaki disease," *Pediatrics in Review*, vol. 39, no. 2, pp. 78–90, 2018.
- [4] N. Makino, Y. Nakamura, M. Yashiro et al., "Descriptive epidemiology of kawasaki disease in Japan, 2011–2012: from the results of the 22nd nationwide survey," *Journal of Epidemiology*, vol. 25, no. 3, pp. 239–245, 2015.
- [5] R. K. Chang, "Hospitalizations for Kawasaki disease among children in the United States, 1988–1997," *Pediatrics*, vol. 109, no. 6, p. e87, 2002.
- [6] R. Kumrah, P. Vignesh, A. Rawat, and S. Singh, "Immunogenetics of kawasaki disease," *Clinical Reviews in Allergy and Immunology*, vol. 59, no. 1, pp. 122–139, 2020.
- [7] B. W. McCrindle, A. H. Rowley, J. W. Newburger et al., "Diagnosis, treatment, and long-term management of kawasaki disease: a scientific statement for health professionals from the American heart association," *Circulation*, vol. 135, no. 17, pp. e927–999, 2017.
- [8] Research Committee of the Japanese Society of Pediatric C, "Cardiac surgery committee for development of guidelines for medical treatment of acute kawasaki D. "Guidelines for medical treatment of acute kawasaki disease: report of the research committee of the Japanese society of pediatric Cardiology and cardiac surgery (2012 revised version)," *Pediatrics International*, vol. 56, no. 2, pp. 135–158, 2014.
- [9] K. S. Hsieh, K. P. Weng, C. C. Lin, T. C. Huang, C. L. Lee, and S. M. Huang, "Treatment of acute Kawasaki disease: aspirin's role in the febrile stage revisited," *Pediatrics*, vol. 114, no. 6, pp. e689–93, 2004.
- [10] K. Durongpisitkul, V. J. Gururaj, J. M. Park, and C. F. Martin, "The prevention of coronary artery aneurysm in Kawasaki disease: a meta-analysis on the efficacy of aspirin and

- immunoglobulin treatment," *Pediatrics*, vol. 96, no. 6, pp. 1057–1061, 1995.
- [11] H. C. Kuo, M. H. Lo, K. S. Hsieh, M. M. Guo, and Y. H. Huang, "High-dose aspirin is associated with anemia and does not confer benefit to disease outcomes in kawasaki disease," *PLoS One*, vol. 10, no. 12, Article ID e0144603, 2015.
- [12] B. Platt, E. Belarski, J. Manaloor et al., "Comparison of risk of recrudescence fever in children with kawasaki disease treated with intravenous immunoglobulin and low-dose vs high-dose aspirin," *JAMA Network Open*, vol. 3, no. 1, Article ID e1918565, 2020.
- [13] A. Dhanrajani, M. Chan, S. Pau, J. Ellsworth, R. Petty, and J. Guzman, "Aspirin dose in kawasaki disease: the ongoing battle," *Arthritis Care & Research*, vol. 70, no. 10, pp. 1536–1540, 2018.
- [14] X. Huang, P. Huang, L. Zhang et al., "Is aspirin necessary in the acute phase of Kawasaki disease?" *Journal of Paediatrics and Child Health*, vol. 54, no. 6, pp. 661–664, 2018.
- [15] F. Dallaire, Z. Fortier-Morissette, S. Blais et al., "Aspirin dose and prevention of coronary abnormalities in kawasaki disease," *Pediatrics*, vol. 139, no. 6, Article ID 20170098, 2017.
- [16] G. B. Kim, J. J. Yu, K. L. Yoon et al., "Medium- or higher-dose acetylsalicylic acid for acute kawasaki disease and patient outcomes," *The Journal of Pediatrics*, vol. 184, pp. 125–129, 2017.
- [17] A. Rahbarimanesh, M. Taghavi-Goodarzi, P. Mohammadinejad, J. Zoughi, J. Amiri, and K. Moridpour, "Comparison of high-dose versus low-dose aspirin in the management of Kawasaki disease," *Indian Journal of Pediatrics*, vol. 81, no. 12, p. 1403, 2014.
- [18] G. Lee, S. E. Lee, Y. M. Hong, and S. Sohn, "Is high-dose aspirin necessary in the acute phase of kawasaki disease?" *Korean Circulation Journal*, vol. 43, no. 3, pp. 182–186, 2013.
- [19] F. T. Saulsbury, "Comparison of high-dose and low-dose aspirin plus intravenous immunoglobulin in the treatment of Kawasaki syndrome," *Clinical Pediatrics*, vol. 41, no. 8, pp. 597–601, 2002.
- [20] X. Jia, X. Du, S. Bie, X. Li, Y. Bao, and M. Jiang, "What dose of aspirin should be used in the initial treatment of Kawasaki disease? A meta-analysis," *Rheumatology*, vol. 59, no. 8, pp. 1826–1833, 2020.
- [21] H. Kato, S. Koike, M. Yamamoto, Y. Ito, and E. Yano, "Coronary aneurysms in infants and young children with acute febrile mucocutaneous lymph node syndrome," *The Journal of Pediatrics*, vol. 86, no. 6, pp. 892–898, 1975.
- [22] M. Yanagisawa, N. Kobayashi, and S. Matsuya, "Myocardial infarction due to coronary thromboarteritis, following acute febrile mucocutaneous lymph node syndrome (MLNS) in an infant," *Pediatrics*, vol. 54, no. 3, pp. 277–281, 1974.
- [23] K. A. Taubert, A. H. Rowley, and S. T. Shulman, "Seven-year national survey of Kawasaki disease and acute rheumatic fever," *The Pediatric Infectious Disease Journal*, vol. 13, no. 8, pp. 704–708, 1994.
- [24] K. Furusho, H. Nakano, K. Tamura et al., "High-dose intravenous gammaglobulin for Kawasaki disease," *The Lancet*, vol. 324, no. 8411, pp. 1055–1058, 1984.
- [25] J. W. Newburger, M. Takahashi, A. S. Beiser et al., "A single intravenous infusion of gamma globulin as compared with four infusions in the treatment of acute Kawasaki syndrome," *New England Journal of Medicine*, vol. 324, no. 23, pp. 1633–1639, 1991.
- [26] S. Jia, C. Li, G. Wang, J. Yang, and Y. Zu, "The T helper type 17/regulatory T cell imbalance in patients with acute Kawasaki disease," *Clinical and Experimental Immunology*, vol. 162, no. 1, pp. 131–137, 2010.
- [27] S. Kamizono, A. Yamada, T. Higuchi, H. Kato, and K. Itoh, "Analysis of tumor necrosis factor- $\alpha$  production and polymorphisms of the tumor necrosis factor- $\alpha$  gene in individuals with a history of Kawasaki disease," *Pediatrics International*, vol. 41, no. 4, pp. 341–345, 1999.
- [28] M.-H. Chiang, H. E. Liu, and J.-L. Wang, "Low-dose or no aspirin administration in acute-phase Kawasaki disease: a meta-analysis and systematic review," *Archives of Disease in Childhood*, vol. 106, no. 7, pp. 662–668, 2021.
- [29] X. Zheng, P. Yue, L. Liu et al., "Efficacy between low and high dose aspirin for the initial treatment of Kawasaki disease: current evidence based on a meta-analysis," *PLoS One*, vol. 14, no. 5, Article ID e0217274, 2019.

## Research Article

# Spray-Dried Griseofulvin-Lactose Matrix for Enhanced Solubility Using a Spray-Drying Biochemical Process

Tian Lan,<sup>1</sup> Jie Yang,<sup>2</sup> Zhi-jie Yang,<sup>1</sup> and Hong-wen Wu<sup>1</sup> 

<sup>1</sup>Department of Pharmacy, Liuzhou Worker's Hospital, The Fourth Affiliated Hospital of Guangxi Medical University, Liuzhou, Guangxi 545007, China

<sup>2</sup>Department of Science and Education, Liuzhou Worker's Hospital, The Fourth Affiliated Hospital of Guangxi Medical University, Liuzhou, Guangxi 545007, China

Correspondence should be addressed to Hong-wen Wu; [dr.hongwen.wu@outlook.com](mailto:dr.hongwen.wu@outlook.com)

Received 21 September 2021; Revised 10 October 2021; Accepted 15 October 2021; Published 5 July 2022

Academic Editor: Weiguo Li

Copyright © 2022 Tian Lan et al. This is an open access article distributed under the Creative Commons Attribution License, which permits unrestricted use, distribution, and reproduction in any medium, provided the original work is properly cited.

Griseofulvin (GF) is a hydrophobic drug with a low solubility. In order to improve the solubility of GF, which has low water solubility, this report uses the spray-drying technique to prepare complexes with lactose to promote the solubility and oral bioavailability of GF. The solution samples were spray dried using different ratios of ethanol or acetone solutions as dissolution media. By characterization of the obtained spray-dried powders, we found that the solubility of the different groups of samples obtained by spray drying was increased, and similarly, their dissolution rates were also increased to different degrees. By comparison, the greatest increase in solubility was obtained in an aqueous acetone solution, showing the greatest ability and efficiency of acetone in promoting the solubility of GF during the spray-drying process.

## 1. Introduction

Griseofulvin, (2S, 6'R)-7-chloro-4, 6-dimethoxybenzofuran-3-one-2-spiro-1'-(2'-methoxy-6'-methylcyclohex-2'-en-4'-one), was primarily isolated from *Penicillium griseofulvum* 1939, and it is one of the first batches of antifungal natural drugs that were found and developed [1]. GF is widely used as an antibiotic and antifungal drug, which inhibits the growth of dermatophytes, possibly by preventing microtubulin polymerization and destroying spindle formation, thus inhibiting fungal mitosis and nucleic acid synthesis. Clinically, GF can be used as the preferred drug for tinea cephalis; meanwhile, it is suitable for treatment in toenail infections and other ringworms. There are some side effects of GF including headaches, gastrointestinal reactions, and skin rash. Since it is mainly distributed in the epidermal stratum corneum, its toxicity to humans is relatively low, so it is generally used for oral treatment of dermatitis [2, 3]. The antibacterial activity of GF is predicted through a computer aided-technique at present [4]. It was also examined that GF has potential antiviral and anticancer effects [5, 6].

GF is a hydrophobic drug with a low solubility. The solubility in the PBS as measured by Petersen et al. [7] is about 7.7( $\mu\text{g}/\text{mL}$ ), while in the water, measured by Thakkar et al. [8], it is about 15( $\mu\text{mL}$ ). As its effective dose is close to the limit of toxicity, the preparation of GF must be carefully designed to achieve maximum absorption. Hence, the water-insolubility characteristics of GF should be improved. In order to increase its solubility in water and improve bioavailability, not only maximum absorption of the drug is achieved but also the dose administered can be reduced and the risk of toxicity is reduced. Solubility in water has become an outstanding factor in improving the efficacy of GF. On the chemical side, changes in molecular structure have been reported to increase the solubility of GF. Amorphous solid dispersion can effectively replace the method of changing molecular structure for increasing solubility [9]. Recently, a series of preparation methods have successfully improved the solubility of GF. For instance, micro- and nano-structured GF is fixed to a silica structure [8], the solvent of GF was prepared into a new polymer dispersion [10], and taking advantage of supercritical fluid- (SCF-) assisted

atomization, we prepared micronized GF [11]. We improve the dissolution performance and bioavailability of the drug by nonionic surfactant vesicles (niosomes) [12], nanocrystalline form, and a self-emulsifying drug delivery system (sedds) [13] for oral administration.

It showed that GF can improve the dissolution behavior of amorphous solid dispersion particles by reducing the particle diameter and inhibiting its recrystallization [14]. The incorporation of surfactants and the preparation of amorphous solid dispersion by spray drying can enhance the miscibility and solubility of GF in water [15]. Through studies and comparisons, the solubility of Gleeevec in ethanol and acetone was found to be quite high [16, 17]. The experiment dissolves the GF into ethanol or acetone and dissolves lactose into water, using the spray drying technique and atomizing the solution or suspensions. The small droplets are quickly dried in the high-temperature airstream to obtain fine powder [18]. In this process, spray-drying techniques transform crystalline hydrophobic drugs into amorphous morphology, and the amorphous drug loose lattice structure has good solubility in water.

The aim of the present article was to develop oral bioavailability of GF through the spray-drying technique (GF dissolved in ethanol/acetone and lactose dissolved in water in certain proportions, respectively) according to suitable parameters to obtain the dried products, and their dissolution properties and various physical and chemical characteristics were characterized.

## 2. Design of Spray-Drying Experiments

**2.1. Preparation of the GF Solution.** For each experiment, a GF solution was freshly prepared at a concentration of 2.5 mg/ml, where the solvent used for sample A was water: ethanol in the ratio of 100:0v/v, sample B water: ethanol in the ratio of 50:50v/v, and sample C water: acetone in the ratio of 50:50v/v. Prior to the configuration of the preceding sample solutions, 9.5g of lactose was first added to the three waters to ensure complete dissolution of the lactose and a consistent ratio of solid components in each sample. After the lactose was completely dissolved, the aqueous lactose solution was slowly poured into ethanol/acetone and then stirred thoroughly at a slow speed (100 rpm/min) to prevent the lactose from precipitating under vigorous stirring. A solution of each sample was obtained, stirred, and set aside.

**2.2. Spray-Drying Process.** The experimental procedure was performed using a small spray dryer (Shanghai YC-015). Spray drying was carried out at a nitrogen gas flow rate of 25 kg/h and a solution flow rate of 12 ml/min using a nozzle of 0.5 mm diameter. The three solutions were completed by three spray processes under the same conditions, respectively. The parameters of the three spray-drying processes were unchanged, fan frequency 50.0 Hz, inlet air temperature  $130 \pm 1^\circ\text{C}$ , outlet air temperature  $120 \pm 3^\circ\text{C}$ , and spray pressure 0.20 MPa. After the completion of the spraying process, the powder of each sample was obtained in the collection hopper, and sample B was dried at a flow rate of 12 ml/min. The samples were sealed and stored.

### 2.3. Characters of Samples

**2.3.1. Dissolution Experiment.** Separate samples of 0.35 g were compressed into tablets under the same pressure and prepared in triplicate to obtain the disintegration dissolution data. The dissolution data were obtained by using an RC1210G solubility meter (Xinzhi, China), the extraction method was the paddle method, the speed was 75 rpm/min, the temperature was  $37.0 \pm 0.1^\circ\text{C}$ , and the sampling height was 750 mL. During the dissolution process, 1.0 ml was sampled separately using a sampling needle at the same interval, and the standard solution was replenished in time until the dissolution process was finished.

**2.3.2. Ultraviolet-Visible Spectrophotometer (UV-Vis).** The solution obtained from the dissolution experiment was filtered into the microporous filter membrane and configured as the required sample, and the absorbance was detected by using a UV-Vis spectrophotometer to draw the dissolution curve; we measured the maximum wavelength at 321 nm. The instrument used was a UV-2401 pc spectrophotometer, Shimadzu, Kyoto, Japan.

**2.3.3. Differential Scanning Calorimetry (DSC).** Thermodynamic analysis of each group of sample powders was carried out using a differential scanning calorimeter (HSC-4 DSC, Henven, China). Samples for DSC determination were prepared in sealed, curled aluminium pans according to standard procedures. Approximately 7.0 mg of each specimen was used for analysis. In the test, the samples were heated from  $30^\circ\text{C}$  to  $350^\circ\text{C}$  at a rate of  $5^\circ\text{C}/\text{min}$ .

**2.3.4. Fourier Transform Infrared Spectroscopy (FTIR).** Fourier transform infrared spectroscopy (FTIR) was used to study each group of samples and the corresponding raw materials. For preparation, KBr particles were predried, ground homogeneously, and mixed with each sample powder, pressed into transparent sheets, and placed in a mold, which were scanned in a Nicolet 6700 FTIR spectrometer (Thermo Fisher Scientific).

**2.3.5. Scanning Electron Microscopy (SEM).** The sample powder was uniformly coated with gold, and subsequently, the sample was placed on an aluminum sample peg with a carbon tape. The gold-plated samples were examined with a JSM-7200F scanning electron microscope (SEM, JEOL Ltd.).

**2.3.6. Thermogravimetric Analyzer (TGA).** Samples were analyzed using a thermogravimetric analyzer (TGA Q5000 V3.17 Build 265). In this process,  $\text{N}_2$  is used as an equilibrium gas. The temperature during thermogravimetric examination is  $35\text{--}350^\circ\text{C}$ , and the heating rate is  $5^\circ\text{C}/\text{min}$ . The sample is placed in an alumina pan to be examined.

**2.3.7.  $\text{N}_2$  Adsorption.** Mesoporous adsorption experiments were performed on the powder samples separately to evaluate the differences in pore size distribution, surface area, and pore volume of the different samples.

**2.3.8. X-Ray Diffraction (XRD).** The powder samples were studied by XRD analysis using a Siemens D5000 diffractometer to investigate the compositional similarities and differences.

### 3. Results and Discussion

The solutions obtained from the dissolution experiments were passed through a  $0.22\ \mu\text{m}$  filter membrane and diluted at the same multiples to obtain test samples. The absorbance was measured with a pc UV-Vis spectrophotometer UV-2401, and the dissolution curves were plotted as shown in Figure 1. For the physical mixture, the solubility of GF in water was low, and after the spray drying treatment, the solubility and dissolution rate of both groups of powders increased. Comparing sample A and sample B, we found that the solubility of GF was significantly higher in sample B, but the dissolution rate was smaller than that of sample A and it took more time to reach dissolution equilibrium. This may be due to the greater proportion of GF dissolved in acetone at the same solid-to-liquid ratio and the fact that more of the GF crystal structure was disrupted during the spray drying process, resulting in a large amount of amorphous solid GF, leading to a significant increase in its solubility. Similarly, in this process, due to the lower solubility of lactose in acetone, more lactose crystals precipitate prior to the high-temperature drying process and the proportion of amorphous lactose is reduced, making the whole system more difficult to break down and dissolve. Various facts show that the amorphous form of GF after dissolution in organic solvents and after the spray-drying process increases the solubility of GF in water considerably.

We measured the IR spectra of raw materials, physical mixtures, and spray-dried samples, as shown in Figure 2. The absorption peaks of the raw material lactose and GF at all wavelengths were present in the physical mixture. For the spray-dried sample, most of its sharp absorption peaks disappeared and merged into flat, blunt absorption peaks, with reduced density and strength of hydrogen bonds and reduced crystallinity, indicating the appearance of amorphous products, whether ethanol or acetone was used as the solvent. Sample B has a smoother peak in the GF characteristic peak region than sample A, indicating the generation of more amorphous GF.

We performed thermal analysis for each raw material and spray-dried samples. By analyzing the DSC curves of the samples (Figure 3), the heat absorption peaks of crystalline water and lactose crystals of lactose appeared at  $148^\circ\text{C}$  and  $209^\circ\text{C}$ , respectively, while the heat absorption peak of GF appeared at  $220^\circ\text{C}$ . In the physical mixture, the position and peak shape of the heat absorption peak of lactose remained basically unchanged. The heat absorption peak of melting GF crystals moved to the low-temperature region to  $215^\circ\text{C}$ , which may be when the less content reduced its melting heat absorption time, resulting in narrowing of the peak width and shift of the peak top position to the low-temperature region. For sample B, the residual acetone boiling point is lower than that of ethanol, which shifts the peak position to the low-temperature region relative to sample A. The heat

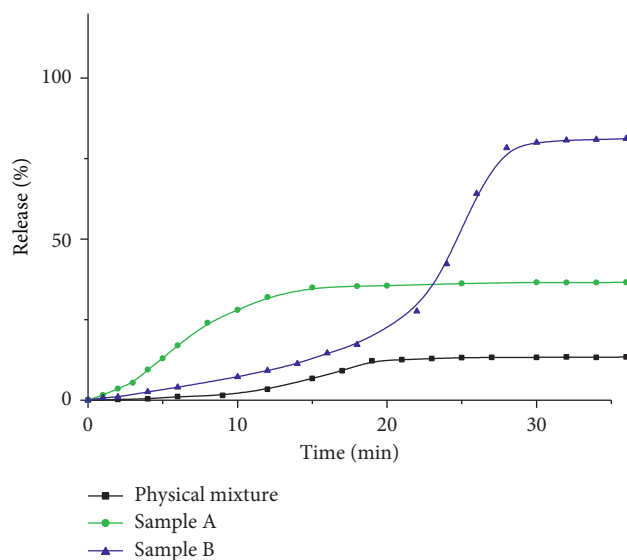


FIGURE 1: Release spectra of GF tablets in the two samples and physical mixture.

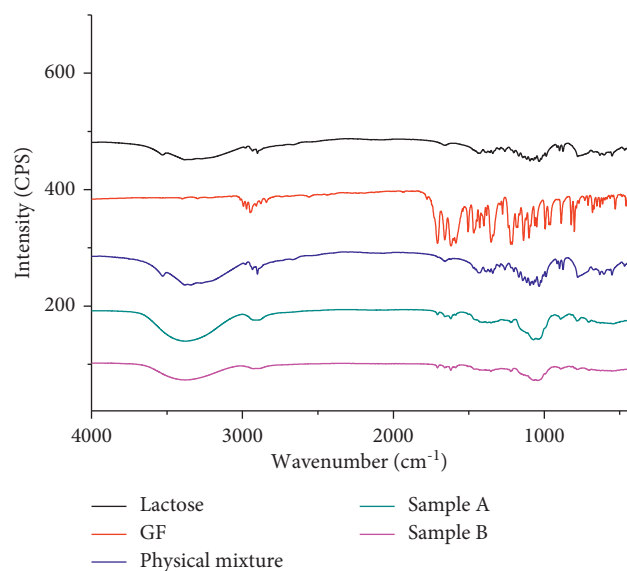


FIGURE 2: FTIR spectra of the raw materials, physical mixture, and samples.

absorption peak similar to that of lactose crystalline water at  $130\text{--}140^\circ\text{C}$  is larger and higher than that of sample B in the TGA curve (Figure 4), and both samples showed the same weight loss trend. However, the derivative weight loss curves suggest that sample B may have a more complex crystalline/noncrystalline structure.

According to the XRD curves (Figure 5), the  $\alpha$ -lactose peaks in both samples were  $12.5^\circ$ ,  $19.1^\circ$ ,  $19.6^\circ$ , and  $19.9^\circ$  at  $2\theta$ , respectively, and the peaks of  $\beta$ -lactose at  $2\theta = 10.5^\circ$  were absent in both samples, suggesting that both ethanol and acetone can inhibit the variable-spin behavior of lactose to some extent [19, 20]. In the interval  $5\text{--}45^\circ$ , the peak positions of the two samples were basically the same, but the lactose peak of sample B was significantly sharper and steeper than

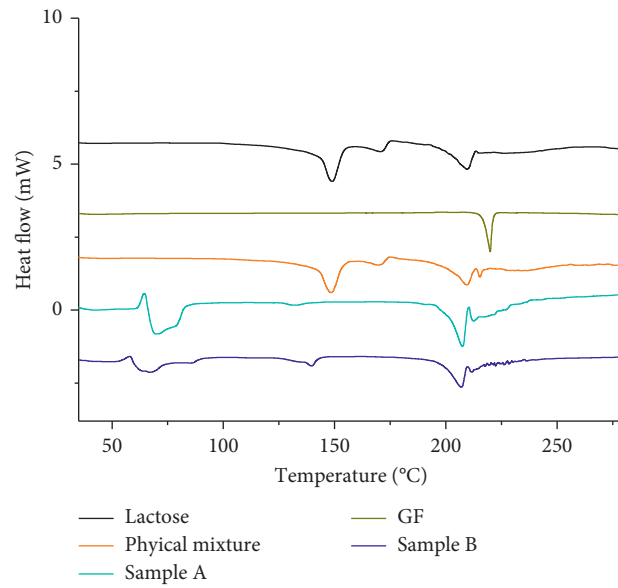


FIGURE 3: DSC curves of the raw materials, physical mixture, and samples.

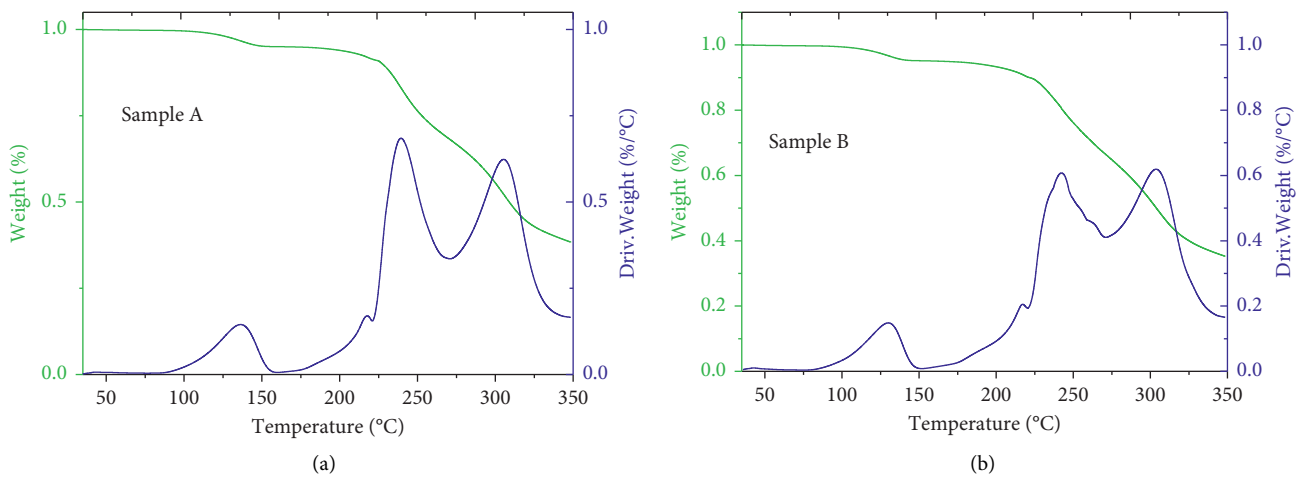


FIGURE 4: The TGA curves of the two spray-dried samples.

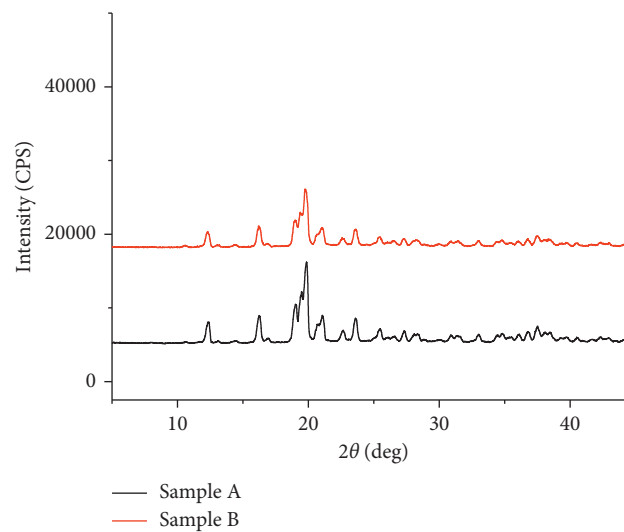


FIGURE 5: XRD curves of the two spray-dried powders.

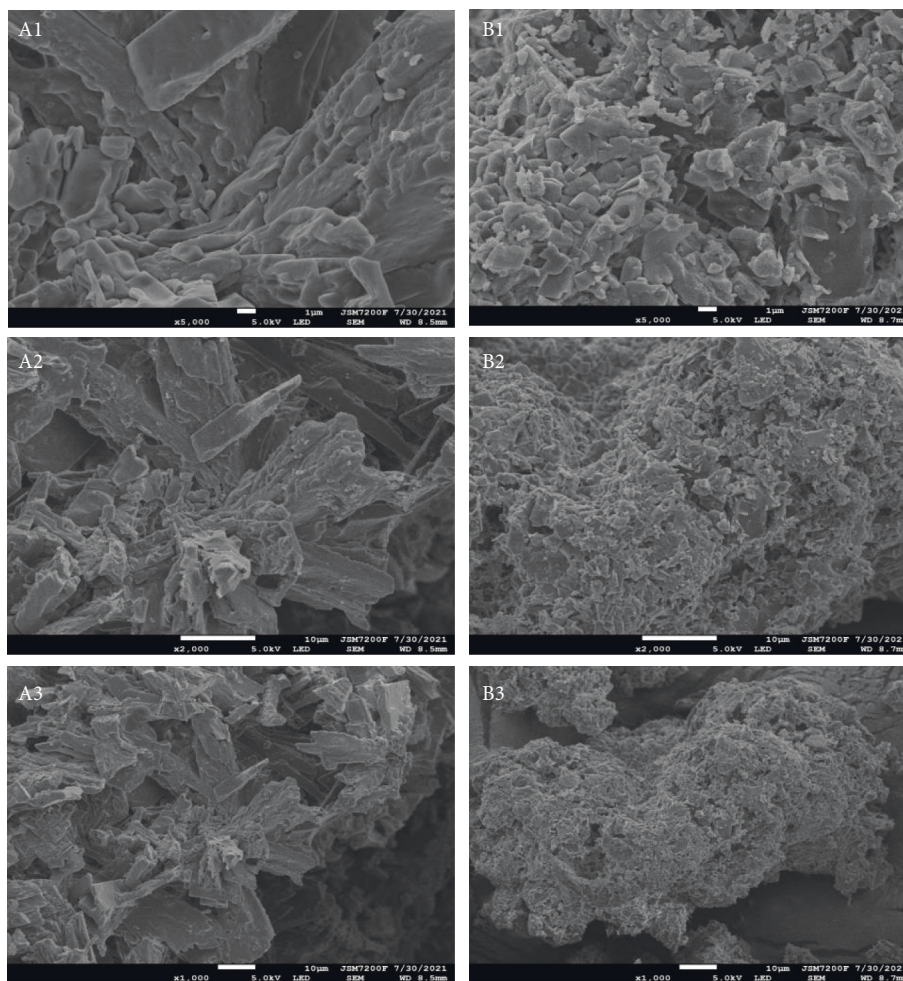


FIGURE 6: SEM images of the two spray-dried powders in 5000x, 2000, and 1000, respectively (A1–3 for sample A; B1–3 for sample B).

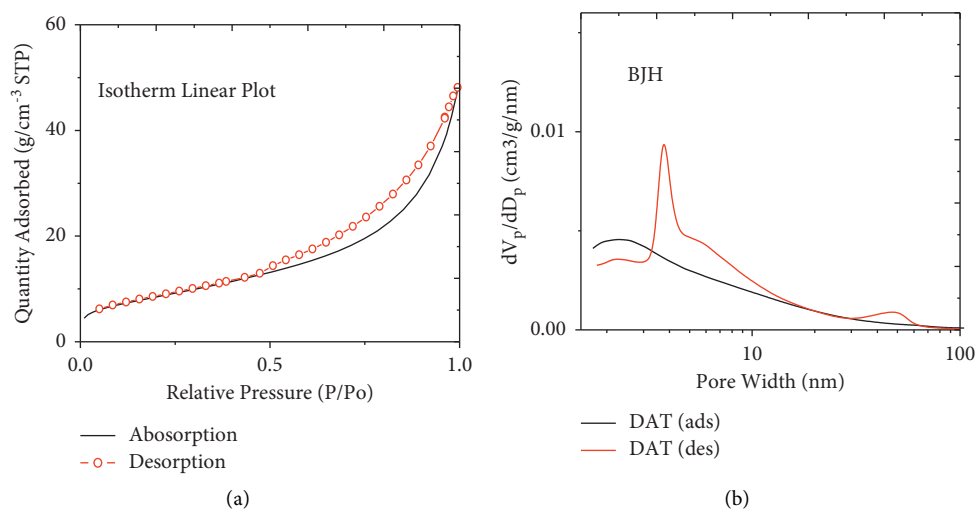


FIGURE 7: The nitrogen adsorption curve. Isotherm linear plot (a) and BJH adsorption  $dV/d\log(w)$  pore volume (b) of sample B.

that of sample A, suggesting the production of more amorphous lactose, which was consistent with the dissolution curves. This can also be observed in the SEM image (Figure 6).

Sample A and sample B exhibit completely different states in the field of view of SEM (Figure 6). Sample A is a lamellar structured aggregate with a smooth surface; sample B exhibits porous aggregates of various fine crystal particles.

The two fields of view indicate different crystalline/non-crystalline states, suggesting that most of the lactose in sample A may be present in an amorphous form. For sample B in the porous state, we performed a nitrogen adsorption experiment to calculate and evaluate its pore structure (Figure 7). Its BET adsorption and desorption curves visually represent its porous nature. The average pore size was calculated by analysis to be about 8.7 nm, cumulative volume of pores between 1.7000 nm and 300.0000 nm width: 0.073814 cm<sup>3</sup>/g, and its large pore volume may provide its better compressibility.

## 4. Conclusions

The solubilisation of insoluble drugs GF is a simple and practical study. In this experiment, we spray-dried GF with ethanol and acetone as dispersion media, respectively, and solubilisation was achieved with both solvents, with a 5–10-fold increase in the solubility of GF after the experimental manipulation. Moreover, the solubilisation efficiency of GF was higher with acetone than with ethanol. Interestingly, the different solvents also had different effects on the properties of the spray-dried excipient lactose. This may provide ideas for programmed manipulation of the solubilisation of insoluble drugs and modulation of their solubilisation behaviour.

## Data Availability

The data used to support the findings of this study are included within the article.

## Conflicts of Interest

The authors declare no conflicts of interest.

## Acknowledgments

The work was supported by Liuzhou Worker's Hospital (The Fourth-Affiliated Hospital of Guangxi Medical University). The authors performed the spray drying and instrumental analysis in Hunan Yaxiang Pharma Co. Pty. The authors thank Bo Wang from Hunan Yaxiang Pharma Co. Pty. for his assistance in spray drying and instrumental analysis. For enquiry of production and analysis, contact Hunan Yaxiang Pharma Co. Pty. via 252856756@qq.com.

## References

- [1] A. B. Petersen, M. H. Rønneest, T. O. Larsen, and M. H. Clausen, "The chemistry of griseofulvin," *Chemical Reviews*, vol. 114, no. 24, pp. 12088–12107, 2014.
- [2] L. De Carli and L. Larizza, "Griseofulvin," *Mutation Research: Reviews in Genetic Toxicology*, vol. 195, no. 2, pp. 91–126, 1988.
- [3] V. Kartsev, A. Geronikaki, A. Petrou et al., "Griseofulvin derivatives: synthesis, molecular docking and biological evaluation," *Current Topics in Medicinal Chemistry*, vol. 19, no. 13, pp. 1145–1161, 2019.
- [4] A. Geronikaki, V. Kartsev, A. Petrou et al., "Antibacterial activity of griseofulvin analogues as an example of drug repurposing," *International Journal of Antimicrobial Agents*, vol. 55, no. 3, Article ID 105884, 2020.
- [5] N. D. Paguigan, M. H. Al-Huniti, H. A. Raja et al., "Chemoselective fluorination and chemoinformatic analysis of griseofulvin: natural vs fluorinated fungal metabolites," *Bioorganic & Medicinal Chemistry*, vol. 25, no. 20, pp. 5238–5246, 2017.
- [6] T. Oda, "Effects of 2'-demethoxy-2'-propoxygriseofulvin on microtubule distribution in Chinese hamster V79 cells," *Journal of Antibiotics*, vol. 59, no. 2, pp. 114–116, 2006.
- [7] A. B. Petersen, G. Konotop, N. H. M. Hanafiah et al., "Strategies for improving the solubility and metabolic stability of griseofulvin analogues," *European Journal of Medicinal Chemistry*, vol. 116, pp. 210–215, 2016.
- [8] M. Thakkar, M. S. Islam, A. Railkar, and S. Mitra, "Antisolvent precipitative immobilization of micro and nanostructured griseofulvin on laboratory cultured diatom frustules for enhanced aqueous dissolution," *Colloids and Surfaces B: Biointerfaces*, vol. 196, Article ID 111308, 2020.
- [9] S. Baghel, H. Cathcart, and N. J. O'Reilly, "Polymeric amorphous solid dispersions: a review of amorphization, crystallization, stabilization, solid-state characterization, and aqueous solubilization of biopharmaceutical classification system class II drugs," *Journal of Pharmaceutical Sciences*, vol. 105, no. 9, pp. 2527–2544, 2016.
- [10] H. Al-Obaidi, R. M. Kowalczyk, R. Kalgudi, and M. G. Zariwala, "Griseofulvin solvate solid dispersions with synergistic effect against fungal biofilms," *Colloids and Surfaces B: Biointerfaces*, vol. 184, Article ID 110540, 2019.
- [11] E. Reverchon, G. D. Porta, A. Spada, and A. Antonacci, "Griseofulvin micronization and dissolution rate improvement by supercritical assisted atomization," *Journal of Pharmacy and Pharmacology*, vol. 56, no. 11, pp. 1379–1387, 2010.
- [12] P. S. Jadon, V. Gajbhiye, R. S. Jadon, K. R. Gajbhiye, and N. Ganesh, "Enhanced oral bioavailability of griseofulvin via niosomes," *AAPS PharmSciTech*, vol. 10, no. 4, pp. 1186–1192, 2009.
- [13] A. I. Arida, M. M. Al-Tabakha, and H. A. J. Hamoury, "Improving the high variable bioavailability of griseofulvin by SEDDS," *Chemical and Pharmaceutical Bulletin*, vol. 55, no. 12, pp. 1713–1719, 2007.
- [14] K. Zheng, Z. Lin, M. Capece, K. Kunnath, L. Chen, and R. N. Davé, "Effect of particle size and polymer loading on dissolution behavior of amorphous griseofulvin powder," *Journal of Pharmaceutical Sciences*, vol. 108, no. 1, pp. 234–242, 2019.
- [15] A. Bhandari, F. Bari, and H. Al-Obaidi, "Evaluation of the impact of surfactants on miscibility of griseofulvin in spray dried amorphous solid dispersions," *Journal of Drug Delivery Science and Technology*, vol. 64, Article ID 102606, 2021.
- [16] S. Zhao, Y. Ma, J. Gong, B. Hou, and W. Tang, "Solid-liquid phase equilibrium and thermodynamic analysis of griseofulvin in twelve mono-solvents," *Journal of Molecular Liquids*, vol. 296, Article ID 111861, 2019.
- [17] X. Zhao, A. Farajtabar, G. Han, and H. Zhao, "Griseofulvin dissolved in binary aqueous co-solvent mixtures of N, N-dimethylformamide, methanol, ethanol, acetonitrile and N-methylpyrrolidone: solubility determination and thermodynamic studies," *The Journal of Chemical Thermodynamics*, vol. 151, Article ID 106250, 2020.
- [18] B. Wang, F. Liu, J. Xiang et al., "A critical review of spray-dried amorphous pharmaceuticals: synthesis, analysis and application," *International Journal of Pharmaceutics*, vol. 594, Article ID 120165, 2021.



- [19] S. Tan, T. Jiang, A. Ebrahimi, and T. Langrish, "Effect of spray-drying temperature on the formation of flower-like lactose for griseofulvin loading," *European Journal of Pharmaceutical Sciences*, vol. 111, pp. 534–539, 2018.
- [20] B. Wang, H. Li, J. Xiang, J. Zheng, and J. Wang, "Fabrication of agglomerated lactose using fluidized bed for good compressibility," *Journal of Nanomaterials*, vol. 2021, Article ID 9918847, 6 pages, 2021.

## Research Article

# Efficacy, Influencing Factors, and Safety of Alteplase Intravenous Thrombolysis in Patients with Acute Ischemic Stroke Combined with Atrial Fibrillation

Yongyin Zhang,<sup>1</sup> Haoye Cai,<sup>2</sup> Hao Shu,<sup>1</sup> Ruqian He,<sup>1</sup> Xuerong Huang <sup>1</sup>,  
and Xiaoyi Song <sup>3</sup>

<sup>1</sup>Department of Neurology, Ruian People's Hospital, Wenzhou 325200, Zhejiang, China

<sup>2</sup>Department of Rehabilitation Medicine, Ruian People's Hospital, Wenzhou 325200, Zhejiang, China

<sup>3</sup>Department of Pharmacy, Ruian People's Hospital, Wenzhou 325200, Zhejiang, China

Correspondence should be addressed to Xuerong Huang; [huangxuerong001@126.com](mailto:huangxuerong001@126.com) and Xiaoyi Song; [songxiaoyi2021@126.com](mailto:songxiaoyi2021@126.com)

Received 7 January 2022; Accepted 9 February 2022; Published 9 March 2022

Academic Editor: Weiguo Li

Copyright © 2022 Yongyin Zhang et al. This is an open access article distributed under the Creative Commons Attribution License, which permits unrestricted use, distribution, and reproduction in any medium, provided the original work is properly cited.

Ischemic stroke is the most common type of stroke. Intravenous thrombolytic therapy with alteplase is currently the most effective method to improve the prognosis of patients with acute cerebral infarction. The purpose of this study was to investigate the efficacy and safety of intravenous thrombolysis with alteplase in patients with acute ischemic stroke combined with atrial fibrillation and to analyze the related influencing factors. It turns out, alteplase intravenous thrombolysis is effective for patients with ICS combined with atrial fibrillation, and the incidence of sICH are lower than those without alteplase intravenous thrombolysis, but the efficacy is worse than that of patients without atrial fibrillation. At the same time, the baseline NHISS score and systolic pressure before the thrombolytic were independent risk factors affecting the efficacy of intravenous thrombolysis with alteplase in ICS patients with atrial fibrillation. This study has provided a scientific basis for making an active decision to perform ultraearly intravenous thrombolysis in our hospital to reduce the mortality and disability rate of stroke in the region.

## 1. Introduction

Acute ischemic stroke (CIS) is the infarction of brain tissue caused by the occlusion of a cerebral artery, accompanied by the damage of neurons, astrocytes, and oligodendrocytes, which has the characteristics of high morbidity, high mortality, and a high disability rate [1, 2]. Evidence-based medical evidence indicates that ultraearly intravenous thrombolysis is currently the most effective drug therapy for CIS. Intravenous recombinant tissue plasminogen activator (rt-PA) within 4.5 hours of onset has been the preferred recommendation in the 2013 American Stroke Association (ASA) guidelines for the diagnosis and treatment of acute ischemic stroke and in the 2014 guidelines for the diagnosis and treatment of acute ischemic stroke in China [3, 4].

Atrial fibrillation is a common arrhythmia and an independent risk factor for CIS. The occurrence of atrial fibrillation not only increases the severity of CIS but also increases the incidence of other complications and poor prognosis [5]. However, the efficacy and safety of intravenous thrombolysis for CIS patients with atrial fibrillation are controversial, as is whether atrial fibrillation affects the efficacy of intravenous thrombolysis for CIS patients [6]. This study analyzed the efficacy, influencing factors, and safety of intravenous thrombolysis with alteplase in patients with CIS complicated with atrial fibrillation, aiming to provide theoretical support for making a positive decision of ultraearly intravenous thrombolysis and reduce the mortality and disability rate of stroke in this region, which was reported as follows.

## 2. Information and Methods

**2.1. General Information.** A total of 355 CIS patients admitted to our hospital from January 2019 to July 2020 were selected as the research objects. There were 198 patients with atrial fibrillation and 157 patients without atrial fibrillation. According to whether to accept alteplase intravenous thrombolysis therapy, 198 patients with atrial fibrillation were divided into group A ( $n = 106$ ) and group B ( $n = 92$ ). And 157 patients without atrial fibrillation were divided into group C.

**2.2. Inclusion Criteria.** The inclusion criteria were as follows: all patients who were confirmed to have ICS by head CT and/or MRI [7]; patients with neurologic impairment symptoms caused by ischemic stroke; patients whose intracranial hemorrhage has been excluded by cerebral CT without imaging changes of early massive cerebral infarction [8]; patients aged  $> 18$  years; patients whose onset time reaches the admission time  $\leq 4.5$  h; and the patient or family members who have signed the informed consent form for intravenous thrombolysis. This study was approved by the ethics committee, and the informed consent form was signed by the patient or his/her family.

**2.3. Exclusion Criteria.** The exclusion criteria were as follows: patients with subarachnoid hemorrhage indicated by medical history and physical examination; Patients who have a history of head trauma, or cerebral infarction, or myocardial infarction within the last 3 months; patients with gastrointestinal or urinary bleeding within the last 3 weeks; patients who had major surgery within the last 2 weeks; patients with a history of artery puncture at the site of hemostasis that is not easy to compress within the past 1 week; patients with a previous history of cerebral hemorrhage; patients with active bleeding or trauma (e.g. fracture) detected by physical examination; patients who were on anticoagulants (INR  $> 1.7$  or PT  $> 15$  s) or who had been on low molecular weight heparin within 24 hours before stroke onset or who had been on thrombin inhibitors or factor Xa inhibitors within 48 hours before stroke onset; patients with platelet count  $< 100 \times 10^9/L$ ; patients with blood glucose  $< 2.8$  mmol/L or  $> 22.22$  mmol/L; CT scan results showed the presence of early large lesions, i.e., in patients with lesion size greater than 1/3 of the MCA distribution or ASPECTS score  $< 5$ ; and patients in pregnancy.

**2.4. Methodology.** The patient was given multifunctional monitoring and oxygen inhalation immediately after weighing. At the same time, bilateral vein channels were established and the vital signs of patients were monitored. The blood pressure of both upper limbs was measured first, and then the upper limb with the higher blood pressure was selected for blood pressure monitoring. All patients had their blood pressure controlled at or below 180/105 mmHg. Patients above this level were given intravenous urapidil to control their blood pressure. And the oxygen saturation

should be kept above 95%. Patients in groups A and C received intravenous thrombolysis with alteplase. The dosage was determined according to the standard of 0.9 mg/kg, and 10% of the total dose was initially measured. The intravenous injection was performed within 1 min, and the remaining dose was administered within 60 min. After 24 hours, the head CT scan was reexamined, and the patient was given routine treatment for ischemic stroke if there was no bleeding. Patients in group B were treated with routine treatment for ischemic stroke after admission.

Patients' clinical data were collected, including basic demographic information such as age, gender, and weight; previous medical history such as hypertension, diabetes, atrial fibrillation, stroke, acute myocardial infarction, heart failure, and smoking; concomitant medication before thrombolysis; emergency examination data such as systolic blood pressure, diastolic blood pressure, blood glucose value, platelet value, LDL value, INR value, NIHSS score, time from admission to intravenous thrombolysis (DNT), and time from onset to intravenous thrombolysis (ONT).

### 2.5. Clinical Efficacy Evaluation

**2.5.1. Short-Term Prognosis.** The NIHSS scores of all patients on day 1 and day 7 after treatment were counted. The neurological changes on days 1 and 7 were observed. Compared with the baseline NIHSS score, a NIHSS score reduction of  $\geq 4$  points or a NIHSS score of 0–1 is effective, a NIHSS score of  $\pm 3$  points showed no change, and a NIHSS score increase of  $\geq 4$  points, or the death turned for the worse [9].

**2.5.2. Long-Term Prognosis.** The modified Rankin scale (mRS) scores of all patients within 3 months after treatment were counted. Three months later, the score of mRS  $\leq 1$  was classified as a good prognostic outcome, while the score of mRS ranged from 2 to 6 was a poor prognostic outcome [10].

### 2.6. Safety Evaluation of Thrombolytic Therapy

- (1) Evaluation of intracranial hemorrhage transformation: hemorrhage transformation was evaluated 24 h after treatment and, according to the secondary analysis Asian acute stroke study (ECASS ii) criteria, it was divided into four types of hemorrhagic infarction-1 (HI-1), HI-2, cerebral parenchymal hemorrhage-1 (PH-1), and PH-2 [11]
- (2) The basis for judging symptomatic intracranial hemorrhage (sICH): cerebral parenchymal hematoma was determined by head CT/MRI examination 24 h after treatment, accompanied by a worsening of clinical symptoms (NIHSS score increase  $\geq 4$  points) [12]
- (3) The case fatality rate within 3 months was observed

**2.7. Statistical Methods.** SPSS26.0 statistical software was used for analysis. The measurement data were expressed as the mean  $\pm$  standard deviation, and independent sample *t*-test was conducted. The enumeration data were subjected to

$\chi^2$  test. The level of statistical significance was defined as a two-sided test. In univariate analysis, variables with  $P \leq 0.05$  were included in the multivariate logistic regression model, and the independent risk factors for poor prognosis were analyzed by multivariate logistic regression.

### 3. Results

*3.1. Comparison of Short-Term and Long-Term Prognosis among the Three Groups.* There were differences in the improvement rate and unchanged rate in the short-term prognosis among the three groups ( $P < 0.05$ ), but there was no difference in the deterioration rate among the three groups ( $P > 0.05$ ). There were differences in long-term prognosis among the three groups ( $P < 0.05$ ; Table 1).

*3.2. Comparison of Safety among the Three Groups.* The bleeding rate in groups A and C was higher than that in group B after thrombolysis for 24 h ( $P < 0.05$ ). The new hemorrhage within 7 days rate of groups A and B was higher than that of group C ( $P < 0.05$ ), but there was no significant difference between group A and group B ( $P > 0.05$ ). The incidence of sICH in groups A and C was lower than that in group B ( $P < 0.05$ ). The mortality of group C was lower than that of group B ( $P < 0.05$ ), but the mortality of group A was not statistically significant compared with that of group B ( $P > 0.05$  Table 2).

*3.3. Single Factor Analysis Affecting the Efficacy of Intravenous Thrombolysis with Alteplase in Patients with ICS Combined with Atrial Fibrillation.* Gender, cycle type, history of hypertension, diabetes, hyperlipidemia, medical history, history of stroke, DNT, ONT, LDL-C, HDL-C, homocysteine, diastolic blood pressure before thrombolysis, random blood glucose, glycosylated hemoglobin, white blood cell count, platelet, neutrophil count, PT, APTT, INR, fibrinogen, and combined drug use before thrombolytic therapy had no correlation with intravenous thrombolytic efficacy of alteplase in ICS patients with atrial fibrillation ( $P > 0.05$ ).

Age, weight, history of heart failure, baseline NHISS, systolic blood pressure before thrombolytic, hemoglobin, and red blood cells were single factors influencing the efficacy of intravenous thrombolysis with alteplase in ICS patients with atrial fibrillation ( $P < 0.05$ ; Table 3).

*3.4. Variable Assignment.* Clinical efficacy (long-term prognosis) was taken as a dependent variable, and the factors with significant differences in Table 3 were taken as independent variables to be included in the logistic regression model. The assignments of the dependent variable and independent variable are shown in Table 4.

*3.5. Analysis of Multiple Factors Affecting the Efficacy of Intravenous Thrombolysis with Alteplase in Patients with ICS Combined with Atrial Fibrillation.* Baseline NHISS score and systolic pressure before thrombolytic were independent risk factors affecting the efficacy of intravenous thrombolysis

with alteplase in ICS patients with atrial fibrillation ( $P < 0.05$ ; Table 5).

### 4. Discussion

Previous studies have shown that ICS occurring in the presence of atrial fibrillation leads to a higher rate of dysfunction and mortality than in patients without atrial fibrillation. ICS is a dynamic process, and restoring blood supply to the ischemic penumbra is the primary objective in the treatment of ICS. However, despite the efficacy of conventional antiplatelet or anticoagulant therapy in ICS, evidence-based medicine indicates that intravenous thrombolytic therapy with retissue-type plasminogen activator remains the dominant approach for ultraearly treatment of ICS [13].

Alteplase can effectively reverse the pathological process of ischemic penumbra after thrombolysis and has become the most widely used intravenous thrombolytic drug in clinical practice [14]. Alteplase has the effect of promoting the activity of the fibrinolytic system in vivo. However, unlike streptokinase and urokinase, since the two cyclic structures have strong affinity for fibrin, they can specifically convert plasminogen in thrombus into plasmin to exert the effect of dissolving thrombus. At present, there are still differences in intravenous thrombolytic therapy of alteplase for patients with acute ischemic stroke complicated with atrial fibrillation at home and abroad, but most studies tend to benefit from thrombolytic therapy [15]. Our study showed that the long-term good prognosis rate of groups A and C was higher than that of group B ( $P < 0.05$ ), confirming the effectiveness of intravenous thrombolysis with alteplase in ICS. The long-term good prognosis rate of group C was higher than that of group A ( $P < 0.05$ ), indicating that the efficacy of alteplase intravenous thrombolysis for patients with ICS combined with atrial fibrillation was worse than that for patients without combined atrial fibrillation [16]. The possible reasons were as follows: The collateral circulation established by the body before thrombolysis is beneficial to reduce the infarct area after thrombolysis, and protecting the brain tissue by reducing the flow and intensity of hypoperfusion [17]. ICS patients with atrial fibrillation or arterial embolism have a worse ability to establish collateral circulation at the obstruction site than those with large artery thrombosis. Patients with ICS with atrial fibrillation are more likely to develop large and old thrombi, and the reaction of large and old thrombi to thrombolytic therapy is lower [18]. Early recanalization after thrombolysis is considered to be a good prognostic indicator for patients with stroke, while atrial fibrillation is associated with lower early recanalization after thrombolysis, which may result in poorer efficacy [19]. Meanwhile, the new hemorrhage within 7 days in group A and group B was not statistically different ( $P > 0.05$ ), and the sICH in group A and group C was significantly smaller than that in group B ( $P < 0.05$ ). Studies have shown that the pharmacological effect of alteplase on plasma free plasmin is not very strong and systemic fibrinolysis will not occur, thus effectively controlling the occurrence of bleeding and intracranial hemorrhage [20].

Further factors influencing the efficacy of intravenous thrombolytic therapy in patients with ICS with atrial

TABLE 1: Comparison of short-term and long-term prognosis among the three groups.

Groups	Short-term prognosis			Long-term prognosis	
	Effective	No change	Worse	Good	Poor
Group A ( <i>n</i> = 106)	55 (51.89)	39 (36.79)	12 (11.32)	50 (47.17)	56 (52.83)
Group B ( <i>n</i> = 92)	15 (16.30)	59 (64.13)	18 (19.56)	27 (29.35)	65 (70.65)
Group C ( <i>n</i> = 157)	91 (57.96)	51 (32.48)	15 (9.55)	95 (60.51)	62 (39.49)
$\chi^2$	43.220	25.517	5.503		22.652
<i>P</i>	<0.001	<0.001	0.064		<0.001

TABLE 2: Comparison of complications and deaths among the three groups.

Groups	Hemorrhage occurred within 24 hours	New hemorrhage within 7 days	sICH	Death
Group A ( <i>n</i> = 106)	21 (19.81)	24 (22.64)	3 (2.83)	18 (16.98)
Group B ( <i>n</i> = 92)	4 (4.35)	20 (21.74)	8 (8.70)	20 (21.74)
Group C ( <i>n</i> = 157)	13 (8.28)	14 (8.92)	2 (1.27)	14 (8.92)
$\chi^2$	14.052	11.370	9.353	8.286
<i>P</i>	0.001	0.003	0.009	0.016

TABLE 3: Single factor analysis of intravenous thrombolysis of alteplase in ICS patients with atrial fibrillation.

Factor	Good group ( <i>n</i> = 50)	Poor group ( <i>n</i> = 56)	$\chi^2/t$	<i>P</i>
Gender				
Male	40 (80.00)	37 (66.07)		
Female	10 (20.00)	19 (33.93)	2.579	0.108
Age (years)	72.50 ± 10.55	77.91 ± 8.49	2.922	0.004
Weight (kg)	63.20 ± 11.62	58.48 ± 11.92	2.057	0.042
Circulation type				
Anterior	39 (78.00)	46 (82.14)		
Posterior	9 (18.00)	7 (12.50)	0.689	0.709
Anterior + posterior	2 (4.00)	3 (5.36)		
History of hypertension				
No	16 (32.00)	14 (25.00)		
Yes	34 (68.00)	42 (75.00)	0.638	0.424
History of diabetes				
No	36 (72.00)	43 (76.79)		
Yes	14 (28.00)	13 (23.21)	0.319	0.572
History of hyperlipidemia				
No	33 (66.00)	38 (67.86)		
Yes	17 (34.00)	18 (32.14)	0.041	0.839
History of stroke				
No	48 (96.00)	53 (94.64)		
Yes	2 (4.00)	3 (5.36)	0.108	0.742
History of heart failure				
No	34 (68.00)	24 (42.86)		
Yes	16 (32.00)	32 (57.14)	6.739	0.009
DNT (min)	56.44 ± 26.49	57.64 ± 23.58	0.247	0.805
ONT (min)	154.62 ± 57.46	156.43 ± 48.49	0.176	0.861
Baseline NHISS (points)	9.32 ± 6.10	15.48 ± 7.96	4.433	<0.001
LDL (mmol/L)	2.58 ± 0.95	2.64 ± 0.95	0.312	0.756
HDL (mmol/L)	1.07 ± 0.27	1.07 ± 0.27	0.023	0.982
Homocysteine (μmol/L)	15.50 ± 13.39	15.77 ± 13.60	0.099	0.921
Systolic pressure before thrombolytic (mmHg)	149.78 ± 28.39	163.29 ± 26.94	2.512	0.014
Diastolic pressure before thrombolytic (mmHg)	83.80 ± 16.06	88.70 ± 18.64	1.440	0.153
Random blood glucose (mmol/L)	7.69 ± 2.94	7.98 ± 3.13	0.490	0.625
Hemoglobin (%)	6.22 ± 1.09	6.18 ± 0.89	0.180	0.858
White blood cell count (×10 <sup>9</sup> /L)	7.43 ± 2.08	7.55 ± 2.23	0.304	0.762
Red blood cell count (×10 <sup>9</sup> /L)	4.55 ± 0.58	4.26 ± 0.63	2.501	0.014
Neutrophil count (×10 <sup>9</sup> /L)	4.80 ± 1.74	4.65 ± 1.98	0.402	0.689
Hemoglobin (g/L)	141.78 ± 18.04	131.68 ± 19.64	2.747	0.007
Platelet count (×10 <sup>9</sup> /L)	167.72 ± 46.43	187.30 ± 56.35	1.939	0.055
PT (s)	11.44 ± 0.92	11.37 ± 1.34	0.345	0.731

TABLE 3: Continued.

Factor	Good group ( <i>n</i> = 50)	Poor group ( <i>n</i> = 56)	$\chi^2/t$	<i>P</i>
APTT (s)	25.80 ± 2.56	25.95 ± 3.12	0.268	0.789
INR	0.98 ± 0.08	0.98 ± 0.11	0.197	0.844
Fibrinogen (g/L)	3.38 ± 2.24	3.28 ± 0.93	0.322	0.748
Na+ (mmol/L)	139.71 ± 2.27	139.40 ± 2.08	0.732	0.466
K+ (mmol/L)	3.68 ± 0.37	3.63 ± 0.49	0.584	0.560
Urea nitrogen (mmol/L)	6.77 ± 1.70	7.36 ± 3.43	1.097	0.245
Aspirin was taken before onset				
No	47 (94.00)	54 (96.43)	0.347	0.556
Yes	3 (6.00)	2 (3.57)		
Clopidogrel was taken before onset				
No	48 (96.00)	54 (96.43)	0.013	0.908
Yes	2 (4.00)	2 (3.57)		
Atorvastatin was taken before onset				
No	47 (94.00)	55 (98.21)	1.292	0.256
Yes	3 (6.00)	1 (1.79)		
Rosuvastatin was taken before onset				
No	49 (98.00)	56 (100.00)	1.131	0.288
Yes	1 (2.00)	0 (0.00)		

TABLE 4: Variable assignment of risk factors affecting the efficacy of intravenous thrombolysis with alteplase in ICS combined with atrial fibrillation.

Variable	The assignment
The dependent variable	
Clinical curative effect	effective = 0, ineffective = 1
The independent variables	
Age	Enter the actual value
Weight	Enter the actual value
History of heart failure	No = 0, Yes = 1
Baseline NHISS	Enter the actual value
Systolic pressure before thrombolytic	Enter the actual value
Hemoglobin	Enter the actual value
Red blood cell	Enter the actual value

TABLE 5: Binary logistic regression analysis of the influence on intravenous thrombolysis of alteplase in ICS patients with atrial fibrillation.

Variable	$\beta$	SE	Wald $\chi^2$	<i>P</i>	OR	95% CI of OR
Age	0.019	0.026	0.510	0.475	1.019	0.968~1.072
Weight	-0.029	0.020	2.091	0.148	0.971	0.934~1.010
History of heart failure	-0.443	0.488	0.823	0.364	0.642	0.246~1.672
Baseline NHISS	0.146	0.040	12.960	0.000	1.157	1.069~1.252
Systolic pressure before thrombolytic	0.019	0.009	4.619	0.032	1.019	1.002~1.037
Hemoglobin	-0.018	0.028	0.409	0.552	0.982	0.929~1.038
Red blood cell	-0.497	0.855	0.338	0.561	0.608	0.114~3.253
Constant	0.656	3.269	0.040	0.841	1.928	-

fibrillation were investigated [21]. In this study, independent risk factors for the efficacy of intravenous thrombolysis with alteplase included baseline NHISS score and systolic pressure before thrombolytic. The NHISS score is a scale for evaluating the neurological functional recovery status of patients with stroke. A high NHISS score indicates how serious the nerve damage is, indicating that the recanalization rate after thrombolysis is low for patients [22]. Therefore, close observation of NHISS score changes in ICS patients with atrial fibrillation and early intervention in patients with high risk factors can help doctors effectively

judge the severity of patients' disease and the outcome of curative effects and improve the effectiveness of clinical treatment. Increased blood pressure plays an important role in the prognosis and mortality of patients with ICS. Hypertension can lead to arteriosclerosis and increased fragility of the vascular wall, and increased irritability of blood pressure after cerebral ischemia. In addition, the increased systolic blood pressure will also increase the permeability of the blood-cerebrospinal fluid barrier and extracellular matrix, causing abnormal situations such as plasma extravasation and edema, and further inducing cerebral

hemorrhage. Therefore, we should strengthen the control of patients' blood pressure before thrombolytic therapy to maintain its relatively stable and normal level.

In summary, alteplase intravenous thrombolysis is effective for patients with ICS combined with atrial fibrillation, and the incidence of sICH are lower than those without alteplase intravenous thrombolysis, but the efficacy is worse than that of patients without atrial fibrillation. At the same time, the baseline NHISS score and systolic pressure before the thrombolytic were independent risk factors affecting the efficacy of intravenous thrombolysis with alteplase in ICS patients with atrial fibrillation. In order to improve the clinical application value of alteplase intravenous thrombolysis, targeted intervention for those combined with high-risk factors should be strengthened in clinics.

### Data Availability

The datasets generated for this study are available from the corresponding author on reasonable request.

### Ethical Approval

This study was approved by the Medical Ethics Committee of Ruian People's Hospital (LZM2018002).

### Conflicts of Interest

The authors declare that there are no conflicts of interest.

### Acknowledgments

This study was supported by the Basic Scientific Research Project of Wenzhou Science and Technology Bureau (Y20180631) and Wenzhou Medical and Health Science Research Project (2018B13).

### References

- [1] J. Beharry, M. J. Waters, R. Drew et al., "Dabigatran reversal before intravenous tenecteplase in acute ischemic stroke," *Stroke*, vol. 51, no. 5, pp. 1616–1619, 2020.
- [2] X. Wang, K.-J. Lee, T. J. Moullaali et al., "Who will benefit more from low-dose alteplase in acute ischemic stroke?" *International Journal of Stroke*, vol. 15, no. 1, pp. 39–45, 2020.
- [3] C.-W. Fang, Y.-T. Tsai, P.-C. Chou et al., "Intravenous thrombolysis in acute ischemic stroke after idarucizumab reversal of dabigatran effect: analysis of the cases from Taiwan," *Journal of Stroke and Cerebrovascular Diseases*, vol. 28, no. 3, pp. 815–820, 2019.
- [4] J.-Q. An, Y.-W. Cheng, Y.-C. Guo et al., "Safety and efficacy of remote ischemic postconditioning after thrombolysis in patients with stroke," *Neurology*, vol. 95, no. 24, pp. e3355–e3363, 2020.
- [5] J. Pretnar Oblak, M. Sabovic, and S. Frol, "Intravenous thrombolysis after idarucizumab application in acute stroke patients—a potentially increased sensitivity of thrombi to lysis?" *Journal of Stroke and Cerebrovascular Diseases*, vol. 28, no. 3, pp. 768–773, 2019.
- [6] H.-M. Wu, C.-P. Chung, and Y.-Y. Lin, "Similar thrombolysis outcomes in acute stroke patients with and without atrial fibrillation if pre-stroke CHA<sub>2</sub>DS<sub>2</sub>-VASc score is low," *Medicine*, vol. 99, no. 2, Article ID e18680, 2020.
- [7] J. Derbisz, K. Nowak, M. Wnuk et al., "Prognostic significance of stroke-associated infection and other readily available parameters in acute ischemic stroke treated by intravenous thrombolysis," *Journal of Stroke and Cerebrovascular Diseases*, vol. 30, no. 2, Article ID 105525, 2021.
- [8] J. Liu, J. Huang, H. Xu, and H. Dai, "Nonatrial fibrillation was associated with early neurological improvement after intravenous thrombolysis with rt-PA in patients with acute ischemic stroke," *The Neurologist*, vol. 25, no. 2, pp. 28–32, 2020.
- [9] D. J. McCarthy, D. A. Tonetti, J. Stone et al., "More expansive horizons: a review of endovascular therapy for patients with low NIHSS scores," *Journal of Neurointerventional Surgery*, vol. 13, no. 2, pp. 146–151, 2021.
- [10] V. Chalos, N. E. LeCouffe, M. Uyttenboogaart et al., "Endovascular treatment with or without prior intravenous alteplase for acute ischemic stroke," *Journal of American Heart Association*, vol. 8, no. 11, Article ID e011592, 2019.
- [11] F. Sun, H. Liu, H.-X. Fu et al., "Predictive factors of hemorrhage after thrombolysis in patients with acute ischemic stroke," *Frontiers in Neurology*, vol. 11, no. 46, Article ID 551157, 2020.
- [12] Y. Fan, X. Liao, Y. Pan, K. Dong, Y. Wang, and Y. Wang, "Intravenous thrombolysis is safe and effective for the cryptogenic stroke in China: data from the thrombolysis implementation and monitor of acute ischemic stroke in China (TIMS-China)," *Journal of Stroke and Cerebrovascular Diseases*, vol. 28, no. 1, pp. 220–226, 2019.
- [13] L. Schlemm, A. Kufner, F. Boutitie et al., "Current smoking does not modify the treatment effect of intravenous thrombolysis in acute ischemic stroke patients—a post-hoc analysis of the WAKE-UP trial," *Frontiers in Neurology*, vol. 10, no. 35, p. 1239, 2019.
- [14] M. Héja, I. Fekete, L. Horváth, S. Márton, and K. E. Fekete, "Experiences with intravenous thrombolysis in acute ischemic stroke by elderly patients—a 'real world scenario'," *Frontiers in Neurology*, vol. 12, no. 5, Article ID 721337, 2021.
- [15] Y. T. Chao, C. J. Hu, and L. Chan, "Thrombolysis in an acute ischemic stroke patient with rivaroxaban anticoagulation: a case report," *Medicine*, vol. 98, no. 8, Article ID e14560, 2019.
- [16] D. Xie, X. Wang, Y. Li et al., "Intravenous thrombolysis after reversal of dabigatran with idarucizumab in acute ischemic stroke: a case report," *Frontiers in Aging Neuroscience*, vol. 13, no. 9, Article ID 765037, 2021.
- [17] T. G. Robinson, B. D. Bray, L. Paley et al., "Applicability of enchanted trial results to current acute ischemic stroke patients eligible for intravenous thrombolysis in England and Wales: comparison with the sentinel stroke national audit programme registry," *International Journal of Stroke*, vol. 14, no. 7, pp. 678–685, 2019.
- [18] A. Mowla, M. Sharifian-Dorche, S. Mehla et al., "Safety and efficacy of antiplatelet use before intravenous thrombolysis for acute ischemic stroke," *Journal of the Neurological Sciences*, vol. 425, no. 1, Article ID 117451, 2021.
- [19] E. Nomura, M. Takemaru, T. Himeno, R. Kono, T. Fukushima, and S. Ota, "Clinical features and efficacy of reperfusion therapy in minor ischemic stroke patients with atrial fibrillation," *Journal of Thrombosis and Thrombolysis*, vol. 50, no. 3, pp. 608–613, 2020.
- [20] C. T. Hong, W. T. Chiu, N. F. Chi et al., "Low-density lipoprotein level on admission is not associated with post-intravenous thrombolysis intracranial hemorrhage in patients with acute ischemic stroke," *Journal of Investigative Medicine*, vol. 67, no. 3, pp. 659–662, 2019.
- [21] Y. F. Tao, Z. B. Ju, C. H. Zhu, Z. P. Son, J. J. Chen, and Y. Ji, "Clinical observation of different reperfusion methods in patients with acute ischemic stroke with atrial fibrillation

within 4.5 hours from onset,” *Zhonghua Yixue Zazhi*, vol. 99, no. 44, pp. 3477–3480, 2019.

- [22] L. Li, X. Ma, L. Zeng et al., “Impact of homocysteine levels on clinical outcome in patients with acute ischemic stroke receiving intravenous thrombolysis therapy,” *Peer-Reviewed Journal*, vol. 8, no. 16, p. e9474, 2020.



## Research Article

# Changes of Cell Adhesion Molecules and T Cell Subset Populations in Acute Myeloid Leukemia Patients Undergoing Intravenous Administration of Cytarabine Supplemented with Idarubicin

Jinhua Piao,<sup>1</sup> Didi Wang,<sup>2</sup> Siying Pei ,<sup>2</sup> Tangdong Ge,<sup>2</sup> Jing Li,<sup>2</sup> and Pengxia Zhang <sup>1</sup>

<sup>1</sup>Key Laboratory of Microecology-Immune Regulatory Network and Related Diseases, School of Basic Medicine, Jiamusi University, Jiamusi, China

<sup>2</sup>Biochemistry Teaching and Research Office, School of Basic Medicine, Jiamusi University, Jiamusi, China

Correspondence should be addressed to Pengxia Zhang; pengxiaz@jmsu.edu.cn

Received 24 December 2021; Accepted 13 January 2022; Published 8 February 2022

Academic Editor: Weiguo Li

Copyright © 2022 Jinhua Piao et al. This is an open access article distributed under the Creative Commons Attribution License, which permits unrestricted use, distribution, and reproduction in any medium, provided the original work is properly cited.

**Objective.** The present study aimed at investigating the efficacy and safety of intravenous administration of cytarabine supplemented with idarubicin in treating acute myeloid leukemia (AML) patients undergoing first attack and its effects on serum levels of cell adhesion molecules, cytokines in response to inflammation, and T cell subset populations in acute myeloid leukemia (AML) patients undergoing first attack. **Methods.** A total of 88 AML patients eligible for inclusion and exclusion criteria participated in the study and were randomly assigned into the control group ( $n = 44$ ) in which the patients received intravenous administration of cytarabine and daunorubicin and the study group ( $n = 44$ ) in which the patients received intravenous administration of cytarabine and idarubicin. Clinical response, incidence of adverse reactions, and quality of life 3 months after therapy were evaluated. Soluble intercellular adhesion molecule-1 (sICAM-1), soluble vascular cell adhesion molecule-1 (sVCAM-1), IL-10, and IL-35 were measured by ELISA methods. Phenotypic characteristics of T cell subsets including CD4<sup>+</sup>, CD8<sup>+</sup>, CD4<sup>+</sup>IL-10 Tregs, and CD4<sup>+</sup>CD25<sup>+</sup>CD127<sup>-</sup>Foxp3<sup>+</sup> Tregs were analyzed by flow cytometry. **Results.** The clinical response rate of the study group was better than that of the control group (65.91% vs. 45.45%) ( $P < 0.05$ ). After treatment, the study group revealed significantly lower levels of sICAM-1, sVCAM-1, IL-10, and IL-35, a lower proportion of Tregs, a higher rate of CD4<sup>+</sup>/CD8<sup>+</sup> T cells, along with increased scores of the Karnofsky Performance Scale (KPS) compared with the control group ( $P < 0.05$ ). The incidence rate of adverse reactions in the study group was lower than that in the control group (34.09% vs. 61.36%) ( $P < 0.05$ ). **Conclusion.** These findings demonstrate that intravenous administration of cytarabine supplemented with idarubicin can improve the immune function and quality of life of AML patients, and this combination drug therapy is effective and safe for AML.

## 1. Introduction

Acute leukemia is classified into acute myeloid leukemia (AML) and acute lymphocytic leukemia according to the presence of different damaged cells [1]. AML is a malignant clonal disease characterized by changes in normal hematopoietic cells, leading to the proliferation of immature progenitor cells and inhibition of cell differentiation. Immature progenitor cells spread through blood to various parts of the body [2]. AML is commonly seen in adults,

especially for these diagnosed at a median age of 68 years, accounting for up to 80% of acute leukemia [3]. AML incidence is positively correlated with age. It was reported about 1.3 cases out of 100 thousand people had the disease and the age was below 65 years old, and 12.2 cases, who aged over 65 years, out of 100 thousand people were subject to the disease [4]. Although the progress of AML treatment is beneficial to significant improvement in the prognosis of young patients, AML is associated with variable prognosis and high mortality. The 5-year overall survival was 40–50%

in younger adults with new diagnosed AML [5]. The prognosis of the elderly, who account for the majority of new cases, is still very poor. 20% of elderly patients died of the disease after 2 years of diagnosis [6], and up to 70% of patients aged 65 or over cannot survive within 1 year after diagnosis [7].

The prognosis of AML is closely related to cytogenetic results and molecular abnormalities at the time of diagnosis. These two factors can predict the complete remission rate, disease-free survival, recurrence risk, and overall survival [8, 9]. Myeloperoxidase activity in fibroblasts found by immunophenotypic and cytochemical analyses or analysis of immunophenotypic surface molecules has been proved to be a specific diagnosis of AML [2]. AML is considered to be a malignant disease with immune dysfunction. The basic role of immune microenvironment in the prognosis of leukemia has been confirmed in many studies [10, 11]. T cells are derived from bone marrow pluripotent stem cells, and the key role of T cells has been recognized in antigen-specific recognition and elimination of malignant cells [12]. Activation of the immune response of cytotoxic T cells is very important for the treatment of viral diseases and tumors [13]. The presence of chronic infection, tumor, and cancer is associated with immune dysfunction.  $CD3^+$ ,  $CD4^+$ , and  $CD8^+$  T cells are involved in immune response and confirmed as effective biomarkers in viral infectious diseases and inflammatory disorders [14, 15]. Regulatory T cells, termed as Tregs, represent a subpopulation of  $CD4^+$  T cells and can inhibit the immune response, which have three classifications according to the cytokines they secrete, including naturally occurring  $CD4^+CD25^+Foxp3^+$  Tregs, interleukin 10 (IL-10)-producing Tregs, and transforming growth factor- $\beta$  (TGF- $\beta$ )-producing Tregs [16]. IL-35, a member of the IL-12 family, is secreted by Treg cells and contributes to the immunosuppressive activity of Tregs, rather than acting in an immunostimulatory or proinflammatory manner [17]. Vascular cell adhesion molecule-1 (VCAM-1) is also known as CD106, and intercellular adhesion molecule-1 (ICAM-1) is also known as CD54, are transmembrane glycoprotein. They are induced by a variety of cytokines, such as tumor necrosis factor  $\alpha$  (TNF- $\alpha$ ), IL-1, and interferon  $\gamma$ , and usually expressed in endothelial cells and immune cells [18]. At present, chemotherapy regimens of cytarabine with daunorubicin or idarubicin are the standard treatment for AML patients [19]. The purpose of this study is to investigate the changes in serum concentrations of soluble VCAM-1 (sVCAM-1), soluble ICAM-1 (sICAM-1), IL-10, and IL-35 along with T cell subsets including  $CD4^+$ ,  $CD8^+$ ,  $CD4^+IL-10$  Tregs, and  $CD4^+CD25^+CD127^+Foxp3^+$  Tregs in the newly diagnosed AML patients receiving intravenous administration of cytarabine and idarubicin.

## 2. Materials and Methods

**2.1. Study Participants.** From June 2019 to August 2020, 88 patients with acute myeloid leukemia (AML) were enrolled in this study. The patients were known to have AML from the diagnostic result of NCCN AML Guidelines [20] and received no treatments after the first attack. All of these

patients aged 20–78 years and were confirmed to have no cognitive impairment. Unqualified patients referred to those with incomplete clinical data, less than 3 months of estimated survival time, hypersensitivity, poor treatment compliance, and who were accompanied by other clinical trials, complicated by systemic infection, organ dysfunction or malignant tumor, and subject to other hematologic disorders. The 88 patients were randomly divided into two groups. The control group ( $n = 44$ ) included 19 males and 25 females (age range, 20–78 years; average age,  $46.43 \pm 4.81$  years). The study group ( $n = 44$ ) included 18 males and 26 females (age range, 20–77 years, average age,  $45.52 \pm 4.83$  years). According to the guideline of morphology, immunology, cytogenetics, and molecular biology (MICM) classification [21], 5 cases of M1, 12 cases of M2, 8 cases of M3, 9 cases of M4, 7 cases of M5, and 2 cases of M6 were found in the control group. The study group consisted of 4 cases of M1, 13 cases of M2, 8 cases of M3, 9 cases of M4, 8 cases of M5, and 2 cases of M6. No significant difference in these data was indicated between the two groups ( $P > 0.05$ ). The Medical Ethics Committee of Jiamusi University approved this prospective study, and a written informed consent was obtained from all participants.

**2.2. Treatment Protocols.** Symptomatic treatments such as myocardial nutrition, liver protection, and stomach protection were carried out to all participants after admission. The control group received intravenous administration therapy involving cytarabine with dosage  $150 \text{ mg}/(\text{m}^2 \cdot \text{d})$  and 1–2 times/d (drug approval number: H20084072, Cisen Pharmaceutical Co., Ltd., China) and a mixture of daunorubicin ( $40 \text{ mg}/(\text{m}^2 \cdot \text{d})$ ) and 10 ml of 0.9% sodium chloride injection (drug approval number: H44024361, Shenzhen Main Luck Pharmaceuticals Inc., China) for successive or alternate administration once a day. The study group was treated with cytarabine which was exactly same as the control group, followed by intravenous injection of idarubicin (drug approval number: H20063284, Yatai Pharma, China) with  $10 \text{ mg}/(\text{m}^2 \cdot \text{d})$  for 3 successive days. Taking 7 days as a course of treatment, both groups were followed up for 3 months after treatment.

**2.3. Outcome Measures.** At 7 days of treatment, the clinical response of all patients was assessed with following criteria: (a) complete remission: normal chromosome, complete remission of morphological and molecular levels, but incomplete recovery of blood cell count; (b) partial remission: less than 5% of immature cell in bone marrow, 50% decline of immature cell in the bone marrow compared with that before treatment; (c) stable disease: absence of improvement or aggravation; (d) exacerbation: progressive exacerbation, even causing death. Total response rate = complete remission rate + partial remission rate. The incidence of adverse reactions, such as nausea and vomiting, bleeding, hair loss, infection (upper respiratory tract, urinary system, skin, and lung infection), was compared between the two groups.

**2.4. Enzyme-Linked Immunosorbent Assay (ELISA).** Before and after 7-day treatment, 5 ml of fasting venous blood was collected from each patient. The blood sample was placed steadily for 2 h prior to centrifugation (10 cm centrifugal radius, 3000 rpm for 15 min). The serum levels of sICAM-1, sVCAM-1, IL-10, and IL-35 were tested by ELISA methods using commercial available kits (all purchased from R&D systems, USA).

**2.5. Flow Cytometric Analysis of T Cell Subsets.** The whole heparinized blood (200  $\mu$ l) was added to the tubes and then centrifuged at 1300 rpm for 8 min, with the supernatant aspirated. The precipitates were added with 1.5 ml PBS and centrifuged at 1300 rpm for 8 min again, with the supernatant aspirated. The precipitates were added with 500  $\mu$ l of 1:10 diluted BD permeabilizing II solution and 1.5 ml PBS and subsequently centrifuged at 1300 rpm for 8 min again, with the supernatant removed. Phenotypic characteristics of T cell subsets were analyzed by the FACSCanto II triple-laser flow cytometer (BD Biosciences, USA) using fluorochrome-labeled monoclonal antibody against CD4 (Cat. no. 562970, BD Biosciences), CD3 (Cat. no. 563423, BD Biosciences), CD8 (Cat. no. 564492, BD Biosciences), IL-10 (Cat. no. 564053), CD25 (Cat. no. 555434, BD Biosciences), CD127 (Cat. no. 560549, BD Biosciences), and Foxp3 (Cat. no. 566526, BD Biosciences).

**2.6. Karnofsky Performance Scale (KPS).** The KPS is a widespread performance scoring system that is used to assess the well-being and functional status of people with illness on a scale ranging from 0 to 100 with intervals of 10. A score of 0 indicates death and a score of 100 indicates normal function with no disease sequel. Before treatment and at 3 months after treatment, AML patients were followed up and required to fill KPS scale for evaluation of their quality of life.

**2.7. Statistical Analysis.** Measurement data normally distributed are described as mean  $\pm$  standard deviation and analyzed by the *t*-test, and counting data were represented by ratio and analyzed by the chi-square test in GraphPad prism software (Version 8.0). A value of *P* less than 0.05 reflects a statistically significant difference.

### 3. Results

**3.1. Intravenous Administration of Cytarabine and Idarubicin Improved Clinical Response Rate in AML Patients.** After 7-day treatment, the clinical response of all patients was evaluated. It was found that the study group showed higher total response rate compared to the control group. As given in Table 1, the rate in the study group and control group was 65.91% and 45.45%, respectively (*P* < 0.05).

**3.2. Intravenous Administration of Cytarabine and Idarubicin Declined Levels of sICAM-1, sVCAM-1, IL-10, and IL-35 in AML Patients.** The levels of sICAM-1, sVCAM-1, IL-10, and IL-35 were measured by ELISA of serum samples. The results

revealed that serum levels of sICAM-1, sVCAM-1, IL-10, and IL-35 were declined significantly in AML patients following intravenous administration of cytarabine supplemented with either idarubicin or daunorubicin (*P* < 0.05), and this decrease was more evident in AML patients following intravenous administration of cytarabine supplemented with idarubicin (*P* < 0.05, Figure 1).

**3.3. Intravenous Administration of Cytarabine and Idarubicin Improved Immune Function of AML Patients.** The proportions of T cell subsets including CD4<sup>+</sup>, CD8<sup>+</sup>, CD4<sup>+</sup>IL-10 Tregs, and CD4<sup>+</sup>CD25<sup>+</sup>CD127<sup>-</sup>Foxp3<sup>+</sup> Tregs were analyzed by flow cytometry. It was observed that, after treatment, increased proportions of CD3<sup>+</sup> T cells, CD4<sup>+</sup> T cells, and CD4<sup>+</sup>/CD8<sup>+</sup> ratio along with decreased proportions of CD8<sup>+</sup> T cells, CD4<sup>+</sup>IL-10 Tregs, and CD4<sup>+</sup>CD25<sup>+</sup>CD127<sup>-</sup>Foxp3<sup>+</sup> Tregs were revealed in peripheral blood in AML patients following intravenous administration of cytarabine supplemented with either idarubicin or daunorubicin (*P* < 0.05, Tables 2 and 3). These changes in AML patients following intravenous administration of cytarabine supplemented with idarubicin were more evident compared to those supplemented with daunorubicin (*P* < 0.05).

**3.4. Intravenous Administration of Cytarabine and Idarubicin Improved Quality of Life in AML Patients.** Before treatment and at 3 months after treatment, AML patients were followed up and required to fill KPS scale to reflect their quality of life. Before treatment, the scores of KPS in the study group and control group were (75.88  $\pm$  3.28) and (76.13  $\pm$  3.20), respectively. At 3 months after treatment, the scores of KPS in the study group and control group were (89.81  $\pm$  6.43) and (81.64  $\pm$  5.51), respectively. The study group and control group showed increased KPS scores after treatment (*t* = 12.800, *P* < 0.001; *t* = 5.736, *P* < 0.001), and this increase was more obvious in the study group (*t* = 6.400, *P* < 0.001).

**3.5. Intravenous Administration of Cytarabine and Idarubicin Led to Reduced Total Incidence Rate of Adverse Reactions in AML Patients.** As given in Table 4, AML patients experienced several adverse reactions, including nausea and vomiting, myelosuppression, infection, and leukopenia after intravenous administration of cytarabine supplemented with either idarubicin or daunorubicin. Two groups of AML exhibited no significant difference in term of the incidence rates of nausea and vomiting, myelosuppression, infection, and leukopenia. However, the total incidence rate of adverse reactions in the study group was evidently lower than that in the control group (34.09% vs. 61.36%, *P* < 0.05).

### 4. Discussion

AML is heterologous tumor, which frequently occurs in adults. It was reported, 19,000 American populations were newly diagnosed with AML and 10,000 patients died of the disease every year [22]. The 5-year overall survival of AML is negatively related to age. It ranged 40–50% in younger

TABLE 1: The clinical response rates of AML patients following intravenous administration of cytarabine supplemented with either idarubicin or daunorubicin.

Group	Case	Complete remission	Partial remission	Stable disease	Exacerbation	Total response rate (%)
Control group	44	14 (31.82)	6 (13.64)	3 (6.82)	21 (47.73)	20 (45.45)
Study group	44	19 (43.18)	10 (22.73)	4 (9.09)	11 (25.00)	29 (65.91)
<i>t</i>						14.175
<i>P</i>						0.001

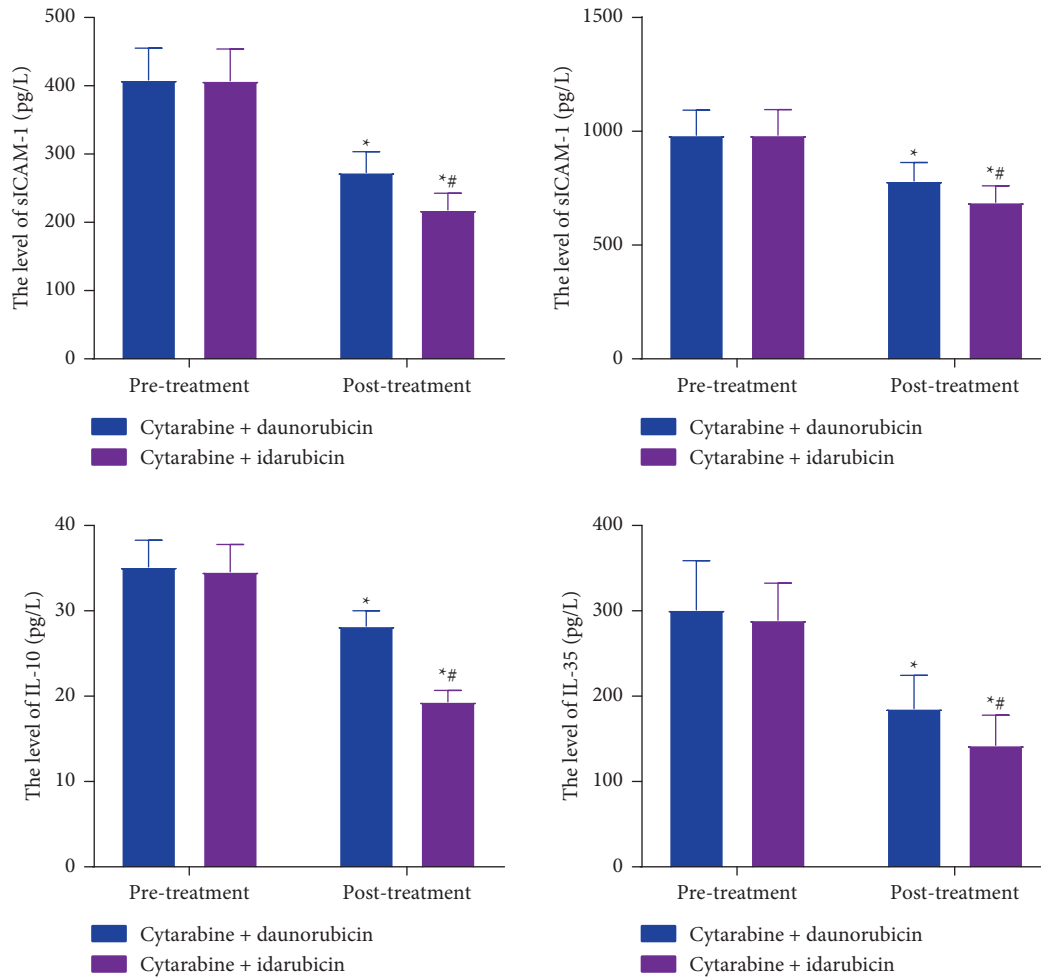


FIGURE 1: The levels of sICAM-1, sVCAM-1, IL-10, and IL-35 measured by ELISA of serum samples in AML patients following intravenous administration of cytarabine supplemented with either idarubicin or daunorubicin.

TABLE 2: The proportions of CD4<sup>+</sup>, CD8<sup>+</sup>, and CD4<sup>+</sup>/CD8<sup>+</sup> ratio in peripheral blood in AML patients following intravenous administration of cytarabine supplemented with either idarubicin or daunorubicin.

Group	Case	Time	CD3 <sup>+</sup> (%)	CD4 <sup>+</sup> (%)	CD8 <sup>+</sup> (%)	CD4 <sup>+</sup> /CD8 <sup>+</sup>
Control group	44	Pretreatment	59.15 ± 6.97	30.14 ± 3.87	34.15 ± 3.41	0.79 ± 0.08
		Posttreatment	62.74 ± 6.03	35.87 ± 3.72	32.96 ± 3.49	1.12 ± 0.12
<i>t</i>			8.125	6.193	0.941	3.618
<i>P</i>			0.001	0.007	0.086	0.029
Study group	44	Pretreatment	59.17 ± 6.99	30.27 ± 3.93	34.11 ± 3.49	0.81 ± 0.09
		Posttreatment	73.80 ± 8.51 <sup>a</sup>	39.91 ± 4.76 <sup>a</sup>	29.74 ± 2.35 <sup>a</sup>	1.39 ± 0.19 <sup>a</sup>
<i>t</i>			12.119	7.374	5.174	4.396
<i>P</i>			0.001	0.001	0.018	0.027

The letter a indicates  $P < 0.05$  compared to the control group.

TABLE 3: The proportions of CD4<sup>+</sup>IL-10 Tregs and CD4<sup>+</sup>CD25<sup>+</sup>CD127<sup>-</sup>Foxp3<sup>+</sup> Tregs in peripheral blood in AML patients following intravenous administration of cytarabine supplemented with either idarubicin or daunorubicin.

Group	Case	Time	CD4 <sup>+</sup> IL-10 Tregs (%)	CD4 <sup>+</sup> CD25 <sup>+</sup> CD127 <sup>-</sup> Foxp3 <sup>+</sup> Tregs (%)
Control group	44	Pretreatment	27.75 ± 3.97	23.31 ± 3.87
		Posttreatment	23.47 ± 2.53	19.89 ± 1.75
<i>t</i>			6.031	5.341
<i>P</i>			<0.001	<0.001
Study group	44	Pretreatment	28.11 ± 3.63	23.07 ± 3.93
		Posttreatment	20.40 ± 2.04 <sup>a</sup>	18.28 ± 1.43 <sup>a</sup>
<i>t</i>			12.280	7.597
<i>P</i>			<0.001	<0.001

TABLE 4: The incidence rate of adverse reactions in AML patients following intravenous administration of cytarabine supplemented with either idarubicin or daunorubicin.

Group	Case	Nausea and vomiting (n, %)	Myelosuppression (n, %)	Infection (n, %)	Leukopenia (n, %)	Total incidence (n, %)
Control group	44	12 (27.27)	5 (11.36)	3 (6.82)	7 (15.91)	27 (61.36)
Study group	44	7 (15.91)	2 (4.55)	2 (4.55)	4 (9.09)	15 (34.09)
<i>t</i>						16.675
<i>P</i>						0.018

patients, but only 10–20% was found in the patients over 60 years old [19, 23]. Clinically, AML is manifested as various symptoms such as infection, fever, bleeding, anemia, and abnormal cell invasion. Most cases are in acute and severe condition, which not only affects the patient's physical condition and life quality but also endangers life. A combination of cytarabine and daunorubicin or idarubicin, also called as 7 + 3 regimen, has been widely applied to most patients with newly diagnosed AML except for clinical studies [24, 25]. Idarubicin is an anthracycline antibiotic targeting tumor and cancer. It removes methoxyl at the C-4 position of daunorubicin and was prepared by Arcamone et al. in 1976 [26]. Idarubicin is a derivative of daunorubicin, which interferes with the activity of topoisomerase II and inhibits nucleic acid synthesis. Comparing to daunorubicin, idarubicin is characterized by higher lipophilicity, cell permeability, stronger immune response, and lower drug resistance [27].

Idarubicin has been widely used in clinical treatment of AML, high-risk myelodysplastic syndrome [28], hepatocellular carcinoma [29], and metastatic breast cancer [30] and turned out to be a treatment scheme to alleviate patients' symptoms. Guiu et al. [29] revealed that the patients with unresectable hepatocellular carcinoma showed better overall survival and objective response rate after interventional therapy of idarubicin-loaded beads. In our study, the patients who received idarubicin showed higher response rate and increased KPS score, suggesting combined intravenous administration of cytarabine and idarubicin was effective on prolonging life and improving life quality. Adhesion molecules on the surface of leukocytes, vascular endothelial cells, or other cells become soluble adhesion molecules after entering blood. sICAM-1 and sVCAM-1 are the members of immunoglobulin superfamily and participate in the migration, proliferation, and differentiation of hematopoietic cells [31]. The present study found that serum levels of sICAM-1, sVCAM-1, IL-10, and IL-35 were declined

significantly in AML patients following intravenous administration of cytarabine supplemented with either idarubicin or daunorubicin ( $P < 0.05$ ), and this decrease was more evident in AML patients following intravenous administration of cytarabine supplemented with idarubicin. The results showed idarubicin has more advantages in maintaining cellular immune balance. Zaccagni et al. also indicated that the patients with systemic lupus erythematosus showed elevated levels of soluble adhesion molecule levels (VCAM-1 and ICAM-1) compared with healthy groups [32]. Low level of sICAM-1 increased cancer-related 5-year survival rate [33]. Increased level of maternal serum and vaginal fluid sVCAM-1 and sICAM-1 was found in pregnant women with preterm prelabour ruptures of membranes. These levels can be used as biomarkers to support diagnosis of the disease [34]. IL-10 exerts anti-inflammatory and immunosuppressive activities by inhibiting the production of cytokines by T cells [35]. Patients with adult T cell leukemia caused by human T cell leukemia virus type I infection showed elevated serum levels of IL-10 [36]. IL-35 is produced by Tregs and responsible for the suppressive activity of Tregs [37]. Tao et al. found that IL-35 was increased in peripheral blood of adult AML patients and correlated with the clinical stages of malignancy [38]. As reported by Wu et al., remarkable higher levels of plasma IL-35 and IL-10 were detected in newly diagnosed AML patients compared with AML patients with complete remission or healthy controls [39].

T cells are the main effector cells of cellular immunity. CD4<sup>+</sup>, CD8<sup>+</sup> T cells, and Tregs have significant heterogeneity in cytokine expression. They produce cytokines, such as interferon- $\gamma$  and tumor necrosis factor- $\alpha$ , in the immune response to mediate inflammation and remove intracellular pathogens [40, 41]. In this study, flow cytometric analysis showed that, after treatment, increased proportions of CD3<sup>+</sup> T cells, CD4<sup>+</sup> T cells, and CD4<sup>+</sup>/CD8<sup>+</sup> ratio along with decreased proportions of CD8<sup>+</sup> T cells, CD4<sup>+</sup>IL-10 Tregs,

and CD4<sup>+</sup>CD25<sup>+</sup>CD127<sup>-</sup>Foxp3<sup>+</sup> Tregs were revealed in peripheral blood in AML patients following intravenous administration of cytarabine supplemented with either idarubicin or daunorubicin. This finding indicated that combined intravenous administration of cytarabine and idarubicin was helpful to reduce virus infection and improve patients' immunity. Another report on AML revealed that increasing CD8<sup>+</sup> T cells were represented in the AML-M5 subtype group compared with the AML-M3 group. Increased CD8<sup>+</sup> T cells were associated with poor response [42]. The patients with chronic lymphocytic leukemia showed significantly higher percentage of CD4<sup>+</sup> than that in healthy volunteers [43]. Guo et al. demonstrated that the patients with acute leukemia had higher absolute count of CD3<sup>+</sup> compared with healthy controls, but with reduced immune function [44]. Xu et al. demonstrated that blocking the interaction between Tregs and AML cells may be a new approach to target leukemia stem cells in the treatment of AML [45]. There was a higher proportion of CD4<sup>+</sup>CD25<sup>+</sup>CD127<sup>-</sup>Foxp3<sup>+</sup> Tregs in newly diagnosed AML patients than healthy controls [46]. All these findings manifested T cells involved in immune response and mediated progress of disease. In addition, this study found that the incidence of adverse reactions in the study group was significantly lower than that in the control group. It suggested that idarubicin improved the safety of chemotherapy in AML patients due to its lower drug resistance and toxicity.

In summary, our data suggest that intravenous administration of cytarabine supplemented with idarubicin can improve the immune function and quality of life of AML patients, and this combination drug therapy is effective and safe for AML, which is worthy of clinical recommendation. However, limited numbers of AML patients in this study might lower the data reliability, and thus, further study should be carried out to confirm these findings.

## Data Availability

The data used to support the findings of this study are included within the article.

## Conflicts of Interest

The authors declare that they have no conflicts of interest.

## Acknowledgments

The study was financially supported by the North Medicine and Functional Food Characteristic Subject Project in Heilongjiang Province (2018-TSXX-02).


## References

- [1] R. D. Brunning, "Classification of acute leukemias," *Seminars in Diagnostic Pathology*, vol. 20, no. 3, pp. 142–153, 2003.
- [2] J. Prada-Arismendy, J. C. Arroyave, and S. Röthlisberger, "Molecular biomarkers in acute myeloid leukemia," *Blood Reviews*, vol. 31, no. 1, pp. 63–76, 2017.
- [3] F. R. Appelbaum, H. Gundacker, D. R. Head et al., "Age and acute myeloid leukemia," *Blood*, vol. 107, no. 9, pp. 3481–3485, 2006.
- [4] I. De Kouchkovsky and M. Abdul-Hay, "Acute myeloid leukemia: a comprehensive review and 2016 update," *Blood Cancer Journal*, vol. 6, no. 7, p. e441, 2016.
- [5] E. M. Stein, C. D. DiNardo, D. A. Pollyea et al., "Enasidenib in mutant IDH2 relapsed or refractory acute myeloid leukemia," *Blood*, vol. 130, no. 6, pp. 722–731, 2017.
- [6] L. Riva, L. Luzi, and P. G. Pelicci, "Genomics of acute myeloid leukemia: the next generation," *Frontiers in Oncology*, vol. 2, p. 40, 2012.
- [7] J. Meyers, Y. Yu, J. A. Kaye, and K. L. Davis, "Medicare fee-for-service enrollees with primary acute myeloid leukemia: an analysis of treatment patterns, survival, and healthcare resource utilization and costs," *Applied Health Economics and Health Policy*, vol. 11, no. 3, pp. 275–286, 2013.
- [8] J. C. Byrd, K. Mrozek, R. K. Dodge et al., "Pretreatment cytogenetic abnormalities are predictive of induction success, cumulative incidence of relapse, and overall survival in adult patients with de novo acute myeloid leukemia: results from cancer and leukemia group B (CALGB 8461)," *Blood*, vol. 100, no. 13, pp. 4325–4336, 2002.
- [9] G. Marcucci, K. Mrózek, and C. D. Bloomfield, "Molecular heterogeneity and prognostic biomarkers in adults with acute myeloid leukemia and normal cytogenetics," *Current Opinion in Hematology*, vol. 12, no. 1, pp. 68–75, 2005.
- [10] K. Melgar, M. M. Walker, L. M. Jones et al., "Overcoming adaptive therapy resistance in AML by targeting immune response pathways," *Science Translational Medicine*, vol. 11, no. 508, 2019.
- [11] M. T. Witkowski, A. Lasry, W. L. Carroll, and I. Aifantis, "Immune-based therapies in acute leukemia," *Trends in Cancer*, vol. 5, no. 10, pp. 604–618, 2019.
- [12] A. Molodtsov and M. J. Turk, "Tissue resident CD8 memory T cell responses in cancer and autoimmunity," *Frontiers in Immunology*, vol. 9, p. 2810, 2018.
- [13] M. A. Oberli, A. M. Reichmuth, J. R. Dorkin et al., "Lipid nanoparticle assisted mRNA delivery for potent cancer immunotherapy," *Nano Letters*, vol. 17, no. 3, pp. 1326–1335, 2017.
- [14] A. Schiffrin, S. Suissa, G. Weitzner, P. Poussier, and D. Lalla, "Factors predicting course of  $\beta$ -cell function in IDDM," *Diabetes Care*, vol. 15, no. 8, pp. 997–1001, 1992.
- [15] L. Ehlers, S. Rohde, S. Ibrahim, and R. Jaster, "Adoptive transfer of CD3<sup>+</sup> T cells and CD4<sup>+</sup> CD 44 high memory T cells induces autoimmune pancreatitis in MRL/MpJ mice," *Journal of Cellular and Molecular Medicine*, vol. 22, no. 4, pp. 2404–2412, 2018.
- [16] S. Sakaguchi, "Regulatory T cells: history and perspective," *Regulatory T Cells*, vol. 707, pp. 3–17, 2011.
- [17] W. Li, R. Gao, T. Xin, and P. Gao, "Different expression levels of interleukin-35 in asthma phenotypes," *Respiratory Research*, vol. 21, no. 1, p. 89, 2020.
- [18] L. Fotis, G. Agrogiannis, I. S. Vlachos et al., "Intercellular adhesion molecule (ICAM)-1 and vascular cell adhesion molecule (VCAM)-1 at the early stages of atherosclerosis in a rat model," *Vivo*, vol. 26, no. 2, pp. 243–250, 2012.
- [19] H. Döhner, D. J. Weisdorf, and C. D. Bloomfield, "Acute myeloid leukemia," *New England Journal of Medicine*, vol. 373, no. 12, pp. 1136–1152, 2015.
- [20] D. A. Pollyea, D. Bixby, A. Perl et al., "NCCN guidelines insights: acute myeloid leukemia, version 2.2021," *Journal of the National Comprehensive Cancer Network*, vol. 19, no. 1, pp. 16–27, 2021.

- [21] D. A. Arber, "The 2016 WHO classification of acute myeloid leukemia: what the practicing clinician needs to know," *Seminars in Hematology*, vol. 56, no. 2, pp. 90–95, 2019.
- [22] T. M. Kadia, F. Ravandi, J. Cortes, and H. Kantarjian, "New drugs in acute myeloid leukemia," *Annals of Oncology*, vol. 27, no. 5, pp. 770–778, 2016.
- [23] H. Döhner, E. H. Estey, S. Amadori et al., "Diagnosis and management of acute myeloid leukemia in adults: recommendations from an international expert panel, on behalf of the European leukemia net," *Blood*, vol. 115, no. 3, pp. 453–474, 2010.
- [24] K. Saleh, N. Khalifeh-Saleh, and H. R. Kourie, "Acute myeloid leukemia transformed to a targetable disease," *Future Oncology*, vol. 16, no. 14, pp. 961–972, 2020.
- [25] F. Ravandi, R. Assi, N. Daver et al., "Idarubicin, cytarabine, and nivolumab in patients with newly diagnosed acute myeloid leukaemia or high-risk myelodysplastic syndrome: a single-arm, phase 2 study," *The Lancet Haematology*, vol. 6, no. 9, pp. e480–e488, 2019.
- [26] F. Arcamone, L. Bernardi, P. Giardino et al., "Synthesis and antitumor activity of 4-demethoxydaunorubicin, 4-demethoxy-7,9-diepidaurubicin, and their beta anomers," *Cancer Treatment Reviews*, vol. 60, no. 7, pp. 829–834, 1976.
- [27] H. Mizutani, C. Shiga, M. Imai et al., "Idarubicin, an anthracycline, induces oxidative DNA damage in the presence of copper (II)," *Anticancer Research*, vol. 40, no. 10, pp. 5399–5404, 2020.
- [28] S. Adige, R. G. Lapidus, B. A. Carter-Cooper et al., "Equivalent doses of daunorubicin and idarubicin for AML: a meta-analysis of clinical trials versus in vitro estimation," *Cancer Chemotherapy and Pharmacology*, vol. 83, no. 6, pp. 1105–1112, 2019.
- [29] B. Guiu, P. Chevallerier, E. Assenat et al., "Idarubicin-loaded beads for chemoembolization of hepatocellular carcinoma: the IDASPHERE II single-arm phase II trial," *Radiology*, vol. 291, no. 3, pp. 801–808, 2019.
- [30] D. Crivellari, D. Lombardi, G. Corona et al., "Innovative schedule of oral idarubicin in elderly patients with metastatic breast cancer: comprehensive results of a phase II multi-institutional study with pharmacokinetic drug monitoring," *Annals of Oncology*, vol. 17, no. 5, pp. 807–812, 2006.
- [31] H. S. Howe, K. O. Kong, B. Y. Thong et al., "Urine sVCAM-1 and sICAM-1 levels are elevated in lupus nephritis," *International Journal of Rheumatic Diseases*, vol. 15, no. 1, pp. 13–16, 2012.
- [32] H. Zaccagni, J. Fried, J. Cornell, P. Padilla, and R. L. Brey, "Soluble adhesion molecule levels, neuropsychiatric lupus and lupus-related damage," *Frontiers in Bioscience*, vol. 9, no. 1-3, pp. 1654–1659, 2004.
- [33] V. S. Schellerer, M. C. Langheinrich, V. Zver et al., "Soluble intercellular adhesion molecule-1 is a prognostic marker in colorectal carcinoma," *International Journal of Colorectal Disease*, vol. 34, no. 2, pp. 309–317, 2019.
- [34] S. Sak, M. Barut, A. Incebiyik et al., "Comparison of sVCAM-1 and sICAM-1 levels in maternal serum and vaginal secretion between pregnant women with preterm prelabour ruptures of membranes and healthy pregnant women," *Journal of Maternal-Fetal and Neonatal Medicine*, vol. 32, no. 6, pp. 910–915, 2019.
- [35] L. Jimbu, O. Mesaros, A. Neaga et al., "The potential advantage of targeting both PD-L1/PD-L2/PD-1 and IL-10-IL-10r pathways in acute myeloid leukemia," *Pharmaceuticals (Basel)*, vol. 14, no. 11, 2021.
- [36] G. Musuraca, S. De Matteis, R. Napolitano et al., "IL-17/IL-10 double-producing T cells: new link between infections, immunosuppression and acute myeloid leukemia," *Journal of Translational Medicine*, vol. 13, no. 1, p. 229, 2015.
- [37] M. E. Turnis, D. V. Sawant, A. L. Szymczak-Workman et al., "Interleukin-35 limits anti-tumor immunity," *Immunity*, vol. 44, no. 2, pp. 316–329, 2016.
- [38] Q. Tao, Y. Pan, Y. Wang et al., "Regulatory T cells-derived IL-35 promotes the growth of adult acute myeloid leukemia blasts," *International Journal of Cancer*, vol. 137, no. 10, pp. 2384–2393, 2015.
- [39] H. Wu, P. Li, N. Shao et al., "Aberrant expression of treg-associated cytokine IL-35 along with IL-10 and TGF- $\beta$  in acute myeloid leukemia," *Oncology Letters*, vol. 3, no. 5, pp. 1119–1123, 2012.
- [40] C. Dong, "Cytokine regulation and function in T cells," *Annual Review of Immunology*, vol. 39, no. 1, pp. 51–76, 2021.
- [41] H.-W. Mittrücker, A. Visekruna, and M. Huber, "Heterogeneity in the differentiation and function of CD8<sup>+</sup> T cells," *Archivum Immunologiae et Therapiae Experimentalis*, vol. 62, no. 6, pp. 449–458, 2014.
- [42] J. Huang, J. Tan, Y. Chen et al., "A skewed distribution and increased PD-1 + V $\beta$  + CD<sup>4</sup>+/CD<sup>8</sup>+ T cells in patients with acute myeloid leukemia," *Journal of Leukocyte Biology*, vol. 106, no. 3, pp. 725–732, 2019.
- [43] E. Allahmoradi, S. Taghiloo, M. Tehrani et al., "CD4<sup>+</sup> T cells are exhausted and show functional defects in chronic lymphocytic leukemia," *Iranian Journal of Immunology*, vol. 14, no. 4, pp. 257–269, 2017.
- [44] W. Guo, C. Xing, A. Dong et al., "Numbers and cytotoxicities of CD3<sup>+</sup>CD56<sup>+</sup>T lymphocytes in peripheral blood of patients with acute myeloid leukemia and acute lymphocytic leukemia," *Cancer Biology & Therapy*, vol. 14, no. 10, pp. 916–921, 2013.
- [45] Y. Xu, J. Mou, Y. Wang et al., "Regulatory T cells promote the stemness of leukemia stem cells through IL10 cytokine-related signaling pathway," *Leukemia*, vol. 36, no. 2, pp. 403–415, 2022.
- [46] Q. Dong, G. Li, C. Fozza et al., "Levels and clinical significance of regulatory B cells and T cells in acute myeloid leukemia," *BioMed Research International*, vol. 2020, Article ID 7023168, 6 pages, 2020.

## Research Article

# Clinical Observation on the Treatment of Chronic Subjective Dizziness by the Herbal-Scraping Duplex Method Based on Holographic Theory

Huanwen Luo,<sup>1</sup> Caidan Liu,<sup>1</sup> Ziwei Xiao,<sup>2</sup> and Yana He <sup>3</sup>

<sup>1</sup>Department of Brain Disease, The First Hospital of Hunan University of Chinese Medicine, Changsha, Hunan 410000, China

<sup>2</sup>Hunan University of Chinese Medicine, Changsha, Hunan 410000, China

<sup>3</sup>Bidding Center of the First Hospital of Hunan University of Chinese Medicine, Changsha, Hunan 410000, China

Correspondence should be addressed to Yana He; 909932870@qq.com

Received 9 December 2021; Accepted 31 December 2021; Published 24 January 2022

Academic Editor: Weiguo Li

Copyright © 2022 Huanwen Luo et al. This is an open access article distributed under the Creative Commons Attribution License, which permits unrestricted use, distribution, and reproduction in any medium, provided the original work is properly cited.

Chronic subjective dizziness (CSD) is a chronic, subjective, nonrotational dizziness and instability caused by mental or physical factors, and patients generally have no existing vestibular system diseases. Clinically, antianxiety drugs are often used for symptomatic treatment with mediocre effects. This study observed the clinical efficacy of the herbal-scraping duplex method in the treatment of CSD based on the holographic theory. 180 patients with CSD were randomly and equally divided into group A ( $n=60$ ) who received fluoxetine hydrochloride, group B ( $n=60$ ) who received fluoxetine hydrochloride combined with holographic soup, and group C ( $n=60$ ) who received fluoxetine hydrochloride, holographic soup, and holographic scraping combined with five-element music. The effects of the 3 different treatment modalities on patients' vertigo symptoms, traditional Chinese medicine (TCM) symptoms, anxiety and depression status, sleep quality, and fatigue level were observed. The safety of medication and the recurrence after discontinuation were observed. The results showed that group C was better than group B and group A in terms of improvement in all of the above indicators, and group B was better than group A ( $P < 0.05$ ). The total efficiency of Chinese and Western medicine was better in groups C and B than in group A ( $P < 0.05$ ). No statistical difference was seen in the comparison of adverse reaction rates between the 3 groups ( $P > 0.05$ ). After 1 month of drug discontinuation, the recurrence rates in groups C and B were lower than those in group A ( $P < 0.05$ ). This suggests that the clinical efficacy and safety of applying the herbal-scraping duplex method based on holographic theory for the treatment of CSD is ideal and has the value of promotion.

## 1. Introduction

Chronic subjective dizziness (CSD) is a group of chronic nonspecific syndromes with high sensitivity to motor signals and low tolerance to visual signals, accompanied by a significant subjective dizziness and instability [1]. Patients often seek medical attention for chronic and persistent head dizziness or a subjective sense of instability, which accounts for approximately 10.6% of all dizziness visits in outpatient clinics and can be twice as common in women as in men [2]. Psychiatric factors such as anxiety, depression, and panic are common triggers, and psychiatric medications are often

applied symptomatically in clinical practice [3]. However, in view of the long treatment cycle of CSD, the safety and compliance of long-term use of such drugs are difficult to guarantee, and some patients have drug resistance or lack of efficacy [4]. Therefore, there is still a need to find a safer and more secure treatment method in the clinic.

CSD belongs to the category of "vertigo" in Chinese medicine. The patient is characterized by head dizziness, which may also be accompanied by complications related to dizziness. The onset is often related to the patient's emotional and mental disorders, improper diet, long-term illness and physical deficiency, old age and physical weakness, or



fall injuries. Treatment can start by regulating the Qi of the whole body and taking into account the overall symptoms. In this study treatment, based on the holographic theory, herbal medicine, scraping, and music therapy, which are highly accepted by the patients, were used as treatment tools. Among them, the application of holographic soup is the result of concentrating the theory of holographic nutrition of herbs and the systemic therapy of Chinese medicine, which has the effect of overall regulation. The application of holographic scraping can achieve the purpose of adjusting the function of the corresponding viscera by stimulating the local information acupoint areas of the patient [5]. The application of five-element music, which combines the patient's condition and psychological state to dialectically play music for treatment, can achieve the effect of stretching the patient's Qi and emotions [6]. The application of all methods, through the combination of overall and local conditioning, is expected to achieve the physiological state of balance between Yin and Yang in CSD patients and ultimately help the body's function to recover as soon as possible and improve the condition. This study observes the clinical efficacy of the herbal-scraping duplex method in the treatment of CSD based on the holographic theory. The report is as follows.

## 2. Materials and Methods

**2.1. Research Object.** Between January 2020 and January 2021, 180 patients with CSD who met the inclusion criteria were randomly and equally divided into the group A ( $n = 60$ ), the group B ( $n = 60$ ), and the group C ( $n = 60$ ). The general data difference analysis in Table 1 of the 3 groups was not statistically significant and could be used for experimental analysis ( $P > 0.05$ ).

**2.2. Diagnostic Criteria.** Western medicine diagnostic criteria refer to the 2017 Bárány Society diagnostic criteria for CSD [7]: nonrotational dizziness or subjective imbalance of balance for  $\geq 3$  months; high sensitivity to movement of things around or of themselves for  $\geq 3$  months; dizziness worsens when performing refined visual tasks or in a complex visual environment. It might be accompanied by a sense of mental unclearness, or anxiety, depression, or somatization symptoms such as palpitations and pain. The diagnostic criteria of TCM referred to the diagnostic criteria of vertigo in the 2007 edition of "Traditional Chinese Medicine Encephalopathy." Main symptoms are obvious vertigo, a sense of shaking and spinning or vision rotation, with chronic onset and recurrent attacks. Secondary symptoms are nausea and vomiting, palpitation and irritability, drowsiness, insomnia and dreaminess, forgetfulness, tinnitus and deafness, fear and suspicion, and sweating and pallor.

**2.3. Inclusion Criteria.** Inclusion criteria were as follows: those with clear diagnostic criteria for CSD in Chinese and Western medicine; 30–70 years old; elementary school education or above, normal mental and cognitive ability, normal communication and understanding ability, and

could cooperate to complete the relevant scale test; those without significant mental illness; those with normal neuroimaging; those with normal or mildly abnormal vestibular function and balance function tests, but not enough to make a diagnosis of abnormality; those who had not received other disease-related treatments within 3 months before treatment; and informed consent, voluntary participants.

**2.4. Exclusion Criteria.** Exclusion criteria were as follows: those whose dizziness was caused by other causes such as drugs, trauma, and poisoning; those who belong to other systemic disease-related dizziness, such as hypotension, hypoglycemia, anemia, hyper or hypothyroidism, and active neurootologic diseases; those with ophthalmoplegia, ocular muscle paralysis, leukemia, disorders of acid-base balance, electrolyte disorders, reduced cardiac ejection, and vascular diseases; those with cervical vertigo, peripheral vertigo, or central vertigo; persons with severe heart, brain, liver, and kidney dysfunction; the presence of a known drug dependency or alcoholism; those with unstable vital signs; pregnant and lactating women.

**2.5. Rejection and Shedding Criteria.** Rejection and shedding criteria were as follows: those whose condition deteriorated rapidly due to serious complications or adverse reactions during the trial, those who developed other diseases that can cause vertigo during the trial, those who caused treatment suspension or the subject withdrew halfway through various factors, those whose medication did not meet the regulations or had low compliance with treatment, those who received other treatments that affect the efficacy during the observation period. Various factors led to loss of follow-up.

### 2.6. Treatment Methods

- (1) Group A: received fluoxetine hydrochloride capsules (Suzhou Yushi Pharmaceutical Co., Ltd., Chinese Medicine Zhunzi H20093454) treatment, once a day, orally 30 minutes after breakfast, 20 mg each time, continuous treatment for 4 weeks.
- (2) Group B: on the basis of group A, holographic soup was added. Holographic soup recipe: 12 g each of Radix Bupleuri and *Alisma orientale* and 10 g each of Guizhi, *Trichosanthes kirilowii*, immature bitter orange, *Allii Macrostemonis Bulbus*, *Magnolia officinalis* cortex, *Paeonia lactiflora* Pall., *Atractylodes sinensis*, dried tangerine or orange peel, *Atractylodes macrocephala*, *Poria cocos*, *Polyporus*, Radix Rehmanniae, Cortex Moutan, ginger, jujube, and licorice. Addition and subtraction for clinical evidence: palpitations and irritability with 12 g each of keel and oyster; fatigue and sleepiness with 110 g of Rhizoma Acori Tatarinowii; tinnitus and deafness with 10 g each of Medulla Tetrapanacis and Rhizoma Acori

TABLE 1: Comparison of the distribution of the 3 groups of general data.

Group	Male/female ( <i>n</i> (%))	Age ( $\bar{x} \pm s$ , years old)	Course of disease ( $\bar{x} \pm s$ , years)
Group A ( <i>n</i> = 60)	18/42 (30.00/70.00)	49.25 $\pm$ 4.64	3.71 $\pm$ 1.05
Group B ( <i>n</i> = 60)	21/39 (35.00/65.00)	48.63 $\pm$ 5.14	4.03 $\pm$ 1.42
Group C ( <i>n</i> = 60)	19/41 (31.67/68.33)	48.71 $\pm$ 4.97	3.87 $\pm$ 1.15
$\chi^2/F$	0.356	0.282	1.038
<i>P</i>	0.837	0.755	0.357

Tatarinowii. All herbal tablets were sourced from the Chinese pharmacy of our hospital. Each dose of Chinese medicine was decocted with 400 mL of water routinely, and patients were instructed to take 200 mL each in the morning and evening after adding warmth. 1 week was 1 course of treatment, continue treatment for 4 courses.

- (3) Group C: on the basis of group B, holographic scraping therapy was added. Holographic scraping and acupoint selection: on Monday, the holographic acupoint area took the middle of the forehead of the head, 1 area of the right side of the forehead, and 2 areas of the left side of the forehead, head, and neck meridian acupoints took the odd points, Sishencong, blood pressure points. On Tuesday, the holographic acupoint area took the posterior 1/3 of the forehead parietal zone and the lower 1/3 of the parietal posterior oblique zone; meridian acupoints took the Baihui-Fengfu of the governor vessel. On Wednesday, the holographic acupoint area took the spleen and stomach correspondence area of the spine, and the meridian acupoints took the Pishu, Weishu, Xinshu, and Shenshu of the bilateral bladder meridian. On Thursday, the holographic acupoint area took the head acupoints and heart acupoints on the radial side of the second metacarpal bone of the hand and palm middle finger, and the meridian acupoints took the Shenmen of the bilateral heart meridian. On Friday, the holographic acupoint area took the hypotensive ditch on the back of the ear, and the meridian acupoints took the Zusanli of bilateral stomach meridian, the Sanyinjiao of bilateral spleen meridian, the Yongquan of bilateral kidney meridian. Operation: before scraping, examine the patient's local skin for ulcers and breaks and ask the patient about contraindications to scraping. When scraping, guide the patient to a comfortable posture and fully expose the scraping area. After routine disinfection, use a flat replenishing-reducing technique for scraping at a speed of 60 times/min. During the period, pay close attention to the patient's local reaction and tolerance. Do not use excessive force and take comfort as the standard, once a day from Monday to Friday, every 20–30 minutes. During each Gua Sha, the five-element music should be played dialectically based on the patient's condition and psychological state. It contains five corresponding pieces of Jiao, Zheng, Gong, Shang, and Yu (all created by the China Medical Audiovisual Publishing House). When playing music, it was

necessary to ensure that the room is not disturbed by other noises or noises, and the playback volume must be controlled below 60 decibels. 1 week was 1 course of treatment; continue treatment for 4 courses.

## 2.7. Observation Indicators

- (1) Dizziness handicap inventory (DHI) score: before and after treatment, the total scores of physical, social function, and emotion factors in the 3 groups of DHI were counted, with a total score of 0–100 points. The higher the score, the more severe the dizziness handicap.
- (2) TCM symptoms score: before and after treatment, the total scores of TCM syndromes of the 3 groups, such as dizziness, nausea and vomiting, palpitations, irritability, drowsiness, insomnia, forgetfulness, tinnitus, and deafness, were counted. The scores (0, 2, 4, and 6) are proportional to the severity of the syndrome (none, mild, moderate, and severe).
- (3) Hamilton anxiety/depression scale (HAMA/HAMD) score: before and after treatment, HAMA/HAMD assessed the degree of anxiety and depression in the 3 groups. The former with a total score of 0–56 points; the latter with a total score of 0–68 points. The higher the score, the greater the anxiety and depression.
- (4) Pittsburgh sleep quality index (SQI) score: before and after treatment, PSQI assessed the total scores of the 3 groups of factors such as sleep quality, sleep time, and sleep latency. The total score is 0–21 points; the higher the score, the more severe the sleep disorder.
- (5) Fatigue severity scale (FSS) score: before and after treatment, FSS assessed the fatigue degree of the 3 groups and their impact on daily functions, with a total score of 9–63 points. The higher the score, the more severe the fatigue.
- (6) Others: during the treatment, the 3 groups of patients were subjected to blood routine, urine routine, stool routine, liver and kidney function, and electrocardiogram and other safety checks, and the occurrence of adverse of the 3 groups was observed such as nausea, vomiting, constipation, skin rash, dry mouth, and so on. After 1 month of drug discontinuation, the recurrence was followed up and counted in the 3 groups.

## 2.8. Efficacy Evaluation

- (1) Western medicine efficacy determination criteria: formulated according to the improvement of the DHI score. (1) Healed: efficacy index  $\geq 75\%$ . (2) Excellent:  $75\% > \text{efficacy index} \geq 50\%$ . (3) Improved:  $50\% > \text{efficacy index} \geq 25\%$ . (4) Ineffective: efficacy index  $< 25\%$ . Efficacy index = (before treatment - after treatment) / before treatment score  $\times 100\%$ . Total effective = (healed + excellent + improved) number.
- (2) Chinese medicine efficacy determination criteria: formulated according to the 2012 edition of the "Diagnosis and Efficacy Criteria for Diseases and Syndromes of Traditional Chinese Medicine." (1) Healed: efficacy index  $\geq 95\%$ . (2) Excellent:  $95\% > \text{efficacy index} \geq 70\%$ . (3) Improved:  $70\% > \text{efficacy index} \geq 30\%$ . (4) Ineffective: efficacy index  $< 30\%$ . Efficacy index = (before treatment - after treatment) / before treatment score  $\times 100\%$ . Total effective = (healed + excellent + improved) number.

**2.9. Statistical Methods.** SPSS 22.0 software was applied. The test level was  $P = 0.05$ . Normally distributed measures were expressed as  $(\bar{x} \pm s)$ , one-way ANOVA was performed for comparisons between multiple groups, and the  $t$ -test was performed for two-way comparisons between groups. Count data were expressed as (%), and  $\chi^2$  was performed. Statistical differences between the data were indicated at  $P < 0.05$ .

## 3. Results

**3.1. Comparison of 3 Groups of DHI and TCM Scores.** After treatment, the total scores of DHI and TCM in the 3 groups were lower than before, and the scores of group C were lower than those of groups B and A, and group B was lower than group A ( $P < 0.05$ ) (Figures 1 and 2).

**3.2. Comparison of 3 Groups of DHI and TCM Scores Treatment Efficiency.** After treatment, in the total effective rate of the DHI score, group C (95.00%)  $>$  group B (86.67%)  $>$  group A (71.67%); in the total effective rate of the TCM score, group C (88.33%)  $>$  group B (81.67%)  $>$  group A (65.00%). After treatment, the total effective rates of DHI and TCM scores of group C and group B were statistically different from those of group A ( $P < 0.05$ ), and there was no statistical difference between group C and group B ( $P > 0.05$ ) (Tables 2 and 3).

**3.3. Comparison of 3 Groups of HAMA and HAMD Scores.** After treatment, the scores of HAMA and HAMD in the 3 groups were lower than before, and the scores of group C were lower than those of groups B and A, and group B was lower than group A ( $P < 0.05$ ) (Figures 3 and 4).

**3.4. Comparison of 3 Groups of PSQI Scores.** After treatment, the PSQI scores of the 3 groups were lower than those before, and the scores of group C were lower than those of groups B

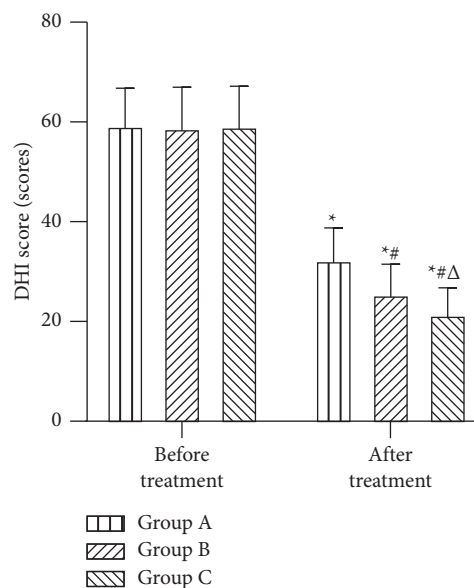


FIGURE 1: Comparison of 3 groups of DHI scores ( $\bar{x} \pm s$ , scores). Compared with the same group before treatment,  $*P < 0.05$ ; compared with group A after treatment,  $\#P < 0.05$ ; compared with group B after treatment,  $\Delta P < 0.05$ .

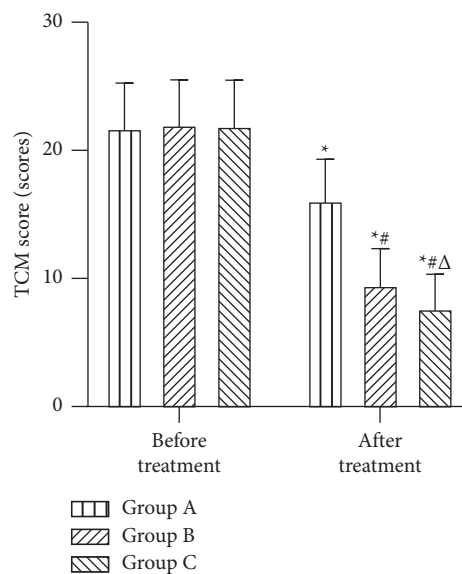


FIGURE 2: Comparison of 3 groups of TCM scores ( $\bar{x} \pm s$ , scores). Compared with the same group before treatment,  $*P < 0.05$ ; compared with group A after treatment,  $\#P < 0.05$ ; compared with group B after treatment,  $\Delta P < 0.05$ .

and A, and group B was lower than group A ( $P < 0.05$ ) (Figure 5).

**3.5. Comparison of 3 Groups of FSS Scores.** After treatment, the FSS scores of the three groups were lower than before, and the scores of group C were lower than those of group B and A, and group B was lower than group A ( $P < 0.05$ ) (Figure 6).

TABLE 2: Comparison of 3 groups of DHI score treatment efficiency ( $n$  (%)).

Group	Healed	Excellent	Improved	Ineffective	Total effective rate (%)
Group A ( $n=60$ )	2	16	25	17	43 (71.67)
Group B ( $n=60$ )	6	29	17	8	52 (86.67)*
Group C ( $n=60$ )	8	36	13	3	57 (95.00)*
$\chi^2$					12.773
$P$					0.002

Compared with group A, \* $P < 0.05$ .

TABLE 3: Comparison of 3 groups of TCM score treatment efficiency ( $n$  (%)).

Group	Healed	Excellent	Improved	Ineffective	Total effective rate (%)
Group A ( $n=60$ )	1	10	28	21	39 (65.00)
Group B ( $n=60$ )	4	25	20	11	49 (81.67)*
Group C ( $n=60$ )	5	30	18	7	53 (88.33)*
$\chi^2$					10.213
$P$					0.006

Compared with group A, \* $P < 0.05$ .

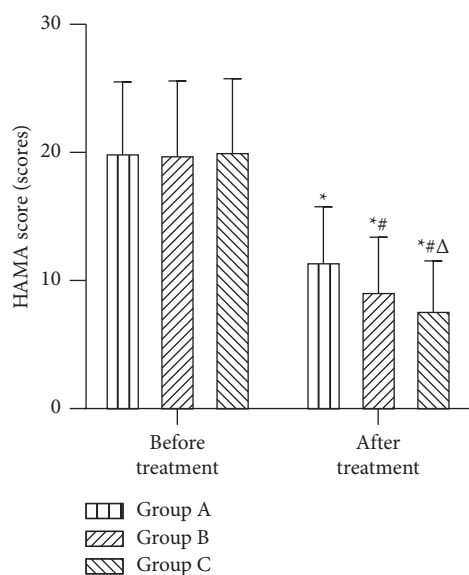


FIGURE 3: Comparison of 3 groups of HAMA scores ( $\bar{x} \pm s$ , scores). Compared with the same group before treatment, \* $P < 0.05$ ; compared with group A after treatment, # $P < 0.05$ ; compared with group B after treatment,  $\Delta P < 0.05$ .

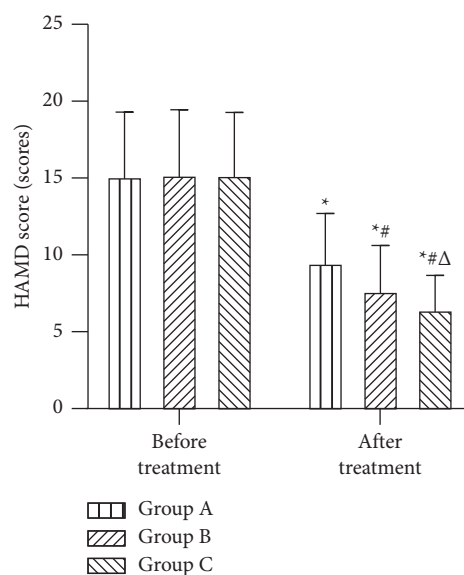


FIGURE 4: Comparison of 3 groups of HAMD scores ( $\bar{x} \pm s$ , scores). Compared with the same group before treatment, \* $P < 0.05$ ; compared with group A after treatment, # $P < 0.05$ ; compared with group B after treatment,  $\Delta P < 0.05$ .

**3.6. Comparison of 3 Groups of the Adverse Reaction Rate and Recurrence Rate.** During the treatment period, 2 patients in group A developed constipation and 2 patients with nausea and retching, with an adverse reaction rate of 6.67%; 2 patients in group B had diarrhea and 1 patient with nausea, with an adverse reaction rate of 5.00%; patients in group C had 1 case of diarrhea, 1 case of headache, and 1 case of dry mouth, and the adverse reaction rate was 5.00%. There was no statistical difference in the adverse reaction rate of the 3 groups ( $P > 0.05$ ). One month after drug withdrawal, 17 cases in group A recurred, with a recurrence rate of 28.33%; 8 cases in group B recurred, with a recurrence rate of 13.33%; and 6 cases in group C recurred, with a recurrence rate of 10.00%. The recurrence rates of group C and group B were statistically

different from group A ( $P < 0.05$ ), and there was no statistical difference between group C and group B ( $P > 0.05$ ) (Figure 7).

#### 4. Discussion

CSD was first called “space motion discomfort,” “phobic positional vertigo,” and “visual vertigo” [8]. All 3 described a phenomenon in which patients have strong discomfort or hypersensitivity to spatial position signals or complex visual signals. In addition, it has been reported that 75% of patients with phobic positional vertigo can be accompanied by significant symptoms of anxiety and depression, and it is also common in patients with visual vertigo [9]. Therefore, chronic dizziness without clear vestibular dysfunction has been called

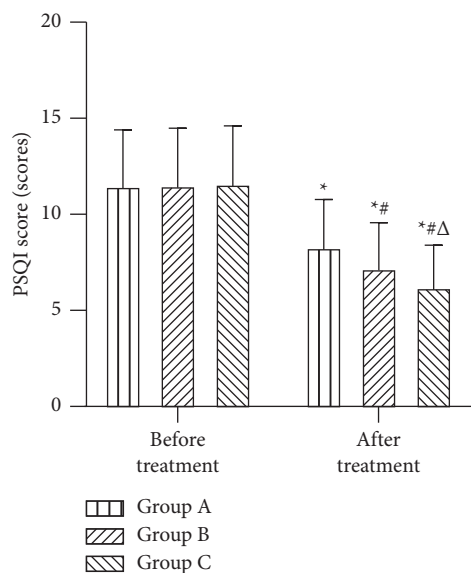


FIGURE 5: Comparison of 3 groups of PSQI scores ( $\bar{x} \pm s$ , scores). Compared with the same group before treatment,  $*P < 0.05$ ; compared with group A after treatment,  $\#P < 0.05$ ; compared with group B after treatment,  $\Delta P < 0.05$ .

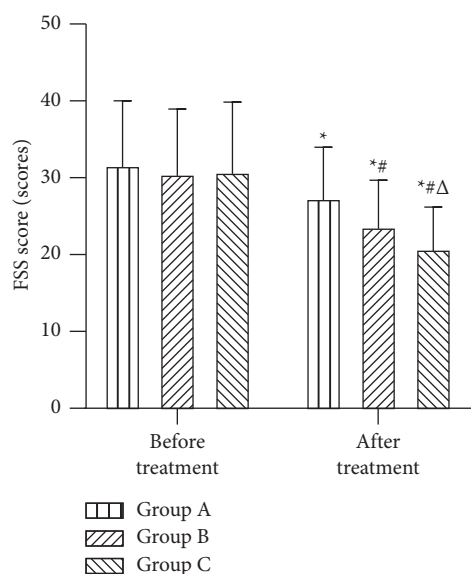


FIGURE 6: Comparison of 3 groups of FSS scores ( $\bar{x} \pm s$ , scores). Compared with the same group before treatment,  $*P < 0.05$ ; compared with group A after treatment,  $\#P < 0.05$ ; compared with group B after treatment,  $\Delta P < 0.05$ .

“mental dizziness” for a long time. From 2004 to 2005, Staab and Ruckenstein integrated the above concepts and proposed the name of CSD [10]. They believe that physical diseases (such as past neurological and otological diseases) or mental diseases (such as anxiety, depressive personality) are the main predisposing factors for CSD [11]. The clinical symptoms of the patients will not disappear with the disappearance of these predisposing factors, but will show a lingering trend with the varying degree of the patient’s condition. Based on the above, the clinical use of selective serotonin reuptake inhibitor (such as

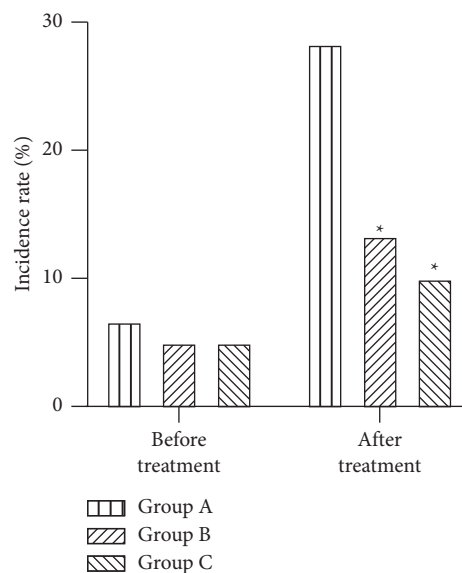


FIGURE 7: Comparison of 3 groups of the adverse reaction rate and recurrence rate ( $n$  (%)). Compared with group A,  $*P < 0.05$ .

fluoxetine, paroxetine, and sertraline) for the treatment of mental and psychological disorders can significantly improve or even completely relieve the clinical symptoms of some patients, but some patients still experience drug resistance reactions or drug side effects in long-term applications or discontinuation reactions such as palpitations, irritability, dizziness, and weakness after discontinuation of the drug [12, 13]. More safe and effective treatments still need to be sought clinically.

Through long-term clinical practice in Chinese medicine, the author found that in addition to the common symptoms of dizziness, patients with CSD may also have a series of symptoms of autonomic dysfunction such as anxiety, depression, insomnia, forgetfulness, tinnitus, lethargy, drowsiness, and dullness. Therefore, the treatment should focus on the whole, with the principle of regulating Yin and Yang, mediating the Qi machine, and dredging the surface, interior, upper, middle, and lower. Based on this, the application of holographic soup in this study is based on the theory of holographic nutrition of Chinese herbs, which believes that a certain material form or nutritional sum in Chinese herbs has the effect of preventing and controlling a corresponding certain disease. It is believed that a certain substance form or total nutrition in Chinese medicinal materials has the effect of preventing and curing corresponding diseases. This formula combines decoction of immature bitter orange, minor bupleurum decoction, cinnamon twig decoction, peptic powder, and Wuling powder in one formula. Among them, decoction of immature bitter orange can dredge Yang and dispel stagnation, resolve phlegm, and promote Qi and treat the syndrome of stagnation of phlegm and Qi in the upper heater [14]. The application of the core herbs Radix Bupleuri and licorice in minor bupleurum decoction can promote Yang and regulate Qi, harmonize Shaoyang, and mediate the gas machine in the middle heater [15]; Cinnamon twig decoction can evacuate the wind chill, reconcile the nutrient and defense,

and clear the head and eyes. Peptic powder can reduce dampness and invigorate spleen, regulate Qi and stomach, and treat the dampness and Qi resistance in the middle heater [16]. The application of Wuling powder can invigorate spleen and dispel dampness, promote Yang and diuresis, and treat the symptom of stagnation of water in the lower heater [17]. In addition, Shengdi and Moutan bark can be used to cool blood and disperse blood stasis, which can treat the syndrome of the heat-stasis in blood. The herbs are combined to unify and regulate triple burner, which has the overall regulating effect of unblocking the surface, interior, upper, middle, and lower, and communicating nutrient, defense, Qi, and blood.

In addition, the theory of TCM believes that the human body is an organic unity, and the physiological activities or pathological changes of any local organs can affect the overall physiological and pathological responses. The dysfunction of the overall function will inevitably lead to the physiological and pathological changes of the local organs. By extension, the phenomenon that a relatively independent part of an organism contains all the information of the whole is a universal law, and this is the holographic law of living things [18]. Based on this theory, the ancients believed that the concepts of the five viscera, six internal organs, Qi and blood, and pulse signs are all holographic embryo or external manifestations of the holographic embryo. They also applied local therapies such as head acupuncture, ear acupuncture, wrist-ankle acupuncture, and foot therapy to regulate the overall functional state of the patient and by stimulating the projections of the body's five internal organs and six internal organs in the corresponding acupuncture areas of the head, hands, and feet to achieve the effect of disease prevention and treatment, which is known as holographic therapy [19, 20]. Based on the above recognition, this study applied holographic scraping and five-element music to CSD patients in group C. The results showed that after treatment, the scores of DHI, TCM, HAMA, HAMD, PSQI, and FSS in the 3 groups were lower than those before, and the scores of group C were lower than those of group B and group A, and group B was lower than group A ( $P < 0.05$ ). After treatment, the total effective rates of DHI and TCM scores of group C and group B were statistically different from those of group A ( $P < 0.05$ ), and there was no statistical difference between group C and group B ( $P > 0.05$ ). This suggests that based on holographic theory, the herbal-scraping duplex method treatment is more effective in improving vertigo symptoms, mental symptoms, sleep disorders, and fatigue symptoms in CSD patients than simple drug treatment. This group of holographic scraping is a type of scraping therapy that promotes blood circulation and removes blood stasis or detoxification to the patient's local area, regulates the corresponding viscera functions, promotes the balance of Yin and Yang, and improves physical fitness. In previous studies, after holographic scraping, the body's antiviral ability and gastrointestinal absorption function of patients with headache after mixed hemorrhoid surgery were significantly improved. In this group of holographic scraping, by appropriately stimulating the patient's holographic and

meridian acupoints, it can promote the decomposition of some tissue cell proteins and the production of histamine or histamine-like and can expand local capillaries and promote blood and lymph microcycle. As a result, the hypoxic state and material metabolism of the patient's local tissues can be improved, which not only helps to achieve the effect of disease prevention and treatment but also can play the role of adjusting the whole by local holographic conditioning; ultimately, patients can fully mobilize their own potential and promote the improvement of disease susceptibility. The coordinated application of the five-element music, combined with patient's illness and mental state dialectically play the corresponding music during holographic scraping, can promote the patient's peace of mind and comfort, and help relieve their anxiety, depression, and other mental symptoms [21]. Therefore, it also has the effect of improving subjective dizziness.

The results of this study also showed that during the treatment period, there was no statistical difference in the adverse reaction rate of the 3 groups ( $P > 0.05$ ). This suggests that the safety of the application of the herbal-scraping duplex method to CSD based on the holographic theory can be guaranteed. In this study, the recurrence rate of the 3 groups was observed after 1 month of drug discontinuation, and the results showed that the recurrence rate of group C was  $10.00\% < 13.33\%$  in group B  $< 28.33\%$  in group A. The recurrence rates of group C and group B were statistically different from group A ( $P < 0.05$ ), and there was no statistical difference between group C and group B ( $P > 0.05$ ). This suggests that integrated traditional Chinese and Western medicine is more effective than simple Western medicine in improving the recurrence rate of patients, and it has a promotion value.

## 5. Conclusion

In conclusion, this study based on the holographic theory of the herbal-scraping duplex method applied to CSD patients had better results in improving symptoms and accelerating healing, and safety was ensured. In terms of reducing short-term recurrence, the two integrated traditional Chinese and Western medicine treatments are better than simple Western medicine treatment, but in the two integrated traditional Chinese and Western medicine treatments, the combined application of the herbal-scraping duplex method has no significant superimposed effect, and the observation of their long-term efficacy and recurrence still needs further in-depth study in the future.

## Data Availability

The primary data used to support the results of this study are available from the corresponding author upon request.

## Ethical Approval

This study was approved by the ethics committee of our hospital.

## Disclosure

Huanwen Luo and Caidan Liu are the co-first authors.

## Conflicts of Interest

The authors declare that they have no conflicts of interest.

## References

- [1] M. Baydan, O. Yigit, and S. Aksoy, "Does vestibular rehabilitation improve postural control of subjects with chronic subjective dizziness?" *PLoS One*, vol. 15, no. 9, Article ID e0238436, 2020.
- [2] M. Ödman and R. Maire, "Chronic subjective dizziness," *Acta Oto-Laryngologica*, vol. 128, no. 10, pp. 1085–1088, 2008.
- [3] X. Chen, J. Cheng, and J. Gong, "Deanxit can improve the dizziness, anxiety, and quality of life of patients with chronic subjective dizziness," *American Journal of Tourism Research*, vol. 13, no. 8, pp. 9348–9355, 2021.
- [4] D. Lochmann and T. Richardson, "Selective serotonin reuptake inhibitors," *Antidepressants*, vol. 250, pp. 135–144, 2019.
- [5] L. Li, P. Zhang, Z. Qin et al., "The effect of holographic meridian scraping therapy combined with free position on the labor process, perineum lateral resection rate, and delivery outcomes of primiparae," *American Journal of Tourism Research*, vol. 13, no. 8, pp. 9846–9852, 2021.
- [6] Q. Wu, Z. Liu, X. Pang, and L. Cheng, "Efficacy of five-element music interventions in perinatal mental health and labor pain: a meta-analysis," *Complementary Therapies in Clinical Practice*, vol. 40, Article ID 101217, 2020.
- [7] J. P. Staab, A. Eckhardt-Henn, A. Horii et al., "Diagnostic criteria for persistent postural-perceptual dizziness (PPPD): consensus document of the committee for the Classification of Vestibular Disorders of the Bárány Society," *Journal of Vestibular Research*, vol. 27, no. 4, pp. 191–208, 2017.
- [8] J. P. Staab, A. Eckhardt-Henn, A. Horii et al., "Diagnostic criteria for persistent postural-perceptual dizziness (PPPD): consensus document of the committee for the Classification of Vestibular Disorders of the Bárány Society," *Journal of Vestibular Research*, vol. 27, no. 4, pp. 191–208, 2017.
- [9] J. Huber, V. L. Flanagan, P. Popp, P. Eulenburg, and M. Dieterich, "Network changes in patients with phobic postural vertigo," *Brain and Behavior*, vol. 10, no. 6, Article ID e01622, 2020.
- [10] D. L. McCaslin, G. P. Jacobson, H. L. Burrows, P. Littlefield, and D. S. Haynes, "Transforming superior canal dehiscence to chronic subjective dizziness: from SCD to CSD," *Journal of the American Academy of Audiology*, vol. 21, no. 05, pp. 293–300, 2010.
- [11] J. P. Staab and M. J. Ruckenstein, "Chronic dizziness and anxiety," *Archives of Otolaryngology - Head and Neck Surgery*, vol. 131, no. 8, pp. 675–679, 2005.
- [12] A. Horii, T. Imai, T. Kitahara et al., "Psychiatric comorbidities and use of milnacipran in patients with chronic dizziness," *Journal of Vestibular Research*, vol. 26, no. 3, pp. 335–340, 2016.
- [13] B. Bandelow, "Current and novel psychopharmacological drugs for anxiety disorders," *Advances in Experimental Medicine & Biology*, vol. 1191, pp. 347–365, 2020.
- [14] Y. Tang, H. Cai, Z. Zhan et al., "Herbal medicine (zhishi xiebai guizhi decoction) for unstable angina," *Medicine*, vol. 97, no. 52, p. e13965, 2018.
- [15] S. Shao, R. Jia, L. Zhao et al., "Xiao-Chai-Hu-Tang ameliorates tumor growth in cancer comorbid depressive symptoms via modulating gut microbiota-mediated TLR4/MyD88/NF- $\kappa$ B signaling pathway," *Phytomedicine*, vol. 88, Article ID 153606, 2021.
- [16] S. P. Hu, "Recurrent respiratory infection in children treated with assistant of Ping-Wei powders--report of 45 cases," *Zhongguo Zhong Xi Yi Jie He Za Zhi*, vol. 28, pp. 85–86, 2008.
- [17] H.-N. Zhou, H.-Y. Li, W.-H. Xu et al., "Study on the action mechanism of Wuling Powder on treating osteoporosis based on network pharmacology," *Chinese Journal of Natural Medicines*, vol. 19, no. 1, pp. 28–35, 2021.
- [18] Y. Luo, M. Yang, T. Liu et al., "Effect of hand-ear acupuncture on chronic low-back pain: a randomized controlled trial," *Journal of traditional Chinese medicine = Chung i tsa chih ying wen pan*, vol. 39, pp. 587–598, 2019.
- [19] Z. L. Wang, L. F. Chen, and W. M. Zhu, "Observation on the transient analgesic effect of abdominal acupuncture TENS on pain of neck, shoulder, loin and legs," *Zhongguo Zhen Jiu*, vol. 27, pp. 657–659, 2007.
- [20] Y. You, T. Zhang, S. Shu, X. Qian, S. Zhou, and F. Yao, "Wrist-ankle acupuncture and Fluoxetine in the treatment of post-stroke depression: a randomized controlled clinical trial," *Journal of traditional Chinese medicine*, vol. 40, pp. 455–460, 2020.
- [21] J. Liao, Y. Wu, Y. Zhao et al., "Progressive muscle relaxation combined with Chinese medicine five-element music on depression for cancer patients: a randomized controlled trial," *Chinese Journal of Integrative Medicine*, vol. 24, no. 5, pp. 343–347, 2018.

## Review Article

# Research Progress in Isolation and Enrichment of Fetal Cells from Maternal Blood

**Ying Tang,<sup>1,2,3</sup> Qiaojin Tang,<sup>4</sup> Haiyan Luo,<sup>1</sup> Xuehui Zhang,<sup>5</sup> Qiuyu Chen,<sup>4</sup>  
Wenyang Tang,<sup>1,2,3</sup> Ting Wang,<sup>1,2,3</sup> Lihua Yang<sup>6</sup> ,<sup>6</sup> and Hongwu Liao<sup>1,2,3</sup> **

<sup>1</sup>The Affiliated Nanhua Hospital, Hengyang Medical School, University of South China, Hengyang 421002, Hunan, China

<sup>2</sup>The School of Nursing, Hengyang Medical School, University of South China, Hengyang 421002, Hunan, China

<sup>3</sup>The Affiliated Nanhua Hospital, Health School of Nuclear Industry, Hengyang Medical School, University of South China, Hengyang 421002, Hunan, China

<sup>4</sup>The Affiliated Nanhua Hospital, Department of Gynecology and Maternity, Hengyang Medical School, University of South China, Hengyang 421002, Hunan, China

<sup>5</sup>The Hengyang Maternal and Child Health Care Hospital, Hengyang 421001, Hunan, China

<sup>6</sup>The Affiliated Hospital of Xiangnan University, Chenzhou 423000, Hunan, China

Correspondence should be addressed to Lihua Yang; 78734460@qq.com and Hongwu Liao; nhyylhw@163.com

Received 21 November 2021; Revised 16 December 2021; Accepted 20 December 2021; Published 5 January 2022

Academic Editor: Weiguo Li

Copyright © 2022 Ying Tang et al. This is an open access article distributed under the Creative Commons Attribution License, which permits unrestricted use, distribution, and reproduction in any medium, provided the original work is properly cited.

Prenatal diagnosis is an important means of early diagnosis of genetic diseases, which can effectively reduce the risk of birth defects. Free fetal cells, as a carrier of intact fetal genetic material, provide hope for the development of high-sensitivity and high-accuracy prenatal diagnosis technology. However, the number of fetal cells is small and it is difficult to apply clinically. In recent years, noninvasive prenatal diagnosis (NIPD) technology for fetal genetic material in maternal peripheral blood has developed rapidly, which makes it possible to diagnose genetic diseases by fetal cells in maternal peripheral blood. This article reviewed the current status of fetal cell separation and enrichment technology and its application in noninvasive prenatal diagnosis technology.

## 1. Introduction

Prenatal diagnosis refers to the detection and diagnosis of an embryo or fetal development or disease before birth. The target population can be divided into the following: advanced maternal age ( $\geq 35$  years), chromosomal abnormalities of previous pregnancies or spouses, presence of genetic disorders in the family, congenital abnormalities, mental retardation, and increased risk of diagnostic testing. Prenatal diagnosis is mainly divided into invasive prenatal diagnosis and noninvasive prenatal diagnosis (NIPD). Invasive prenatal diagnosis uses interventional means to obtain fetal genetic material for analysis, including amniocentesis, umbilical cord puncture, and transcervical villus biopsy (TC-CVS) and transabdominal villus biopsy (TA-CVS), which can be performed in early pregnancy, but they have a 0.3–0.1% risk of procedural miscarriage [1, 2]. Some of these

technologies have come into play late, while others are limited to a few specific abnormalities and disease detection, and they have limitations in terms of timeliness, sensitivity, and scope of detection. Therefore, noninvasive prenatal diagnosis is becoming a hot topic. Compared with invasive prenatal diagnosis, NIPD has no risk of abortion, infection, and other risks, is simple to operate, and is more easily accepted by pregnant women who need further testing.

NIPD mainly includes diagnosis technology based on plasma cell-free fetal DNA (cffDNA) and prenatal diagnosis technology by obtaining fetal cells in maternal peripheral blood and rare fetal cells in exfoliated cells. DNA fragment diagnosis technology based on placental cells circulating in maternal blood has been widely accepted in clinic for detecting common chromosomal aneuploidy [3–5]. Although fetal cffDNA is abundant and readily available in maternal plasma, prenatal screening based on cffDNA has



been used to diagnose trisomy (13, 18, 21) and other genetic diseases (e.g., thalassemia). However, *cffDNA*-based diagnosis has some disadvantages: (1) due to *cffDNA* fragmentation, it is difficult to diagnose chromosomal mosaicism, duplication, deletion, and other abnormalities; (2) *cffDNA*-based diagnosis requires deep sequencing with high cost and low sensitivity [6–8]. Compared with the former, fetal cells contain complete cell structure and a full set of genomic information, and, with the progress of single-cell genomic detection technology, research results show that fetal cells have been able to analyze single-cell DNA accurately and specifically [9–11]. If these fetal cells were successfully isolated and their genomic DNA was amplified on a genome-wide scale, many types of genetic changes, including chromosome reversals and translocations, could be clearly detected and, in principle, repeated amplification could be done. Therefore, this cell-based NIPD is considered as a potential diagnostic test [12, 13]. Circulating fetal cells have been reported to be rare cells shed from trophoblast or umbilical cord blood into the maternal peripheral blood. Usually 1 mL of peripheral blood contains  $1 \times 10^9$  red blood cells and  $1 \times 10^6$  white blood cells but may contain only 1–10 fetal cells. Although fetal cells contain complete fetal genome information, due to the small number of these cells, effective isolation, enrichment, and identification are the primary premise of using fetal cells for related genetic analysis. This paper reviews the research progress of fetal DNA noninvasive prenatal testing based on fetal cells and prospects the future development of this field.

## 2. Classification of Fetal Cells in Maternal Peripheral Blood

Fetal cells in the peripheral blood of pregnant women are mainly divided into four categories: fetal nucleated red blood cells (FNRBC), trophoblasts, leukomonocyte, and granulocyte may form the cells.

Studies have shown that fetal cells exist in maternal peripheral blood during pregnancy; compared with maternal peripheral blood cells and epithelial cells, fetal cells in maternal peripheral blood content are very small; usually 6–8 fetal cells may only exist in 1 ml of maternal blood. The number of fetal cells in maternal blood at a given time is reproducible and can therefore be assessed by cytogenetic methods [14]. DNA has been successfully isolated from fetal cells circulating in the blood of pregnant women and can be used to diagnose fetal sex [3]. However, fetal lymphocytes and granulocytes may develop maternal tolerance to the fetus, or to maternal autoimmune diseases, and it can continue for many years [15]. This persistence makes circulating fetal lymphocytes and granulocytes unsuitable for NIPD, as their presence in subsequent pregnancies may influence test results. In contrast, FNRBC and trophoblast cells were cleared from the maternal circulation rapidly after delivery and were not detected after  $\geq 8$  weeks [16]. Therefore, at present, trophoblast cells and fetal nucleated red cells are mainly studied as fetal cells in prenatal diagnosis. However, despite cell-based enrichment methods, fetal cells are difficult to grow without contamination because only a very small number of them are present in maternal blood [3].

**2.1. Fetal Nucleated Red Blood Cells.** Among fetal cells in the maternal peripheral blood, fetal nucleated red blood cells are the most ideal cells for prenatal screening. Because FNRBC have complete fetal genetic information, the accuracy of identification in maternal blood cell populations is high, and the survival time and life cycle of FNRBC are short. After delivery, they will disappear completely in the maternal peripheral blood within 3 months. Prenatal examination Time will not be affected by past pregnancies [10]. However, its amount in the maternal blood circulation is very small, which affects the direct use of it for prenatal diagnosis. After pregnancy, the placenta becomes the communication bridge between the mother and the fetus. Similarly, maternal and fetal cells can exchange through the placenta, and the fetal cells pass through or fall off the villi and sinus space and enter the maternal circulation. The number of fetal nucleated red blood cells in the maternal peripheral blood can be affected by many factors, such as the number of red blood cells produced by the fetus itself, the integrity of the placental structure, and the immune status between the mother and the fetus. In addition, different cell capture and sorting methods can draw different conclusions because of their different sensitivity and specificity. Studies at home and abroad have shown that, under pathological pregnancy conditions with abnormal maternal placenta, such as gestational hypertension and gestational diabetes, the number of fetal nucleated red blood cells in maternal blood is significantly increased [17]. FNRBC can be seen in the peripheral blood of pregnant women in early pregnancy, with short survival time, significant morphological characteristics, and certain cell surface markers [3]. At present, the identifiable markers of fetal nucleated red blood cells include FNRBCs surface or intracellular specific antigens, such as CD71, GPA, globin, CD36, HLA-G, and EPO-R. The cells can be labeled and screened by these positive markers. Zhang et al. [18] used a microfluidic chip coated with anti-CD71 antibodies to identify 5–35 FNRBCs per 2 ml of maternal blood starting from 7 weeks of pregnancy, and SRY-PCR confirmed the fetal origin. However, studies have shown that these positive antibodies are not highly specific, leading to large false positives [14, 19]. It shows that, for rare fetal cells, the loss of fetal cells can be derived from the positive antibody enrichment method. Therefore, in subsequent research, a combination of positive antibody labeling and negative antibody labeling was used, and the combination of cell surface labeling and intracellular labeling was used to improve the capture efficiency.

**2.2. Trophoblasts.** Circulating trophoblast (CTB) cells are a type of placental-derived cells. Because of their large size, special morphology, and easy identification, they are the easiest cells to separate in theory. Compared with cell-free DNA, an important advantage of trophoblasts is that they carry the entire fetal genome without maternal DNA contamination. The first cells found in the mother's body are trophoblast cells, which are different from fetal lymphocytes and fetal bone marrow cells. They will not stay in the mother's body for many years after delivery, which will affect

the test results. Therefore, they have a unique shape and are closely related to the mother's body, and they are considered to have the biggest potential to isolate fetal cells. However, there are still some problems in the application of trophoblasts: ① the best diagnosis time of trophoblasts is early pregnancy, but only a few trophoblasts exist in the peripheral blood circulation of pregnant women. ② Because trophoblasts are large in size, they are easy to stay in the lung tissue, resulting in a small amount of maternal peripheral blood. ③ The specificity of trophoblast monoclonal antibody HLA-G and CD105 is not high. ④ Because trophoblasts come from placenta, polynuclear characteristics and chimeric karyotype of aggregated trophoblasts will interfere with the analysis of genetic results. Chung-Er Huang et al. [20] used a specific antibody, EpCAM, to connect to a silicon-based nanostructured microfluidic chip to immunoadsorb the trophoblasts in the maternal peripheral blood and then used cytokeratin-7 (+)/HLA-G(+)/DAPI(+) immunofluorescence staining to identify fetal trophoblasts, HSH, aCGH, STR analysis, and NGS technology for prenatal diagnosis of chromosomal diseases. Studies have shown that rare trophoblast cells can be used to diagnose 47, XXY, T18, and T13 syndromes [10]. To sum up, the fetal cells in the maternal peripheral blood contain the complete genetic information of the fetus and are one of the ways to diagnose single-gene diseases. However, due to their small number and difficulty in isolation, clinical transformation is limited.

**2.3. Lymphocytes.** Since the discovery of the karyotype of the male fetal lymphocytes in the peripheral blood of pregnant women in 1969, a scientific research team has successfully isolated the fetal lymphocytes from the maternal blood, but the fetal lymphocytes enter the maternal blood circulation relatively late. Due to the slow circulation of fetal lymphocytes into the mother's blood, the number of early pregnancy in the mother's blood is small, not in the prime of prenatal diagnosis. Secondly, lymphocytes still exist in the maternal peripheral blood for many years after delivery, which affects the prenatal diagnosis results of the second pregnancy [3]. In addition, fetal lymphocytes lack specific monoclonal antibodies. Therefore, fetal lymphocytes are difficult to use for prenatal diagnosis.

**2.4. Granulocyte.** The results of fetal granulocyte research are very rare. Only one team successfully isolated granulocytes from the mother's peripheral blood. The team used Ficoll density gradient centrifugation and flow cytometry to separate cells from the peripheral blood of a female who had not given birth to a male baby and used FISH to identify Y signal. This report may be due to a technical error or male cells are derived from a previous pregnancy history. Fetal granulocytes also account for 0.13%–0.26% of maternal peripheral blood mononuclear cells, but there is no effective data showing that fetal granulocytes can be used for fetal cell separation and noninvasive prenatal diagnosis.

### 3. Main Methods of Separation and Enrichment of Fetal Cells in Pregnant Women's Peripheral Blood

Because fetal cells contain 1 fetal cell in about 105 to 109 maternal cells in the peripheral blood of the mother and their number is very small, it must be separated and enriched before it can be used for noninvasive prenatal testing. The commonly used methods so far are density gradient centrifugation (DGC), filtration on chip, magnetic activated cell sorting (MACS), fluorescence activated cell sorting (FACS), microscope operation method, and so forth. The above methods have different fetal cell recovery rates and extraction purity. Therefore, a combination of different techniques and methods is usually used to improve sample purity and enrichment efficiency. Each enrichment and separation method has its own advantages and disadvantages.

**3.1. Density Gradient Centrifugation (DGC).** The density gradient centrifugation method uses the density difference between the fetal cells in the maternal blood and other cells in the peripheral blood to mix and centrifuge the Ficoll of the appropriate density with the peripheral blood and place the target cell layer in a specific density zone to separate the target cells. Studies have proved the role of this method in enriching nucleated cells and removing maternal red blood cells. According to the density of the medium used, it can be divided into single-density gradient centrifugation, double-density gradient centrifugation, and discontinuous density gradient centrifugation. Studies have shown that fetal cells can be separated from maternal blood by double-density gradient centrifugation [21]. In 2018, Feng et al. used density gradient centrifugation to initially separate fetal nucleated red blood cells and then captured them on a microfluidic chip coated with CD147 antibody and finally obtained 22–56 cells per milliliter of peripheral blood [22]. Domestic scholars Xu et al. [23] used density gradient centrifugation to concentrate peripheral blood mononuclear cells (PBMCs) from whole blood for the first time, greatly increasing the number of nucleated cells.

DGC is relatively simple in operation, short in time, and low in cost, but it is usually used as the first step of FNRBC enrichment, and then the target cells are further purified, because the number of enriched fetal cells is small and the purity is low.

**3.2. Fluorescence Activated Cell Sorting (FACS).** FACS is a technology to enrich and separate the target cell population by using the surface antigen of the target cell which specifically binds to fluorescent antibody. In 2017, Chen et al. [19] developed a double negative selection (DNS) method to isolate fetal cells from maternal peripheral blood. The method includes first using red blood cell lysate to remove red blood cells and then using magnetic beads to couple monoclonal antibodies against leukocyte surface antigen CD45, using the principle of antigen-antibody specific

binding to remove leukocytes, and then using FACS to further remove nontarget cells to obtain a suspension of a large number of target cells, and finally single cells are selected by the morphology of the fetal cells. In 2021, a study took male pregnancy cases as the research object, and FNRBC was isolated from the blood of pregnant women through FACS [24]. In order to isolate fetal cells from endocervical specimens and try to identify possible abnormalities, Erkan et al. [25] used human leukocyte antigen (HLA) G233 and placental alkaline phosphatase (PLAP) antibodies to separate fetal cells from cervical intima specimens by fluorescence activated cell sorting (FACS) and magnetic activated cell sorting (MACS). The results showed that the percentages of HLA-G233 and placental alkaline phosphatase (PLAP) positive cells were 4.55% and 84.59%, respectively. The positive rate of the two markers was 14.75%.

FACS enrichment is reliable, and the specificity of its antibody determines the purity of sorted cells. However, the cost of experimental reagents and equipment is high, the application is difficult and takes a long time, and it requires professional operations.

**3.3. Microfluidic Chip Filtration Method.** Microfluidic chip filtration method is to separate target cells by using chip microchannels and the specific size and shape of cells themselves. In 2015, Han et al. [26] reported that a microfluidic chip was used to separate FNRBC from maternal blood by a two-step cascade enrichment method. In 2017, Chinese scholar Zhao et al. [27] developed a biocompatible nanostructured microfluidic chip, which can not only separate FNRBC from maternal peripheral blood very effectively but also realize the in situ bioanalysis of FNRBC on the chip. Foreign scholars Benjamin Thierry et al. [28] published an inertial-based microfluidic chip technology to separate trophoblast cells in 2018. By removing red blood cells, the cells were introduced into the chip, and the target cells were separated according to the different sizes of white blood cells and trophoblast cells and the inertia received in the chip. Finally, the target cells were identified by fluorescence in situ hybridization (FISH) and gene sequencing, and the results were analyzed. The recovery rate can reach 79%.

The microfluidic chip method has high sensitivity, but, due to the high technical and laboratory requirements and expensive equipment, there may be a greater risk of sample contamination or loss. Therefore, the technology needs to be further optimized, and the fetal cell sorting effect needs further research.

**3.4. Magnetic Activated Cell Sorting (MACS).** MACS uses the antibody labeled by magnetic beads to specifically bind to the target cell antigen and uses the strong adsorption of magnetic beads such as attaching magnetic frame to separate the target cells, which is relatively cheaper than FACS and is widely used in the study of fetal nucleated red cells sorting. In 2019, Liesbeth Vossaert et al. used the MACS method to enrich trophoblast cells and finally enriched to 5.38 cells per

28.5 ml in maternal peripheral blood [29]. Foreign scholar Dragos Nemescu et al. [21] first separated fetal cells from maternal blood by double-density gradient centrifugation and then selected magnetic cells according to the paramagnetism of NRBC hemoglobin, converted into methemoglobin, or used anti-CD71 monoclonal antibody for positive magnetization activated cell sorting enrichment. Finally, the cells are identified by fluorescence in situ hybridization with specific chromosome X and Y probes.

MACS sorting method has the advantages of short time and relatively low cost of separating multiple samples at the same time, and the cells remain active after separation. The disadvantage is that, like FACS, the separation purity of MACS depends on the specificity of antibody, and it is difficult to avoid mother cell contamination, so it should be used in combination with other methods.

**3.5. Microscope Operation Method.** Microscope operation method is to accurately separate the target cells according to the characteristics of cells to be separated. Under the operation of platform and system, the whole operation process can be clearly seen, thus avoiding the loss of cells and the mixing of nontarget cells. Katarina Ravn et al. [30] collected blood from 13 pregnant women, used MACS method to separate and enrich circulating fetal trophoblast cells, stained with anti-cytokeratin antibody, and identified target cells using MetaSystems fluorescence microscope scanner. The advantage of this method is that it can identify and obtain a single target cell from the morphology, and the cell purity is high, which can help us distinguish the fetal origin and maternal origin of fetal cells, but it is rare in the blood circulation of pregnant women. In the separation of target cells, due to the existence of a large number of nontarget cells, the micromanipulation separation method takes too long and the workload is huge, which is not conducive to the preservation and separation of rare samples. At the same time, it also has the disadvantages of expensive operating equipment and high requirements for operating technology.

**3.6. Method Based on Nanometer Material and Microsphere Material.** The method based on nanomaterials and microsphere materials is to add microfluidic sorting platform or microsphere sorting platform to the original antibody capture, which significantly improves the antibody capture efficiency. In 2017, Tseng et al. [10] used PLGA nano-substrate structure combined with a herringbone microfluidic chip to realize the separation and capture of cTBs. Domestic scholar Lin Cheng et al. [31] used density gradient centrifugation for preliminary separation in 2019 and then captured FNRBC with SiO<sub>2</sub> microspheres coated with CD147 antibody and obtained 42–93 FNRBC/ml in peripheral blood. Wei et al. [32] combined with nucleated red blood cells by using microspheres coated with CD147 and separated by high-density Percoll centrifugation and finally enriched nucleated red blood cells with an efficiency of 84% and a purity of 80%. In summary, on the basis and with application of a large number of experiments, we found that a single method is difficult to achieve stable and efficient fetal

cell separation. It requires multiple conditions for simultaneous separation, and the efficiency, time, and cost are as close as possible to the clinical requirements.

#### 4. Identification and Application of Fetal Cells of Pregnant Women

The fetal cells enriched and purified by the above methods are not all fetal sources. Studies have shown that about 22–50% of nucleated red blood cells enriched and purified from pregnant women's peripheral blood come from mothers [33]. Therefore, purified fetal cells from pregnant women must be identified as fetal-derived or maternally derived before they can be used for prenatal testing. At present, the commonly used methods are as follows.

**4.1. Fluorescence In Situ Hybridization (FISH).** Fluorescence in situ hybridization uses specific sites of Y chromosome to design fluorescent probes, and, after hybridization, fluorescent staining can identify male fetal cells. FISH technology, which can be used as a cytogenetic method in maternal blood, is one of them. It can directly screen out abnormal chromosome cells. In 2020, foreign scholars [21] collected the peripheral blood of 27 pregnant women and enriched and separated fetal cells through DGC and MACS. The FISH analysis found at least one XY cell in 81.5% and 61.5% of cases, respectively, for paramagnetic and anti-CD71 selection. Some studies have used FNRBC specific antibodies (anti-CD147) to modify gelatin-coated silica beads to capture target cells in blood samples and then purify them. Then the released cells are analyzed by real-time PCR to verify their fetal origin, and FISH is used to detect fetal chromosomal abnormalities. The final test showed that 2 pregnant women with male fetuses were confirmed; 4 fetuses with 21-tris syndrome and 3 fetuses with trisomy 13 were confirmed [32]. He et al. [27] used an immunoaffinity chip to separate FNRBC from maternal blood and confirmed the fetal origin of the separated cells by FISH analysis.

FISH identification is short in time, low in price, and high in accuracy, but the disadvantage is that it cannot be used for quantitative analysis of cells, and the identified cells cannot be used for other detection methods, which is a loss of cell quantity.

**4.2. Polymerase Chain reaction (PCR).** PCR refers to the technique of obtaining exponentially amplified DNA sequences by repeating the DNA replication cycle, each cycle including DNA denaturation, primer annealing, primer elongation, and other processes. It can amplify the specific sequence of the entire fetal genome, obtain enough DNA for analysis, and use a minimum number of cells and quantitative analysis to identify the source of the cells. Yang et al. [34] used multiplex PCR, target capture, and next-generation sequencing to perform noninvasive prenatal diagnosis of thalassemia. Guissart et al. [35] used a universal detection method for indirect diagnosis of cystic fibrosis (CF) based on fluorescence multiplex PCR and large and small fragment analysis. The results showed that noninvasive prenatal

diagnosis from maternal peripheral blood was successfully applied 30 couples. The human leukocyte antigen sequence is specifically expressed by fetal cells, not limited to male fetal cells, and can also be identified and quantified by PCR technology. At present, the sensitivity of this type of technology has been improved, and target gene amplification can be achieved in single cells.

**4.3. Whole Genome Amplification (WGA).** Single-cell whole-genome sequencing technology is a technology to amplify and sequence the entire genome at the single-cell level. The main principle is to amplify a small amount of whole-genome DNA in a single cell. Then, after obtaining a high-coverage whole genome, high-throughput sequencing is performed. The prerequisite for obtaining accurate and comprehensive sequencing results is high-coverage, high-fidelity whole-genome amplification products. At present, there are three main methods for the more commonly used WGA: degenerate oligonucleotide PCR technology, multiple displacement amplification, and so forth. For cells fixed with soluble polytetrafluoroethylene PFA, various WGA methods need to be optimized. In 2016, the whole-genome approach was used to explore NIPD whole-genome sequencing for single-gene genetic diseases, combined with a series of bioinformatics screening, to increase the positive predictive value of new fetal mutation detection to 74% [36]. Scholar Weymaere et al. [37] discussed the effectiveness and evidential value of STR and SNP genotyping methods for 24 single cells after WGA in three families, using formaldehyde-fixed cells and unfixed cells in the offspring-parent combination. The results showed that the two genotyping methods could be used in all test conditions and scenarios, and the sensitivity and specificity are 100%, and the evidence values for fixed cells and nonfixed cells are similar. In addition, sequence-based SNP genotyping has higher evidential value than length-based STR genotyping after WGA, which cannot be observed using a large number of high-quality progenitor DNA samples.

**4.4. High-Throughput Sequencing Technology (NGS).** High-throughput sequencing technology can comprehensively analyze the genome and transcriptome of a species. Compared with traditional PCR or FISH, NGS can provide high-throughput and basic-level genetic analysis information more quickly, and NGS can detect and analyze multiple gene loci at the same time, which is the gold standard for maternal and fetal cell recognition. It does not need multiple restriction endonuclease digestion reactions, and the accuracy rate is higher than that of traditional methods, reaching 100%, which is the direction of cell recognition in the future. NGS still has some disadvantages, such as high cost and inconvenient separation of target cells. Hua et al. [38] found in 2015 that the whole-genome sequencing (WGS) method can successfully detect aneuploidy diseases in individual FNRBC. With the increasing optimization of technology, those diseases caused by insertion/deletion and point mutation are expected to be confirmed by fetal cells in maternal blood. Yu et al. [39] used NGS to detect fetal aneuploidy, and

NIPD was used to detect aneuploidy in 26 fetuses, of which 18 fetal aneuploidies occurred in only one fetus of twins. The aneuploidy rates of double-chorionic twins were 1.3% and 0.5% of single-chorionic twins. The incidence of aneuploidy was 1.2% in the spontaneous pregnancy group and 1.1% in the assisted reproductive technology group. Huada Gene Research Group, for the first time, confirmed that the fetal cells separated by double negative selection combined with deep sequencing (used for screening single-gene diseases) had high-coverage rate of WGS (86.8%) and allele loss rate of 24.90% [19]. In 2021, the scholar Noriko et al. [24] have found that FNRCs in the maternal circulation can be selectively separated by single-cell sorting, and their fetal origin can be confirmed by real-time PCR and WGS.

Fetal cells in the peripheral blood of pregnant women can be used as a source of genetic material for prenatal testing after identification, and corresponding molecular biology techniques can be used to detect diseases. At present, FNRBC has been applied to noninvasive prenatal diagnosis, detecting fetal-related phenotype and diseases such as fetal sex, the blood type, chromosome abnormality, and HLA polymorphism. Some scholars [31] carried out prenatal testing of the fetal ABO blood type by capturing FNRBC and testing the obtained samples. It was shown that the results of testing the fetal blood type were consistent with the results after birth. In 2018, Zhang et al. [18] used fetal nucleated red blood cells to conduct gender identification. Experiments showed that the gender of 20 samples of fetuses was consistent with the detection results of free DNA. At present, FNRBC can be labeled and screened by corresponding markers, such as CD36, HLA-G, globin, and CD71.

In recent years, due to the discovery of new antigens on the surface of trophoblasts and the introduction of new enrichment methods, the application of trophoblasts in prenatal diagnosis has attracted people's attention. A study in 2016 pointed out that the multisite STR and SNP sequencing analysis of the enriched trophoblast cells found that their genotypes are completely consistent with the placental genotypes [40]. Vossaert et al. showed in 2018 that circulating trophoblast cells can be separated by single cells for the detection of chromosome microdeletion, with a resolution of up to 1 to 2 Mb [41].

For fetal lymphocytes and granulocytes, fetal lymphocytes are similar to maternal lymphocytes in immunology, and it is not easy to find fetal specific antibodies, so it is not the best choice for prenatal diagnosis. At present, there is no report of successful isolation of fetal granulocytes, so it is rarely used in prenatal diagnosis.

With the development of technology, fetal cells in maternal peripheral blood will play an important role in monogenic genetic diseases. Besides, these cells can also be used to understand fetal ABO type [31]. It has a certain significance for the diagnosis of neonatal hemolysis. NGS can be used to identify the fetal genotype, which is also of guiding significance to the nutrition absorption during pregnancy and prenatal and postnatal care.

## 5. Problems and Prospects

In conclusion, maternal peripheral blood fetal cells have a wide range of applications and development prospects in prenatal diagnosis and prenatal screening, and technical optimization and clinical data demonstration are still needed to evaluate whether it can truly surpass the existing NIPT detection and become a real technical method for clinical application. At present, the enrichment and detection methods of fetal cells in maternal peripheral blood are not perfect. Therefore, we need to further search for more effective and more sensitive identification methods. In addition, a unified quality evaluation standard should be established for the various enrichment and detection methods developed, which is more conducive to promoting the clinical transformation of circulating fetal cells. It is believed that, with the continuous development and optimization of science and technology, its application prospect is more and more broad. The detection methods of fetal cells in peripheral blood of pregnant women will get more choices and be widely used in prenatal diagnosis.

## Data Availability

The data used to support the findings of this study are included within the article.

## Disclosure

Ying Tang and Qiaojin Tang are the co-first authors.

## Conflicts of Interest

The authors declare that they have no conflicts of interest.

## Acknowledgments

This work was supported by the Science and Technology Innovation Program of Hunan Province (2018SK51712 and 2018SK51713).

## References

- [1] L. J. Salomon, A. Sotiriadis, C. B. Wulff, A. Odibo, and R. Akolekar, "Risk of miscarriage following amniocentesis or chorionic villus sampling: systematic review of literature and updated meta-analysis," *Ultrasound in Obstetrics and Gynecology*, vol. 54, no. 4, pp. 442–451, 2019.
- [2] "Practice bulletin No. 162: prenatal diagnostic testing for genetic disorders," *Obstetrics & Gynecology*, vol. 127, no. 5, pp. e108–e122, 2016.
- [3] S. H. Guseh, "Noninvasive prenatal testing: from aneuploidy to single genes," *Human Genetics*, vol. 139, no. 9, pp. 1141–1148, 2020.
- [4] L. Hui, "Noninvasive approaches to prenatal diagnosis: historical perspective and future directions," *Prenatal Diagnosis*, vol. 1885, pp. 45–58, 2019.
- [5] J. R. Vermeesch, T. Voet, and K. Devriendt, "Prenatal and pre-implantation genetic diagnosis," *Nature Reviews Genetics*, vol. 17, no. 10, pp. 643–656, 2016.

- [6] B. Renga, "Non invasive prenatal diagnosis of fetal aneuploidy using cell free fetal DNA," *European Journal of Obstetrics & Gynecology and Reproductive Biology*, vol. 225, pp. 5–8, 2018.
- [7] O. M. Y. Ngan, H. Yi, and S. Ahmed, "Service provision of non-invasive prenatal testing for Down syndrome in public and private healthcare sectors: a qualitative study with obstetric providers," *BMC Health Services Research*, vol. 18, no. 1, p. 731, 2018.
- [8] X. Li, T. Yang, C. S. Li, L. Jin, H. Lou, and Y. Song, "Prenatal detection of thalassemia by cell-free fetal DNA (cffDNA) in maternal plasma using surface enhanced Raman spectroscopy combined with PCR," *Biomedical Optics Express*, vol. 9, no. 7, pp. 3167–3176, 2018.
- [9] A. M. Breman, J. C. Chow, L. U'Ren et al., "Evidence for feasibility of fetal trophoblastic cell-based noninvasive prenatal testing," *Prenatal Diagnosis*, vol. 36, no. 11, pp. 1009–1019, 2016.
- [10] S. Hou, J.-F. Chen, M. Song et al., "Imprinted NanoVelcro microchips for isolation and characterization of circulating fetal trophoblasts: toward noninvasive prenatal diagnostics," *ACS Nano*, vol. 11, no. 8, pp. 8167–8177, 2017.
- [11] S. Kølvrå, R. Singh, and E. A. Normand, "Genome-wide copy number analysis on DNA from fetal cells isolated from the blood of pregnant women," *Prenatal Diagnosis*, vol. 36, no. 12, pp. 1127–1134, 2016.
- [12] C. Pin-Jung, T. Pai-Chi, and Y. Zhu, "Noninvasive prenatal diagnostics: recent developments using circulating fetal nucleated cells," *Curr Obstet Gynecol Rep*, vol. 8, no. 1, pp. 1–8, 2019.
- [13] O. Pös, J. Budiš, and T. Szemes, "Recent trends in prenatal genetic screening and testing," *F1000Research*, vol. 8, p. 764, 2019.
- [14] K. Krabchi, F. Gros-Louis, J. Yan et al., "Quantification of all fetal nucleated cells in maternal blood between the 18th and 22nd weeks of pregnancy using molecular cytogenetic techniques," *Clinical Genetics*, vol. 60, no. 2, pp. 145–150, 2001.
- [15] D. W. Bianchi, K. Khosrotehrani, S. S. Way, T. C. MacKenzie, I. Bajema, and K. O'Donoghue, "Forever connected: the lifelong biological consequences of fetomaternal and maternofetal microchimerism," *Clinical Chemistry*, vol. 67, no. 2, pp. 351–362, 2020.
- [16] A. Looij, R. Singh, L. Hatt et al., "Do fetal extravillous trophoblasts circulate in maternal blood postpartum?" *Acta Obstetrica et Gynecologica Scandinavica*, vol. 99, no. 6, pp. 751–756, 2020.
- [17] G. Hu, R. Guan, and L. Li, "Nucleated red blood cell count in maternal peripheral blood and hypertensive disorders in pregnant women," *The American Journal of the Medical Sciences*, vol. 351, no. 2, pp. 140–146, 2016.
- [18] H. Zhang, Y. Yang, X. Li et al., "Frequency-enhanced transferrin receptor antibody-labelled microfluidic chip (FETAL-Chip) enables efficient enrichment of circulating nucleated red blood cells for non-invasive prenatal diagnosis," *Lab on a Chip*, vol. 18, no. 18, pp. 2749–2756, 2018.
- [19] F. Chen, P. Liu, Y. Gu et al., "Isolation and whole genome sequencing of fetal cells from maternal blood towards the ultimate non-invasive prenatal testing," *Prenatal Diagnosis*, vol. 37, no. 13, pp. 1311–1321, 2017.
- [20] C.-E. Huang, G.-C. Ma, H.-J. Jou et al., "Noninvasive prenatal diagnosis of fetal aneuploidy by circulating fetal nucleated red blood cells and extravillous trophoblasts using silicon-based nanostructured microfluidics," *Molecular Cytogenetics*, vol. 10, no. 1, p. 44, 2017.
- [21] D. Nemescu, D. Constantinescu, V. Gorduza, A. Carauleanu, L. Caba, and D. B. Navolan, "Comparison between paramagnetic and CD71 magnetic activated cell sorting of fetal nucleated red blood cells from the maternal blood," *Journal of Clinical Laboratory Analysis*, vol. 34, no. 9, Article ID e23420, 2020.
- [22] C. Feng, Z. He, B. Cai et al., "Non-invasive prenatal diagnosis of chromosomal aneuploidies and microdeletion syndrome using fetal nucleated red blood cells isolated by nanostructure microchips," *Theranostics*, vol. 8, no. 5, pp. 1301–1311, 2018.
- [23] S. Xu, L. Wu, Y. Qin et al., "Sequential ensemble-decision aliquot ranking isolation and fluorescence in situ hybridization identification of rare cells from blood by using concentrated peripheral blood mononuclear cells," *Analytical Chemistry*, vol. 93, no. 6, pp. 3196–3201, 2021.
- [24] N. Ito, K. Tsukamoto, K. Taniguchi et al., "Isolation and characterization of fetal nucleated red blood cells from maternal blood as a target for single cell sequencing-based non-invasive genetic testing," *Reproductive Medicine and Biology*, vol. 20, no. 3, pp. 352–360, 2021.
- [25] E. Yurtcu, D. Karçaaltincaba, H. H. Kazan et al., "Is cervical swab an efficient method for developing a new noninvasive prenatal diagnostic test for numerical and structural chromosome anomalies?" *Turkish Journal of Medical Sciences*, vol. 51, no. 3, pp. 1043–1048, 2021.
- [26] Y. Byeon, C. S. Ki, and K. H. Han, "Isolation of nucleated red blood cells in maternal blood for Non-invasive prenatal diagnosis," *Biomedical Microdevices*, vol. 17, no. 6, pp. 118–18, 2015.
- [27] Z. He, F. Guo, C. Feng et al., "Fetal nucleated red blood cell analysis for non-invasive prenatal diagnostics using a nanostructure microchip," *Journal of Materials Chemistry B*, vol. 5, no. 2, pp. 226–235, 2017.
- [28] Marnie, Winter, and Tristan, "Isolation of circulating fetal trophoblasts using inertial microfluidics for noninvasive prenatal testing," *Advanced materials technologies*, vol. 3, no. 7, p. 1800066, 2018.
- [29] L. Vossaert, Q. Wang, R. Salman et al., "Validation studies for single circulating trophoblast genetic testing as a form of noninvasive prenatal diagnosis," *The American Journal of Human Genetics*, vol. 105, no. 6, pp. 1262–1273, 2019.
- [30] K. Ravn, R. Singh, L. Hatt et al., "The number of circulating fetal extravillous trophoblasts varies from gestational week 6 to 20," *Reproductive Sciences*, vol. 27, no. 12, pp. 2170–2174, 2020.
- [31] L. Cheng, X. Wei, Z. Wang et al., "Silica microbeads capture fetal nucleated red blood cells for noninvasive prenatal testing of fetal ABO genotype," *Electrophoresis*, vol. 41, no. 10-11, pp. 966–972, 2020.
- [32] X. Wei, Z. Ao, L. Cheng et al., "Highly sensitive and rapid isolation of fetal nucleated red blood cells with microbead-based selective sedimentation for non-invasive prenatal diagnostics," *Nanotechnology*, vol. 29, no. 43, Article ID 434001, 2018.
- [33] A. Mavrou, E. Kouvidi, A. Antsaklis, A. Souka, S. Kitsiou Tzeli, and A. Kolialexi, "Identification of nucleated red blood cells in maternal circulation: a second step in screening for fetal aneuploidies and pregnancy complications," *Prenatal Diagnosis*, vol. 27, no. 2, pp. 150–153, 2007.
- [34] X. Yang, Y. Ye, D. Fan et al., "Non-invasive prenatal diagnosis of thalassemia through multiplex PCR, target capture and next-generation sequencing," *Molecular Medicine Reports*, vol. 22, no. 2, pp. 1547–1557, 2020.
- [35] C. Guissart, F. Tran Mau Them, V. Debant et al., "A broad test based on fluorescent-multiplex PCR for noninvasive prenatal diagnosis of cystic fibrosis," *Fetal Diagnosis and Therapy*, vol. 45, no. 6, pp. 403–412, 2019.

- [36] K. C. A. Chan, P. Jiang, K. Sun et al., "Second generation noninvasive fetal genome analysis reveals de novo mutations, single-base parental inheritance, and preferred DNA ends," *Proceedings of the National Academy of Sciences*, vol. 113, no. 50, pp. E8159–E8168, 2016.
- [37] J. Weymaere, A.-S. Vander Plaetsen, L. Tilleman et al., "Kinship analysis on single cells after whole genome amplification," *Scientific Reports*, vol. 10, no. 1, Article ID 14647, 2020.
- [38] R. Hua, A. N. Barrett, T. Z. Tan et al., "Detection of aneuploidy from single fetal nucleated red blood cells using whole genome sequencing," *Prenatal Diagnosis*, vol. 35, no. 7, pp. 637–644, 2015.
- [39] W. Yu, Y. Lv, S. Yin et al., "Screening of fetal chromosomal aneuploidy diseases using noninvasive prenatal testing in twin pregnancies," *Expert Review of Molecular Diagnostics*, vol. 19, no. 2, pp. 189–196, 2019.
- [40] C. V. Jain, L. Kadam, M. van Dijk et al., "Fetal genome profiling at 5 weeks of gestation after noninvasive isolation of trophoblast cells from the endocervical canal," *Science Translational Medicine*, vol. 8, no. 363, Article ID 363re4, 2016.
- [41] L. Vossaert, Q. Wang, R. Salman et al., "Reliable detection of subchromosomal deletions and duplications using cell-based noninvasive prenatal testing," *Prenatal Diagnosis*, vol. 38, no. 13, pp. 1069–1078, 2018.

## Research Article

# Mechanism of Baclofen Inhibiting the Proliferation and Metastasis of GBM by Regulating YAP

Lin Zhu,<sup>1,2</sup> Juan Lu,<sup>3</sup> Zhijun Bao,<sup>2</sup> and Shiwen Guo<sup>1</sup> 

<sup>1</sup>Department of Neurosurgery, The First Affiliated Hospital of Xi'an, Jiaotong University, Xi'an 710061, China

<sup>2</sup>Department of Neurosurgery, Affiliated3201 Hospital of Xi'an Jiaotong University, Han Zhong 723000, China

<sup>3</sup>School of Foreign Studies, Shaanxi University of Technology, Han Zhong 723000, China

Correspondence should be addressed to Shiwen Guo; zhr6962012@163.com

Received 30 October 2021; Accepted 27 November 2021; Published 29 December 2021

Academic Editor: Weiguo Li

Copyright © 2021 Lin Zhu et al. This is an open access article distributed under the Creative Commons Attribution License, which permits unrestricted use, distribution, and reproduction in any medium, provided the original work is properly cited.

This study explores the effect of baclofen on the malignant phenotype of glioblastoma (GBM) and the growth of xenograft tumors and investigates the related mechanisms, aiming to reveal the effect of baclofen on the occurrence and development of GBM. The development of new therapeutic drugs for GBM lays a theoretical and experimental foundation. Research results show that baclofen could inhibit GBM cell proliferation and migration and promote GBM cell apoptosis; baclofen dose- and time-dependently could induce GBM cell YAP phosphorylation. YAP participated in the effect of baclofen on GBM cell proliferation and migration inhibition. Baclofen induced YAP phosphorylation in GBM cells through the GABABR2-Gs-Lats1/2 signaling pathway. Baclofen could inhibit the expression of survivin and Bcl2. Baclofen inhibits subcutaneous tumors by inducing YAP phosphorylation in vivo.

## 1. Introduction

Glioma is the most important and common central nervous system tumor and fatal primary brain tumor [1]. It is estimated that glioblastoma (GBM) accounts for 55% of all brain tumors [2]. Although radiation therapy, chemotherapy, and surgery have made great progress in the treatment of tumors, the prognosis of malignant GBM is still very poor, and the average survival time of patients is less than 1.5 years [3]. GBM is high malignant glioma. The molecular mechanism of GBM is a multistep development process of multigene changes [4]. In clinicopathology, the occurrence of GBM can be expressed in two different ways: primary and recurrent, suggesting that there may be some differences in molecular genetic changes between primary and recurrent GBM [5]. Previous efforts in GBM genome characterization identified GBM genes including growth factor receptors (EGFR, KIT, PDGFRA, FGFR1, FGFR3, and MET), mitogen-activated protein kinase (MAPK), and phosphoinositide 3-kinase (PI3K) signaling pathways, which includes PTEN, PIK3CA, NF1, BRAF, cell cycle pathways (MDM2, TP53,

CDK4/6, and RB1), and others (IDH1, MYC, and MYCN) [6]. With the further understanding of the molecular pathways driving malignant tumors in malignant GBM, various biomarkers and several drugs targeting specific molecular pathways in malignant cells have been developed. Despite the progress of current treatment, the prognosis of GBM is still poor, and the median survival time is only 12–15 months [7, 8]. In addition, in GBM, rapid tumor development and resistance to chemotherapy and radiotherapy are common, resulting in low 1-year survival. Therefore, further research is needed to explore the molecular mechanism of glioma progression and find new and effective glioma treatment strategies.

The Hippo pathway is an evolutionary conserved kinase cascade. The mammalian Hippo pathway consists of a dual kinase module, in which Mst1 and mst2 (Hippo homology in *Drosophila*) cooperate with their binding partner SAV1 to phosphorylate and activate Lats1/2. With the help of co-factor mob-1, they directly phosphorylate YAP and TAZ, resulting in cytoplasmic retention and proteomic degradation. In the “Hippo OFF” state, YAP/TAZ is set free of



inhibitory phosphorylation [9]. When the upstream kinase is inactivated, dephosphorylated YAP/TAZ translocates to the nucleus, binds to TEAD1-4, and induces the expression of target genes [10]. Hippo signaling pathways play pivotal roles in governing organ size through balancing cell proliferation and apoptosis; moreover, accumulating evidence suggests that the Hippo pathway is dysregulated in GBM [11]. Studies have found that YAP-expressed GBM cells showed stronger tumorigenicity and caused enhanced tumor growth [12]. Nicholas Artinian et al. discovered that Ser<sup>760</sup>-phosphorylated AMOTL2 is incapable of binding YAP and leads to YAP-induced GBM cell migration and invasiveness [13]. Although the overexpression of YAP promotes the proliferation and invasion of GBM cancer cell lines, the role of YAP in the formation and progression of new cancers remain unclear. Understanding the molecular mechanism of heterogeneous tumor cell population in brain tumors may have a far-reaching impact on treatment management.

$\gamma$ -Aminobutyric acid (GABA) is an important inhibitory neurotransmitter in the central nervous system. It has good water solubility and thermal stability. It has been proved that GABA, as a small molecular weight nonprotein amino acid, has edible safety and can be used in the production of beverages and other foods. Studies have shown that a certain amount of GABA can improve the body's sleep quality and reduce blood pressure. GABA acts on two different types of receptors and provides a powerful inhibitory effect based on their physiological and pharmacological properties. GABA type A (GABAA) receptor is a ligand-gated chloride channel which mediates fast inhibitory signals through rapid postsynaptic membrane hyperpolarization, whereas the metabotropic GABAB receptor produces slow and prolonged inhibitory signals via G proteins and second messengers. GABAB receptors are members of class CG protein-coupled receptor (GPCR) family. GABAB receptors are prototypical heterodimers of R1 and R2 subunits; it is necessary for GABAB receptors to form R1/R2 heterodimers to produce GABA-mediated GPCR functions. Recent studies suggest that the Hippo pathway is a downstream branch of GPCR signaling. Many GPCRs mediated signals can modulate YAP/TAZ activity depending on the type of downstream G proteins [10]. However, GABA signaling remains extremely complex, and the multiple possible interaction of GABA (B) subunits with the Hippo pathway in GBM has not been well established. The mechanism of action of related proteins is shown in Figure 1.

Baclofen, ( $\pm$ )-4-amino-3-(p-chlorophenyl)-butanoic acid, is a structural analog of GABA. Baclofen can cross the blood-brain barrier via neutral amino acid transporters, acting as agonist of the GABAB receptor [14–16]. Baclofen was shown to reduce hepatocellular carcinoma, gastric, and colon cancer development in vitro and in vivo [17, 18], but its relationship with GMB has not yet been reported so far. In this study, we found that baclofen could inhibit the proliferation and migration of GBM cells, which reduce the invasiveness of GBM, in a dose- and time-dependent manner. Molecular mechanisms underlying the baclofen's effects are related to YAP of the Hippo pathway. What is more, baclofen induced phosphorylation of YAP in GBM cells through the GABABR1/2-Gs-Lats1/2 signaling pathway, which leads to the degradation

of YAP, and pYAP could not activate the downstream surviving genes such as survivin and Bcl2, and lower level of proliferation-associated genes may be the reason of tumor inhibition. This may explain baclofen GBM cancer inhibition mechanism.

## 2. Methods

**2.1. Cell Culture and Transfection.** U251 cells were purchased from Cell bank of representative culture preservation Committee of Chinese Academy of Sciences. U251 cells were cultured in DMEM (Dulbecco's modified Eagle's medium, ThermoFisher, Shanghai, China) supplemented with 10% FBS (fetal bovine serum, ThermoFisher, Shanghai, China) and cultured at 37°C in a 5% CO<sub>2</sub> incubator. GABABR2 shRNA plasmids (sc-42463-SH) were purchased from Santa Cruz; YAP downregulated and upregulated lentiviruses were constructed and obtained from GeneChem (Shanghai, China). The transfection process was carried out according to the manufacturer's guidance.

**2.2. Proliferation Assay [19].** Cell Counting Kit-8 (APEX-BIO, USA) was purchased for detecting the cell proliferation rate.  $1 \times 10^3$  treated cells were seeded in 96-well plates per well and cultured at 37°C and 5% CO<sub>2</sub> for 24 hours. Cells were cultured after 12, 24, and 48 hours, respectively, and incubated with CCK-8 testing solution for 2 hours. Then, absorbance was measured at the wavelength of 450 nm to represent the cell proliferation ability.

**2.3. Transwell Assay [19].** Cell suspension was prepared, and  $1 \times 10^5$  cells/well were inoculated into the supraventricular cavity of Transwell. 100  $\mu$ L serum-free DMEM medium was added to the superior chamber: 15% fetal bovine serum and 600  $\mu$ L DMEM medium. The cells were routinely cultured for 24 hours. Then, the cells on the surface of the lower membrane were fixed with 4% paraformaldehyde and stained with crystal violet. The migrated cells were fixed and counted.

**2.4. Western Blot.** The total protein of GBM cells was extracted, and the protein concentration was measured. Make SDS-polyacrylamide gel to separate the protein and transfer it to PVDF membrane (Millipore, USA). 5% nonfat milk was used to block the transferred PVDF membrane. Then, phospho-YAP (1 : 1000), YAP (1 : 1000), GABABR1 (1 : 500), anti-GABABR2 (1 : 2000), Lats1 (1 : 1000), Lats2 (1 : 1000), survivin (1 : 1000), and Bcl2 (1 : 1000) primary antibodies were incubated overnight at 4°C, and secondary antibodies (1 : 10000) were incubated for 1 hour. ECL chemiluminescent kit and Quantity One software were used to detect the protein expression level.

**2.5. Apoptosis [19].** FAM-FLICA® caspase-3/7 assay kit was used to detect the apoptosis rate. FLICA was added to each sample at 1 : 30 and incubated for 1 hour. Then, the fluorescence microscope was used to detect the caspase3/7 activity. FAM-FLICA excites at 492 nm and emits at 520 nm.

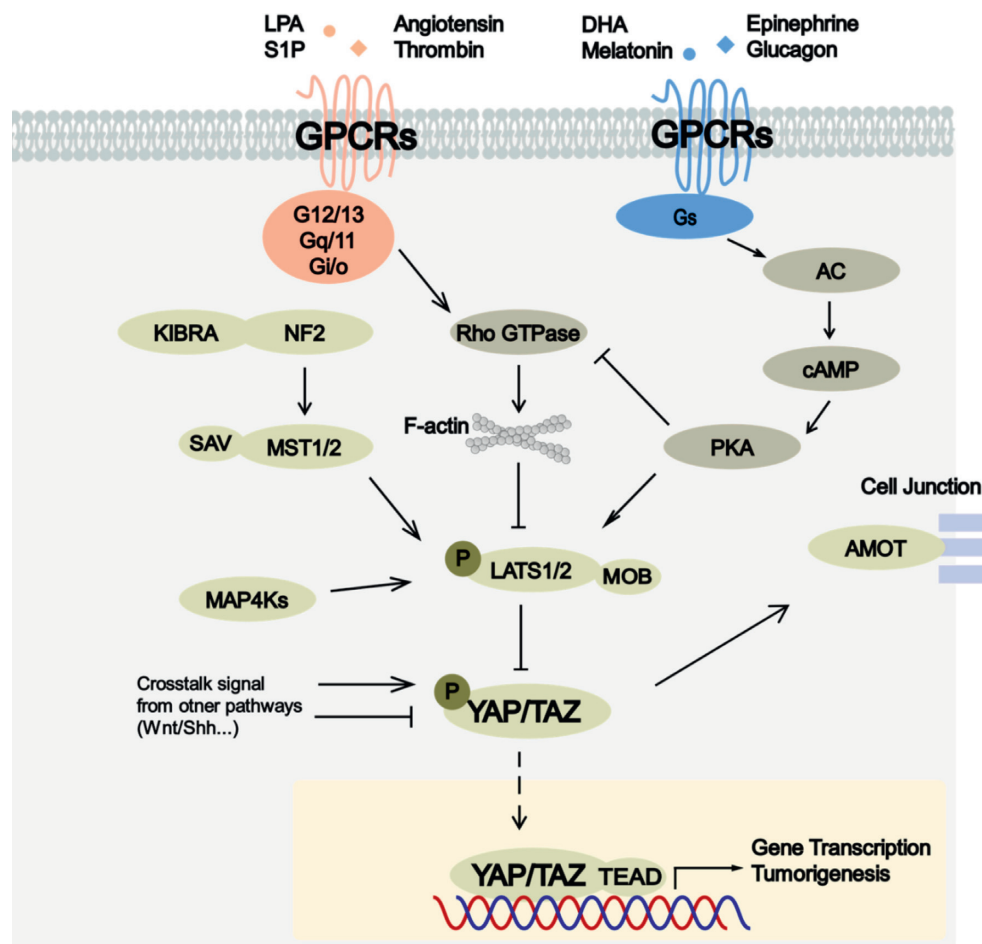


FIGURE 1: Diagram of the mechanism of protein action.

**2.6. Animal Model.** Ten four-week-old nude mice were recruited (18–22 g, Beijing Weitong Lihua Laboratory Animal Technology Co., Ltd.). We used  $2 \times 10^6$  U251 cells to subcutaneously inject into the left flank of the nude mice. Mice were randomly classified into the control group (0.9% NaCl injected from tail vein) and baclofen treatment group (100  $\mu\text{M}$  baclofen injected from tail vein). Thirty days later, the tumor was collected, and the changes of various proteins in the tumor tissue were detected. Tumor volume was calculated as  $0.5 \times \text{length} \times \text{width}^2$  every third day.

**2.7. Statistics.** The statistics analysis was conducted, and figures were graphed using GraphPad Prism 8.2. Student's *t*-test was used to evaluate the differences between two groups. One-way ANOVA was used to investigate the statistical significance among multiple groups.  $P < 0.05$  was thought to be statistically significant.

### 3. Results

**3.1. Baclofen Inhibited Proliferation and Migration and Promoted Apoptosis of GBM Cells.** In order to investigate the function of baclofen, we treated GBM cells (U251) with 10, 50, 100, and 120  $\mu\text{M}$  baclofen for 18 hours. After that, we found that 100  $\mu\text{M}$  or more baclofen could significantly

suppress the viability of U251 (Figure 2(a)). Moreover, baclofen could inhibit the migration of and promote the apoptosis of GBM cells (Figures 2(b) and 2(c)).

**3.2. Baclofen Dose- and Time-Dependently Induced Phosphorylation of YAP in GBM Cells.** We treated U251 cell line with 10, 50, 100, and 120  $\mu\text{M}$  baclofen, respectively. The results turned out that YAP phosphorylation was induced when treated with 50  $\mu\text{M}$  baclofen; besides, 100  $\mu\text{M}$  baclofen was the optimal concentration in inducing the phosphorylation of YAP (Figure 3(a)). Furthermore, we used 100  $\mu\text{M}$  baclofen to treat U251 cell line for 12, 18, 24, and 36 hours and found that the phosphorylation of YAP was induced on the condition that baclofen was incubated with U251 cell line for at least 18 hours (Figure 3(b)).

**3.3. YAP Involved in Baclofen-Induced Inhibition of Proliferation and Migration of GBM Cells.** After downregulating the expression of YAP, the proliferation and migration ability of U251 were significantly suppressed (Figures 4(a) and 4(b)). Besides, the overexpression of YAP resulted in increased proliferation and migration rate (Figures 4(c) and 4(d)). We then increased the YAP expression in baclofen-incubated U251 cell line, and we noticed that baclofen-

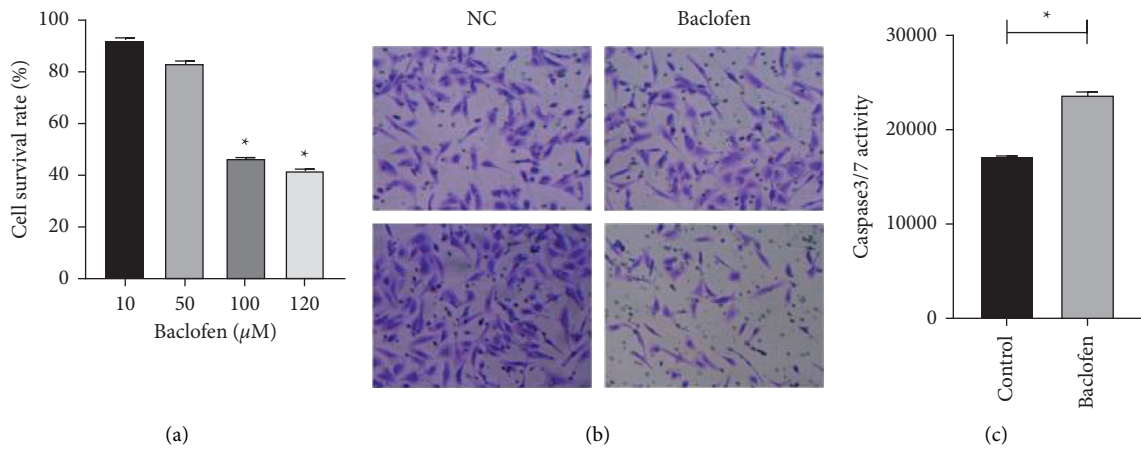


FIGURE 2: Baclofen inhibited proliferation and migration and promoted apoptosis of GBM cells. \*Statistical significance compared with the control group.

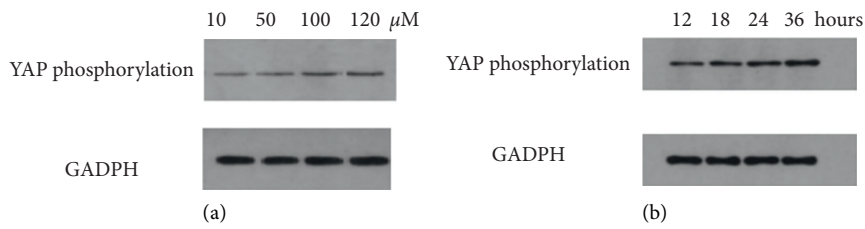


FIGURE 3: Baclofen dose and time-dependently induced phosphorylation of YAP in GBM cells.

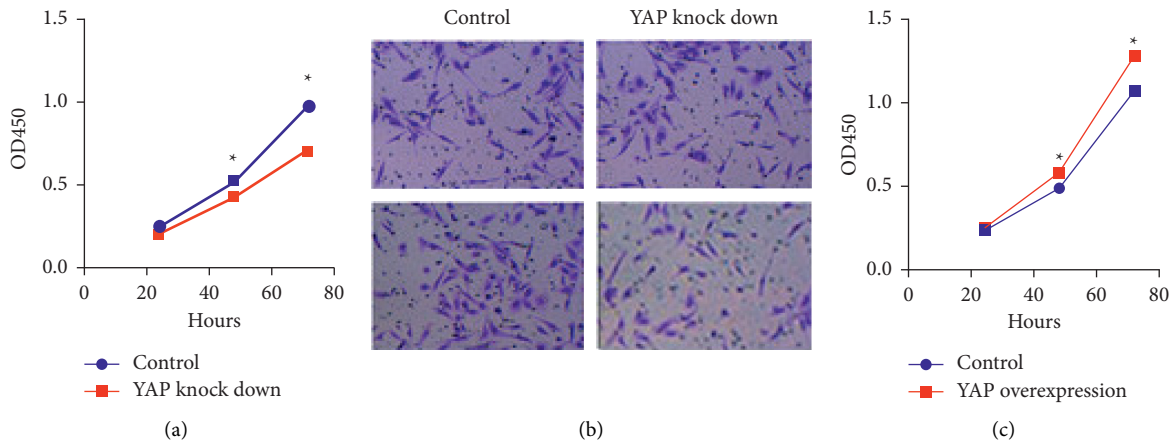


FIGURE 4: Continued.

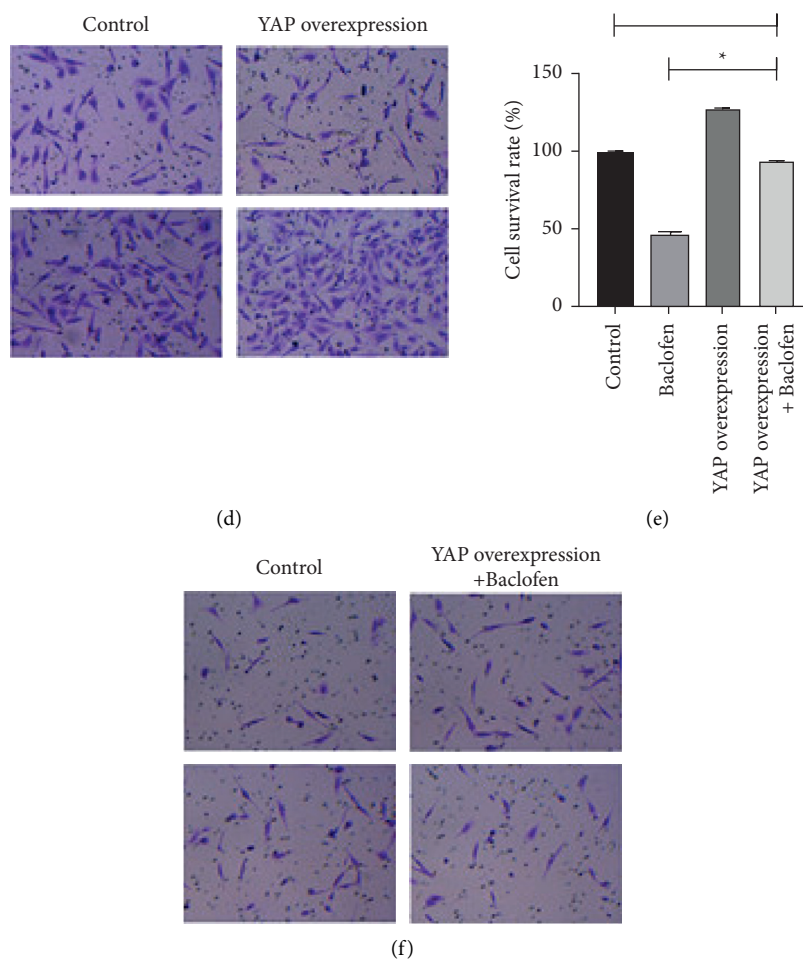


FIGURE 4: YAP involved in baclofen-induced inhibition of proliferation and migration of GBM cells. \*Statistical significance compared with the control group.

induced inhibition of cell viability was significantly suppressed (Figure 4(e)). Moreover, Transwell assay showed that the baclofen-related suppression on migration ability was rescued by YAP overexpression as well (Figure 4(f)).

**3.4. Baclofen-Induced Phosphorylation of YAP in GBM Cells through GABABR2-Gs-Lats1/2 Signaling Pathway.** We found that CGP 35348, a GABAB receptor antagonist, could reverse the baclofen-induced inhibition of proliferation of GMB cells; however, SR 95531 hydrobromide, a GABAB receptor antagonist showed a limited effect on baclofen-mediated proliferation inhibition (Figures 5(a) and 5(b)). After treated with baclofen, we detected the significant increase in the expression of GABABR2 and Lats1; however, the expression of Lats2 was not significantly influenced (Figure 5(c)). After downregulating the expression of GABABR1 and GABABR2, respectively, we found that only GABABR2 knock down reversed the baclofen-induced inhibition of proliferation of GMB cells, suggesting that it is GABABR2 not GABABR1 that acted as the potential downstream target of baclofen (Figures 5(d) and 5(e)). Furthermore, we detected an increased expression of cAMP in U251 after treating with

baclofen, indicating that GABABR2-Gs might be activated (Figure 5(f)).

**3.5. Survivin and Bcl2 Acted as Downstream of YAP.** We found that survivin and Bcl2 expression can be suppressed by baclofen treatment (Figure 6(a)). We assumed that survivin and Bcl2 were the downstream target of YAP. Therefore, we downregulated the expression of YAP and found that the expressions of survivin and Bcl2 were suppressed (Figure 6(b)); meanwhile, YAP overexpression led to upregulation of survivin and Bcl2 (Figure 6(c)).

**3.6. Baclofen Inhibited Subcutaneous Tumors Generated by Inducing YAP Phosphorylation In Vivo.** We have recruited 10 mice and classified them into treatment (baclofen) and control group (0.9% NaCl). We found that baclofen significantly decreased the tumor growth in vivo (Figures 7(a) and 7(b)).

**3.7. Changes of Transplanted Tumor Tissues in Nude Mice after Baclofen Treatment.** Compared with the control group, the expression level of phosphorylated YAP protein in the

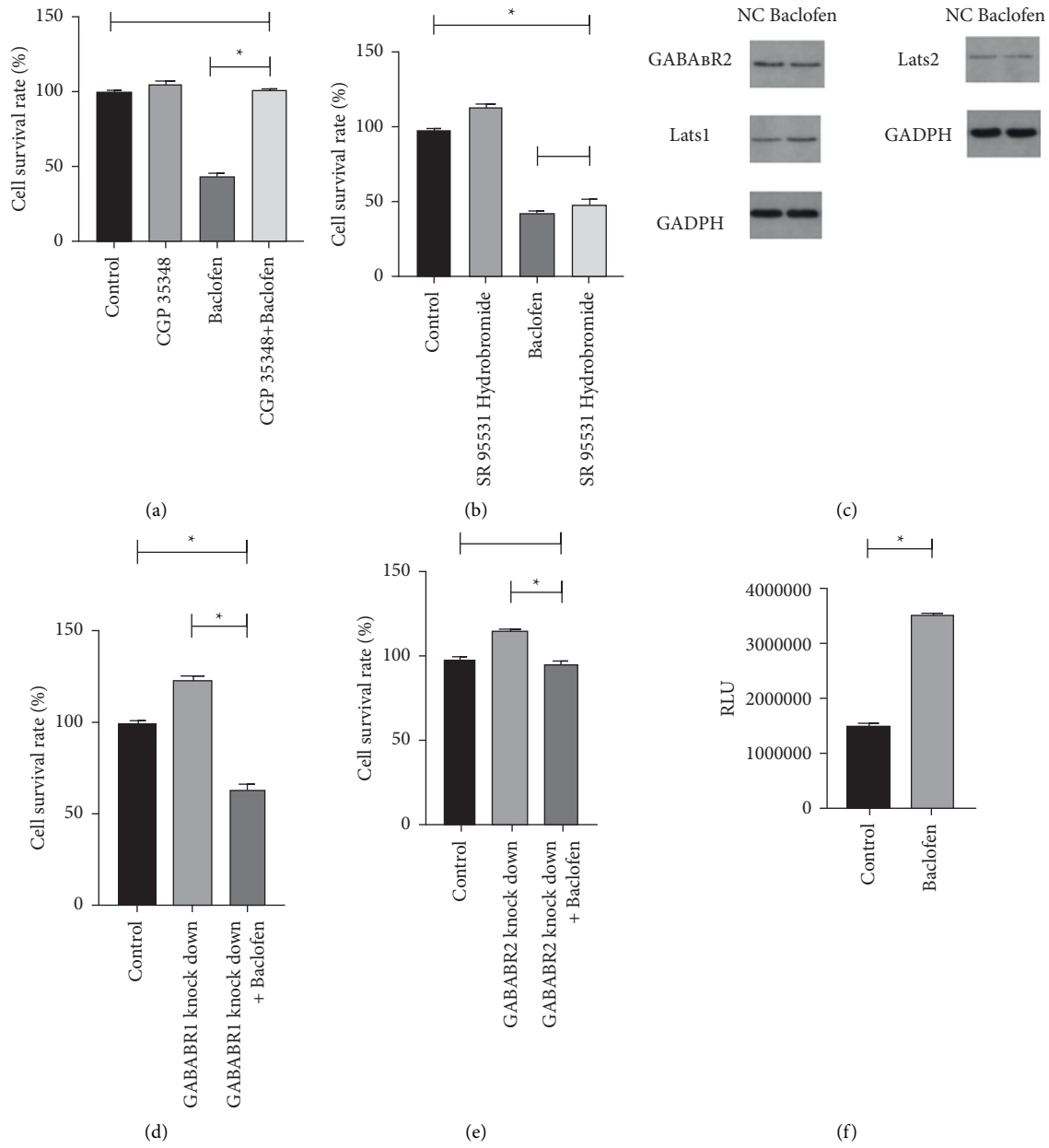


FIGURE 5: Baclofen-induced phosphorylation of YAP in GBM cells through the GABA<sub>B</sub>R2-Gs-Lats1/2 signaling pathway. \*Statistical significance compared with the control group.

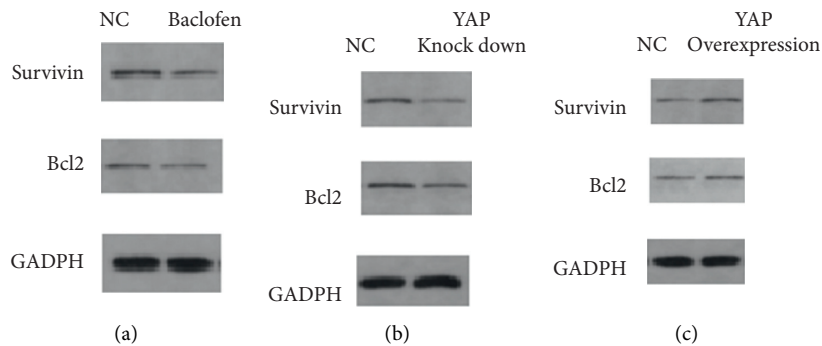


FIGURE 6: Survivin and Bcl2 acted as downstream of YAP.

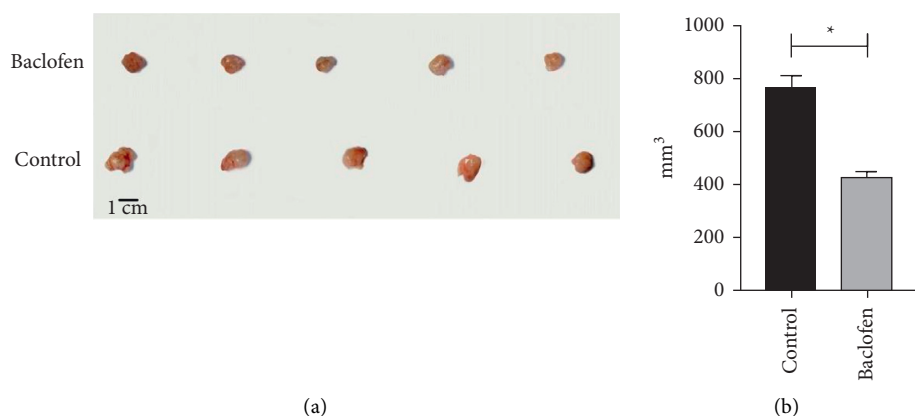


FIGURE 7: Baclofen inhibited subcutaneous tumors generated by inducing YAP phosphorylation in vivo. \*Statistical significance compared with the control group.

transplanted tumor tissue of nude mice after the treatment of baclofen was significantly increased, indicating that the phosphorylation of YAP could also be induced by baclofen in vivo (Figure 8(a)). The expression levels of GABABR2 and Lats1 proteins in transplanted tumor tissues after the treatment of baclofen were significantly higher than those in the control group, indicating that baclofen can also promote the expression of GABABR2 and Lats1 proteins in vivo (Figure 8(b)). The expression levels of survivin and Bcl2 proteins in transplanted tumor tissues after baclofen treatment were significantly lower than those in the control group, suggesting that survivin and Bcl2 proteins expression could also be inhibited by baclofen in vivo (Figure 8(c)).

#### 4. Discussion

GBM is the most frequent and most aggressive malignant primary brain tumor in adults, representing a highly heterogeneous group of neoplasms that are among the most aggressive and challenging cancers to treat. These tumors are typically associated with dismal prognosis and poor quality of life. It is the most frequent primary brain tumor, with a median overall survival (OS) between 10 and 20 months. High-grade gliomas are the leading cause of central nervous system (CNS) cancer-related death in both children and adults. Most people suffering from GBM, especially the elderly, have a lower survival within one year [4]. In GBM, the clinical trials of targeted therapy for most patients have a limited success rate, indicating that the current medical community still lacks understanding of the pathophysiology of gliomas.

Studies have shown that the GABAB signaling pathway participates in the occurrence of GBM through metabolic reprogramming and genetic transformation and accelerates the replication and progression of glioma. GABAB can upregulate cytoskeleton protein and intracellular  $\text{Ca}^{2+}$  level and increase the release of glutamate, so as to promote the formation of synaptic-like connection and the surrounding cell microenvironment [20]. GHB (4-hydroxybutyrate) exists in human brain and can act on

GABA receptor (GABABR). GABABR is mainly the main inhibitory neurotransmitter in the somatosensory system. Research has showed that GHB inhibits proliferation of GBM stem-like cells and alleviated tumor aggressiveness [21]. Therefore, GPCR is the main target of drugs at present, and the GPCR-Hippo signal pathway is a complex signal network. Drugs targeting GPCRs, G protein, or downstream signal nodes may affect effectors such as YAP/TAZ [10].

The main functions of YAP/TAZ include regulating cell proliferation and survival, maintaining the self-renewal of adult stem cells, participating in organ development, tissue size regulation, tissue regeneration, and so on. The Hippo signal pathway is a common YAP/TAZ upstream signal pathway, which was first found in the screening of tumor suppressor genes in *Drosophila*. Subsequently, the four core components of the signal pathway were revealed successively, including Wars, Salvador (SAV1/WW45), Hippo, and Mats. When the Hippo signaling pathway is turned on, YAP/TAZ is phosphorylated by Lats1/2 at multiple sites, interacts with 14-3-3, and is retained in the cytoplasm; phosphorylation also leads to YAP/TAZ polyubiquitination and degradation [22]. When Hippo signaling is off, its dephosphorylated morphology could translocate into the nucleus to bind TEAD and VGLL4 to regulate target gene transcription. The functional mechanism of YAP/TAZ protein is shown in Figure 9.

Studies have shown that YAP phosphorylation can be mediated through relevant contact between cells, transmission of mechanical signals, induction of stress signals, cell polarity/structure, and cell cycle [23]. GPCR and Rho can promote YAP/TAZ nuclear localization and transcriptional activities. Stimulation of  $G\alpha$ -coupled receptors by multiple ligands, including lysophospholipids sphingosine 1-phosphate (S1P), lysophosphatidic acid (LPA), thrombin, estrogens, and acetylcholine, results in YAP/TAZ activation through the promotion of a RhoGTPase-regulated F-actin cytoskeleton in a manner that is either Lats1/2-dependent or independent. When tumors occur, the dysfunction of the Hippo signaling pathway can lead to the dephosphorylation and activation of YAP, which in turn

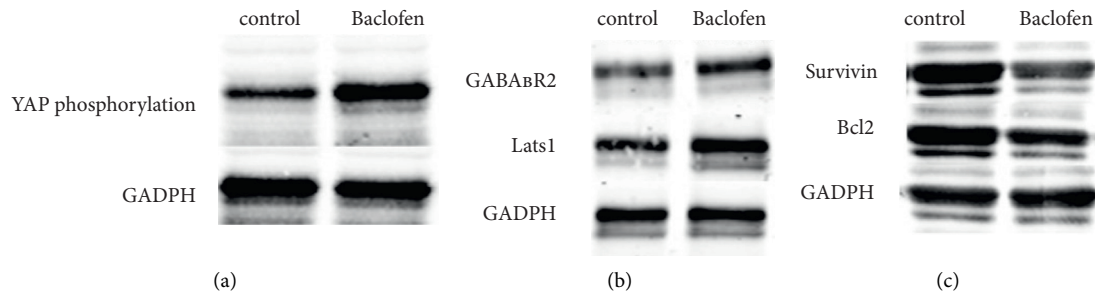
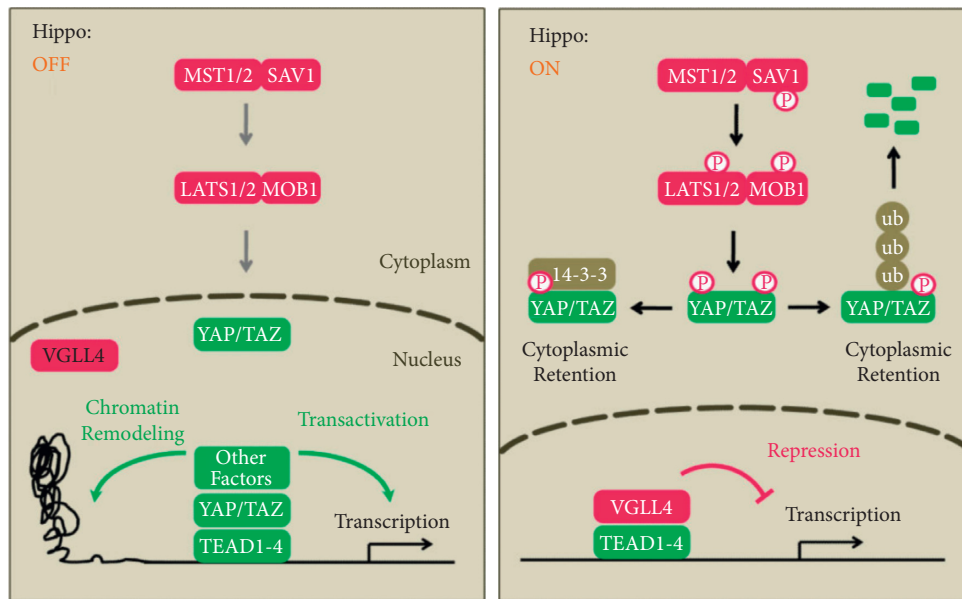


FIGURE 8: Changes of transplanted tumor tissues in nude mice after baclofen treatment.



Hippo pathway components and major functions.

Drosophila	Mammals	Major functions in Hippo pathway
Hippo (Hpo)	MST1/2	Phosphorylate LATS1/2, MOB1, and SAV1, leading to LATS1/2 activation
Salvador (Sav)	SAV1	Interacts with MST1/2, promotes phosphorylation of LATS1/2 by MST1/2
Warts (Wts)	LATS1/2	Phosphorylate and inactivate YAP/TAZ
Mats	MOB1A/B	Scaffold protein of LATS1/2
Yorkie (Yki)	YAP/TAZ	Transcription co-activator, major effectors of the Hippo pathway
Scalloped (Sd)	TEAD1-4	Transcription factors mediate the effect of YAP/TAZ
Tgi	VGLL4	Competes with YAP/TAZ for TEADs, inhibits YAP/TAZ functions
misshapen (Msn)	MAP4K4	Activates LATS1/2
Merlin (Mer)	Merlin/NF2	May form a complex and mediates upstream signals (from plasma membrane) to MST1/2. NF2 may bring LATS1/2 to plasma membrane and facilitate its activation by MST1/2
Kibra	KIBRA	
Expanded (Ex)	FRMD6?	
	AMOT	Sequesters YAP/TAZ to cell junctions, binding and indirectly activates LATS1/2; a substrate of LATS1/2

FIGURE 9: Diagram of the functional mechanism of YAP/TAZ protein.

induces Ki67, c-Myc, SOX4, H19, AFP, BIRC5/survivin, BIRC2/cIAP1, and other cell proliferation-related genes, and apoptosis inhibits high expression [22].

Animal experiments show that YAP activation can cause tissue overgrowth, injury, and multiple organ lesions, resulting in tumor formation [24]. TAZ upregulation is

detected in most GBMs, and high TAZ mRNA levels are associated with reduced survival. High levels of YAP expression are found in all levels of glioma subsets and are associated with shorter survival in glioma patients. SCID mice were injected with primary GBM cell line in situ, and TAZ gene knockout impaired tumor formation [11].

Baclofen has been used in treating this tumor in neuroscience for quite a time, but the precise mechanism of how baclofen inhibits GBM remains elusive. In this study, we have proved that baclofen can inhibit GBM cells invasion. The CCK-8 test and Transwell test proved that baclofen can inhibit GMB cells' proliferation and migration. Baclofen could induce phosphorylation of YAP; as shown in Figure 9, the phosphorylated YAP retained in the cytoplasm and is degraded, leaving the downstream genes inactivated. Western blot analysis shows that the level of phosphorylated YAP is dose and time-dependent of baclofen. This may be the possible mechanism of baclofen in inhibiting the progression of GBM.

In most cases, soluble factors regulate YAP through their homologous G protein-coupled receptors and related G protein subunits through the Hippo pathway, so as to bind to small GTPase, RhoA, and rock, resulting in the change of Lats1/2 activation [23]. To determine which receptor was involved, siRNAs against the catalytic subunits of GABABR1/R2 and Gs and YAP upstream Lats1/2 were used. Western blot results show that baclofen-induced pYAP was reversed by these siRNAs, suggesting that YAP is activated by the GABABR1/2-Gs signaling pathway and is likely to be a direct substrate of Lats1/2.

We further examined the role of baclofen as a downstream effector in the expression of survivin and Bcl2. As shown in Figure 4, baclofen significantly decreased survivin and Bcl2 expression in both mRNA and protein levels, which means pYAP could not activate the transcription of genes that promote cellular survival, such as survivin and Bcl2, which means baclofen could inhibit tumor progression in affecting the expression of the survival genes, and lower level of proliferation-associated genes may be the reason of tumor-inhibition.

Bcl2 family members can counteract the BAK/BAX's ability to induce apoptosis; when in stress, BH3 members activate BAK/BAK, resulting in mitochondrial outer membrane permeabilization (MOMP). MOMP results in cytochrome c release, activation of downstream caspase, and finally cell death. During tumorigenesis, antiapoptotic Bcl2 is upregulated to make cancer cells survive. [25] The beta-catenin YAP1-TBX5 complex transcriptionally upregulated Bcl2 family members, thus suppressing the mitochondrial-induced apoptosis pathway in cancer cells [26]. Other than Bcl2 family proteins, a second gene family called inhibitor of apoptosis protein (IAP) has been identified, which regulates various important aspects of cell survival. Survivin (encoded by BIRC5) is a member of the IAP family, which is over-expressed in most of the malignancies and totally absent in most of the normal tissues. Survivin has two main functions in cancer cells: (1) regulate mitosis by forming chromosome passenger complex (CPC) with other proteins and (2) inhibition of apoptosis by direct inhibition of active caspases

[27]. It is reported that survivin is a target of YAP because the level of survivin increases significantly when YAP is activated. Here, we determined the functional relationship between YAP and survivin in GBM environment.

## 5. Conclusion

Together these studies suggest the following:

- (1) GABAB inhibits the GBM
- (2) For the first time, we proved that baclofen could be used as a drug against GBM
- (3) Baclofen takes effect by the GABAB signaling pathway
- (4) YAP could promote GMB
- (5) Thus, our findings confirm the regulatory relationship between YAP/TAZ and GABA signaling pathway.

## Data Availability

The data used and analyzed during the current study are available from the corresponding author upon request.

## Conflicts of Interest

The authors declare that they have no conflicts of interest.

## References

- [1] D. F. Quail and J. A. Joyce, "The microenvironmental landscape of brain tumors," *Cancer Cell*, vol. 31, no. 3, pp. 326–341, 2017.
- [2] A. Omuro and L. M. Deangelis, "Glioblastoma and other malignant gliomas," *Journal of the American Medical Association*, vol. 310, no. 17, pp. 1842–1850, 2013.
- [3] V. Frattini, V. Trifonov, J. M. Chan et al., "The integrated landscape of driver genomic alterations in glioblastoma," *Nature Genetics*, vol. 45, no. 10, pp. 1141–1149, 2013.
- [4] D. N. Louis, H. Ohgaki, O. D. Wiestler et al., "The 2007 WHO classification of tumours of the central nervous system," *Acta Neuropathologica*, vol. 114, no. 2, pp. 97–109, 2007.
- [5] D. Sturm, S. Bender, D. T. W. Jones et al., "Paediatric and adult glioblastoma: multifactorial (epi)genomic culprits emerge," *Nature Reviews Cancer*, vol. 14, no. 2, pp. 92–107, 2014.
- [6] M. Touat, A. Idhahbi, M. Sanson, and K. L. Ligon, "Glioblastoma targeted therapy: updated approaches from recent biological insights," *Annals of Oncology*, vol. 28, no. 7, pp. 1457–1472, 2017.
- [7] H. Ohgaki and P. Kleihues, "Epidemiology and etiology of gliomas," *Acta Neuropathologica*, vol. 109, no. 1, pp. 93–108, 2005.
- [8] A. Tobias, A. Ahmed, K.-S. Moon, and M. S. Lesniak, "The art of gene therapy for glioma: a review of the challenging road to the bedside," *Journal of Neurology, Neurosurgery & Psychiatry*, vol. 84, no. 2, pp. 213–222, 2013.
- [9] A. Totaro, T. Panciera, and S. Piccolo, "YAP/TAZ upstream signals and downstream responses," *Nature Cell Biology*, vol. 20, no. 8, pp. 888–899, 2018.
- [10] J. Luo and F. X. Yu, "GPCR-hippo signaling in cancer," *Cells*, vol. 8, no. 5, 2019.



- [11] F. Zanconato, M. Cordenonsi, and S. Piccolo, "YAP/TAZ at the roots of cancer," *Cancer Cell*, vol. 29, no. 6, pp. 783–803, 2016.
- [12] Z. Liu, P. P. Yee, Y. Wei, Z. Liu, Y. I. Kawasawa, and W. Li, "Differential YAP expression in glioma cells induces cell competition and promotes tumorigenesis," *Journal of Cell Science*, vol. 132, no. 5, 2019.
- [13] N. Artinian, C. Cloninger, B. Holmes, A. Benavides-Serrato, T. Bashir, and J. Gera, "Phosphorylation of the Hippo pathway component AMOTL2 by the mTORC2 kinase promotes YAP signaling, resulting in enhanced glioblastoma growth and invasiveness," *Journal of Biological Chemistry*, vol. 290, no. 32, pp. 19387–19401, 2015.
- [14] M. Terunuma, "Diversity of structure and function of GABAB receptors: a complexity of GABAB-mediated signaling," *Proceedings of the Japan Academy, Series B*, vol. 94, no. 10, pp. 390–411, 2018.
- [15] A. Shergalis, A. Bankhead, U. Luesakul, N. Muangsin, and N. Neamati, "Current challenges and opportunities in treating glioblastoma," *Pharmacological Reviews*, vol. 70, no. 3, pp. 412–445, 2018.
- [16] R. Sanchez-Ponce, L.-Q. Wang, W. Lu, J. von Hehn, M. Cherubini, and R. Rush, "Metabolic and pharmacokinetic differentiation of STX209 and racemic baclofen in humans," *Metabolites*, vol. 2, no. 3, pp. 596–613, 2012.
- [17] T. Wang, W. Huang, and F. Chen, "Baclofen, a GABAB receptor agonist, inhibits human hepatocellular carcinoma cell growth in vitro and in vivo," *Life Sciences*, vol. 82, no. 9-10, pp. 536–541, 2008.
- [18] M. Fève, J.-M. Saliou, M. Zeniou et al., "Comparative expression study of the endo-G protein coupled receptor (GPCR) repertoire in human glioblastoma cancer stem-like cells, U87-MG cells and non malignant cells of neural origin unveils new potential therapeutic targets," *PLoS One*, vol. 9, no. 3, Article ID e91519, 2014.
- [19] T. Sun, K. Li, K. Zhu, R. Yan, C. Dang, and D. Yuan, "SNHG6 interacted with miR-325-3p to regulate cisplatin resistance of gastric cancer by targeting GITR," *OncoTargets and Therapy*, vol. 13, pp. 12181–12193, 2020.
- [20] Z. Pei, K.-C. Lee, A. Khan, G. Erisnor, and H.-Y. Wang, "Pathway analysis of glutamate-mediated, calcium-related signaling in glioma progression," *Biochemical Pharmacology*, vol. 176, p. 113814, 2020.
- [21] E. A. El-Habr, L. G. Dubois, F. Burel-Vandenbos et al., "A driver role for GABA metabolism in controlling stem and proliferative cell state through GHB production in glioma," *Acta Neuropathologica*, vol. 133, no. 4, pp. 645–660, 2017.
- [22] C.-L. Da, Y. Xin, and J. Zhao, "Significance and relationship between Yes-associated protein and survivin expression in gastric carcinoma and precancerous lesions," *World Journal of Gastroenterology*, vol. 15, no. 32, pp. 4055–4061, 2009.
- [23] X. Li, L. Yao, Q. Liang, H. Qu, and H. Cai, "Propofol protects hippocampal neurons from hypoxia-reoxygenation injury by decreasing calcineurin-induced calcium overload and activating YAP signaling," *Oxidative medicine and cellular longevity*, vol. 2018, Article ID 1725191, 2018.
- [24] W. Zhang, Y. Gao, F. Li et al., "YAP promotes malignant progression of lkb1-deficient lung adenocarcinoma through downstream regulation of survivin," *Cancer Research*, vol. 75, no. 21, pp. 4450–4457, 2015.
- [25] J. Cui and W. J. Placzek, "Post-transcriptional regulation of anti-apoptotic BCL2 family members," *International Journal of Molecular Sciences*, vol. 19, no. 1, 2018.
- [26] J. Rosenbluh, D. Nijhawan, A. G. Cox et al., " $\beta$ -Catenin-Driven cancers require a YAP1 transcriptional complex for survival and tumorigenesis," *Cell*, vol. 151, no. 7, pp. 1457–1473, 2012.
- [27] Z. Khan, A. A. Khan, H. Yadav, G. B. K. S. Prasad, and P. S. Bisen, "Survivin, a molecular target for therapeutic interventions in squamous cell carcinoma," *Cellular and Molecular Biology Letters*, vol. 22, no. 1, p. 8, 2017.

## Research Article

# Screening of Active Components and Key Targets of Radix Codonopsis in the Treatment of Gastric Cancer

Lijun Tang,<sup>1</sup> Jinhui Chen,<sup>1</sup> Jin Yin,<sup>2</sup> and Mingli Fang<sup>1,2</sup> 

<sup>1</sup>Hunan Provincial People's Hospital, The First-Affiliated Hospital of Hunan Normal University, Changsha 410005, China

<sup>2</sup>Hunan Provincial Center for Disease Control and Prevention, Changsha 410005, China

Correspondence should be addressed to Mingli Fang; fangmily@163.com

Received 26 September 2021; Accepted 16 October 2021; Published 8 November 2021

Academic Editor: Weiguo Li

Copyright © 2021 Lijun Tang et al. This is an open access article distributed under the Creative Commons Attribution License, which permits unrestricted use, distribution, and reproduction in any medium, provided the original work is properly cited.

Gastric cancer is the fifth most common cancer type in the world. The incidence and mortality of gastric cancer in China ranks second among malignant tumors in the country. At present, the main treatment method of gastric cancer is still surgical resection combined with chemotherapy. However, chemotherapy drugs will cause serious toxic and side effects on other normal tissues and cells. At the same time, chemotherapy drugs can make patients develop drug resistance and seriously affect the curative effect. By contrast, Chinese medicine has more advantages in the treatment of cancer. Dangshen (Radix Codonopsis), a traditional Chinese medicine, has been proved to be effective for the clinical treatment of gastric cancer. However, due to the complex components of Dangshen, the main active components and pharmacological mechanism for its treatment of gastric cancer are still unclear. In this study, the main active components and pharmacological mechanism of Radix Codonopsis in the treatment of gastric cancer were preliminarily explored based on network pharmacology and molecular docking. We obtained bioactive compounds and targets from Radix Codonopsis from the Chinese Medicine System Pharmacology Database (TCMSP) and constructed the active ingredient-target network of *Codonopsis pilosula*. We then obtained targets related to gastric cancer from the disease database. The common targets of Radix Codonopsis and gastric cancer were the key target of Radix Codonopsis for the treatment of gastric cancer. Then, we used Metascape database to conduct functional enrichment analysis on the key targets of Radix Codonopsis for the treatment of gastric cancer to clarify the mechanism of Radix Codonopsis for the treatment of gastric cancer. We constructed a network to screen the main bioactive compounds and therapeutic targets, assessed the prognostic value of the main target genes by survival analysis, and finally assessed the binding affinity of the main target genes and main bioactive compounds of Radix Codonopsis for the treatment of gastric cancer by molecular docking. The results showed that the main active compounds of *Codonopsis pilosula* in treating gastric cancer were luteolin and cryptotanshinone, which played a role in the treatment of gastric cancer through the multitarget and multipathway mechanism.

## 1. Introduction

Gastric cancer is the fifth most common cancer type in the world and the third leading cause of cancer death in the world. Its incidence and mortality rate ranks second among malignant tumors in China, seriously affecting people's quality of life and social and economic development [1]. The occurrence of gastric cancer is mainly related to smoking [2], advanced age [3], heredity [4], and *Helicobacter pylori* [5]. At present, the main treatment methods of gastric cancer are still surgical resection and chemotherapy [6]. However, chemotherapy drugs will produce serious toxic and side

effects on other normal tissues and cells. At the same time, chemotherapy drugs can make patients develop drug resistance and seriously affect the curative effect [7]. By contrast, Chinese medicine has more advantages in the treatment of cancer due to its advantages of small toxicity and side effects. Studies have also shown that Chinese medicine not only has a unique advantage in the treatment of tumors but also plays an important role in promoting the recovery of tumor patients after tumor resection [8]. In China, Chinese medicine plays an important role in the comprehensive treatment of gastric cancer, among which *Codonopsis pilosula* plays an important role in the treatment

of gastric cancer. *Codonopsis pilosula*, as a traditional Chinese medicine, has many pharmacological activities and important medicinal value and can be used in combination with other traditional Chinese medicines to treat various diseases. The pharmacological activities of *Codonopsis pilosula* mainly include regulating immunity [9], cardiovascular protection [10], neuroprotection [11], regulation of gastrointestinal function [12], antibacterial [13], antiaging, and antioxidant effects [14]. At present, China's Food and Drug Administration has approved nearly 200 kinds of health food containing Radix *Codonopsis*. Radix *Codonopsis* has the efficacy of invigorating the spleen and tonifying the lung, which has a significant therapeutic effect on gastric cancer clinically. However, due to the complex components of Radix *Codonopsis*, the main active components and pharmacological mechanism of Radix *Codonopsis* in the treatment of gastric cancer are still unclear.

As the cutting edge of Chinese medicine research, network pharmacology technology integrated chemical, medical, and biological data and integrated the ideas of system biology and multidirectional pharmacology. Currently, it has been applied to many fields, such as target recognition of new drugs, discovery of lead compounds, research on action mechanism, and screening of material basis [15]. The network pharmacology combined with molecular docking provided a feasible method for elucidating the multicomponent and multitarget action mechanism of Chinese medicinal compound preparations [16]. In this study, network pharmacology and molecular docking were used to preliminarily explore the main active components and pharmacological mechanism of Radix *Codonopsis* in the treatment of gastric cancer, study the interaction between the chemical components of Radix *Codonopsis* and antigastric cancer targets, and establish the target network of chemical components, to provide the basis for elucidating the molecular mechanism of Radix *Codonopsis* antigastric cancer effect. This study provided a scientific basis for the treatment of gastric cancer with Radix *Codonopsis*, and it was of practical significance to guide its clinical medication.

## 2. Methods

**2.1. Active Compounds and Targets of the *Codonopsis pilosula*.** We searched TCMS (http://tcmsp.com/tcmsp.php) for the keyword "dangshen." Taking oral bioavailability (OB)  $\geq 30\%$  and drug-like property (DL)  $\geq 0.18$  as screening conditions, we screened the active components of *Codonopsis pilosula*. We collected the protein targets of the active ingredients of *Codonopsis pilosula* with the help of Herb database (http://herb.ac.cn/) and finally screened them through Excel to remove the duplicate targets, thus obtaining the final targets of the active compounds.

**2.2. Targets of *Codonopsis pilosula* in Treating Gastric Cancer.** We used the keyword "gastric carcinoma" in GeneCards Database (https://www.genecards.org/) to search for gastric cancer-related targets. Then, using online Venny 2.1 Venn

diagram (http://www.bioinformatics.com.cn/static/others/jvnn/example.html), we matched and mapped the active component targets of Radix *Codonopsis* with disease-related targets. The intersection part was the key target of Radix *Codonopsis* for the treatment of gastric cancer, and the corresponding active component was the key component.

**2.3. Functional Enrichment Analysis and Its Clustering Network Construction.** We used Metascape (https://metascape.org/gp/index.html#/main/step1) to conduct functional enrichment analysis on the target of Radix *Codonopsis* for the treatment of gastric cancer. The GO functional enrichment analysis mainly included biological process (BP), molecular function (MF), and cellular component (CC). The protein target was introduced into Metascape database, and GO analysis and KEGG pathway analysis are carried out on the action target of *Codonopsis pilosula*. Terms with a  $p$  value  $< 0.01$ , a minimum count of 3, and an enrichment factor  $> 1.5$  (the enrichment factor is the ratio between the observed counts and the counts expected by chance) were collected and grouped into clusters based on their membership similarities; each color represents a group.  $p$  values were calculated based on the accumulative hypergeometric distribution. Kappa scores were used as the similarity metric when performing hierarchical clustering on the enriched terms, and subtrees with a similarity of  $> 0.3$  are considered a cluster. The final result showed the top 20 clusters, and the most statistically significant term within a cluster was chosen to represent the cluster.

**2.4. Construction of Compound-Target Network and Protein-Protein Interaction Network.** In order to scientifically explain the therapeutic effect of Radix *Codonopsis* on gastric cancer by network pharmacology, we constructed a visual network to predict the relationship between compounds and targets. We constructed the compound-target network using Cytoscape 3.6.1 software. The node in the network represented the compound components and targets. If a compound might act on a potential target, they were connected by an edge. In addition, we used the Metascape (https://metascape.org/gp/index.html#/main/step1) to build an interaction network between proteins, in which each color represents a clustering module.

**2.5. Construction of Network Modules and Screening of Core Targets.** The molecular complex detection (MCODE) algorithm has been applied to identify densely connected network components. Pathway and process enrichment analysis has been applied to each MCODE component independently, and the three best-scoring terms by  $p$  value have been retained as the functional description of the corresponding components. Finally, we chose a relatively important module from the seven modules to construct the target-component network, so as to find the key components and targets.

**2.6. Survival Analysis of the Core Target Genes.** Kaplan-Meier plotter is a popular online site tool based on the databases of EGA, TCGA, and GEO for evaluating gene

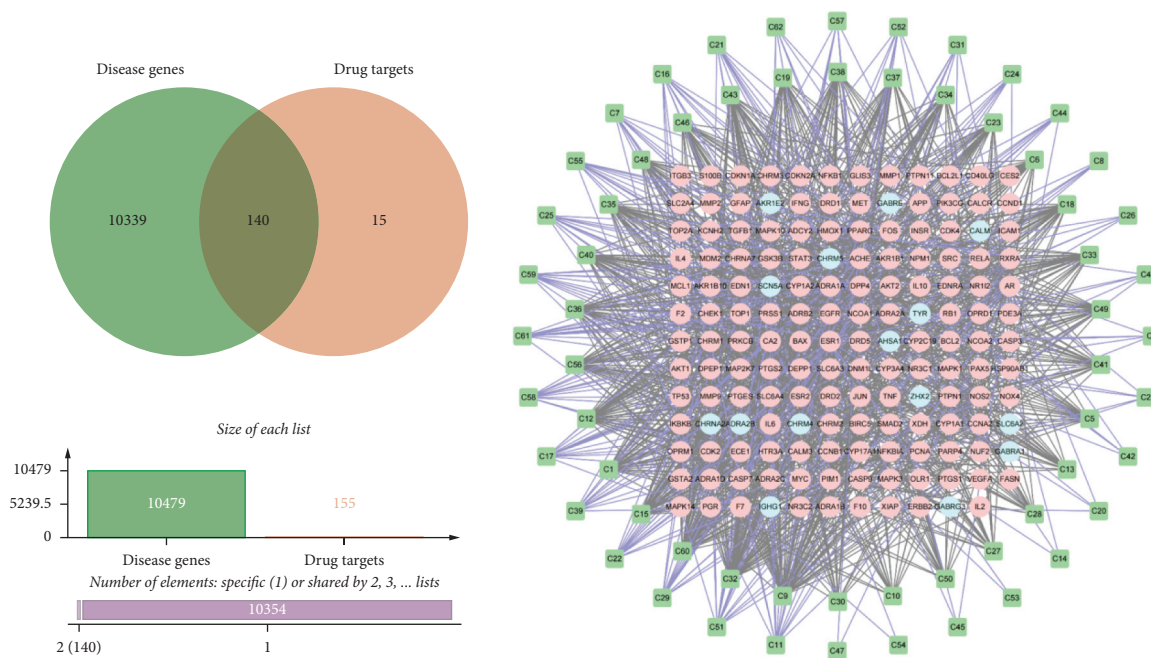


FIGURE 1: Screening of therapeutic targets and construction of its component network.

effects on survival [17]. The cancer species was set as “gastric carcinoma,” and the key core target genes screened above were analyzed for survival by K–M plotter. Finally, we screened out genes that affected the overall survival of gastric cancer.

**2.7. Molecular Docking Analysis.** We chose the MCODE2 network to construct the component-target network, found the targets and components with relatively high degree, and took them as docking objects. AutoDock Vina 1.1.2 software is used for docking, and PyMOL 2.4.1 software is used for visualization of docking results [18]. Finally, the results are further verified by docking score.

### 3. Results

**3.1. Screening of Related Targets of *Codonopsis pilosula* in the Treatment of Gastric Cancer.** In TCMSP database, we searched 134 compounds in *Codonopsis pilosula*. In order to screen the potential active compounds, we evaluated the ADME properties of the compounds and screened out the compounds with OB value  $\geq 30\%$  and DL  $\geq 0.18$ . A total of 62 potential active compounds were screened out. Through searching the action targets of these active compounds from the Herb database, 155 protein targets were collected. Then, in order to search for disease genes, we searched for the keyword “gastric cancer” in GeneCards database and found 10,479 gastric cancer-related targets. Finally, 140 common targets are obtained by mapping the disease targets with the component action targets (Figure 1), which we regard as the related targets of *Codonopsis pilosula* in treating gastric cancer.

**3.2. Construction of *Codonopsis pilosula* Composition-Target Network.** After screening the common targets, we constructed a component-target network (Figure 1). In the network, the green squares on the periphery represent 62 active components, among which the degree value of the inner ring components is larger than that of the outer ring components, and the components in each ring are arranged clockwise according to the degree value. In order to show the target number of components more intuitively, we use two different-colored connecting lines to distinguish the action relationship between inner and outer ring components and target points. Circles in the network represent action targets, among which pink targets are 140 gastric cancer-related targets. From the network, we can see that compared with the outer ring component, the inner ring component has a higher degree of importance in the network. In addition, we can also find that most of the targets of *Codonopsis pilosula* are related to gastric cancer, suggesting that this medicine is more targeted for the treatment of gastric cancer.

**3.3. Functional Enrichment Analysis of Therapeutic Targets for Gastric Cancer.** We analyzed the GO functional enrichment and KEGG pathway enrichment of the above 140 key targets by using Metascape database (<http://metascape.org/>) (Figures 2 and 3). GO analysis includes biological processes (BP), cellular components (CC), and molecular functions (MF), which together describe the functions of gene products. We will further cluster the obtained terms according to the similarity of members and show the first 20 clusters. Each cluster selects a term with the most statistical significance to represent the cluster.

KEGG enrichment analysis mainly involves pathways in cancer, AGE-RAGE signaling pathway in diabetic

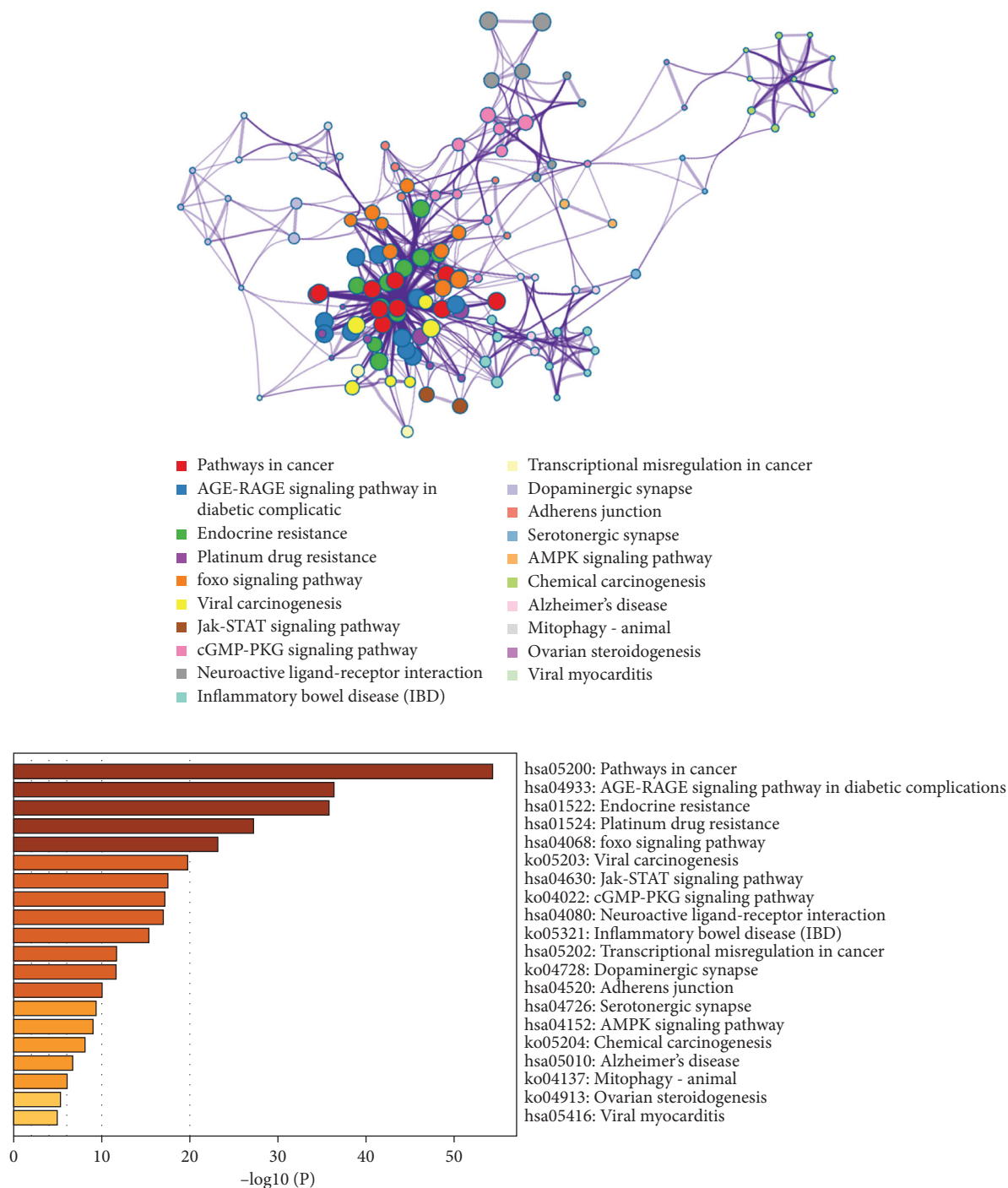


FIGURE 2: The KEGG pathway enrichment analysis.

complications, endocrine resistance, platinum drug resistance, FOXO signaling pathway, viral carcinogenesis, JAK-STAT signaling pathway, cGMP-PKG signaling pathway, neuroactive ligand-receptor interaction, inflammatory bowel disease (IBD), and so on. GO analysis of *Codonopsis pilosula* in treating gastric cancer mainly involved cellular response to organic cyclic compound, response to drug, positive regulation of protein phosphorylation, response to inorganic substance, response to steroid hormone,

circulatory system process, response to radiation, response to oxygen levels, response to growth factor, aging, etc.

Enrichment analysis showed that 140 interaction targets between drugs and diseases were concentrated in cancer pathways, age-rage signaling pathways in diabetic complications, endocrine resistance, and other clusters. In addition, we also built an interaction network among terms, in which the cluster represented by “paths in cancer” is located in the center of the network. It is suggested that *Codonopsis*

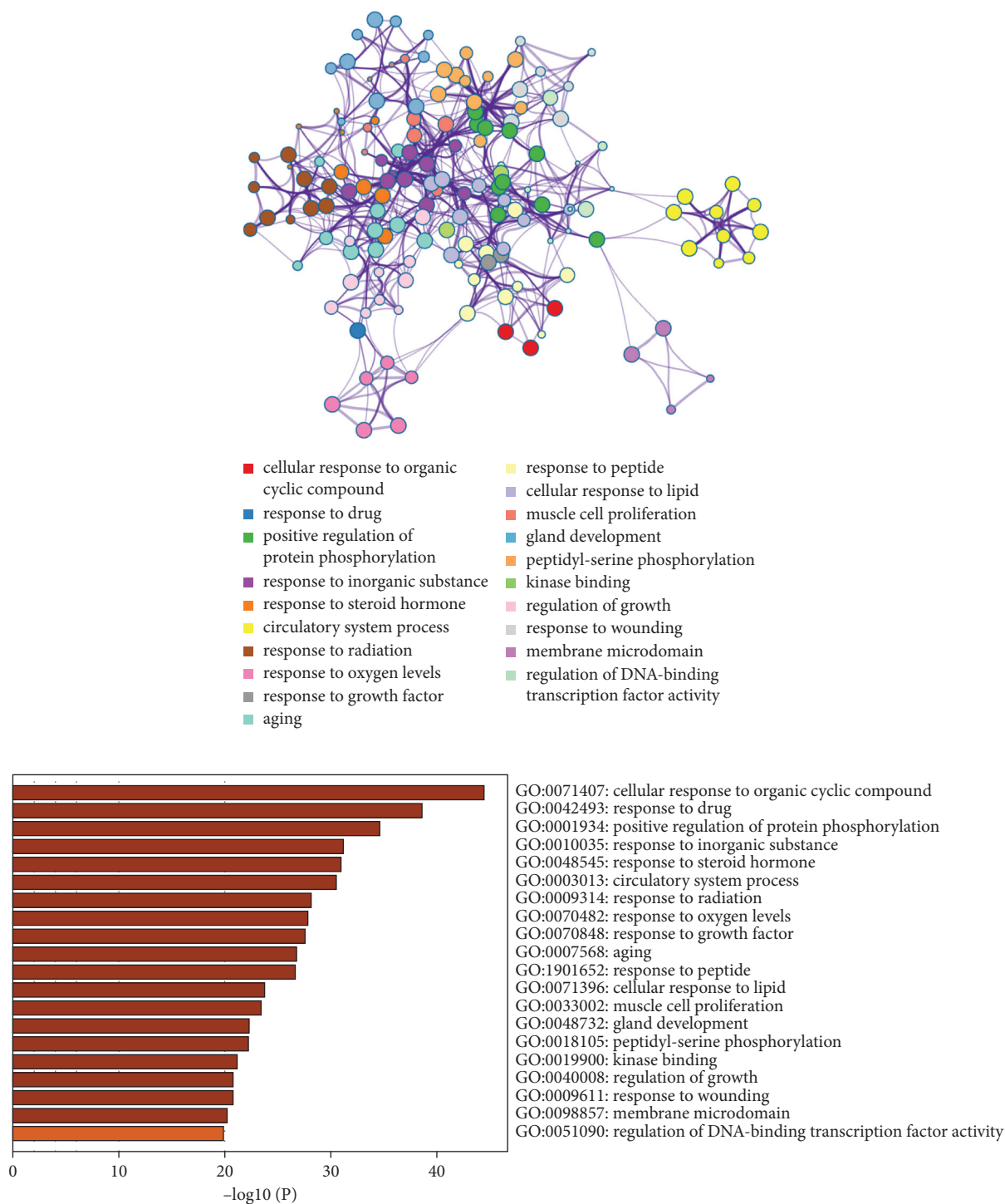


FIGURE 3: The GO enrichment analysis.

*pilosula* may act on multiple targets through various signal pathways in this cluster and play a role in the treatment of gastric cancer. At the same time, it also provides reference value for further searching for key core targets and compounds.

**3.4. Construction of Protein-Protein Interaction Network and Its Module Extraction.** In order to explore the relationship between action targets, we constructed a protein-protein

interaction network and further carried out cluster analysis through modular extraction (Figure 4). We obtained seven types of modules from the target interaction network, representing each cluster with different colors. The size of the target in the network represents the degree of the target in the network, reflecting the number of targets interacting with it. The larger the target, the greater the weight of network participation and the more important it is in the network. It can be seen from the network that the targets in

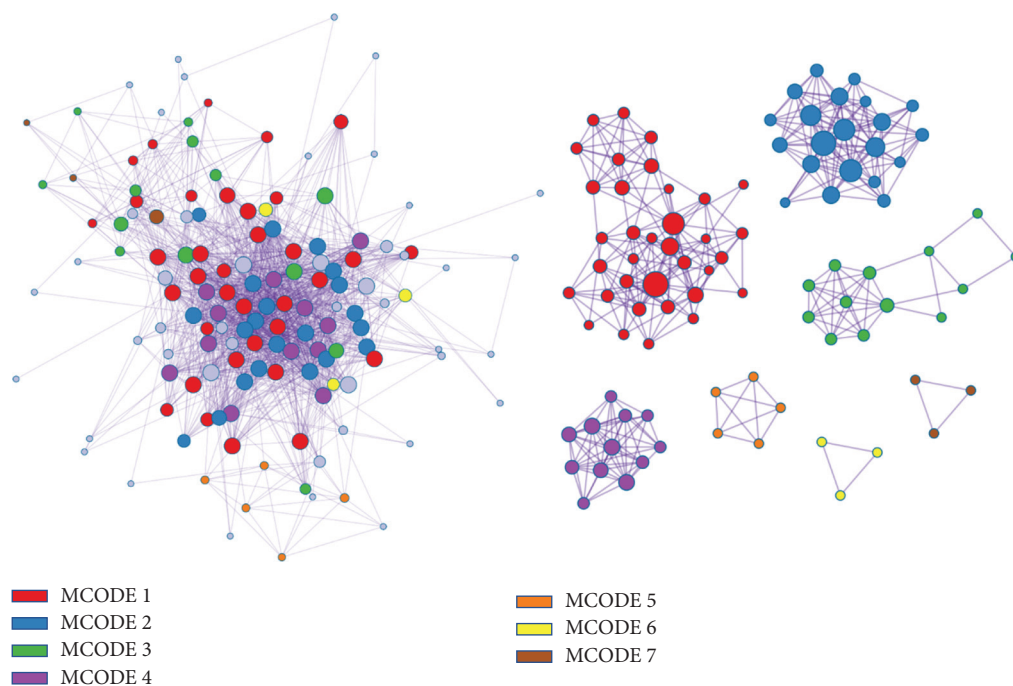


FIGURE 4: Protein-protein interaction network.

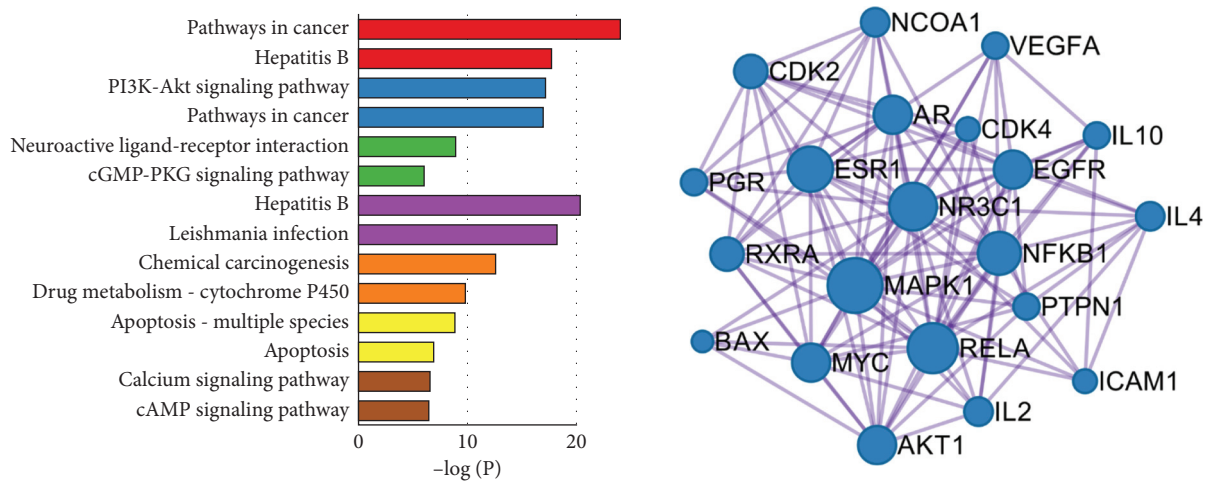


FIGURE 5: Pathway enrichment analysis of MCODE2.

red MCODE1 and blue MCODE2 are relatively large, and the two modules are relatively located in the center of the PPI network, indicating that these two modules may play a leading role in the network.

In order to understand the pathways in which each module participated, we conducted enrichment analysis on seven clusters again (Figure 5) and found that the pathway in which the former two clusters participated involved the term “pathways in cancer,” which occupied the largest weight in the pathway analysis network of the previous 140 related targets, indicating that compared with other modules, these two modules might play a more critical role. By comparing the other entries in the two modules (MCODE 1: Hepatitis B; MCODE2: PI3K-Akt signaling pathway), we focused on

the modules that were more related to gastric cancer and thus screened out MCODE2 as the core subnetwork.

**3.5. Prognostic Analysis of Genes in Modules and Identification of Core Targets.** We further used the K-M plotter to analyze the prognosis information of the core targets of MCODE 2. As shown in Figure 6, the results showed that VEGFA, IL10, AR, PGR, ESR1, EGFR, MAPK1, IL4, MYC, RELA, ICAM1, BAX, IL2, and AKT1 were correlated with the overall survival time of gastric cancer. Among these targets related to the total survival time of gastric cancer, MYC, MAPK1, and BAX have better prognosis, while other targets have poorer prognosis. In this modular network, most genes have

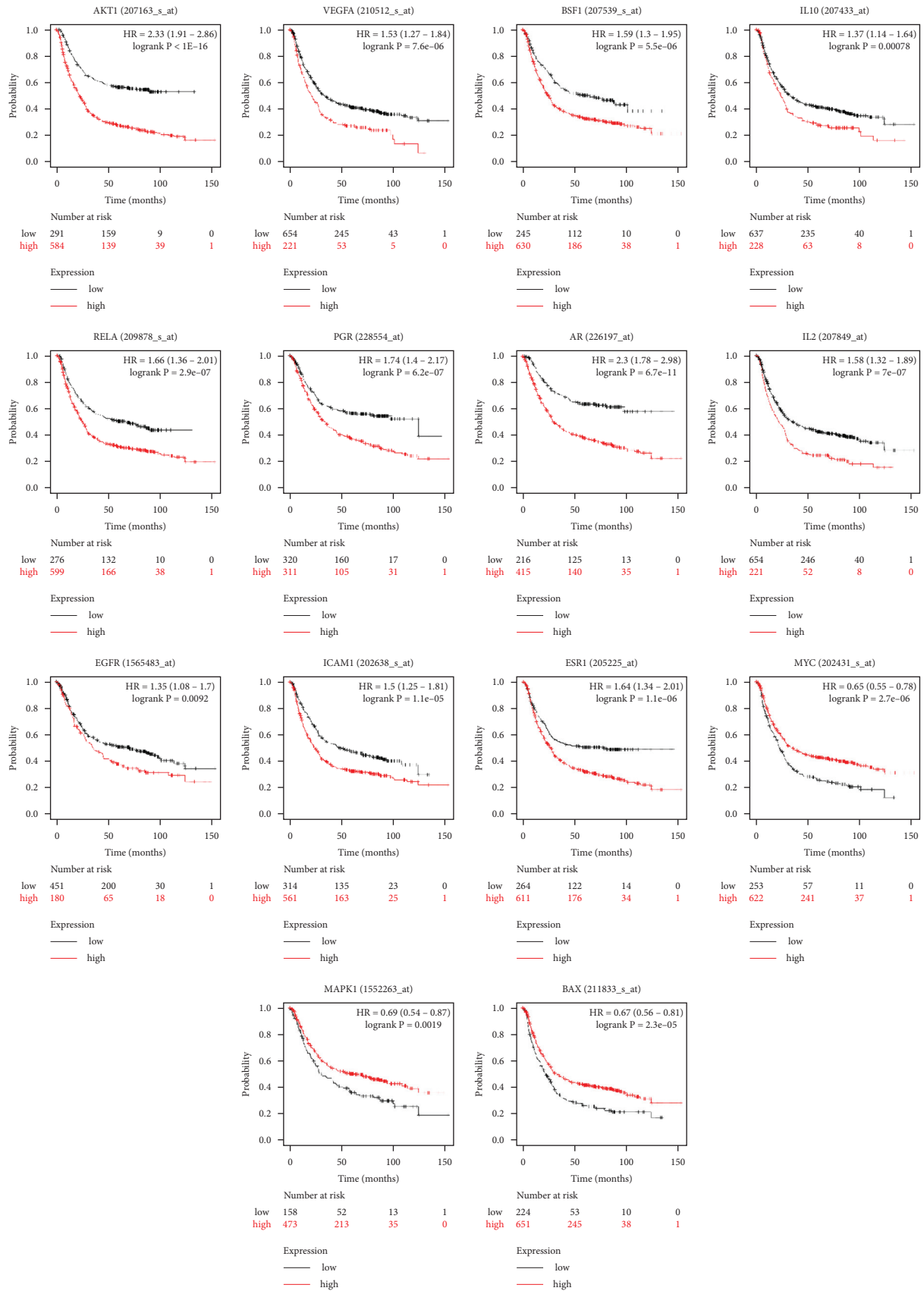


FIGURE 6: Survival analysis of the core target genes.



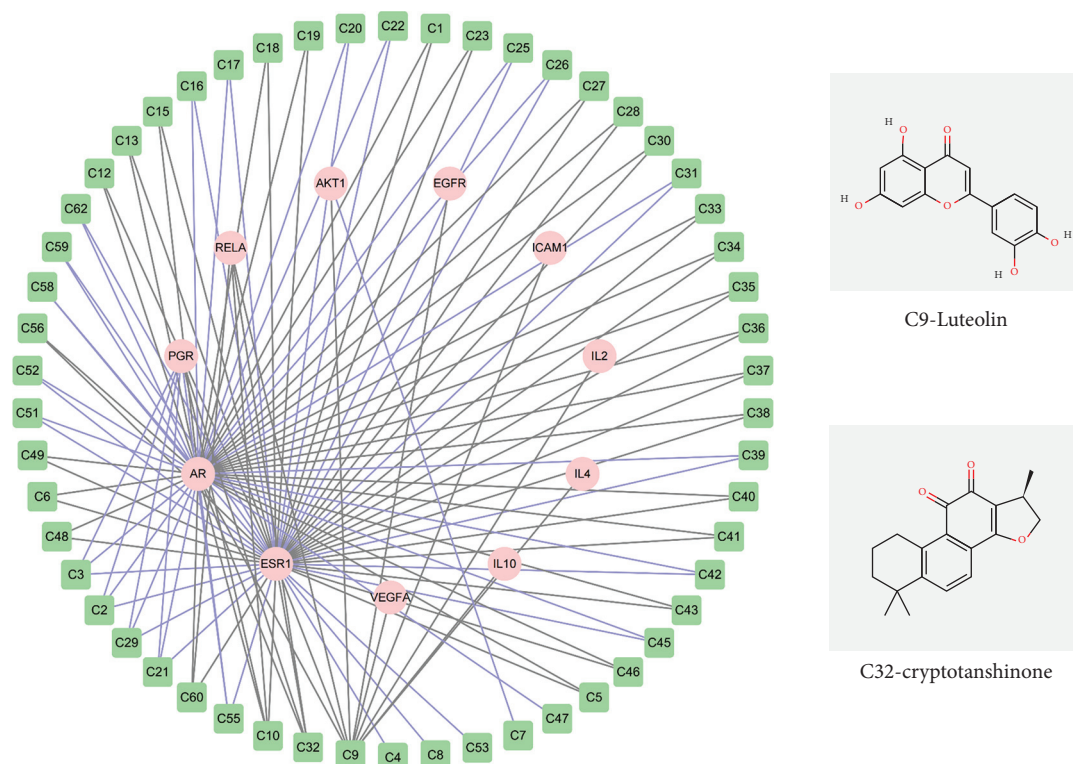


FIGURE 7: Key active compounds in *Codonopsis pilosula*.

prognostic value, and the components acting on them may affect the whole treatment network through these prognostic targets. In addition, among the 14 prognosis-related targets, 11 have poor prognosis, and the components interacting with these targets may play the role of small molecule inhibitors and thus play a therapeutic role.

**3.6. Construction of Core Target-Component Network and Molecular Docking Analysis.** To determine the key components, we further constructed the component network of targets with poor prognosis (Figure 7). The green squares on the periphery of the network represent the components interacting with 11 targets with poor prognosis. By sorting them clockwise according to the magnitude of degree, we can see that the top ranked components are C9, C32, C10, C55, C60, C21, etc., and among the 11 targets, AR and ESR1 have significantly more related components. Therefore, next, we further verify the matching score of the core components. We selected the first two components C9-luteolin and C32-cryptotanshinone with a higher degree to match AR and ESR1, respectively. It is generally believed that the binding energy is less than 0, and the compound and protein can bind spontaneously. The lower the binding energy is, the greater the possibility of interaction is. It is generally believed that the docking score  $\leq -5.0$  kJ mol<sup>-1</sup> indicates a good binding activity. As shown in Figure 8, the core components predicted in this study have strong binding ability with key targets, which confirms the reliability of the prediction results of network pharmacology.

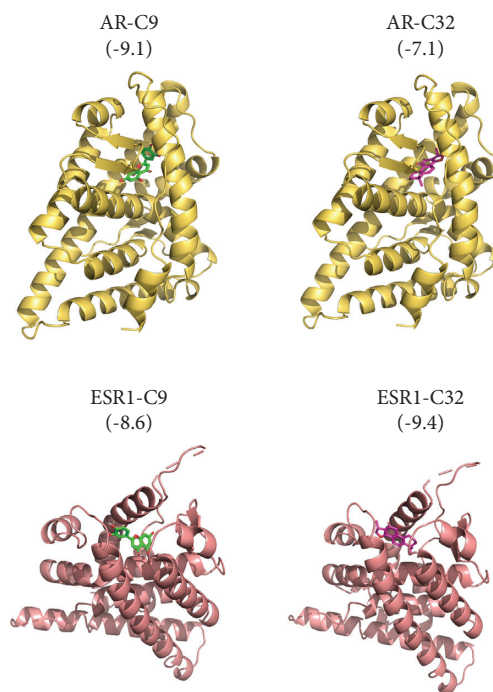


FIGURE 8: Results of molecular docking.

## 4. Discussion

In recent years, the systematic and complete construction of network pharmacology platform has provided us with an opportunity to explore the mechanism of Radix Codonopsis

in the treatment of gastric cancer. Network pharmacology is applicable to the multicomponent, multitarget, and multi-channel characteristics of Chinese medicine to analyze the interaction network of drugs, genes, and diseases. In this study, the main components, action targets, and signaling pathways of Radix Codonopsis in the treatment of gastric cancer were explored by using the network pharmacology platform, which laid a scientific foundation for the clinical application and further research of Radix Codonopsis in the treatment of gastric cancer. We screened and obtained 62 compounds from Radix Codonopsis, and these compounds acted on 155 targets. We obtained a total of 10,479 targets related to gastric cancer. Finally, the obtained common targets of the Radix Codonopsis action target and the gastric cancer-related targets were a potential action target of Radix Codonopsis for treating gastric cancer, and the compound corresponding to the targets may be a component that plays an important role in the treatment of gastric cancer by Radix Codonopsis. We selected an important module from the protein-protein interaction network for in-depth analysis, and the potential action targets mainly included NCOA1, VEGFA, IL10, CDK4, AR, CDK2, PGR, ESR1, NR3C1, EGFR, RXRA, NFKB1, MAPK1, IL4, MYC, PTPN1, RELA, ICAM1, BAX, IL2, AKT1, HSP90AA1, CDK2, AKT1, and JUN. We analyzed the prognosis information of these targets, and the results showed that VEGFA, IL10, AR, PGR, ESR1, EGFR, MAPK1, IL4, MYC, RELA, ICAM1, BAX, IL2, and AKT1 correlated with the overall survival time of gastric cancer. Among these targets related to the total survival time of gastric cancer, MYC, MAPK1, and BAX have better prognosis, while other targets have poor prognosis.

Frycz et al. studied the relationship between mRNA expression of NCOA1, AR, ESR 2, and other genes and clinical pathological characteristics of patients with gastric cancer. The results showed that the levels of AR and NCOA 1 in gastric cancer tissues were significantly reduced. The abnormal expression of AR and NCOA 1 might be related to the occurrence and development of gastric cancer [19]. Studies have shown that tumor angiogenesis plays an important role in the growth and metastasis of gastric cancer. There are many factors that promote tumor angiogenesis, and vascular endothelial growth factor (VEGF) is one of the important factors that promote tumor angiogenesis. The results of the study by Ding S et al. showed significant decreases in serum and plasma VEGFA levels in patients with gastric cancer after surgical resection of the tumor, suggesting that VEGFA may be produced by tumor secretion [20]. IL-10 is a multidirectional cytokine that can regulate tumor suppressor gene. The methylation rate of a CGI fragment of the IL-10 gene in tumor patients was obviously lower than that in normal cells, and the methylation of IL-10 was related to gastric cancer [21]. Through screening, we have obtained that the key active components of Radix Codonopsis in the treatment of gastric cancer are C9-luteolin and C32-cryptotanshinone. Luteolin is one of the common flavonoid compounds with anticarcinogenic effects. The study by Wu et al. has revealed that luteolin has antiproliferation and chemotherapy sensitization effects on human gastric cancer cells [22]. Liu et al. found that

cryptotanshinone can induce extracellular apoptosis and cell cycle arrest through ROS-mediated MAPK and AKT signaling pathways to achieve the effect of treating gastric cancer [23]. Our results are consistent with those in the previous studies and further verified by the molecular docking findings.

## Data Availability

All data supporting this work are included within the paper.

## Conflicts of Interest

The authors declare no conflicts of interest.

## Acknowledgments

This work was supported by the Health Commission of Hunan Province, China (a general project led by Lijun Tang and a research project led by Liming Fang with no. 202112051631). This work was also supported by the Clinical Medical Technology Innovation Guidance Project, Hunan Science and Technology Department (a project led by Jinhui Chen).

## References

- [1] F. Bray, J. Ferlay, I. Soerjomataram, R. L. Siegel, L. A. Torre, and A. Jemal, "Global cancer statistics 2018: GLOBOCAN estimates of incidence and mortality worldwide for 36 cancers in 185 countries," *CA: A Cancer Journal for Clinicians*, vol. 68, no. 6, pp. 394–424, 2018.
- [2] D. Praud, M. Rota, C. Pelucchi et al., "Cigarette smoking and gastric cancer in the stomach cancer pooling (StoP) project," *European Journal of Cancer Prevention*, vol. 27, no. 2, pp. 124–133, 2018.
- [3] S. Hisamichi, R. Sasaki, N. Sugawara, T. Yanbo, and S. Yamagata, "Stomach cancer in various age groups (Japan) as detected by gastric mass survey," *Journal of the American Geriatrics Society*, vol. 27, no. 10, pp. 439–443, 1979.
- [4] H. Sun, X. Wu, F. Wu et al., "Associations of genetic variants in the PSCA, MUC1 and PLCE1 genes with stomach cancer susceptibility in a Chinese population," *PLoS ONE*, vol. 10, no. 2, Article ID e0117576, 2015.
- [5] C. A. González, N. Sala, and T. Rokkas, "Gastric cancer: epidemiologic aspects," *Helicobacter*, vol. 18, pp. 34–38, 2013.
- [6] P. Xia, C.-L. Song, J.-F. Liu, D. Wang, and X.-Y. Xu, "Prognostic value of circulating CD133+ cells in patients with gastric cancer," *Cell Proliferation*, vol. 48, no. 3, pp. 311–317, 2015.
- [7] L. E. Van Vlerken and M. M. Amiji, "Multi-functional polymeric nanoparticles for tumour-targeted drug delivery," *Expert Opinion on Drug Delivery*, vol. 3, no. 2, pp. 205–216, 2006.
- [8] Y. Chen, G. Zhang, X. Chen et al., "Jianpi bushen, a traditional Chinese medicine therapy, combined with chemotherapy for gastric cancer treatment: a meta-analysis of randomized controlled trials," *Evidence-based Complementary and Alternative Medicine*, vol. 2018, 2018.
- [9] T. Jia and H. L. Benjamin, "The enhancing effect of Chinese medicine radix pilosulae on J774 macrophage (党参对鼠 J774 巨噬细胞吞噬活性的增强效应)," *Lishizhen Medicine and*

- Materia Medica Research* (时珍国医国药), vol. 119, Article ID 769F770, 2000.
- [10] Y. Li, Q. Wu, and Q. Lin, "Effect of radix codonopsis and milkvetch root on hemodynamics in chronic heart failure rats," *Chinese Journal of Basic Medicine in Traditional Chinese Medicine*, vol. 7, 2010.
- [11] J. B. Weon, B.-R. Yun, J. Lee et al., "Neuroprotective effect of steamed and fermented codonopsis lanceolata," *Biomolecules & Therapeutics*, vol. 22, no. 3, pp. 246–253, 2014.
- [12] C. Shaofu, H. Li, and Z. Zhuo, "Effects of codonopsis pilosula on gastrin and somatostatin of gastroduodenal mucosa in rabbits," *Journal of China University of Medical Sciences*, vol. 313, pp. 164–165, 2002.
- [13] P. Qiao-na, C. Bei-mi, and S. Wen-guang, "Chemical composition and antibacterial activity of secondary metabolites from endogenesis bacteria gbl18-2 on root nodule of radix astragali," *Acta Agriculturae Jiangxi*, vol. 10, 2008.
- [14] Z. Sun, J. Shao, and M. Guo, "Research progress of Codonopsis pilosula chemical component and pharmacological effects," *Journal of Anhui Agricultural Sciences*, vol. 33, pp. 174–176, 2015.
- [15] C.-x. Liu, R. Liu, H.-r. Fan et al., "Network pharmacology bridges traditional application and modern development of traditional Chinese medicine," *Chinese Herbal Medicines*, vol. 7, no. 1, pp. 3–17, 2015.
- [16] L. Shao and B. Zhang, "Traditional Chinese medicine network pharmacology: theory, methodology and application," *Chinese Journal of Natural Medicines*, vol. 112, pp. 110–120, 2013.
- [17] A. M. Szász, A. Lánckzy, Á. Nagy et al., "Cross-validation of survival associated biomarkers in gastric cancer using transcriptomic data of 1,065 patients," *Oncotarget*, vol. 7, no. 31, pp. 49322–49333, 2016.
- [18] O. Trott, A. J. Olson, and A. Vina, "Improving the speed and accuracy of docking with a new scoring function, efficient optimization, and multithreading," *Journal of Computational Chemistry*, vol. 312, pp. 455–461, 2010.
- [19] B. A. Frycz, D. Murawa, M. Borejsza-Wysocki et al., "mRNA expression of steroidogenic enzymes, steroid hormone receptors and their coregulators in gastric cancer," *Oncology Letters*, vol. 13, no. 5, pp. 3369–3378, 2017.
- [20] S. Ding, S. Lin, X. Dong et al., "Potential prognostic value of circulating levels of vascular endothelial growth factor-a in patients with gastric cancer," *In Vivo*, vol. 194, pp. 793–795, 2005.
- [21] J. Tang, R. Pan, L. Xu et al., "Il10 hypomethylation is associated with the risk of gastric cancer," *Oncology Letters*, vol. 214, p. 1, 2021.
- [22] B. Wu, Q. Zhang, W. Shen, and J. Zhu, "Anti-proliferative and chemosensitizing effects of luteolin on human gastric cancer AGS cell line," *Molecular and Cellular Biochemistry*, vol. 313, no. 1-2, pp. 125–132, 2008.
- [23] C. Liu, H.-N. Sun, Y.-H. Luo et al., "Cryptotanshinone induces ROS-mediated apoptosis in human gastric cancer cells," *Oncotarget*, vol. 8, no. 70, pp. 115398–115412, 2017.

## Research Article

# Study on the Mechanism of *Salvia miltiorrhiza* in the Treatment of Traumatic Bone Defects

Qian Tan, Yaoxi Liu, Ting Lei, Weihua Ye, Xin Hu, Haibo Mei , and Ge Yang 

Pediatric Orthopedic Lab, Department of Orthopedic Surgery, The Hunan Children's Hospital, Changsha 410007, Hunan, China

Correspondence should be addressed to Haibo Mei; [meihaiboprof@outlook.com](mailto:meihaiboprof@outlook.com) and Ge Yang; [yangge@csu.edu.cn](mailto:yangge@csu.edu.cn)

Received 8 September 2021; Accepted 18 September 2021; Published 1 October 2021

Academic Editor: Weiguo Li

Copyright © 2021 Qian Tan et al. This is an open access article distributed under the Creative Commons Attribution License, which permits unrestricted use, distribution, and reproduction in any medium, provided the original work is properly cited.

Traumatic bone defect is one of the major orthopedic diseases in clinics, and its incidence is increasing year by year. And repairing traumatic bone defects is a very difficult problem in clinics at present. The surface of medical titanium-based alloy has good biological properties, and its implant has a certain role in promoting bone in bone tissue. However, titanium-based materials are biologically inert and have no biological activity. As a traditional Chinese medicine, *Salvia miltiorrhiza* has the efficacy of treating bone diseases and promoting bone healing. The curative effect can be better exerted by loading the traditional Chinese medicine active compound *Salvia miltiorrhiza* on the surface of the titanium implant in a certain way. At present, due to the complex chemical composition of *Salvia miltiorrhiza*, the mechanism of its use for the treatment of traumatic bone defects is still unclear. Therefore, in this study, we mainly discussed the potential target and mechanism of *Salvia miltiorrhiza* in the treatment of traumatic bone defects through network pharmacology, which may provide a scientific basis for the treatment of traumatic bone defects with *Salvia miltiorrhiza* loaded on the surface of medical titanium-based alloy. We screened out effective compounds and targets of *Salvia miltiorrhiza* and targets related to traumatic bone defects with the help of relevant databases. The targets of *Salvia miltiorrhiza* for traumatic bone defects were analyzed by STRING and GeneCards databases, and the results were visualized by constructing a compound-target network, protein-protein interaction network, and compound-target-disease network with Cytoscape 3.7.1 analysis software. Finally, the selected core targets carried out GO and KEGG enrichment. The results showed that 60 main active components were screened from *Salvia miltiorrhiza* Bunge, which could act on 149 targets. There were 33 active components and 70 targets related to traumatic bone defects, respectively. The core targets of *Salvia miltiorrhiza* in the treatment of traumatic bone defects were MAPK1, MAPK10, MAPK14, TGFB1, and TNF. The results of enrichment analysis showed that *Salvia miltiorrhiza* might treat traumatic bone defects through an osteogenic differentiation pathway.

## 1. Introduction

Bone is an organ that maintains the normal posture and movement of the human body and has the function of protecting internal organs [1]. Traumatic bone defect is one of the most common, most frequent, and serious diseases in orthopedics and traumatology and even poses a certain threat to patients' lives in severe cases [2]. In recent years, with the continuous development of transportation and construction industry, as well as the deepening of the aging of the population, the incidence of traumatic bone defects is increasing, which has seriously affected the quality of life [3]. The repair and treatment of traumatic bone defects is a very difficult problem in clinical practice at present, and the

treatment of bone defects is mainly through surgery and drug treatment. With the application of orthopedic implants in tissue engineering and the emergence of drugs on the surface of many implants, the combination of traditional Chinese medicine for bone repair and modern biomaterials for bone repair has become a promising treatment for bone defects [4]. Bone defects must be filled and implanted with appropriate substances to accelerate bone repair [5]. Autograft is the preferred filler material due to its biocompatibility and bone induction potential, but its application is limited by the limited number of autologous bones and the surgical trauma it can cause at the donor site [6]. Therefore, at present, we mainly use synthetic bone materials instead of autograft for filling, so as to realize the complete integration

of nonliving implants and living bones [7]. Among them, medical titanium-based alloy is a new generation of medical metal materials developed after medical stainless steel and medical Co-Cr-Mo alloy, which has more excellent biocompatibility and other properties and is more suitable as an implant for the treatment of bone defects [8]. Drug treatment is mainly the use of traditional Chinese medicine internal and external application, the combination of western medicine, etc. The external traditional Chinese medicine can directly reach the focus and has stronger targeting, which can improve the drug concentration in the bone microenvironment [9]. At the same time, the traditional Chinese medicine can avoid liver first-off effect generated after the oral administration of drugs and has the advantages of no gastrointestinal tract stimulation, small toxic and side effects, good patient compliance, and the like so that the traditional Chinese medicine has better clinical effect and more advantages in treating traumatic bone defects [10]. The implant is a biologically inert material with no biological activity and can exert its curative effect by loading externally applied Chinese herbs with bone-promoting effects on the implant. *Salvia miltiorrhiza* is a traditional Chinese medicine and has certain curative effects in treating bone diseases and promoting bone healing. *Salvia miltiorrhiza* loaded on the surface of the titanium implant in a certain way can better exert the curative effect. However, the components of *Salvia miltiorrhiza* Bunge are complex so that the mechanism of *Salvia miltiorrhiza* in the treatment of traumatic bone defects is still unclear, which hinders the application and promotion of *Salvia miltiorrhiza* in the treatment of bone defects to a certain extent. On the basis of the biological network, Chinese medicine network pharmacology analyzes the relationship of the compound, target, and disease in the network by means of database retrieval, high-throughput omics data analysis, and computer simulation to reflect and describe the interaction [11]. In this work, we explored the potential mechanism of *Salvia miltiorrhiza* in the treatment of traumatic bone defects through network pharmacology, which played a positive role in promoting the clinical application of *Salvia miltiorrhiza* in the treatment of bone defects and the development of related drugs.

## 2. Methods

**2.1. Screening of Effective Components and Targets of *Salvia miltiorrhiza*.** We used the Chinese Medicine System Pharmacology Database (TCMSP) to screen. We entered *Salvia miltiorrhiza* under the column "Herb name" to perform search and set the screening conditions as oral bioavailability  $OB \geq 30\%$ , and drug-likeness  $DL \geq 0.18$ . And we obtained the qualified active components of *Salvia miltiorrhiza* [12]. Target proteins related to effective active ingredients of *Salvia miltiorrhiza* were searched separately under the column of "Related Targets." With the help of the UniProt database (<https://www.uniprot.org/>), we standardized the human gene name corresponding to the target protein and finally obtained the target of *Salvia miltiorrhiza*.

**2.2. Screening of Related Targets for Traumatic Bone Defects and Potential Core Targets for Treatment.** We searched the disease-related targets in the GeneCards database and OMIM database with Traumatic bone defect and Traumatic fracture as key words, respectively. Then, we merged and removed the duplicate targets to get the related targets of the traumatic bone defect. The online Venny 2.1 Venn diagram was used to intersect the disease-related targets and drug targets. After that, we obtained the intersection targets of *Salvia miltiorrhiza* and traumatic bone defect, which were the potential therapeutic targets of *Salvia miltiorrhiza* in treating traumatic bone defects.

**2.3. Construction of the Compound-Target Network and Protein-Protein Interaction Network.** We constructed the Chinese medicine regulatory network of "drug-active ingredient-disease-target" using Cytoscape V3.8.2 software for visualization [13]. Finally, we obtained the most effective active ingredients according to the degree analysis. In order to clarify the role of target protein at the level of the biological network system, we introduced the target of *Salvia miltiorrhiza* in treating traumatic bone defects obtained in Section 2.2 into STRING (<https://string-db.org/cgi/input.pl>) to construct the protein-protein interaction network. The setting conditions were as follows: we chose *Homo sapiens* for species, deleted the free target, and set the minimum confidence level to 0.4. We downloaded the corresponding TSV file and imported it into Cytoscape to generate the PPI network and used CytoNCA plugin to analyze the PPI network [14].

**2.4. Enrichment Analysis.** We used DAVID databases (<https://David.ncifcrf.gov/home.jsp>) to perform GO (gene ontology) functional enrichment analysis of core targets [15]; GO functional analysis describes the function of genes, which is divided into molecular biological function (MF), biological process (BP), and cellular components (CC). The KEGG database was used for pathway enrichment analysis of core targets to comprehensively predict the regulatory pathways of *Salvia miltiorrhiza* in the treatment of traumatic bone defects [16].

## 3. Results

**3.1. Composition and Target of *Salvia miltiorrhiza* and Compound-Target Network.** We used the Chinese Medicine System Pharmacology Database (TCMSP) to search the components of *Salvia miltiorrhiza* with setting the screening conditions as oral bioavailability  $OB \geq 30\%$  and drug-likeness  $DL \geq 0.18$ . We obtained 65 kinds of active ingredients through screening and then searched the corresponding target proteins of these 65 components. Five of these 65 components have no corresponding targets. Finally, we integrated targets and removed the duplicate targets to get a total of 149 targets which were the target points of *Salvia miltiorrhiza*. With Cytoscape V3.8.2 software, we built a compound-target network for visualization. As shown in Figure 1, the square node in the middle represents the target, and the darker the square node is, the more compounds act on it. The round nodes represent the

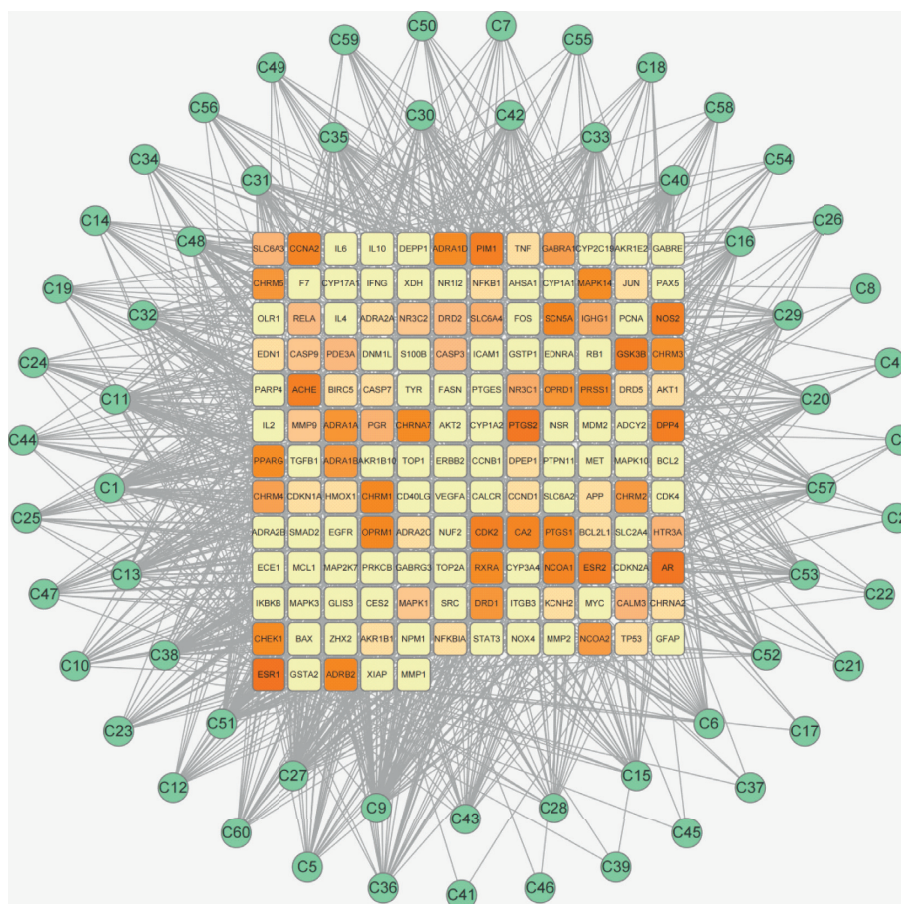


FIGURE 1: Compound-target network.

active components in *Radix Salviae Miltiorrhizae*, and the lines represent the interaction relationship between the active components and the targets. In the network, the components with more targets, which had darker color in the network diagram, may play an important role in the pharmacological function of *Salvia miltiorrhiza*.

**3.2. The Core Target of *Salvia miltiorrhiza* in the Treatment of Traumatic Bone Defects.** We searched the disease-related targets in the GeneCards database and OMIM database with Traumatic bone defect and Traumatic fracture as key words, respectively, and obtained 1700 targets in the GeneCards database and 608 targets in the OMIM database. We finally obtained 1482 targets related to traumatic bone defects after merging and removing the duplicate targets. As shown in Figure 2, we used Venny 2.1 to intersect these 1482 disease-related targets with the above 149 drug targets to get 70 common targets, which were potential therapeutic targets of *Salvia miltiorrhiza* for traumatic bone defects.

**3.3. Protein-Protein Interaction Network.** We introduced the above 70 common target genes into STRING and chose *Homo sapiens* for species, deleted the free target, and set the minimum confidence level to 0.4. Through the information of the database, we obtained the interaction relationship

between the protein and constructed PPI network, as shown in Figure 3. There were 70 nodes and 895 lines in the network graph, and the average nodal degree was 25.6. The nodes represented target proteins, and each line represented the interaction between target proteins. We processed the downloaded TSV file with CytoNCA plugin and finally obtained 14 core target proteins such as MAPK1, MAPK10, MAPK14, TGFB1, TNF, JUN, ITGB3, CALCR, FOS, AKT1, PPARG, IFNG, RELA, and NFN1 (Figure 4). We associated these 14 core targets with the active components of *Salvia miltiorrhiza* and found that 33 active components of *Salvia miltiorrhiza* involve these 14 targets. As shown in Figure 5, rectangular nodes represented key target genes, circular nodes represented active ingredients in *Salvia miltiorrhiza*, and lines represented the interaction relationship between active ingredients and targets. The more lines corresponding to the target meant that more active ingredients acted on the target. The more lines corresponding to the active ingredient represented that there were more targets for the action of this active ingredient. Therefore, the more active ingredients and targets corresponding to the lines may be the key active ingredients and targets of *Salvia miltiorrhiza* in the treatment of traumatic bone defects. Among them, the more important active components and targets were luteolin,  $\alpha$ -amyrin, cryptotanshinone, tanshinone IIA, PPARG, and MAPK14, respectively.

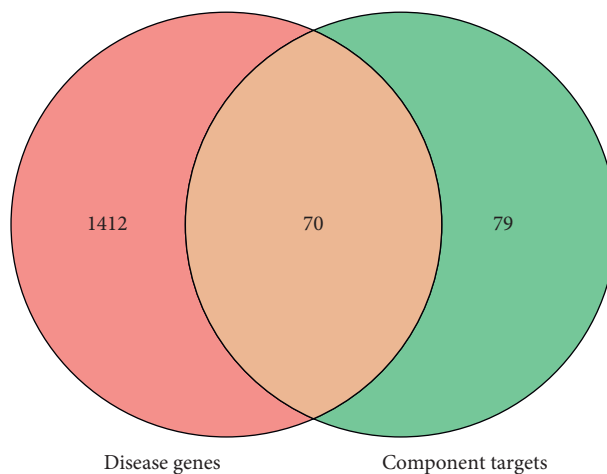


FIGURE 2: Potential therapeutic targets of *Salvia miltiorrhiza* for traumatic bone defects.



FIGURE 3: Network of interactions between proteins.

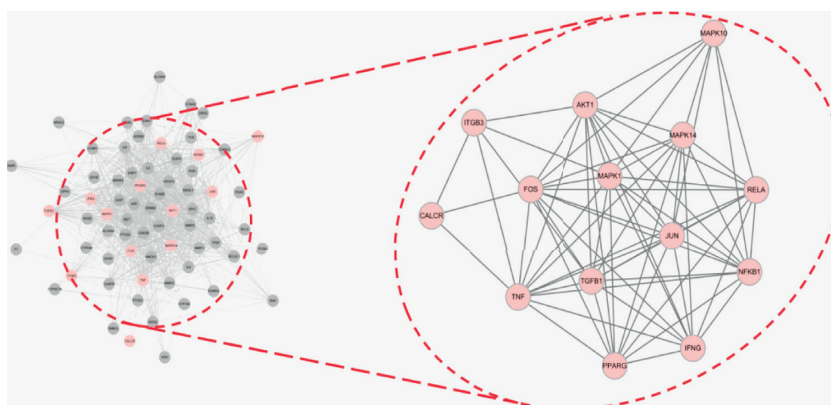


FIGURE 4: The key core targets of *Salvia miltiorrhiza* in the treatment of traumatic bone defects.

**3.4. Enrichment Analysis.** GO functional enrichment analysis consists of three parts: biological process, cellular component, and molecular function. We performed GO

functional enrichment analysis on the common targets of the targets of *Salvia miltiorrhiza* and disease-related targets, as shown in Figure 6, with the vertical axis representing the

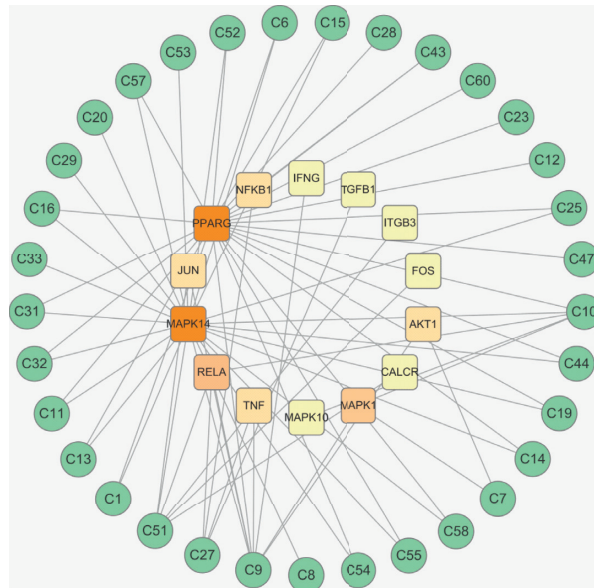


FIGURE 5: Active components corresponding to key core targets.

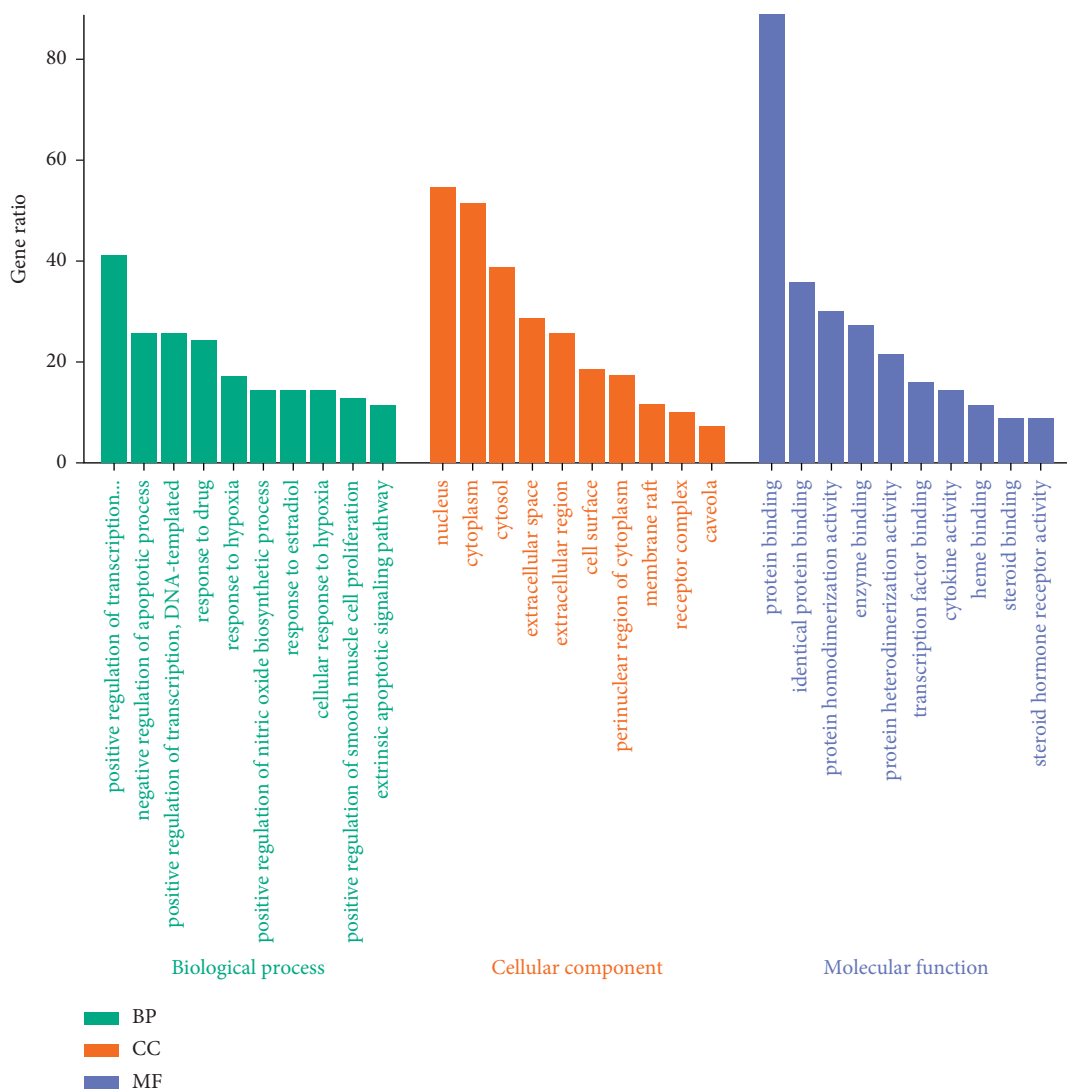


FIGURE 6: GO functional enrichment analysis of 149 targets.





FIGURE 7: The KEGG pathway enrichment analysis of 149 targets.

name of the pathway and the horizontal axis representing the proportion of enriched genes. The results showed that biological processes involved in GO functional enrichment analysis were concentrated in the positive regulation of transcription from the RNA polymerase II promoter, response to the drug, positive regulation of the nitric oxide biosynthetic process, positive regulation of smooth muscle cell proliferation, extrinsic apoptotic signaling pathway in the absence of the ligand, positive regulation of transcription, DNA-templated, etc. The process of cellular components was mainly related to the extracellular space, cell surface, receptor complex, membrane raft, perinuclear region of the cytoplasm, nucleus, extracellular region, cytoplasm, and so on. And the process of molecular functions was mainly related to enzyme binding, identical protein binding, protein homodimerization activity, protein binding, protein heterodimerization activity, cytokine activity, steroid binding, transcription factor binding, heme binding, etc. 149 common target genes were analyzed by KEGG pathway enrichment analysis, and 111 pathways were

obtained. Set the bar chart showing the first 30 paths with the smallest  $p$  value, as shown in Figure 7. And in Figure 7, the abscissa represented the number of enrichment analyses, and the ordinate represented the  $p$  value. The smaller the  $p$  value, redder the color. The results of KEGG pathway enrichment analysis were mainly involved in osteoclast differentiation (hsa04380), apoptosis (hsa04210), PI3K-Akt signaling pathway (hsa04151), T-cell receptor signaling pathway (hsa04660), HIF-1 signaling pathway (hsa04066), TNF signaling pathway (hsa04668), amyotrophic lateral sclerosis (hsa05014), neurotrophin signaling pathway (hsa04722), and so on. Among them, osteoclast differentiation pathway (Figure 8) was closely related to the bone repair.

#### 4. Discussion

Every year, more than 2 million people in the world suffer from bone defects with an economic burden of 3 billion dollars, which seriously affects the quality of life of patients.

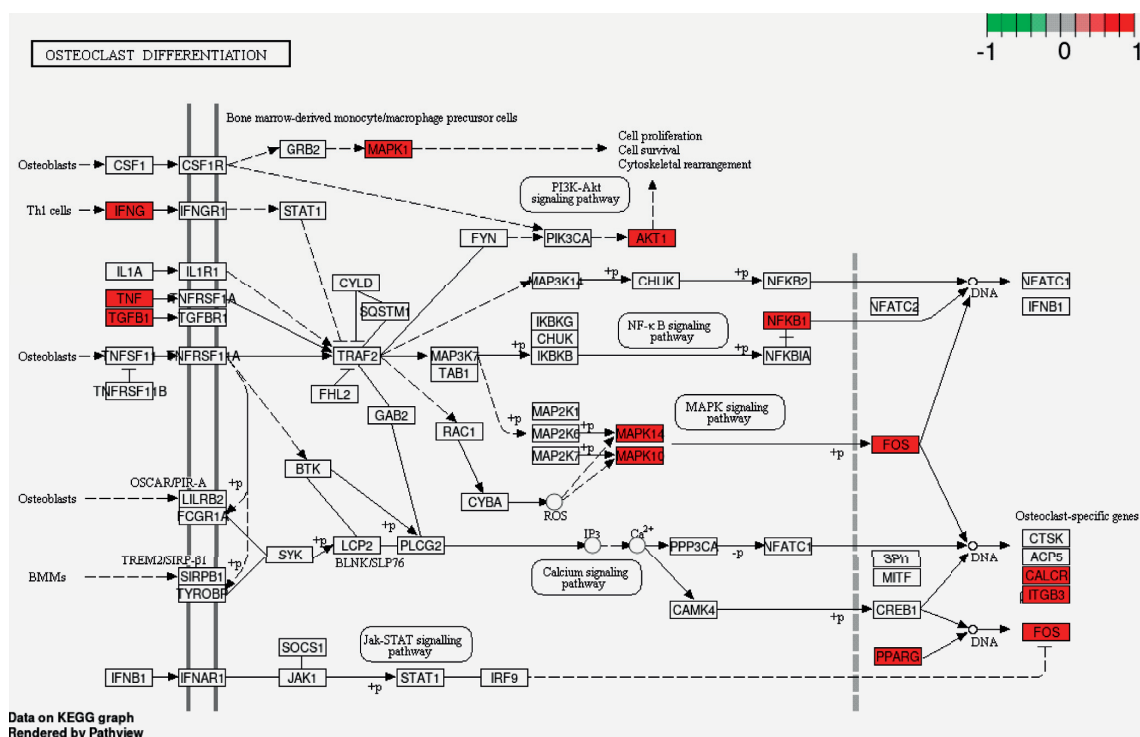


FIGURE 8: The diagram of the osteogenic differentiation pathway.

Bone transplantation is one of the most commonly used surgical operations. Autologous bone is the preferred filling material, but the number of autologous bones is limited [17]. At present, with the application of orthopedic implants in tissue engineering and the emergence of many drugs on the surface of implants, the combination of traditional Chinese medicine bone repair medicine and modern bone repair biomaterials has become a promising treatment method for bone defects. *Salvia miltiorrhiza* has the effect of repairing bone defects, but its mechanism is unclear because of its complex composition. This study preliminarily studied the possible mechanism of *Salvia miltiorrhiza* in treating traumatic bone defects by using the network pharmacology method. The results showed that *Salvia miltiorrhiza* had the characteristics of multicomponent and multitarget in treating traumatic bone defects, and one component of *Salvia miltiorrhiza* can act on multiple targets. According to the analysis of Cytoscape degree values, the ones with the highest component degree values were luteolin,  $\alpha$ -amyrin, cryptotanshinone, and tanshinone IIA, which may be the key components of *Salvia miltiorrhiza* in the treatment of traumatic bone defects. Bone repair depended on bone resorption and bone formation. Excessive osteoclast formation was not conducive to the repair of traumatic bone defects and led to a series of orthopedic diseases such as osteoporosis and rheumatoid arthritis. And our results were consistent with previous studies. Kim found that luteolin, which is a flavonoid compound, can inhibit the differentiation of bone marrow nuclear cells and Raw264.7 cells into osteoclasts and can reduce bone loss in osteoporosis by reducing the differentiation and function of osteoclasts [18].  $\alpha$ -Amyrin is a pentacyclic triterpenoid. Related studies have

shown that  $\alpha$ -amyrin can affect some pathways in skeletal muscle cells. Giacomani-Martínez et al. found that  $\alpha$ -amyrin can induce translocation of glucose transporter 4 (GLUT4) mediated by activated protein kinase (Ampk) and peroxisome proliferator-activated receptors (PPAR  $\delta/\gamma$ ) in C2C12 myoblasts [19]. Cryptotanshinone belongs to a quinone compound. Studies showed that cryptotanshinone can alleviate osteoarthritis in mice. And its mechanism may be that cryptotanshinone can inhibit the production of PGE2 and NO induced by IL-1 $\beta$ , inhibit the expression of ADAMTS-5, COX-2, MMP-3, MMP-13, and iNOS, and achieve it by inhibiting the activation of NF- $\kappa$ B and MAPK pathway [20]. The study showed that tanshinone IIA can inhibit the differentiation of osteoclasts and inhibit the differentiation of osteoclast precursor cells by inhibiting the expression of c-FOS and NFATC1 induced by the NF- $\kappa$ B ligand receptor activator [21]. In this study, it was found that the key targets of *Salvia miltiorrhiza* in the treatment of traumatic bone defects were MAPK1, MAPK10, MAPK14, TGF $\beta$ 1, TNF, JUN, ITGB3, CALCR, FOS, AKT1, PPAR $\gamma$ , IFNG, RELA, and NFNB1. FOS and JUN are members of the AP-1 transcription factor complex and are regulators of many cellular functions. JUN is associated with many inflammatory diseases [22]. FOS is a key regulator of bone cell differentiation, which can induce NFATC1 expression and inhibit osteoclast differentiation under the action of the active ingredient tanshinone IIA [21]. AKT1 is one of the key regulatory molecules of bone synthesis factor signaling and is highly expressed in bone cells [23]. Naohiro Kawamura et al. found that AKT1 can promote bone formation, and its mechanism may be through IGF-I and insulin-mediated osteoblast bone formation [24]. Tang et al. demonstrated

that TGFBI has the function of regulating bone resorption and promoting bone formation. And regulating TGFBI may be an effective method for repairing bone defects. [25]. And PPARG can also regulate bone resorption and bone formation [26]. P38 mitogen-activated protein kinase (MAPK) signaling pathway plays an important role in regulating bone development and maintenance. MAPK14 belongs to the p38 mitogen-activated protein kinase family and is the most abundant member in bone cells in the p38 mitogen-activated protein kinase family [27]. We also found that osteoclast differentiation was an important signaling pathway through GO biological functions and KEGG pathway enrichment analysis, which corresponded to the above main components and targets. Therefore, the active components luteolin,  $\alpha$ -amyrin, cryptotanshinone, and tanshinone IIA in Radix Salviae Miltiorrhizae may play an important role in the treatment of traumatic bone defects, and its mechanism may be related to the regulation of MAPK1, MAPK10, MAPK14, TGFBI, TNF, JUN, ITGB3, CALCR, FOS, AKT1, PPARG, IFNG, RELA, and NFNB1 on the osteogenic differentiation pathway, so as to achieve the therapeutic effect. In this work, we preliminarily discussed the mechanism of *Salvia miltiorrhiza* in treating traumatic bone defects through network pharmacology, which laid a scientific foundation for the clinical application of *Salvia miltiorrhiza*. Math tools are very important in medical applications [28–31]. We think the work benefits the field.

## 5. Conclusion

In this study, we analyzed the mechanism of Radix Salviae Miltiorrhizae in the treatment of traumatic bone defects based on network pharmacology. We found a total of 65 active components in Radix Salviae Miltiorrhizae. Furthermore, through network analysis and screening, we obtained 33 main active components and 70 action targets, which were related to traumatic bone defects. The results showed that its mechanism of treating traumatic bone defects may be that luteolin,  $\alpha$ -amyrin, cryptotanshinone, and tanshinone IIA acted on MAPK1, MAPK10, MAPK14, TGFBI, TNF, JUN, ITGB3, CALCR, FOS, AKT1, PPARG, IFNG, RELA, and NFNB1 by the osteogenic differentiation pathway.

## Data Availability

All the data supporting this work are included within the article.

## Conflicts of Interest

The authors declare no conflicts of interest.

## Acknowledgments

This work was supported by the Clinical Research Center for Limb Deformity of Children in Hunan Province (2019SK4006), the Major Science and Technology Projects for Collaborative Prevention and Control of Birth Defects in Hunan Province (2019SK1010), the Clinical Medical

Technology Innovation Guidance Project, Hunan Province (2020SK50517), and Natural Science Foundation of Hunan Province (2021JJ70081).

## References

- [1] K. Gulati, M. S. Aw, D. Findlay, and D. Losic, "Local drug delivery to the bone by drug-releasing implants: perspectives of nano-engineered titania nanotube arrays," *Therapeutic Delivery*, vol. 3, no. 7, pp. 857–873, 2012.
- [2] P. Haentjens, J. Magaziner, C. S. Colón-Emeric et al., "Meta-analysis: excess mortality after hip fracture among older women and men," *Annals of Internal Medicine*, vol. 152, no. 6, pp. 380–390, 2010.
- [3] S. Maher, A. Mazinani, M. R. Barati, and D. Losic, "Engineered titanium implants for localized drug delivery: recent advances and perspectives of titania nanotubes arrays," *Expert Opinion on Drug Delivery*, vol. 15, no. 10, pp. 1021–1037, 2018.
- [4] L. Mohan, C. Anandan, and N. Rajendran, "Drug release characteristics of quercetin-loaded TiO<sub>2</sub> nanotubes coated with chitosan," *International Journal of Biological Macromolecules*, vol. 93, pp. 1633–1638, 2016.
- [5] M. Kikuchi, S. Itoh, S. Ichinose, K. Shinomiya, and J. Tanaka, "Self-organization mechanism in a bone-like hydroxyapatite/collagen nanocomposite synthesized in vitro and its biological reaction in vivo," *Biomaterials*, vol. 22, no. 13, pp. 1705–1711, 2001.
- [6] C. J. Damien and J. R. Parsons, "Bone graft and bone graft substitutes: a review of current technology and applications," *Journal of Applied Biomaterials*, vol. 2, no. 3, pp. 187–208, 1991.
- [7] B. S. Liu, C. H. Yao, Y. S. Chen, and S. H. Hsu, "In vitro evaluation of degradation and cytotoxicity of a novel composite as a bone substitute," *Journal of Biomedical Materials Research Part A*, vol. 67A, no. 4, pp. 1163–1169, 2003.
- [8] J. Li, Y. Ying, H. Xie et al., "Dual regulatory role of CCNA2 in modulating CDK6 and MET-mediated cell-cycle pathway and EMT progression is blocked by miR-381-3p in bladder cancer," *The FASEB Journal*, vol. 33, no. 1, pp. 1374–1388, 2019.
- [9] S. Rahman, K. Gulati, M. Kogawa et al., "Drug diffusion, integration, and stability of nanoengineered drug-releasing implants in bone ex-vivo," *Journal of Biomedical Materials Research Part A*, vol. 104, no. 3, pp. 714–725, 2016.
- [10] C.-Y. Lin, J.-S. Sun, S.-Y. Sheu, F.-H. Lin, Y.-J. Wang, and L.-T. Chen, "The effect of Chinese medicine on bone cell activities," *American Journal of Chinese Medicine*, vol. 30, no. 02n03, pp. 271–285, 2002.
- [11] H. Yuan, Q. Ma, H. Cui et al., "How can synergism of traditional medicines benefit from network pharmacology?" *Molecules*, vol. 22, no. 7, p. 1135, 2017.
- [12] J. Ru, P. Li, J. Wang et al., "TCMSP: a database of systems pharmacology for drug discovery from herbal medicines," *Journal of Cheminformatics*, vol. 6, no. 1, pp. 13–16, 2014.
- [13] P. Shannon, A. Markiel, O. Ozier et al., "Cytoscape: a software environment for integrated models of biomolecular interaction networks," *Genome Research*, vol. 13, no. 11, pp. 2498–2504, 2003.
- [14] Y. Tang, M. Li, J. Wang, Y. Pan, and F.-X. Wu, "CytoNCA: a cytoscape plugin for centrality analysis and evaluation of protein interaction networks," *Biosystems*, vol. 127, pp. 67–72, 2015.
- [15] G. Dennis, B. T. Sherman, D. A. Hosack et al., "DAVID: database for annotation, visualization, and integrated discovery," *Genome Biology*, vol. 4, no. 5, pp. P3–P11, 2003.

- [16] M. Kanehisa and S. Goto, "KEGG: kyoto encyclopedia of genes and genomes," *Nucleic Acids Research*, vol. 28, no. 1, pp. 27–30, 2000.
- [17] W. Sun, M. Li, L. Xie et al., "Exploring the mechanism of total flavonoids of *Drynariae rhizoma* to improve large bone defects by network pharmacology and experimental assessment," *Frontiers in Pharmacology*, vol. 12, p. 1303, 2021.
- [18] T.-H. Kim, J. W. Jung, B. G. Ha et al., "The effects of luteolin on osteoclast differentiation, function in vitro and ovariectomy-induced bone loss," *The Journal of Nutritional Biochemistry*, vol. 22, no. 1, pp. 8–15, 2011.
- [19] A. Giacomán-Martínez, F. Javier Alarcón-Aguilar, A. Zamilpa et al., " $\alpha$ -amyrin induce GLUT4 translocation mediated by AMPK and PPAR $\delta/\gamma$  in C2C12 myoblasts," *Canadian Journal of Physiology and Pharmacology*, vol. 99, no. 9, 2021.
- [20] Z. Feng, W. Zheng, X. Li et al., "Cryptotanshinone protects against IL-1 $\beta$ -induced inflammation in human osteoarthritis chondrocytes and ameliorates the progression of osteoarthritis in mice," *International Immunopharmacology*, vol. 50, pp. 161–167, 2017.
- [21] H. B. Kwak, D. Yang, H. Ha et al., "Tanshinone IIA inhibits osteoclast differentiation through down-regulation of c-Fos and NFATc1," *Experimental & Molecular Medicine*, vol. 38, no. 3, pp. 256–264, 2006.
- [22] E. Wagner, "Bone development and inflammatory disease is regulated by AP-1 (Fos/Jun)," *Annals of the Rheumatic Diseases*, vol. 69, no. Suppl 1, pp. i86–i88, 2010.
- [23] M. Almeida, L. Han, T. Bellido, S. C. Manolagas, and S. Kousteni, "Wnt proteins prevent apoptosis of both uncommitted osteoblast progenitors and differentiated osteoblasts by  $\beta$ -Catenin-dependent and -independent signaling cascades involving src/ERK and phosphatidylinositol 3-kinase/AKT," *Journal of Biological Chemistry*, vol. 280, no. 50, pp. 41342–41351, 2005.
- [24] N. Kawamura, F. Kugimiya, Y. Oshima et al., "Akt1 in osteoblasts and osteoclasts controls bone remodeling," *PLoS One*, vol. 2, no. 10, Article ID e1058, 2007.
- [25] Y. Tang, X. Wu, W. Lei et al., "TGF- $\beta$ 1-induced migration of bone mesenchymal stem cells couples bone resorption with formation," *Nature Medicine*, vol. 15, no. 7, pp. 757–765, 2009.
- [26] L. A. Stechschulte, P. J. Czernik, Z. C. Rotter et al., "PPARG post-translational modifications regulate bone formation and bone resorption," *EBioMedicine*, vol. 10, pp. 174–184, 2016.
- [27] C. Thouverey and J. Caverzasio, "Focus on the p38 MAPK signaling pathway in bone development and maintenance," *Bonekey Reports*, vol. 4, 2015.
- [28] M. Z. Yang, B. B. Zhang, J. C. Huang et al., "Network pharmacology reveals polyphyllin II as one hit of nano Chinese medicine monomers against nasopharyngeal carcinoma," *Bioinorganic Chemistry and Applications*, vol. 2021, Article ID 9959634, 10 pages, 2021.
- [29] N. Xu, B. B. Zhang, X. N. Huang et al., "S100A8/A9 molecular complexes promote cancer migration and invasion via the p38 MAPK pathway in nasopharyngeal carcinoma," *Bioinorganic Chemistry and Applications*, vol. 2021, Article ID 9913794, 11 pages, 2021.
- [30] X. He, L. Chen, H. Chen, Y. Feng, B. Zhu, and C. Yang, "Diagnostic accuracy of procalcitonin for bacterial infection in liver failure: a meta-analysis," *Bioinorganic Chemistry and Applications*, vol. 2021, Article ID 5801139, 8 pages, 2021.
- [31] M. Liu, X. Lin, Q. Tan, and X. Han, "Evidence-based analysis of the emergency temporary cardiac pacing (electrical stimulation from metal wire electrode)," *Bioinorganic Chemistry and Applications*, vol. 2021, Article ID 5677598, 9 pages, 2021.

## Research Article

# SPSS Analysis of Pain Factors in Rotator Cuff Repair

Yi Zhou,<sup>1</sup> Huali Chen ,<sup>2</sup> Jing Wang,<sup>1</sup> Hui Wu,<sup>1</sup> Yuanjie Zeng,<sup>1</sup> Xiaohui Yi,<sup>1</sup>  
and Yan Zhang <sup>3,4</sup>

<sup>1</sup>Department of Orthopedics (Department of Osteoarticular and Sports Medicine), Hunan Provincial People's Hospital (The First-Affiliated Hospital of Hunan Normal University), Changsha 410005, China

<sup>2</sup>Quality Control Office of Nursing Department, Hunan Provincial People's Hospital (The First-Affiliated Hospital of Hunan Normal University), Changsha 410005, China

<sup>3</sup>Department of Cardiovascular Internal Medicine, Hunan Provincial People's Hospital (The First-Affiliated Hospital of Hunan Normal University), Changsha 410005, China

<sup>4</sup>Hunan Provincial Heart Failure Clinical Medical Research Center, Hunan Provincial People's Hospital (The First-Affiliated Hospital of Hunan Normal University), Changsha 410005, China

Correspondence should be addressed to Yan Zhang; zhangyan.01@outlook.com

Received 4 September 2021; Accepted 15 September 2021; Published 29 September 2021

Academic Editor: Weiguo Li

Copyright © 2021 Yi Zhou et al. This is an open access article distributed under the Creative Commons Attribution License, which permits unrestricted use, distribution, and reproduction in any medium, provided the original work is properly cited.

In this study, the matched case-control study was used. Nineteen cases of severe pain in the early postoperative period among 55 patients were set as the observation group, and 57 cases of simultaneous rotator cuff repair without severe pain were matched in a 1:3 ratio as the control group. Patients' general information, disease characteristics, anesthesia and analgesia scheme, and operation information were collected. Frequency statistics, Wilcoxon signed rank sum test, regulatory effect analysis, and Poisson regression analysis were performed on these data. Some findings are included in the analysis. (1) There was a markable difference of 0.01 between the preoperative 48 h maximum pain value and the postoperative 48 h maximum pain value in the observation group. (2) There was a markable difference of 0.01 between the size and shape of the wound tear and the maximum pain value at 48 h after operation in the observation group. (3) When the number of opioid use affected the maximum pain value at 48 h after operation, the regulatory variables (type, quantity, and number of days of postoperative analgesics) were at different levels, and the impact amplitude had markable differences. (4) Age has a markable negative impact on the postoperative hospital stay. (5) The operation duration has a markable positive relationship with the postoperative hospital stay. (6) The analgesic pump had a markable positive impact on the postoperative hospital stay. (7) The location of injury did not affect the postoperative hospital stay.

## 1. Introduction

Rotator cuff suture reduces the postoperative adhesion of the shoulder joint in wound treatment and can restore the shoulder joint function of patients to the maximum degree [1, 2]. Compared with the previous incision treatment, the rotator cuff suture has the advantages of less trauma [3], smaller incision, and more beautiful appearance after operation [4, 5].

SPSS is very useful in data analysis [6]. The pain problem before and after surgery has been widely discussed by scholars, and mathematical analysis is gradually used more

frequently [7–9]. Many studies have discussed rotator cuff sutures with the method of mathematical analysis [10–12]. There are many other studies that have been conducted prospectively in patients with rotator cuff sutures [13, 14]. Derwin and Sahoo [15] studied factors such as the number of suture anchors used in rotator cuff repair and pain. Some researchers have described the magnitude of pain after rotator cuff suture [16]. Pain-related studies in rotator cuff sutures also include predictions of surgical outcomes and discussion of the size and shape of a patient's wound [17, 18].

The above observations indicate that the pain factors in patients undergoing rotator cuff repair deserve further

analysis. In this work, we analyzed preoperative and postoperative pain in 55 patients to observe disease characteristics, anesthesia and analgesia regimens, operative information, and so on. SPSS software was used for frequency statistics, Wilcoxon signed rank sum test, adjustment effect analysis, and Poisson regression analysis. This work can further discuss the situation of pain factors in rotator cuff sutures.

## 2. Objective and Methods

The statistic analysis of the frequency for 55 patients is given in Table 1.

Table 1 provides the results of the frequency analysis for 55 patients. The original information is shown in Supplementary Materials. SPSS was used to analyze the results. As can be seen from the above table, on the distribution of the affected side in the observation group, most of the samples were “right shoulder,” and the proportion was 76.92%. The proportion of “women” in the observation group was 53.85% and that of the male sample was 46.15%. The proportion of “right shoulder” in the control group was 64.29%. There was also left shoulder in 35.71% of samples. The highest proportion of females in the control group was 69.05%. 30.95% of the samples were male.

## 3. Results and Discussion

The paired sample Wilcoxon analysis results are given in Table 2.

It can be seen from Table 2 that the Wilcoxon signed rank-sum test is used to study the differences of experimental data. Among the two paired datasets, one actually presented a difference ( $p < 0.05$ ). The specific analysis shows that there is a markable difference of 0.01 level between the presurgery and postsurgery 48 h maximum pain values in the observation group ( $p < 0.01$ ), and the specific comparison difference shows that the presurgery median value (3.000) in the observation group is markably lower than the median value of postsurgery 48 h maximum pain value (8.000). Therefore, the observation group data were true and valid. Next, the observation group data were analyzed.

It can be seen from Table 3 that the Wilcoxon signed rank-sum test is used to study the differences of experimental data. The paired data of the two groups showed differences ( $p < 0.05$ ). The specific analysis showed that there was a markable difference of 0.01 between the wound tear size and the maximum pain 48 h after surgery in the observation group ( $p = 0.003 < 0.01$ ). By specific comparison, the median tear size (1.500) was markably lower than the median maximum pain 48 h after surgery (8.000).

There was a markable difference at the 0.01 level between wound tear shape and wound retraction ( $p = 0.009 < 0.01$ ), and the median tear shape (2.000) was markably higher than the median retraction.

A total of 2 sets of paired data will all present differences.

As given in Table 4, some information of patients is missing the variables to be investigated in this analysis, so  $n = 13$ . The regulatory effects were divided into three models, with the independent variable (opioid use times) included in

model 1. Model 2 included regulatory variables (type, quantity, and number of days of postoperative analgesics) on the basis of model 1, and model 3 included interactive terms (the product term of independent variables and regulatory variables) on the basis of model 2.

Model 1 was used for studying the effect of independent variable (opioid use times) on dependent variable (maximum pain 48 h after surgery) without considering the interference of regulatory variables (type, quantity, and number of days of postoperative analgesics). As given in the above table, the independent variable (number of opioid use) showed markable ( $t = 0.696$ ,  $p = 0.501 > 0.05$ ). This means that, regardless of the effects of regulatory variables (type, quantity, and number of days of postoperative analgesics), the number of opioid use did not have a markable impact on the maximum pain value at 48 h after surgery, which should still be investigated for further regulatory effects.

The adjustment effect can be viewed in two ways. The first way is to view the significance of  $F$  value change from model 2 to model 3. The second way is to check the significance of the interaction items in model 3. The regulation effect is analyzed in the second way this time.

As given in the above table, the interaction between the number of opioid use and the type, quantity, and number of days of postoperative analgesics was statistically markable ( $t = -2.874$ ,  $p = 0.018 < 0.05$ ). It meant that when the number of opioid use affected the maximum pain value at 48 h after operation, the magnitude of impact was markably different when the regulatory variables (type, quantity, and number of days of postoperative analgesic drugs) were at different levels.

As given in Table 5, age, operation duration, analgesic pump, and injury site in the observation group were regarded as independent variables, while the postoperative hospital stay was regarded as dependent variable for Poisson regression analysis. Only 10 cases met the requirements when the data of age, operation time, analgesic pump, and injury site of the observation group were available. Therefore, only these ten cases were analyzed. The model pseudo- $R$  formula (McFadden  $R$  formula) was 0.487, which meant that age, operation duration, analgesic pump, and injury site could explain 48.7% of the change in the postoperative hospital stay. It can be seen from the above table that the model formula was  $\log(u) = 5.979 - 0.122^* \text{age} + 0.015^* \text{operation duration} + 1.513^* \text{analgesic pump} - 0.045^* \text{injury site}$  (where  $U$  represents the expected mean).

The regression coefficient value of age was  $-0.122$  and showed a markable value at 0.01 level ( $Z = -5.394$ ,  $p < 0.01$ ), which meant that age had a markable negative impact on the postoperative hospital stay. An OR of 0.885 meant a 0.885-fold change in postoperative hospital stay as age increased by one unit.

The regression coefficient value of the operation duration was 0.015, and the significance was shown at 0.05 level ( $z = 2.260$ ,  $p = 0.024 < 0.05$ ), indicating that the operation duration had a markable positive impact on the postoperative hospital stay. An OR of 1.015 indicated a 1.015-fold increase in postoperative hospital stay with a unit increase in procedure duration.

TABLE 1: Statistic analysis of the frequency for 55 patients.

Name	Option	Frequency	Percentage (%)
Affected side of the observation group ( $n = 13$ )	Right shoulder	10	76.92
	Left shoulder	3	23.08
Gender ( $n = 13$ )	Woman	7	53.85
	Man	6	46.15
Affected side of the control group ( $n = 42$ )	Right shoulder	27	64.29
	Left shoulder	15	35.71
Gender ( $n = 42$ )	Woman	29	69.05
	Man	13	30.95
Add up to			100.0

TABLE 2: Paired sample Wilcoxon analysis results.

Name	Paired (median)		Difference (pair 1-pair 2)	Statistical value, $z$	$P$
	Pair 1	Pair 2			
Maximum pain 48 h after preoperative pairing in the observation group	3.000	8.000	-5.000	3.208	$\leq 0.001^{**}$
Patients in the control group were paired with the maximum pain value at 48 h after operation	3.000	3.000	0.000	0.493	0.622

$**P < 0.01$ .

TABLE 3: Paired sample Wilcoxon analysis results.

Name	Paired (median)		Difference (pair 1-pair 2)	Statistical value, $z$	$P$
	Pair 1	Pair 2			
The size of wound tear in the observation group was paired with the maximum pain value at 48 h after operation	1.500	8.000	-6.500	2.944	0.003 $^{**}$
Does the tear shape pair retract	2.000	0.000	2.000	2.598	0.00 $^{**}$

$**P < 0.01$ .

TABLE 4: Adjustment effect analysis results ( $n = 13$ ).

Name	Model 1			Model 2			Model 3			
	Standard error	$t$	$P$	Standard error	$t$	$P$	Standard error	$t$	$P$	
Constant	0.184	41.298	$\leq 0.001^{**}$	0.191	39.78	$\leq 0.001^{**}$	0.147	51.686	$\leq 0.001^{**}$	
Number of opioid uses	0.103	0.696	0.501	0.107	0.714	0.492	0.092	-0.488	0.637	
Type, quantity, and number of days of postoperative analgesic				0.066	0.455	0.659	0.056	-0.665	0.523	
Number of opioid use*, type, quantity, and number of days of postoperative analgesics							0.028	-2.874	0.018*	
$R^2$		0.042			0.062			0.511		
Adjust $r$		-0.045			-0.126			0.347		
Variance ratio		$F(1, 11) = 0.485, p = 0.501$			$F(2, 10) = 0.328, p = 0.728$			$F(3, 9) = 3.130, p = 0.080$		
$\Delta R^2$		0.042			0.019			0.449		
$\Delta F$ value		$F(1, 11) = 0.485, p = 0.501$			$F(1, 10) = 0.207, p = 0.659$			$F(1, 9) = 8.258, p = 0.018$		

Dependent variable: maximum pain 48 h after surgery in the observation group. \* $P < 0.05$ . \*\* $P < 0.01$ .

The regression coefficient value of the analgesic pump was 1.513, and the significance was shown at 0.01 level ( $z = 3.212, p < 0.01$ ), which meant that the analgesic pump had a markable positive impact on the postoperative hospital stay. An odds ratio (OR value) of 4.540, which means a 4.540-fold change in postoperative hospital days, occurred when the analgesic pump was increased by one unit.

The regression coefficient value for the injury site was -0.045, but it was not markable ( $z = -0.195, p = 0.845 > 0.05$ ), suggesting that the injury site did not affect the postoperative hospital stay.

According to the summary and analysis, it can be seen that the operation duration and analgesic pump have a markable positive impact on the postoperative hospital

TABLE 5: Summary of Poisson regression analysis results ( $n = 10$ ).

Item	Coefficient of regression	Standard error	Z value	P value	OR value	OR value, 95% CI
Observation group age	-0.122	0.023	-5.394	$\leq 0.001^{**}$	0.885	0.846-0.925
Duration of surgery	0.015	0.006	2.260	0.024	1.015	1.002-1.028
Analgesic pump	1.513	0.471	3.212	$\leq 0.001^{**}$	4.540	1.804-11.428
Injury site	-0.045	0.232	-0.195	0.845	0.956	0.606-1.507
Intercept	5.979	1.668	3.584	$\leq 0.001^{**}$	395.129	15.024-10391.750

Dependent variable: postoperative hospital stay in the observation group. McFadden  $R$  formula, 0.487.

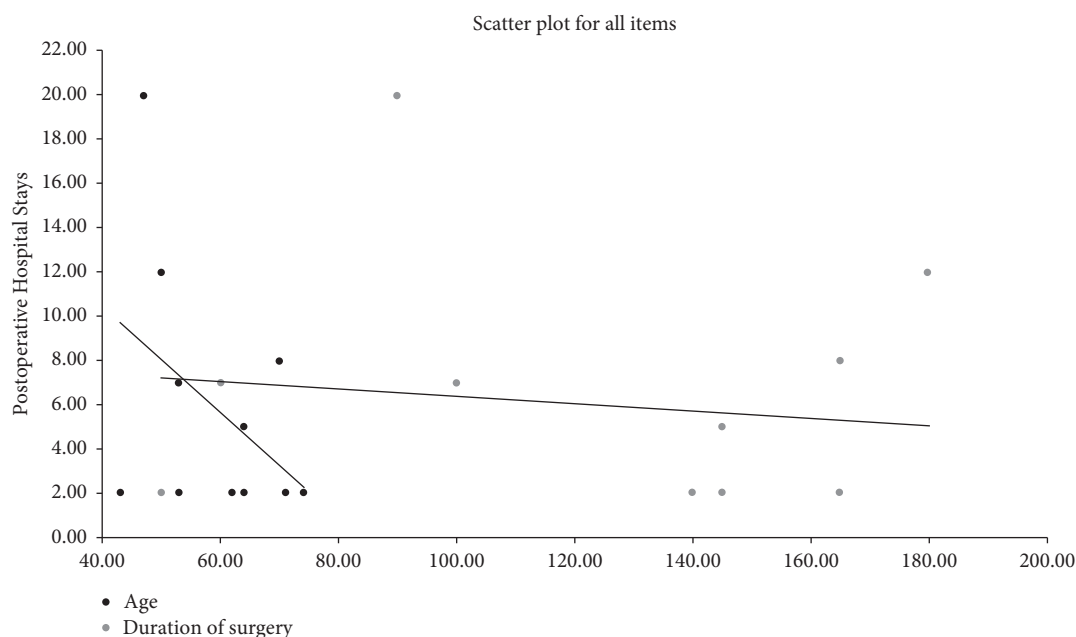


FIGURE 1: Scatter plot for 3 items.

stay, and age has a markable negative impact on the postoperative hospital stay. However, the injury site did not affect the postoperative hospital stay. The scatter plot of age, operation duration (analgesia pump was not good for making trend chart, so it was excluded), and postoperative hospital days in the observation group is shown in Figure 1.

#### 4. Conclusions

Data analysis was performed on 55 patients. In the matched case-control study, 19 cases with severe pain in the early postoperative period were set as the observation group, and 57 cases without severe pain who underwent rotator cuff repair at the same time were matched according to the ratio of 1:3 as the control group. The general data, disease characteristics, anesthesia and analgesia scheme, and operation information of the patients were collected. The data were subjected to frequency statistics, Wilcoxon signed rank-sum test, adjustment effect analysis, and Poisson regression analysis. Some findings were included in the analysis. (1) There was a markable difference of 0.01 between the preoperative 48 h maximum pain value and the postoperative 48 h maximum pain value in the observation group. (2) There was a markable difference of 0.01 between

the size and shape of the wound tear and the maximum pain value at 48 h after operation in the observation group. (3) When the number of opioid use affected the maximum pain value at 48 h after operation, the regulatory variables (type, quantity, and number of days of postoperative analgesics) were at different levels, and the impact amplitude had markable differences. (4) Age has a markable negative impact on the postoperative hospital stay. (5) The operation duration has a markable positive relationship with the postoperative hospital stay. (6) The analgesic pump had a markable positive impact on the postoperative hospital stay. (7) The location of injury did not affect the postoperative hospital stay.

#### Data Availability

The data used to support the findings of this study are included within the article and the Supplementary Materials.

#### Ethical Approval

Ethical approval for this work was obtained from the Ethical Review Committee of Hunan Provincial People's Hospital (the First Affiliated Hospital of Hunan Normal University).



## Conflicts of Interest

The authors declare that they have no conflicts of interest.

## Acknowledgments

This work was supported by Health Commission of Hunan Province, China (Project No. 202104072141).

## Supplementary Materials

Raw data for the analysis. (*Supplementary Materials*)

## References

- [1] R. Prasetya, B. Sukhapradit, and B. Chernchujit, "Clinical features and repair integrity after knotless-in situ suture bridge technique in high-grade bursal side rotator cuff tears," *Journal of Orthopaedics*, vol. 20, pp. 352–358, 2020.
- [2] N. A. Zurita Uroz, F. Abat, and A. Calvo Diaz, "All-suture repair for compressive rotator cuff tears: reducing the traction of the tissue," *Arthroscopy Techniques*, vol. 6, no. 2, pp. e499–e503, 2017.
- [3] H. Van der Bracht, T. Van den Langenbergh, M. Pouillon, S. Verhasselt, P. Verniers, and D. Stoffelen, "Rotator cuff repair with all-suture anchors: a midterm magnetic resonance imaging evaluation of repair integrity and cyst formation," *Journal of Shoulder and Elbow Surgery*, vol. 27, no. 11, pp. 2006–2012, 2018.
- [4] M. P. McCabe, "Editorial commentary: choose wisely: rotator cuff all-suture anchors," *Arthroscopy: The Journal of Arthroscopic & Related Surgery*, vol. 36, no. 11, pp. 2812–2813, 2020.
- [5] J. Buckup, D. Smolen, F. Hess, C. Sternberg, and J. Leuzinger, "The arthroscopic triple-row modified suture bridge technique for rotator cuff repair: functional outcome and repair integrity," *Journal of Shoulder and Elbow Surgery*, vol. 29, no. 2, pp. 308–315, 2020.
- [6] Q. Tan and W. Shao, "Investigation on Health promotion by the typical sports for teenagers with self-efficacy and sports commitment questionnaires," *Evidence-Based Complementary and Alternative Medicine: eCAM*, vol. 2021, Article ID 8677182, 7 pages, 2021.
- [7] M. A. Röling, B. Hesselting, N. M. C. Mathijssen, and R. M. Bloem, "Hip arthroscopy for femoroacetabular impingement syndrome results in 2 recovery patterns based on preoperative pain and on arthritis: improvers and non-improvers," *Arthroscopy, Sports Medicine, and Rehabilitation*, 2021.
- [8] K. Powezka, T. Adjei, W. von Rosenberg et al., "A pilot study of preoperative heart rate variability predicting pain during local anesthetic varicose vein surgery," *Journal of Vascular Surgery: Venous and Lymphatic Disorders*, vol. 7, no. 3, pp. 382–386, 2019.
- [9] X. He, L. Chen, H. Chen, Y. Feng, B. Zhu, and C. Yang, "Diagnostic accuracy of procalcitonin for bacterial infection in liver failure: a meta-analysis," *Bioinorganic Chemistry and Applications*, vol. 2021, Article ID 5801139, 8 pages, 2021.
- [10] G. Villatte, R. Erivan, J. Barth, N. Bonneville, S. Descamps, and S. Boisgard, "Progression and projection for shoulder surgery in France, 2012–2070: epidemiologic study with trend and projection analysis," *Orthopaedics & Traumatology: Surgery & Research*, vol. 106, no. 6, pp. 1067–1077, 2020.
- [11] M. Liu, X. Lin, Q. Tan, and X. Han, "Evidence-based analysis of the emergency temporary cardiac pacing (electrical stimulation from metal wire electrode)," *Bioinorganic Chemistry and Applications*, vol. 2021, Article ID 5677598, 9 pages, 2021.
- [12] J. Johnson, M. Pinto, E. Brabston et al., "Attitudes and awareness of suture anchor cost: a survey of shoulder surgeons performing rotator cuff repairs," *Journal of Shoulder and Elbow Surgery*, vol. 29, no. 3, pp. 643–653, 2020.
- [13] R. Dukan, P. Ledinot, J. Donadio, and P. Boyer, "Arthroscopic rotator cuff repair with a knotless suture bridge technique: functional and radiological outcomes after a minimum follow-up of 5 years," *Arthroscopy: The Journal of Arthroscopic & Related Surgery*, vol. 35, no. 7, pp. 2003–2011, 2019.
- [14] P. Belón-Perez and A. I. Cuesta-Vargas, "Immediate effects of thoracic spine manipulation upon shoulder functionality in patients with sutured rotator cuff repair: a prospective study," *Journal of Manipulative and Physiological Therapeutics*, vol. 41, no. 7, pp. 589–595, 2018.
- [15] K. A. Derwin, S. Sahoo, A. Zajichek et al., "Tear characteristics and surgeon influence repair technique and suture anchor use in repair of superior-posterior rotator cuff tendon tears," *Journal of Shoulder and Elbow Surgery*, vol. 28, no. 2, pp. 227–236, 2019.
- [16] K. Yamakado, "A prospective randomized trial comparing suture bridge and medially based single-row rotator cuff repair in medium-sized supraspinatus tears," *Arthroscopy: The Journal of Arthroscopic & Related Surgery*, vol. 35, no. 10, pp. 2803–2813, 2019.
- [17] D. Goutallier, J.-M. Postel, X. Chevalier, J. Beaudreuil, and S. Zilber, "Intermediate term functional outcome prediction following full thickness rotator cuff tear reparative or not reparative surgery," *Orthopaedics & Traumatology: Surgery & Research*, vol. 96, no. 7, pp. 727–733, 2010.
- [18] E. Buess, K.-U. Steuber, and B. Waibl, "Open versus arthroscopic rotator cuff repair: a comparative view of 96 cases," *Arthroscopy: The Journal of Arthroscopic & Related Surgery*, vol. 21, no. 5, pp. 597–604, 2005.

## Review Article

# Application of Nanooptics in Photographic Imagery and Medical Imaging

Yunrun Liu,<sup>1,2</sup> Na Pang,<sup>3</sup> Yunzhou Cai,<sup>1</sup> Yanqing Yang,<sup>1</sup> Chunyu Zeng,<sup>1</sup>  
and Yuehong Wang<sup>1</sup> 

<sup>1</sup>Hunan Key Laboratory of Oral Health Research & Hunan 3D Printing Engineering Research Center of Oral Care & Hunan Clinical Research Center of Oral Major Diseases and Oral Health & Academician Workstation for Oral-Maxillofacial and Regenerative Medicine & Xiangya School of Stomatology, Central South University, Changsha 410008, China

<sup>2</sup>Beijing Normal University-Hong Kong Baptist University United International College (UIC), Zhuhai 519087, China

<sup>3</sup>Pangna Dental Clinic, Yantai 265400, Shandong, China

Correspondence should be addressed to Yuehong Wang; wangyuehong1999@csu.edu.cn

Received 25 August 2021; Accepted 3 September 2021; Published 28 September 2021

Academic Editor: Weiguo Li

Copyright © 2021 Yunrun Liu et al. This is an open access article distributed under the Creative Commons Attribution License, which permits unrestricted use, distribution, and reproduction in any medium, provided the original work is properly cited.

**Background.** At present, with the continuous development of nanotechnology, great changes have taken place in people's lives in medical treatment, production, daily leisure, and so on. Nanooptical technology is entirely based on nanotechnology that laser and visible light are limited to submicron structures (nanopores, nanoslits, and nanoneedles). Due to the great development potential of nanooptical technology in nanoscale sensors, TOF camera applications, THz imaging technology, and other imaging equipment materials and applications, people have been interested in it, recently. **Scope and Approach.** In this review, the importance of good practices for nanooptical technology used in equipment as both nanometer scale sensors and optical auxiliary equipment is described. Based on recent reports, this work discussed the development of nanooptical technology in daily photography and medical imaging from both the positive and the negative sides and compared the engineering techniques. **Key Findings and Conclusions.** As a kind of new optical technology, nanooptical technology can produce the plasmonic effect under the intense collision of atoms and electrons in nanostructures. It has significant effects in superresolution nanolithography, high-density data storage, near-field optics, and other fields. Although the current nanooptical technology is not extremely mature, the results obtained from current works are pointing out that nanooptical technology is the future of daily imaging and medical imaging, and it also will play a positive role in the improvement of people's health and ecological environment quality. As a trend, nanooptical technology is developing in the direction of energy-saving, portability, high efficiency, and low pollution, and in the upsurge of environmental protection in the world, nanooptical technology will surely achieve amazing development in the field of daily photography and medical imaging. Under the huge market demand and innovation power, nanophotonics technology will cover all emerging technologies that share the same research field with it and take advantage of each technology (terahertz, cell and molecular microscopy, and nanoscale probes) to develop an unprecedented new century in nanoscience. The future trends of research contain finding new imaging equipment with nanostructure, designing nanooptical products, and improving engineering techniques.

## 1. Introduction

With the development of industrialization, optics, an ancient subject, has developed rapidly. In recent years, optics has evolved into many branches, such as nanooptics, metasurface, terahertz, and so on. As a result, in information

transmission, more and more channels are needed, the storage density is higher than before, and the processing speed is faster. Therefore, the size of the unit device is required to be smaller, and in the final size to break through the diffraction limit, the space distance of the device is also smaller. With the increasing demand for information in the

21st century, nanophotonics as a new optical technology has unimaginable development potential in digital imaging and digital storage.

Nanophotonics is the combination of nanotechnology and photonics, which are two major technologies in the 21st century. Its main advantage is that it can realize many new functions on the basis of local electromagnetic interaction. In nanophotonics, the traditional concepts of interference and diffraction are no longer applicable, but replaced by some new concepts. In the near-field condition, the size of the unit device is tens of nanometers, and the corresponding energy transmission time is tens of picoseconds. Compared with the current electronic integration technology, these parameters are undoubtedly a leap [1]. Since 1999, the integration technology of nanophotonic devices based on surface plasmon and near-field optics has developed rapidly [2]. Japan, the United States, France, Germany, and other developed countries have invested huge human and financial resources to study this frontier subject, in order to achieve the "3T target" of the information age in the 21st century. The calculation speed reaches 1 Tbit/s and storage density up to 1 Tbit/in<sup>2</sup> [3]. Therefore, nanophoton firmware with high computing power can control the computing power in the millisecond level. In the millisecond level, medical equipment and nanooptical special equipment used in life are expected to be error-free, and nanooptical instruments at this level may help operators to perform a series of complex and difficult mechanical operations through remote operation of instruments [4].

Under this trend of nanophotonics development, it can not only make the digital storage technology get better but also can make the digital imaging become more precise. Nanophotonics-assisted polymer materials realize five-dimensional optical storage including spatial domain, time domain, polarization, and other dimensions, which is two-dimensional more than blue light three-dimensional DVD. It has the storage capacity of tb (1 tb = 1024 gb) or even Pb (1 PB = 1024 tb), which is equivalent to the storage capacity of 10000 DVDs. This is also the first time in the world for scientists to use the principle of two beam superresolution to break through the optical diffraction limit in polymers and realize the optical storage technology of 9 nm characteristic size [5]. As a result of this, there will be a lot of demand of nanophotonics in the future market and industry. Due to the popularity of digital cameras and mobile phones, there is a huge market demand for image sensing and imaging devices. International leading enterprises, such as STMicronics and Panasonic, have invested a lot in the research of complementary metal oxide semiconductor and other COMS-related devices. Nanophotonics is expected to make great breakthroughs in sensing imaging, sensing measurement, display, and medical image. The surface plasma photonics used to enhance magnetic storage, nanophotonics, and nanoimaging technology for diagnosis and treatment and drug delivery will significantly improve the efficiency of imaging and information transmission in the field of professional photography and medical imaging [6]. For example, Purdue University recently developed a new ultrasensitive medical imaging technology. It uses a near-

infrared laser to irradiate the skin to detect tiny gold nanorods that are injected into the blood to make them shine. In experiments with mice, the images produced by the nanorods are about 60 times brighter than those produced by conventional fluorescent dyes, including rhodanine, which is widely used in the study of biological imaging in cells and molecules. So, it is possible to develop nanorods into an advanced medical imaging tool for early detection of cancer. Nanophotonics technology can use photon statistics and far-field microscopic spatial response to reconstruct the high-resolution image; we can display nanoquantity, and even the sensitivity is below the photon counting level [7]. In this situation, nanophotonics can undertake the important research and development of human society, such as electronic information storage and transmission, nanooptical imaging, medical diagnosis, and so on. As a new technology, it can bring great changes and new creation to human science and technology in the next decade or a hundred years. It has the strength to prove that nanophotonics can subvert the development direction of the next generation of human science and technology and will be able to provide a variety of change ways for the development of science industry, cultural industry, medicine, and even cultural inheritance.

There have been many research studies of nanooptics or nanophotonics published in the recent years, with increasing numbers of publication and citation. A few review studies of nanophotonics, such as all-optical routing, surface plasmon photonics for enhanced magnetic storage, nanoimaging, and nanophotonics, are used in diagnosis, treatment, and drug delivery to explore the development potential of nanophotonics in the field of photography and medical imaging. Here, we review the past research studies, discuss the topics related to the development of science and technology to change life, and observe from the positive (development of science and technology, engineering techniques innovation) to the negative (development difficulty and social or environmental hazards). Compare the engineering methods/techniques for the production of nanophotonics products, discuss the last findings and conclusions in literature, and propose the possible research directions for future works relative to nanooptics. This review study may benefit researchers, manufacturers, and government and relative agency officials to design their nanophotonics-based products with most up-to-date and necessary information readily available here.

## 2. Functional Properties

Figure 1 shows the main applications of nanooptics in the field of medical imaging and photographic imaging. Nowadays, it is in daily life to unlock smart phones through face recognition. However, the public rarely understand that it is a time-consuming and energy-consuming process behind this; first, the optical information of the face is collected by sensors and sent to the neural network in the computer, and the visual information is converted into electronic information through electronic hardware, and then, the image information is displayed. With the help of nanophotonics,

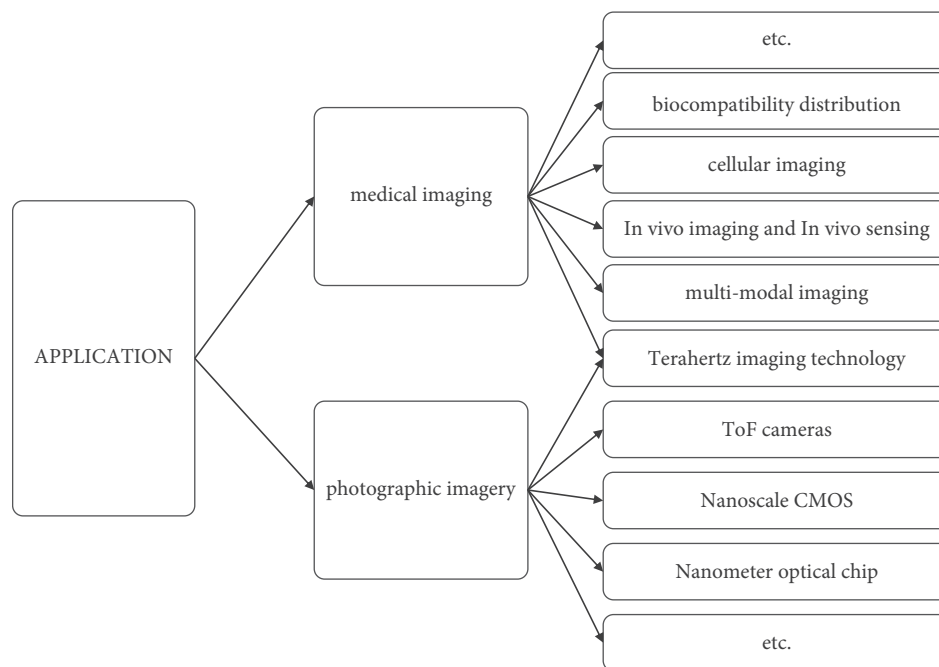


FIGURE 1: The main applications of nanooptics in the field of medical imaging and photographic imaging.

these functional optoelectronic devices can become more high speed, efficient, and energy-saving. The firmware can be applied to medical imaging, intelligent driving, art appreciation, and satellite image processing. Compared with the existing solutions, they occupy less space and consume less energy and cost. The upper limit of computing power of our reasoning perceptron in visible and near-infrared bands printed by nanooptical technology is 400 exaflops (1018 flops per second for floating operation). Compared with diffraction equipment and integrated photonic hardware in millimeter wave, microwave, and other bands, the number of operations per second increases by 3–5 orders of magnitude [8]. Using superresolution 3D nanofabrication technology, we can directly integrate AI optical devices into the existing CMOS image sensor, which is equivalent to placing customized smart glasses for specific tasks on the image sensor, which can process the incoming optical information before detecting it [9].

Furthermore, nanostructured optical filters can also be widely used in photography and medical imaging. Periodic refractive index or photonic crystal nanostructures can adjust and control the transmission and reflection spectra. In this case, the overlapping of multiple grooves with different periods can theoretically control the light of each color. Different from the traditional Bayer filter method, all colors can be sorted by surface plasmon resonance, and even a single nanostructured metal film can achieve fine color selection. The basic principle of the traditional Bayer process, as a chemical stationary process for more than 100 years, is the process of obtaining alumina. First, bauxite is dissolved out with NaOH solution under high temperature and high pressure, so that alumina hydrate in bauxite reacts rightwards according to the above formula to obtain sodium aluminate solution, and impurities such as iron and silicon

enter red mud [10]. Adding varieties to the sodium aluminate solution after thoroughly separating red mud, decomposing under the conditions of continuous stirring and gradual cooling, make the above formula react to the left to precipitate aluminum hydroxide and obtain a mother liquor containing a large amount of sodium hydroxide [11]. The mother liquor is evaporated and concentrated and then returned for dissolving out a new batch of bauxite. The aluminum hydroxide is calcined and dehydrated to obtain the product aluminum oxide. In this study, through the improvement of nanooptical materials, the chemical process in the past 100 years has undergone new changes, which can make a breakthrough in the production process and automation equipment. As early as ten years ago, it has been confirmed that the infrared receiver based on nanophotonics can be fully compatible with CMOS technology in the imaging process and can be used as a sensor, which is very important in daily mobile phone camera and medical imaging [12].

In recent studies, terahertz imaging under the extension of nanophotonics technology is more obvious for medical imaging. Terahertz technology can be used not only for MRI but also for skin cancer detection. Compared with X-ray, terahertz wave has lower photon energy (1 THz = 4.1 MeV), which can avoid the side effects of X-ray medical imaging. In addition, water molecules show strong absorption for terahertz wave. The research shows that the terahertz wave radiation from air plasma is quite different from that from water. For example, longer laser pulse duration increases the amount of THz radiation energy generated from water, but the opposite is true for air plasma: shorter pulse will increase THz radiation [13]. Moreover, when away from the normal incident angle of optical excitation, the terahertz radiation intensity from water depends on the polarization of laser

beam, while the terahertz radiation from air plasma is polarization independent [14]. Therefore, terahertz spectroscopy can be used in medicine to observe the difference between the water content of tumor tissue and normal cells, so as to judge the development of tumor, and also can be used to identify normal tissue and inflammatory skin tissue. The terahertz spectrum of matter contains abundant information of molecular structure. Most of the lattice vibrations of matter and the transitions between the rotational and vibrational energy levels of molecules correspond to the terahertz band. The position, intensity, and shape of the transmission absorption spectrum of each matter are different in this band. Therefore, the terahertz spectrum can reflect the subtle changes of molecular species and structures, making them have the same unique characteristics as fingerprints, so the terahertz spectrum is also known as molecular fingerprints. According to the molecular fingerprint characteristics of terahertz spectroscopy, we can analyze and study the material composition, microstructure, and their interaction relationship. According to the existing research results, the transmission properties of terahertz radiation to polar dielectrics, electrodeless dielectrics, and metal conductors are very different. There is an equivalent dipole moment in polar dielectrics and a large number of free moving charges in metal conductors. When they interact with terahertz waves, resonance absorption occurs, so the penetration of terahertz waves to these two materials is very low. However, electrodeless dielectrics have no resonance absorption effect on the terahertz wave, so they have strong penetrability. Thus, terahertz imaging can distinguish different materials. Many packaging materials, such as plastics, cartons, cloth, wood, and so on, belong to electrodeless dielectrics, but they are opaque to visible light. Therefore, terahertz perspective imaging of opaque objects can be combined with corresponding technologies, which can be used as a supplement to X-ray and ultrasonic imaging technologies to detect internal defects of materials and items in sealed packaging [15].

The human trial conducted by Woodward et al. [16] is the first experiment for terahertz pulse scanning imaging of the skin and other cancers performed. The experiment shows that the cancerous tissue contains more water than normal tissue, and water molecules and other polar molecules will absorb a lot of terahertz wave; normal tissue, cancerous tissue, and inflammatory tissue can be easily distinguished in terahertz wave imaging results, so that terahertz wave imaging of cancerous tissue can have great practical significance. Terahertz wave imaging technology is used to distinguish normal tissue from tumor tissue [17]. The results further prove that healthy tissue and tumor tissue have different echo characteristics in terahertz reflection signal and are basically consistent with the actual pathological analysis results [18]. Three-dimensional images of tooth tissue were successfully constructed by using the terahertz pulse imaging system, and it can measure enamel thickness directly and accurately [19].

With the continuous maturity of terahertz imaging technology, researchers have higher and higher requirements for the resolution of the imaging samples. Then, the

next step is to study the confocal imaging. Through the nanometer optical pinhole, the medical samples are precisely collected, and the image information collection is controlled in the accurate plane. It will not be interfered by signals from other positions on the specimen. After removing the influence of background fluorescence and increasing the signal-to-noise ratio, the contrast and resolution of the confocal image are significantly improved compared with the traditional field illumination fluorescence image. At present, terahertz imaging research focuses on the nature of tumor tissue, such as skin basal cell carcinoma, liver cancer, cervical cancer, and other cancerous cells [20]. The United States, Australia, and China have made remarkable achievements in those regards [21].

Metasurface as same as terahertz is an important part of nanophotonics. First of all, the metasurface was first recognized by people in 2011, and in the latest experiments, it shows that the supersurface can jointly control the multiple degrees of freedom of the electromagnetic wave, so as to control the phase, amplitude, polarization, and other degrees of freedom of the electromagnetic wave at the same time. For example, through the joint control of the phase and amplitude of the electromagnetic wave, the stereoscopic superholography can be realized, and through the joint control of the phase and polarization of the electromagnetic wave, the vector vorticity can be realized. The joint control of the phase and frequency of the electromagnetic wave can realize the function of nonlinear superlens. Based on metasurface, some researchers using Pancharatnam–Berry phase is by the rod-shaped metal nanoantenna along the axis direction of  $0\text{--}180^\circ$ . Different angles of rotation achieve  $0\text{--}2\pi$  phase coverage of the system. In this design, the incident light is circularly polarized light wave, and the experimental results show that the rotation angle and abrupt phase have a linear ratio of twice. According to this relationship, the unit structure can be arranged and designed as a bipolar metalens [22].

As a derivative function of nanooptics, superlens can use the structure and operation mechanism of our human eyes and the adaptability of superlens to upgrade the human body. It is essentially a flat, electronically controlled artificial eye. Due to the breakthrough of superlens and artificial muscle technology, this kind of instrument can not only complete real-time focusing but also is not as bulky as traditional spherical lens. It can even do things that the human eye cannot do. Moreover, the adaptive superlens has established the ability of dynamic correction of astigmatism and image motion, which cannot be achieved naturally by human eyes. Because the superlens can focus light and eliminate spherical aberration through the dense mode of nanostructures, each structure is smaller than the wavelength of light [23]. Due to the use of nanostructures, the information density in each lens is very high. If you switch from a 100 micron lens to a 1 cm lens, you will add 10000 pieces of information you need to describe the lens [24]. Every time we try to zoom in, the file size expands to GB or even TB. From a certain level, adaptive superlens can replace the heavy and miscellaneous lens and use the characteristics of human eyes to assist human beings in a series of scientific

and artistic shooting activities (Alan She et al.2019). This technology makes it possible to combine semiconductor manufacturing with lens manufacturing. Superlens can be embedded into glasses, lens, mobile phone, VR, AR, and other industrial products relying on semiconductor components, which make the process of zoom and auto focus in daily optical imaging and microoptics light become simpler. Moreover, in medical imaging, hyperlens also has excellent performance. The lens made of high-purity hBN crystal can distinguish the virus details on the surface of living cells. In the process of preparation, the light loss is significantly reduced, and the lifetime of polarized phonons is increased by three times, which makes their propagation distance increased by three times. Therefore, the inherent diffraction limit can be broken by using hBN crystal. In principle, the target image with the size of 30 nm can be captured. In addition, the current use is very small hBN sheet, and the future use of larger crystals is expected to obtain better performance (Joshua Caldwell et al., 2017).

In the new study, scientists at the University of California have developed a new, record breaking, ultra-metalens that uses a series of small, interconnected waveguides, similar to fishnets, to focus light at wavelengths ranging from visible to infrared with record efficiency. So, the lens is called fishnet-achromatic-metalens, and the research shows that this kind of superlens is flat and compact and can be made small enough to meet the needs of increasing miniaturization. This technological development will lead to revolutionary progress in solar energy, virtual reality technology, medical imaging, optical information processing, and other optical dependent applications. At present, fishnet-achromatic-metalens is the thinnest, most efficient, and widest flat lens in the world [25]. At the same time, some researchers use nanoforce to make the liquid crystal penetrate between these microcolumns, so that the microcolumns can shape and diffract light in a new way and “adjust” the focusing force to achieve this. Here, liquid crystals are particularly useful because they can be thermally, electrically, magnetically, or optically manipulated, which is expected to bring about “flexible” or “reconfigurable” lenses. By controlling the liquid crystal, they make the new superlens develop in a new direction of science and technology to produce reconfigurable structured light. They hope that liquid crystals can be reproductively infiltrated into state-of-the-art superlens (made of 150 million nanometer diameter glass columns) and their ability to significantly change their focusing characteristics, indicating that the exciting technology I am looking forward to will emerge from reconfigurable planar optics in the future [26]. Based on this technology, the lens used in mobile phones, computers, and other electronic devices can be smaller, and it has exceeded the ability of traditional glass cutting and glass bending technology, so these fine, thin, and flat lenses can replace the existing bulky glass lens and further miniaturize the sensors and medical imaging equipment [27].

According to the existing research reports, nanophotonics can attract more and more attention in the practical application range, especially in photography and imaging, lens upgrading, nanomaterials, and medical

imaging system. Nanophotonics has a lot of intersection with other disciplines, and the development of nanophotonics will certainly drive the progress of related disciplines. For example, the new type of photographic instrument, due to the strict alignment of light on the sensor, its structure of all components, and assembly accuracy will also reach the nanometer level, so the nanophotonics method may be used [28]. It can be seen that nanooptics can not only reduce the light to a small amount in the combination of optoelectronics and microelectronics but also be absorbed and detected by a small detector, so as to achieve the characteristics of low noise, high speed, low voltage, and low power consumption. It is also possible to use lithography or exposure to make integrated circuits and make very small transistors and integrate light into very clear images, so as to improve the image processing ability of the current camera sensor. Nanooptical technology can also use the characteristics of spectroscopy coupled with nanophotonics to produce peak intensity, reduce the given amount of light energy to a smaller volume, and study the high-sensitivity spectrum by increasing the intensity of hot spots to assist the current medical imaging technology. Or to fit in with the microscope, use near-field optical scanning to achieve the same goal of obtaining images with resolution much lower than the wavelength [29]. The target is also included in the grating imaging surface with a very sharp tip or a very small aperture [30], so as to obtain more clear and easy to identify medical etiology or biological research in the image.

### 3. Adverse Effects

The researchers not only doubted the effectiveness of nanophotonic technology in the experimental process of nanocontrol but also could not fully determine the potential harm of nanophotonic technology. Some researchers have shown that nanophotons may pose a risk leading to cancer in patients in medical experiments studying nanoscale photons. As we know, nanoparticle is known to be very small, thousands of times smaller than a cell. Nanomaterials have special physical and chemical properties due to a small size effect, quantum effect, and large specific surface area [31]. After entering the living body, the chemical properties and biological activities generated by their interaction with the living body are very different from the conventional substances with the same chemical composition. Nanomaterials have special physical and chemical properties due to the small size effect, quantum effect, and large specific surface area [32]. After entering the living body, the chemical characteristics and biological activities generated by their interaction with the living body are very different from those of the conventional substances with the same chemical composition, which may cause serious damage to human health and become the inducer of many major diseases [33]. The Great Smog of London is a well-known example. After the Great Smog, there were many sudden deaths in London. The scientists analyzed the results of the study and concluded that the main cause was a large increase in fine nanoparticles in the air [34]. Studies have shown that some artificial nanoparticles in very small doses are also easy to

cause inflammation in target organs, easy to cause brain damage, easy to cause oxidative stress in the body, and easy to enter cells and even the nucleus. Moreover, the cost of nanooptical technology is very high.

Second, for inorganic mineral drug particles, the physical and chemical properties of the drug will change greatly, the probability of side reactions will increase, and the preparation process is complex, which requires reasonable ratio and accurate calculation, and it will also involve social and ethical issues. Not only have the dangers of nanotechnology and materials have been discovered in medical science but also the potential negative effects of nanooptics have been discovered in imaging and electronics [5]. CNT as an important carbon nanotube, due to its good mechanical, electrical, and chemical properties, can be used as superfiber, stealth materials, high-power supercapacitors, and sensors, known as the “star material” [35]. However, in practice and application, the current toxicological studies of CNT have shown that CNT inhalation and exposure can cause pulmonary inflammation and fibrosis reactions in experimental animals, and the tendency of local granuloma and stromal tumor appears. However, what is more worrying is the practical significance of CNT respiratory exposure in people’s daily life. In addition to the atmospheric release of CNT in the production workplace, CNT has been detected in air samples from Paris, the United States, and other places (especially the site of 9/11) [36]. A 2015 report showed CNT was detected in lung lavage fluid samples from 64 children with asthma in the Paris area. The potential impact of carbon nanotubes in the atmosphere on human health has become a practical issue of widespread concern. However, until now, CNT respiratory exposure has been mostly confined to pulmonary or cardiovascular diseases, and studies on systemic effects and long-term health effects have been lacking [37]. At the University of Birmingham, the researchers found four different graphene nanomaterials (GFNs) and found that the cytotoxicity of the different modified group is the main reason; through the cell vitality, membrane damage and ROS found their toxicity levels are different, and finally, nontarget metabolomics metabolite changes in nerve cells after detecting material processing technology. It was found that GFNs produced toxic effects mainly by disrupting the glucose metabolism, lipid synthesis, and antioxidant pathways [38].

Similarly, in the derivative application of nanophotonic technology, due to the characteristics of productivity and materials, the processing of nanophotonic technology is extremely difficult and the process is very complex. Moreover, the substantial increase of cost makes it impossible to promote the nanophotonic technology in a large area in a short time. In the current field of nanoscale lithography, the progress from 28 nm to 22/20 nm, limited by the 193i lithography, necessitates the use of double pattern exposure (DP). When it is further developed to 16/14 nm, FINFET technology is mostly used. Now, the FINFET technology is also upgraded generation by generation, plus the extension of 193i optical technology, using SADP and SAQP, so in the future to 10 nanometers or even 7 nanometers, basically the same equipment can be used; it seems that there is no doubt,

but the manufacturing cost of the chip will increase rapidly [39]. That will be a hurdle; however, because if the EUV is not ready, it will be forced to adopt a five-step graphic exposure (FP) technology that has already caught the attention of the global industry.

According to the current situation, there will be a certain negative impact in the field of electronic photography and medical imaging. From a series of studies, the nanophotonic hypersurface lens is also faced with huge difficulties and research bottlenecks. The U-shaped metal nanometer antenna, with its structural elements arranged into a parabolic phase array shape, can suppress the background light of the same polarization state of the incident light wave, retain only cross-circularly polarized light during the exit, and achieve beam bending and focusing when approaching the diffraction limit [40]. However, to some extent, the structure also inhibits cross-circularly polarized light, and its transmission efficiency value is relatively small, only about 10%. In a word, a common problem with bar, V-shaped, or U-shaped metal antennas is that they are very inefficient (Li Jensen, 2012).

In terahertz research, some researchers also believe that the nanoscale optical research need to make further adjustments; they in the terahertz system on the accuracy of the living skin imaging studies, experiments show that the imaging process, over time, increase or decrease water content on the surface of the skin surface to block increases (5 min before the biggest change). This leads to an increase in the refraction index of THz wave, which affects the accuracy of THz wave imaging [41]. To do this, the researchers created a model to eliminate unwanted effects. It is also proposed that there are many uncertain factors in the process of terahertz wave imaging of living skin, and we need to further establish a model to improve the accuracy of imaging [42]. At present, nanooptics research related to photography, imaging, and medical imaging technology cannot be large-scale production and application. The most of nanophotonics technology is still in research and a small amount in the production stage. Moreover, due to technical problems and other problems between theoretical research and actual production, it is easy to cause deviation, and the implementation also needs to invest high cost. The development of low-cost and large-scale manufacturing will also require new technologies to avoid the current reliance on expensive materials and other technologies.

However, science and technology are still constantly updated and developed, and the cost of nanophotonic technology has been reduced. For example, nanooptics has made a very small TOF camera based on TOF technology. In the field of medical imaging, this camera uses the TOF sensor to obtain the dense three-dimensional model of the patient’s chest and abdomen at a speed of more than 15 frames per second [43]. Then, different planes are fitted to different regions of the patient’s torso through data-driven algorithm, so as to carry out the three-dimensional model of the chest and abdomen. The results show that the TOF camera modeling method can be used to track the patient’s breathing movement with an accuracy of 0.1 mm without labeling, 3D, real-time [44]. In medical imaging, the

application of the TOF camera for three-dimensional posture imaging is to provide image data with the TOF three-dimensional image navigation on the endoscope. It shows a visual page for doctors, which can effectively avoid unnecessary harm to the human body caused by physical interactive devices [45].

Nanophotonics has had an important impact on people's daily life, and there is a strong market demand for nanophotonics devices products, so the results of its research can be quickly converted into commercial products [46]. In the near future, the current negative effects of nanophotonics technology will be eliminated by the development of science and technology. Its development is driven not only by people's strong interest in the micro/nanoscale or the subwavelength scale of light properties change but also from the huge market demand and strong investment from the industry. "Optical technology has a limitless future not only used in face recognition but also in artificial intelligence, VR/AR and other fields." About the use of 3D vision VCSEL and HCG technology [47], for example, the latest HCG technology, which is only a very thin film on the surface, about 1/1000 or 1/500 of the hair can be obtained by photolithography [48], which can effectively reduce the loss of light power, thus greatly reducing the cost [49]. Some research results have proved that in the field of related medical imaging, the research of nanooptics will not cause harm to human health under controllable circumstances [50]. Nanoparticle exists as a single particle around the cell membrane, endocytosis into the cell and distribution in the cytoplasm as a small aggregation state, and quickly along the microtubules to the nucleus and lysosome, and in the vicinity of the nucleus and lysosome, it exists as a large aggregation state. The assimilation mechanism of gold nanoparticles was observed by controlling the temperature [51]. When the temperature decreased, the phagocytosis decreased, indicating that the assimilation depended on energy. Fluorescence and plasma imaging demonstrated that the transport speed of gold nanoparticles depends on the size of the particle cluster rather than on the type of organelle (e.g., endosomes and lysosomes). This study proposes an effective nanometer diagnostic treatment method and provides a guarantee for the effective health management of nanobiologic medicine [52].

#### 4. Novel Engineering Techniques

Figure 2 shows the current major technologies in nanophotonics. Nanophotonic technology is currently used in many areas closely related to people's lives, such as daily mobile phone cameras, medical imaging, and sensors. From every tiny part, we can see a wide and deep world of nanophotons [53]. Nowadays, the information society requires more and more integration of integrated circuits, which also urges people to explore ways to break through the size limit of devices [54]. Thus, nanophotonics came into being. Using nanooptics, it will be possible to start with individual molecules and build a substance that functions exactly as a chip, storing data and acting as an electronic channel switch [55]. In addition, new methods such as

biomolecular detection, photothermal therapy, photodynamic therapy, and targeted drug delivery based on nanomaterials are gradually becoming important diagnostic and treatment methods in the field of biomedicine. However, due to the limitations of traditional nanomaterials or the defects of the treatment methods, the current nanomedical technology has many problems, such as the low drug utilization rate, large toxic and side effects, and low therapeutic effect [56]. By combining nanotechnology with photonics, the interaction between light and matter can be precisely controlled on the nanometer scale, making biomedical diagnosis and treatment more accurate and stable. Bioluminescence imaging and multispectral fluorescence imaging were used to visualize the whole process of drug delivery to tumor therapy [57]. In addition, drug release and distribution, vector location and degradation, and tumor were further described based on real-time imaging localization and tracking the interrelationship between growth or inhibition. The visualization of drug delivery systems provides a new approach to the study of nanomedicine mechanisms [58].

In the medical field, the development of almost all key technologies for the research of cutting-edge biomedical problems depends more or less on the introduction of new photonic technologies. With the help of nanophotonics technology, many medical problems that were previously unsolvable can now be solved [59]. Cell tracer technology, modified some markers in the specific cell-cell tracer, can get on two dimensions of space and time in real-time with relevant information; these cells in the body, distribution of survival, differentiation, migration, and outcome of dynamic monitoring, and at the cellular level reveal many important mechanism related to the origin of life [60]. As an important technical tool, cell tracer technology has been widely used in modern biomedical basic research and clinical applications [61]. With the development of biomedical technology, people gradually realize that the cells of the group with average effect of the tracer study is likely to cover up a lot closely related to the origin of life or disease of important individual information, so the biomedical research is more and more emphasis on the individual cells specificity information acquisition; it is also for cell tracer technology development to put forward new requirements. In order to achieve more accurate of biomedical research, the researchers used nanoparticles and quantum dots connected to small molecules such as protein or virus, real-time monitoring of protein or virus inside cells that interact with other substances, and study its impact on the host cell in the process of life change, in which biomedical field provides a more accurate means of detection [62]. In the research field of the cancer mechanism, how to prevent metastatic cells from invading other parts of the body has always been the core problem to be solved. In the course of the study, the researchers found that among seemingly identical cancer cells, there may be specific individual cancer cells that act as cancer seeds, resistant to chemotherapy and leading to cancer recurrence years later [63]. Nanophotonics, combined with medical imaging, could enable the seeds of these cancers to be better tracked and assisted in cancer treatment through gene editing. At present, gene editing technology is



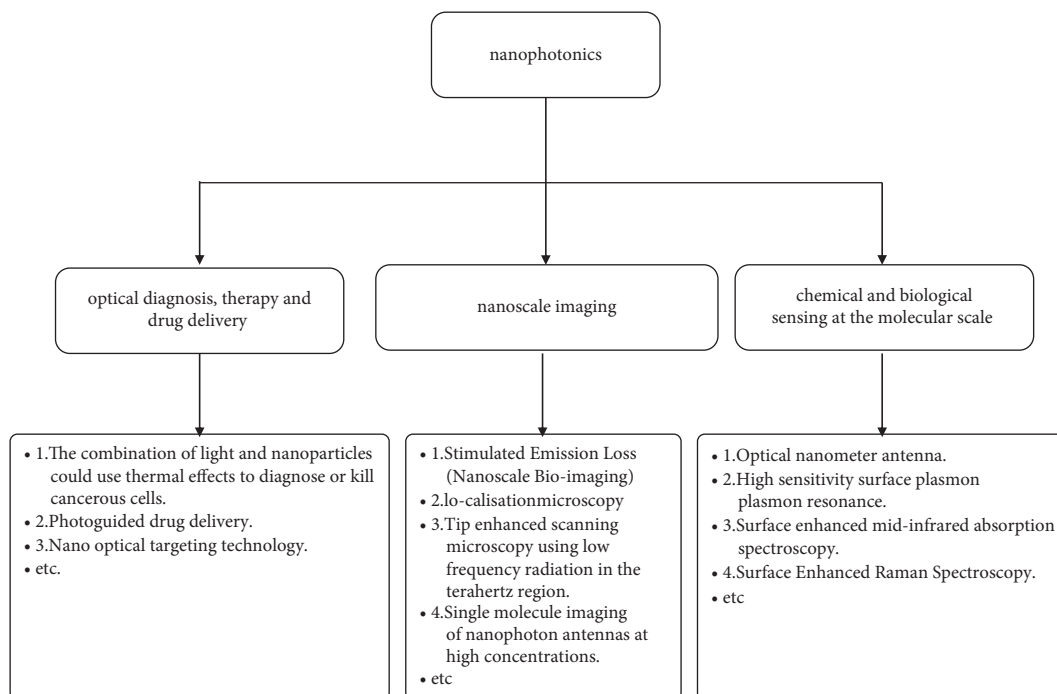


FIGURE 2: Current major technologies in nanophotonics.

the most successful multicell-specific target labeling technology [64]. On the premise of not affecting cell function, the use of gene editing techniques for each cell differentiation is to modify the corresponding article “the code” DNA fragments, it is like each item in the supermarket with a bar code on the back, so it can go through the cell genetic screening after the experiment, from nearly 4000 cells found in the community of 10 targets labeled cells [65]. Nanooptical technology has high spatial resolution and high temporal resolution, and it plays an important role in tumor detection, gene expression, protein molecular detection, drug screening, and drug efficacy evaluation by nondestructive real-time dynamic monitoring of the activity and response of labeled cells in living small animals [66].

In terms of modern imaging technology, nanophotonics has also seen a huge innovation in engineering techniques. As the most important nanoscale imaging technology at present, STED technology plays an important role in the field of technical testing and quality control of nanomanufacture. Localisation microscopy can be used in a controlled environment, for example, by combining photonic statistics and far-field microscopic spatial response to reconstruct high-resolution images, which can show nanoscale organisms in details below 50 nm, which with sensitivity below the level of photon counting [67]. A fluorescent probe based on arsenate was successfully synthesized by our team at Shenzhen University. The probe has good bleaching resistance and can specifically bind to o-dimercaptin-VDPs in mitochondrial membrane. The probe can be used for STED imaging of mitochondria of living HeLa cells, and the distribution of VDPs in mitochondria can be observed well. Last year, a team developed a new enhanced acrylic acid variant dye (MITOESQ-635),

which has low saturation intensity and high optical stability, making it an ideal choice for long-term STED imaging of living cells. By labeling the mitochondrial intima in living HeLa cells, they achieved 50 min of STED superresolution imaging at 35.2 nm. Meanwhile, a team from Anhui University has developed a novel probe, TPSPYM, which can specifically label both mitochondria and endoplasmic reticulum in living cells and distinguish them by fluorescence intensity [68]. The probe has good photostability and is suitable for STED living cell imaging. Using this probe, they labeled STED images of living cells and not only observed the superresolution structure of the ER-mitochondrial contact site but also observed the three-dimensional dynamic process of the interaction between ER and mitochondria after starved cells [7].

Now, there is a new imaging technology, structured illumination visible microtechnology (SIM). This technique usually requires only 9 original images to be captured, which can significantly improve the temporal resolution of imaging compared to Storm’s acquisition of tens of thousands of original images, and is also much faster than STED based on scanning imaging. Some scholars have introduced total internal reflection fluorescence (TIRF) excitation into SIM [69]. TIRF can only stimulate a small layer on the surface of the sample, which can effectively eliminate the characteristics of defocusing background signal. Simultaneously, a high NA TIRF-SIM method was proposed in combination with a high numerical aperture (NA = 1.7) objective lens to achieve dynamic superresolution imaging of the plasma membrane of living cells. The resolution was about 84 nm at a subsecond acquisition speed. The dynamic relationship between actin and myosin in mouse embryonic fibroblasts was also observed. Furthermore, they proposed the PA

NL-SIM method on this basis, which can obtain higher resolution [70]. In the following studies, in order to solve the problem that it is impossible to image many organelles inside living cells, the researchers developed GI-SIM technology based on the glance incident structured light illumination, which realized the superresolution imaging of various organelle structures in living cells and the observation of the dynamic process of the interaction between organelles [71]. Many new discoveries are possible only if the imaging is fast enough and the resolution is high enough. The superresolution structure of cytoskeletal microtubules in living COS-7 cells (resolution 97 nm) was obtained at 9.2 FPS, which was helpful to observe the dynamic changes of cytoskeletal microtubules. The superresolution structure of the endoplasmic reticulum of living COS-7 cells was obtained at 266 FPS [72]. It was not only observed that most of the endoplasmic reticulum was composed of tubular matrices but also that the formation and disappearance of the contracted parts of the endoplasmic reticulum were observed by the real-time imaging of the endoplasmic reticulum tubules [73].

Terahertz, as one of the core technologies in nanophotonics, has irreplaceable advantages in many fields because of its unique physical properties. It plays a great role in medical imaging and other everyday imaging units. Terahertz waves are different from millimeter waves or X-rays, which have unique imaging capabilities and application scenarios [74]. Terahertz waves do not penetrate metals, but have good penetration for many nonmetallic and nonpolar materials. So, terahertz waves can be used to “see through” objects such as clothes, shoes, bags, and suitcases to detect potentially dangerous objects such as metal knives or guns. And because of their low photon energy, terahertz waves do not pose a health hazard to users [75]. In recent years, some researchers have proposed to modulate probe beams to determine the spatial distribution of terahertz radiation and generate terahertz radiation transmission samples by means of an optical rectifier [76]. The probe light with a wavelength of 800 nm is spatially encoded by a spatial light modulator and then reflected by beam-splitting crystal to ZnTe crystal and propagates collinearly with the terahertz beam. Through a 1/4 wave plate and a Wollaston prism, it enters the balanced photodiode for electrooptic sampling. The experimental data can be obtained by using this research method [77]. Some other researchers proposed the method of electrooptic sampling (EOS) to shoot real-time images with the CCD camera, making it possible for real-time terahertz imaging. The laser source is a titanium gem laser with a pulse time of less than 50 fs, and the terahertz radiation is produced by using GaAs wafer [78]. The terahertz radiation was focused on a Zn Te crystal with a thickness of 0.9 mm, an area of 6 mm × 8 mm, and a crystal orientation of <110> using an off-axis parabolic mirror. The diameter of the probe beam is larger than that of the terahertz beam [79]. After passing through the mutual perpendicular polarizer and polarization analyzer, the two-dimensional electric field distribution in the sensor crystal is converted into the two-dimensional light intensity distribution and the optical image is recorded by the CCD camera [80]. This method can

provide effective data support for terahertz experiment of nanometer optical imaging with clear and accurate sampling images (Jiang Y, Deng B, Qin Y, et al., 2017).

Based on the development of these technologies, more nanoscale insights have been put forward in optics, and hence, the TOF camera [81]. This new imaging technology based on nanometer optics is to transmit continuous infrared light pulses of specific wavelengths to the target, receive the light signal from the object under test through a specific sensor, and calculate the time of flight or phase difference of the light to and from the object under test to get the 3D depth information of the object under test [82]. The brightness image and depth information of the TOF camera can be connected through the model to achieve fast and accurate face matching and detection [81]. In the aspect of interactive entertainment, researchers proposed a method of tracking and recognizing human body posture based on depth image [83]. The motion estimation algorithm adopted the three-step search method to track human body motion trajectory. Finally, the recognition of human body motion posture was realized based on bone coordinates. In the medical field, researchers use the TOF camera for three-dimensional gesture imaging and successfully applied in medical imaging [84]. The data are captured by the TOF camera on the endoscope to present a visual interface to the medical personnel [85]. This method reduced the damage caused by the physical device to the patient's organs, and the recognition rate reached 94.3% [45]. In people's daily life scenes, the TOF camera has been able to assist people in a series of motion capture, 3D modeling, and other tasks that previously needed large equipment to complete the microcamera of the mobile phone, home projection equipment, and monitoring equipment in public places by using nanooptical technology [86]. All of this complexity has been made easier by the advent of the TOF camera [87]. In summary, nanophotonics has demonstrated excellent theoretical basis and experimental results both in medical industry and in people's daily imaging applications [88]. And it to the modern related scientific research and technological innovation has provided a broad stage. But due to volume limit, this review focuses on the methods with higher prevalence and more evidence and, therefore, does not cover all existing techniques.

## 5. Future Trends

Figure 3 shows the future directions of nanooptics in medical imaging and photographic imaging. In literature, nanophotonics has showed the beneficial effects of medical imaging and photography-related imaging technologies, such as optical diagnosis, therapy, and drug delivery [89], single molecule imaging of nanophotonic antenna in high concentration [90], three-dimensional laser direct writing, stimulated radiation lithography, nanoprinting, terahertz imaging technology, and terahertz spectroscopy technology [91], and a series of new optical technologies based on nanophotonics, such as superlens. In this review, as different from previous reviews, we have presented the up-to-date research works on nanooptics, advance imaging, and

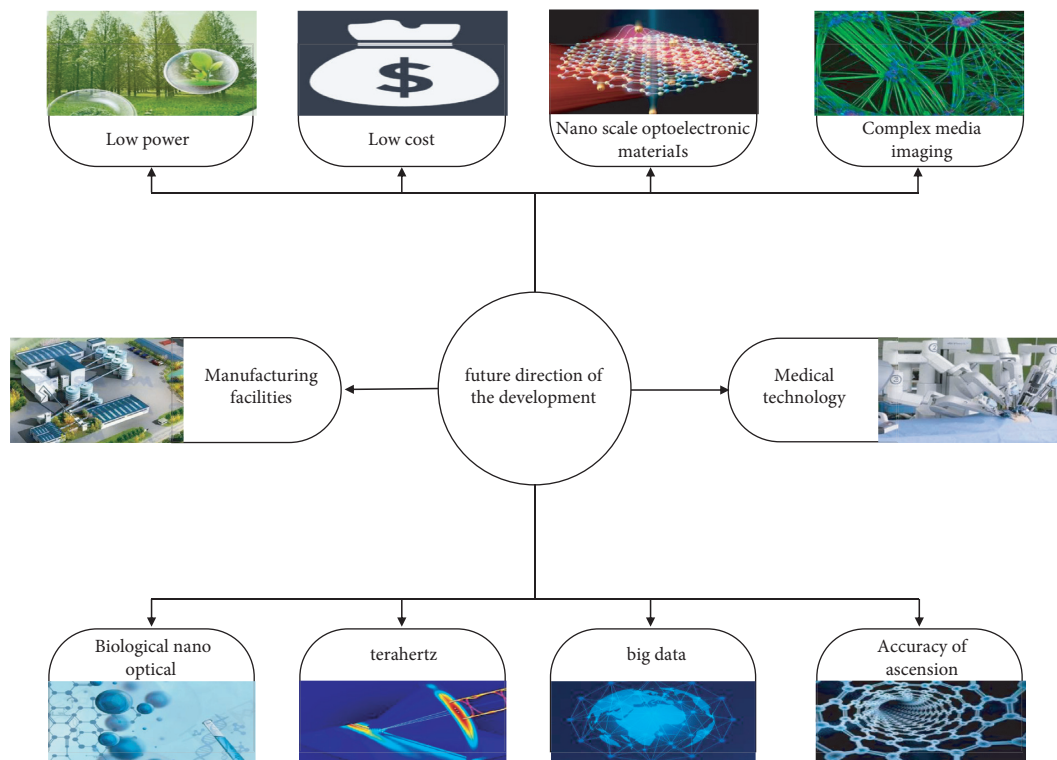


FIGURE 3: Future directions of nanoptics in medical imaging and photographic imaging.

nanophotonics [92]. We provide convincing evidence to nanophotonics, metasurface, terahertz, surface-enhanced Raman spectroscopy, STED, ToF camera, and other technologies available for medical imaging and daily imaging [93]. Also, we illustrate the benefits of the field of human health research and many technologies that can help human daily life [94]. In conclusion, nanooptical technology can bring advantages to the stability, accuracy, treatment mechanism research, and the development of new diagnostic and therapeutic methods of nanobiomedicine [95]. In the future research work, multifunctional nanophotonics technology (such as photogenetic technology, gene editing technology, and cell tracking), as a new generation of biomedical fine research means, is of great significance to biomedical basic and clinical application research [96]. According to those works, it can be seen that nanooptical technology can help people's life in many ways, promote the development of human science and technology, and stimulate the progress of scientific research in many fields. However, there are still many difficulties and defects in the medical field and photography [97]. First of all, the blockade of related technologies leads to that researchers in various countries and institutions cannot quickly obtain the research platform they need, which leads to that researchers need to spend a lot of time and energy to do unnecessary research on basic science. Among them, nanotoxicology research report will also make researchers pay more attention to the potential harm of nanooptical technology to human body [98]. Second, nanooptics is an emerging discipline; just out of infancy, there are still many unknown factors and challenges waiting for researchers, which will lead to the cost of early

research and development is unpredictable. In the research process, it is very likely that a variety of research technologies will be developed at the same time, each with its own advantages and obvious disadvantages [99]. Because we cannot distinguish which method is the best in a short time, the research and practice of nanophotonics are still uncertain. Third, the current nanooptical technology is in its infancy, and a large number of technology industry preparations are not perfect. Therefore, in the process of commercialization and marketization, the application of nanooptical technology in medical imaging and photography needs to go through a transitional period and experimental period to test the adaptability of new technology to the market demand and then correct and improve it [100, 101].

According to the possible side effects of nanooptical technology, many countries have established relevant research institutions and research organizations founded by researchers. At the same time, many universities cooperate with each other internationally to share resources, so as to achieve the effect of mutual assistance and joint research and development. These organizations and institutions are committed to the development of nanooptics applications in various fields in the future and can achieve maximum returns and nanosafety management, such as the National Nanotechnology Plan issued by the US government aims to promote world-class nanotechnology R&D projects, promote the commercialization of new technological achievements, maintain and develop educational resources and labor force, promote the establishment of nanotechnology dynamic infrastructure, and support and be responsible for the development of nanotechnology. Similarly, the

University of Southampton and the University of Manchester in the UK have developed the latest nanolevel optical microscope with the joint efforts of the national nanoinstitution some time ago, and these British scientists think that they can use the microscope to find smaller images of objects in the future. Moreover, China's nanoresearch institutions and many scholars at home and abroad maintain close ties. For example, the Institute of Nanophotonics of Jinan University maintains close ties with optical research institutions in the UK, and the Nano-optical Measurement Laboratory of Huazhong University of Science and Technology, the National Optoelectronic Research Center, National Digital Manufacturing Equipment and Technology Laboratory, and National Natural Science and Technology Foundation always maintain close scientific research cooperation. At the same time, scientific researchers also maintain close scientific exchanges in the world. For example, the International Conference on Nanophotonics and Micro/Nano-optics 2020 (NANOP) held in Paris recently attracted a large number of scholars at home and abroad to exchange and discuss with each other. More than 2500 famous experts and scholars from all over the world in the field of nanophotonics discussed the main development directions of nano-optical technology in the future, such as nano-optical imaging and the application of nanophotonics. It can be seen that the development of nanometer optical technology is promising in the future. In the future development, there will be three directions. The first is to strengthen the cooperation between different universities, research institutes, regions, and departments and to take advantage of the convenience of the region and the priority of science and technology to help the research and development of nano-optics with the fastest progress. Besides, the government will establish regional nanomachining centers for free use or fabrication by surrounding researchers, so as to enhance the market adaptability of nanomachining technology, enhance its commercial nature, increase production capacity, and promote the development of a range of research technologies and, on the other hand, sharing of testing equipment. Compared with other researches, nano-optical prototype trial manufacturing and measuring equipment are expensive, and equipment sharing among different units can make full use of resources. In the process of application, we should unify research methods and use excellent research plans and tools to shorten research time and reduce research costs. The research on nanophotonics at China and other counties is making continuous breakthroughs, and its research on suprasurface, terahertz, and nanoscale optical materials has gradually revealed a broad application prospect, which is bound to become one of the key technologies of future medical and daily imaging systems [102]. However, there are also some shortcomings, such as low efficiency, high processing cost, complex manufacturing process, and unsatisfactory focusing effect, which still need to be improved continuously. Therefore, more and better nano-optical technology with better performance and more suitable for the development of the time need to be studied [5].

In future works, the following four directions may be largely conducted, including the following. (1) In the field of medical imaging, it supports innovative basic research in nanophotonics to facilitate advances in quantitative nano-imaging, systems nanobiology, medicine and neuroscience, and biomarker technologies. (2) The size of the equipment should be improved, and the accuracy of the wavelength of the emitted nanowave should be solved through technological innovation [103]. (3) The problem of the cancer cells, tumor cells, and other newborn cells cannot be marked by the imaging system in the process of medical diagnosis and treatment [104]. (4) How to break through the order of magnitude in the running speed, bandwidth, efficiency, energy consumption, and integration of nanometer optical components, so that the research level and calculation rate of nanometer optical technology can be improved. In fact, the nanoscale size not only facilitates its integration with existing technologies but also enables it to exhibit many unique and excellent new physical properties. In the future world of modern science, nano-optics will become even more important [105].

In conclusion, governments, researchers, and the media around the world are interested in nano-optical technology and its application in medical imaging and photography because of their many beneficial effects. Based on the evidence reported so far, this review presents the importance of nano-optics as a good practice for use in projects such as 3D imaging and ranging for potential medical imaging and everyday people's lives [106]. The main conclusions of this review include the following [107]. As a strong technological, economic, research, and development potential of the multifunction emerging nanotechnology, nanophotonics because of its small volume, the future cost control scope, and imaging effect obvious features, a series of the treatment and diagnosis diseases (including cancer cells, tumor cells, and a series of difficult to mark cells) show as optical technology in the field of medical benefits [108]. The important function of nano-optics can facilitate its applications in imaging for security protection, lithography, and lens manufacturing. However, the toxicology of nanotechnology and its potential harms and development costs remain largely unknown [109]. Though completely with nano-optical technology in production and life of controversy still exists, the results obtained from the present study suggests that they support the nano-optical technology as the next ten years or twenty years development of the main optical research, and there were some studies that have shown that in certain cases, nano-optical technology, with no obvious potential adverse impact on metabolic health. In particular, there are adverse effects on technical operators [110]. Nowadays, nano-optical technology has been applied to many fields of research. In the field of medical imaging, medical researchers and workers from all over the world have obtained a lot of valuable data through continuous practice in clinical cases [111]. Researchers use these data combined with nanoscale materials to make the error smaller and smaller. The stability of the technology will become higher and higher in the future. At the same time, it will become more mature and

applied to the medical market to help many patients. All about that, opportunities and challenges coexist, and it is quite reasonable that a series of nanophotonics technologies have great development potential in the field of medical imaging and photography. Future research efforts may involve research into nano-optical technologies and new discoveries of their side effects, new designs for medical imaging and photography including nano-optical technologies, and new engineering techniques for high quality processing.

### Data Availability

All data supporting this work are included within the article.

### Conflicts of Interest

The authors declare that they have no conflicts of interest.

### Acknowledgments

This work was partially supported by the National Natural Science Foundation of China (81901020) and Natural Science Foundation of Hunan Province, China (2020JJ4458).

### References

- [1] M. Ohtsu and H. Hori, "Lasers, photonics, and electro-optics," *Near-Field Nano-Optics*, Springer, New York, NY, USA, 1999.
- [2] K.-T. Lee, J.-Y. Jang, S. J. Park et al., "Nanoimprint lithography: angle-insensitive and cmos-compatible sub-wavelength color printing (advanced optical materials 11/2016)," *Advanced Optical Materials*, vol. 4, no. 11, p. 1695, 2016.
- [3] S. Bao, "The marriage of nanotechnology and photonics-nanophotonics," *Knowledge of Modern Physics*, vol. 21, no. 5, pp. 52–55, 2009.
- [4] Y. Lei, "A review of nanophotonics," *Journal of Quantitative Economics*, vol. 3, pp. 374–378, 2006.
- [5] Z. Gu, "Book review: nanostructures in electronics and photonics," *Journal of Nanophotonics*, vol. 3, no. 1, p. 30204, 2009.
- [6] G. Sun, L. Zhang, and L. Hang, "Key developments of nanophotonics over the next decade," *Physics*, vol. 10, pp. 47–55, 2013.
- [7] D. Wildanger, E. Rittweger, J. Buckers, R. Medda, and S. W. Hell, "Sted and related concepts for far-field optical nanoscopy," in *Proceedings of the Lasers and Electro-Optics Society Annual Meeting-LEOS*, pp. 353–354, Belek-Antalya, Turkey, October 2009.
- [8] E. Goi, "Nanoprinted high-neuron-density optical linear perceptrons performing near-infrared inference on a CMOS chip," *Light Science and Applications*, vol. 10, p. 40, 2021.
- [9] S. Clemmen, A. Hermans, E. Solano et al., "Atomic layer deposited second-order nonlinear optical metamaterial for back-end integration with cmos-compatible nanophotonic circuitry," *Optics Letters*, vol. 40, no. 22, pp. 5371–5374, 2015.
- [10] A. Hocini and A. Harhouz, "Modeling and analysis of the temperature sensitivity in two-dimensional photonic crystal microcavity," *Journal of Nanophotonics*, vol. 10, no. 1, Article ID 016007, 2016.
- [11] S. C. Hohng, Y. C. Yoon, D. S. Kim, V. Malyarchuk, and Q. H. Park, "Light emission from the shadows: surface plasmon nano-optics at near and far fields," *Applied Physics Letters*, vol. 81, no. 17, pp. 3239–3241, 2002.
- [12] G. Sun, L. Zhang, and L. Hang, "Key development fields of nanophotonics in the next decade," *Journal of Physics*, vol. 10, pp. 724–732, 2013.
- [13] B. Wang, W. Liu, M. Yu, Q. Yang, D. Liu, and Y. Gao, "Application research of terahertz imaging technology," *Journal of Measurement and Control Technology*, vol. 240, pp. 1–7, 2021.
- [14] E. Esarey, K. Ledingham, C. B. Schroeder, K. Spohr, F. J. Grner, and P. Mckenna, "Laser acceleration of electrons, protons, and ions iii; and medical applications of laser-generated beams of particles iii," *Journal of Nanoparticle Research An Interdisciplinary Forum for Nanoscale Science & Technology*, vol. 9514, no. 1, pp. 1–15, 2015.
- [15] L. Han, Y. Jiao, and W. Ning, "A review of the medical applications of terahertz imaging and spectroscopy," *Journal of Chongqing University of Posts and Telecommunications (Natural Science Edition)*, vol. 2, pp. 242–252, 2021.
- [16] N. D. Woodward, S. E. Purdon, H. Y. Meltzer, and D. H. Zald, "A meta-analysis of cognitive change with haloperidol in clinical trials of atypical antipsychotics:dose effects and comparison to practice effects," *Schizophrenia Research*, vol. 89, no. 1-3, pp. 211–224, 2007.
- [17] W. E. Moerner, P. J. Schuck, D. P. Fromm, A. Kinkhabwala, and R. J. Twieg, *Nanophotonics and Single Molecules*, Springer Berlin Heidelberg, Berlin, Germany, 2007.
- [18] E. Pickwell, B. E. Cole, A. J. Fitzgerald, M. Pepper, and V. P. Wallace, "In vivo study of human skin using pulsed terahertz radiation," *Physics in Medicine and Biology*, vol. 49, no. 9, pp. 1595–1607, 2004.
- [19] D. Porterfield, J. Hesler, T. Crowe, W. Bishop, and D. Woolard, "Integrated terahertz transmit/receive modules," in *Proceedings of the 33rd European Microwave Conference*, Munich, Germany, October 2003.
- [20] Z. Lijie and T. J. Webster, "Nanotechnology and nanomaterials: promises for improved tissue regeneration," *Nano Today*, vol. 4, no. 1, 2009.
- [21] L. Tong, "Frontiers in nanophotonics research," 2014.
- [22] Z. Y. Tan, F. Fan, and S. J. Chang, "Active broadband manipulation of terahertz photonic spin based on gyrotropic pancharatnam-berry metasurface," *IEEE Journal of Selected Topics in Quantum Electronics*, vol. 26, 2020.
- [23] N. C. Lindquist, P. Nagpal, K. M. Mcpeak, D. J. Norris, and S. H. Oh, "Engineering metallic nanostructures for plasmonics and nanophotonics," *Reports on Progress in Physics*, vol. 75, no. 3, Article ID 036501, 2012.
- [24] S. J. Liao, S. F. Wang, and M. H. Chiu, "A new method for measuring a small displacement by using the critical angle method and confocal technology," in *Proceedings of the Nanophotonics, Nanostructure, and Nanometrology*, Beijing, China, February 2005.
- [25] B. Kanté, "Plasmonic topological metasurface by encircling an exceptional point," *Science*, vol. 373, 2021.
- [26] A. L. Capasso, A. Y. Zhu, J.-S. Park et al., "Optical properties of metasurfaces infiltrated with liquid crystals," *Proceedings of the National Academy of Sciences*, vol. 117, no. 34, 2019.
- [27] J. Cong, Z. Ming-Ming, L. Hong-Tao, C. Xiao-Yu, S. Chen, and X. Peng, "Smartphone-based fundus imaging system," *China Optics*, vol. 12, no. 1, pp. 97–103, 2019.

- [28] C. Li, "The origin, present state and future of photonics. Analysis of the road map for > in traditional optics-modern optics-photonics-nanophotonics," in *The 5th National Photonics Congress*, Huangshan, China, 2004.
- [29] A. J. Huber, F. Keilmann, J. Wittborn, J. Aizpurua, and R. Hillenbrand, "Terahertz near-field nanoscopy of mobile carriers in single semiconductor nanodevices," *Nano Letters*, vol. 8, no. 11, p. 3766, 2008.
- [30] M. Ohtsu, K. Kobayashi, T. Kawazoe, S. Sangu, and T. Yatsui, "Nanophotonics: design, fabrication, and operation of nanometric devices using optical near fields," *IEEE Journal of Selected Topics in Quantum Electronics*, vol. 8, no. 4, pp. 839–862, 2002.
- [31] Y. Bai, *Nanotoxicology Research Is on the Fast Track*, China Medical News, Beijing, China, 2012.
- [32] B. S. Williams, "Terahertz quantum-cascade lasers," *Nature Photonics*, vol. 1, no. 9, pp. 854–856, 2007.
- [33] B. E. Cole, J. B. Williams, B. T. King, M. S. Sherwin, and C. R. Stanley, "Coherent manipulation of semiconductor quantum bits with terahertz radiation," *Nature*, vol. 410, no. 6824, pp. 60–63, 2001.
- [34] Z. Chen, X. Shao, and J. Duan, "The impact of the combination of nanotechnology and photonics on modern technology," in *Western Photonics Academic Conference*, Xian, China, 2011.
- [35] M. N. Patel, P. Looney, K. Young, and M. D. Halling-Brown., "Automated collection of medical images for research from heterogeneous systems: trials and tribulations," in *Proceedings of SPIE-The International Society for Optical Engineering*, vol. 9039, San Diego, CA, USA, 2014.
- [36] A. J. Fitzgerald and E. Al, "Terahertz pulsed imaging of human breast tumors," *Radiology*, vol. 239, no. 2, 2006.
- [37] J. Kolosnjaj-Tabi and F. Moussa, "Anthropogenic carbon nanotubes and air pollution," *Emission Control Science and Technology*, vol. 3, no. 1, pp. 1–3, 2017.
- [38] I. Lynch, S. Halappanavar, J. D. Ede et al., "A methodology for developing key events to advance nanomaterial-relevant adverse outcome pathways to inform risk assessment," *Nanotoxicology*, vol. 15, no. 3, 2020.
- [39] M. Pelusi, F. Luan, T. D. Vo et al., "Photonic-chip-based radio-frequency spectrum analyser with terahertz bandwidth," *Nature Photonics*, vol. 3, no. 3, pp. 139–143, 2009.
- [40] T. Jing, X. Xiang, H. Tian, and Z. Pan, "3d reconstruction of non-rigid shapes using one top camera," *Jisuanji Fuzhu Sheji Yu Tuxingxue Xuebao/Journal of Computer-Aided Design and Computer Graphics*, vol. 23, no. 3, pp. 377–384, 2011.
- [41] A. V. Zayats, I. I. Smolyaninov, and A. A. Maradudin, "Nano-optics of surface plasmon polaritons," *Physics Reports*, vol. 408, no. 3–4, pp. 131–314, 2005.
- [42] Y. Chen, L. Wang, and J. Song, "Multifunctional nanophotonics technology for precision biomedicine applications," *Chinese Journal of Lasers*, vol. 3, pp. 22–31, 2018.
- [43] S. F. Salmeron, G. A. Ribas, J. Andrade-Cetto, and C. T. Genís, "Object modeling using a tof camera under an uncertainty reduction approach," in *Proceedings of the IEEE International Conference on Robotics and Automation*, Anchorage, AK, USA, May 2010.
- [44] J. Penne, C. Schaller, J. Hornegger, and T. Kuwert, "Robust real-time 3d respiratory motion detection using time-of-flight cameras," *International Journal of Computer Assisted Radiology and Surgery*, vol. 3, no. 5, pp. 427–431, 2008.
- [45] S. Soutschek, J. Penne, J. Hornegger, and J. Kornhuber, "3-d gesture-based scene navigation in medical imaging applications using time-of-flight cameras," in *Proceedings of the 2008 IEEE Computer Society Conference on Computer Vision and Pattern Recognition Workshops*, Anchorage, AK, USA, June 2008.
- [46] I. Yoneda, S. Mikami, T. Ota, T. Koshiba, and T. Higashiki, "Study of nanoimprint applications toward 22nm node cmos devices-art," in *Proceedings of SPIE-The International Society for Optical Engineering*, vol. 4, San Jose, CA, USA, March 2008.
- [47] O. Ferhanoglu, "3D-printed microsystems for opto-medical imaging," in *Proceedings of the 2019 International Conference on Optical MEMS and Nanophotonics (OMN)*, Daejeon, South Korea, July 2019.
- [48] J. F. O'Hara, R. Singh, I. Brener, E. Smirnova, and W. Zhang, "Thin-film sensing with planar terahertz metamaterials: sensitivity and limitations," *Optics Express*, vol. 16, no. 3, 2008.
- [49] C. Chang-Hasnain and L. Zhu, "Actively controllable color using high contrast metastructures," Alexandria, VA, USA United States Patent 10114238, 2018.
- [50] Y. Lu, D. Su, F. Ai, and J. Ma, "Effects of nanometer antibacterial materials on human health," *Chinese Journal of Clinical Rehabilitation*, vol. 13, pp. 164–165, 2006.
- [51] L. Vicarelli, M. S. Vitiello, D. Coquillat et al., "Graphene field-effect transistors as room-temperature terahertz detectors," *Nature Materials*, vol. 11, no. 10, pp. 865–871, 2012.
- [52] F. Yue, *Study on New Methods and Techniques of Subhundred Nanometer Superresolution Optical Microscopy Imaging*, Zhejiang University, Hangzhou, China, 2017.
- [53] L. Tizei and M. Kociak, "Spatially resolved quantum nano-optics of single photons using an electron microscope," *Physical Review Letters*, vol. 110, no. 15, pp. 164–170, 2013.
- [54] S. Manipatruni, M. Lipson, and I. A. Young, "Device scaling considerations for nanophotonic cmos global interconnects," *IEEE Journal of Selected Topics in Quantum Electronics*, vol. 19, no. 2, p. 8200109, 2013.
- [55] S. Manipatruni and C. J. Hardy, "Nanophotonic System for Optical Data and Power Transmission in Medical Imaging Syste," US20120146646 A1, 2012.
- [56] Y. Chen, T. Zhang, H. Lin, L. Cui, and N. An, "Nir-sensitive ucnp@mSiO<sub>2</sub> nanovehicles for on-demand drug release and photodynamic therapy," *RSC Advances*, vol. 6, no. 31, pp. 26479–26489, 2016.
- [57] K. Kawase, Y. Ogawa, Y. Watanabe, and H. Inoue, "Non-destructive terahertz imaging of illicit drugs using spectral fingerprints," *Optics Express*, vol. 11, no. 20, pp. 2549–2554, 2003.
- [58] F. Gan and Y. Wang, "Breakthrough the optical diffraction limit, the development of nano optics and photonics," *Journal of the Optical*, vol. 9, pp. 57–65, 2011.
- [59] C. Long, "Book review of fullerenes: nanochemistry, nanomagnetism, nanomedicine, nanophotonics," *Journal of the American Chemical Society*, vol. 133, no. 38, p. 15220, 2011.
- [60] M. Mikhailova, N. Stoyanov, I. Andreev, B. Zhurtanov, and Y. Yakovlev, "Optoelectronic sensors on gas- and inas-based heterostructures for ecological monitoring and medical diagnostics," in *Proceedings of SPIE-The International Society for Optical Engineering*, p. 6585, Prague, Czech Republic, 2007.
- [61] M. F. Kircher, J. Grimm, and S. S. Gambhir, "Noninvasive cell-tracking methods," *Nature Reviews. Clinical Oncology*, vol. 8, 2011.

- [62] L. Gardini, M. Capitanio, and F. S. Pavone, "3d tracking of single nanoparticles and quantum dots in living cells by out-of-focus imaging with diffraction pattern recognition," *Forestry Report*, vol. 5, no. 1, Article ID 16088, 2015.
- [63] S. Linden, C. Enkrich, M. Wegener, J. Zhou, T. Koschny, and C. M. Soukoulis, "Magnetic response of metamaterials at 100 terahertz," *Science*, vol. 306, 2004.
- [64] J. He, S. Yan-Mei, M. Yu-Tao et al., "A nano-metallic-particles-based cmos image sensor for dna detection," *Chinese Physics B*, vol. 21, no. 7, 2012.
- [65] C. Yu, A. M. Mannan, G. M. Yvone, K. N. Ross, and T. R. Golub, "High-throughput identification of genotype-specific cancer vulnerabilities in mixtures of barcoded tumor cell lines," *Nature Biotechnology*, vol. 34, no. 4, 2016.
- [66] Y. P. Ho, H. H. Chen, K. W. Leong, and T. H. Wang, "Spatially-resolved analysis of dna nanocomplex self-assembly enabled by integrating nanophotonics and microfluidics," *Biophysical Journal*, vol. 96, no. 3, p. 313a, 2009.
- [67] M. Kociak, O. Stéphan, A. Gloter et al., "Seeing and measuring in colours: electron microscopy and spectroscopies applied to nano-optics," *Comptes Rendus-Physique*, vol. 15, no. 2–3, pp. 158–175, 2014.
- [68] E. Rittweger, K. Y. Han, S. E. Irvine, C. Eggeling, and S. W. Hell, "Sted microscopy reveals crystal colour centres with nanometric resolution," *Nature Photonics*, vol. 3, no. 3, pp. 144–147, 2015.
- [69] S. Ye, W. Yan, M. J. Zhao, X. Peng, J. Song, and J. Qu, "Low-saturation-intensity, high-photostability, and high-resolution STED nanoscopy assisted by CsPbBr<sub>3</sub> quantum dots," *Advanced Materials*, vol. 30, no. 23, pp. 1–9, 2018.
- [70] D. Li, L. Shao, B.-C. Chen et al., "Extended-resolution structured illumination imaging of endocytic and cytoskeletal dynamics," *Science*, vol. 349, 2015.
- [71] J. Zhang, Q. He, Z. Wu, B. Yu, J. Qu, and D. Lin, "Application and development of superresolution microscopic imaging technique in living cell imaging," *Progress in Biochemistry and Biophysics*, vol. 3, pp. 1–15, <https://kns.cnki.net/kcms/detail/11.2161.q.20210427.1442.003.html>, 2021.
- [72] X. Wang, M. Rosol, S. Ge, D. Peterson, and G. Mcnamara, "Dynamic tracking of human hematopoietic stem cell engraftment using in vivo bioluminescence imaging," *Blood*, vol. 102, no. 10, pp. 3478–3482, 2003.
- [73] G. Jing, "New developments in cutting-edge optical technology," *Space Return and Remote Sensing*, vol. 3, pp. 1–4, 2019.
- [74] Y. S. Yi and B. Liu, "Scintillator detectors with integrated nanophotonics for medical imaging," *Photonics Spectra*, vol. 49, no. 4, pp. 58–62, 2015.
- [75] V. P. Wallace, A. J. Fitzgerald, S. Shankar, N. Flanagan, and D. D. Arnone, "Terahertz pulsed imaging of basal cell carcinoma ex vivo and in vivo," *British Journal of Dermatology*, vol. 151, no. 2, pp. 424–432, 2015.
- [76] D. M. Gill, J. E. Proesel, C. Xiong et al., "Demonstration of a high extinction ratio monolithic cmos integrated nanophotonic transmitter and 16 gb/s optical link," *IEEE Journal of Selected Topics in Quantum Electronics*, vol. 21, no. 4, pp. 212–222, 2015.
- [77] J. Zhao, E. Yiwen, K. Williams, X. C. Hang, and R. W. Boyd, "Spatial sampling of terahertz fields with sub-wavelength accuracy via probe-beam encoding," *Light: Science & Applications*, vol. 8, 2019.
- [78] J. S. Jensen and O. Sigmund, "Topology optimization for nano-photonics," *Laser & Photonics Reviews*, vol. 5, no. 2, pp. 308–321, 2011.
- [79] H. Ohtake, Y. Ichikawa, Y. Uehara, K. Tanaka, and M. Nagai, "Terahertz wave generating apparatus and terahertz wave generating method," US20100054296 A1, 2010.
- [80] L. M. Lechuga, B. Sepulveda, S. Jose, F. Blanco, A. Calle, and C. Dominguez, "Integrated micro- and nano-optical biosensor silicon devices cmos compatible," *Proceedings of SPIE - The International Society for Optical Engineering*, vol. 13, pp. 54–64, 2004.
- [81] S. Hussmann and T. Liepert, "Robot vision system based on a 3D-TOF camera," in *Proceedings of the Instrumentation & Measurement Technology Conference*, May 2007.
- [82] J. Wei, H. Qu, Y. Wang, J. Zhu, and Y. Guan, "A review of 3D camera research based on time of flight method," *Journal of Infrared Technology*, vol. 1, pp. 60–67, 2021.
- [83] J. K. Udupa, T. Jie, and D. C. Hemmy, "Pentium pc-based craniofacial 3d imaging and analysis system," in *Proceedings of Spie the International Society for Optical Engineering*, Newport Beach, CA, USA, 1997.
- [84] M. Lindner and A. Kolb, "Calibration of the intensity-related distance error of the pmd tof-camera," in *Proceedings of Spie the International Society for Optical Engineering*, Boston, MA, USA, 2007.
- [85] Y. Deng and L. Tang, "Organizing and accessing methods for massive medical microscopic image data," in *Proceedings of SPIE-The International Society for Optical Engineering*, vol. 6789, pp. 678910–678916, Wuhan, China, 2007.
- [86] M. Jian, *Design and Implementation of Advertising Media Screen Interactive Software Based on TOF Sensor*, Dalian University of Technology, Dalian, China, 2018, <https://kns.cnki.net/KCMS/detail/detail.aspx?dbname=CMFD201901&filename=1018869442.nh%20dbname=CMFD201901&filename=1018869442.nh%20>.
- [87] H. Rapp, "Experimental and theoretical investigation of correlating TOF-camera systems," Heidelberg University, Heidelberg, Germany, 2007.
- [88] H. B. Barber, L. R. Furenlid, H. N. Roehrig, M. Ye, and Y. S. Yi, "Improvement of medical imaging with enhanced light extraction of scintillators by integrated nanophotonics," *Medical Applications of Radiation Detectors*, vol. 9594, p. 95940D, 2015.
- [89] R. Bardhan, W. Chen, M. Bartels, C. Perez-Torres, and A. Joshi, "Tracking of multimodal therapeutic nano-complexes targeting breast cancer in vivo," *Nano Letters*, vol. 10, no. 12, pp. 4920–4928, 2010.
- [90] L. Novotny and N. van Hulst, "Antennas for light," *Nature Photonics*, vol. 5, pp. 83–90, 2011.
- [91] G. Yangjiuzhou and X. Peng, "Research progress of terahertz rapid imaging technology," *Journal of Chongqing University of Posts and Telecommunications (Natural Science Edition)*, vol. 2, pp. 218–229, 2021.
- [92] V. G. Kravets, F. Schedin, R. Jalil et al., "Singular phase nanoptics in plasmonic metamaterials for label-free single-molecule detection," *Nature Materials*, vol. 12, no. 4, pp. 304–309, 2013.
- [93] M. V. Exter, C. Fattinger, and D. Grischkowsky, "Terahertz time-domain spectroscopy of water vapor," *Optics Letters*, vol. 14, no. 20, pp. 1128–1130, 1989.
- [94] J. R. Krenn and J. C. Weeber, "Surface plasmon polaritons in metal stripes and wires: one contribution of 13 to a Theme <Nano-optics and near-field microscopy>," *Philosophical Transactions Mathematical Physical & Engineering Sciences*, vol. 362, no. 1817, pp. 739–756, 2004.
- [95] P. H. Siegel, "Terahertz technology in biology and medicine," *International Microwave Symposium Digest, IEEE*, vol. 52, no. 10, , 2004.

- [96] T. Endo, "Development of nanophotonics-based bio-analytical devices," *Bunseki Kagaku*, vol. 64, no. 10, pp. 751-757, 2015.
- [97] Z. Zhu, "The impact of nanotechnology on human health," *Journal of New Chemical Materials*, vol. 2, pp. 78-80, 2007.
- [98] F. Nemati, M. M. Heravi, and R. S. Rad, "Nano-technology and nano-toxicology," *Chinese Journal of Catalysis*, vol. 33, no. 11, pp. 1825-1831, 2012.
- [99] N. Singh, B. Manshian, G. Jenkins et al., "Nanogenotoxicology: the dna damaging potential of engineered nanomaterials," *Biomaterials*, vol. 30, no. 23-24, pp. 3891-3914, 2009.
- [100] H. N. Wang, X. Meng, K. Zhou, Q. Reng, and G. Sun, "Application of molecular imaging probes-quantum dots in cancer imaging and early detection," 2015.
- [101] G. Rui, E. C. Kinzel, L. Yan, S. M. Uppuluri, A. Raman, and X. Xu, "Three-dimensional mapping of optical near field of a nanoscale bowtie antenna," *Optics Express*, vol. 18, no. 5, p. 4961, 2010.
- [102] K. Wang and D. M. Mittleman, "Metal wires for terahertz wave guiding," *Nature*, vol. 432, no. 7015, pp. 376-379, 2004.
- [103] Y. Yifat and J. Scheuer, "Theoretical analysis for active coupled resonator optical waveguide arrays and applications," *Journal of Nanophotonics*, vol. 5, no. 1, p. 51822, 2011.
- [104] B. J. Skutnik, "High-NA hpcs optical fibers for medical diagnosis and treatment," in *Proceedings of SPIE-The International Society for Optical Engineering*, San Francisco, CA, USA, 2010.
- [105] Y. Chen, L. Wang, and J. Song, "Multi-functional nanophotonics technology for precise biomedical applications," *Chinese Journal of Lasers*, vol. 3, pp. 28-37, 2018.
- [106] B. Li, G. E. Christensen, J. Dill, E. A. Hoffman, and J. M. Reinhardt, "3D intersubject warping and registration of pulmonary CT images for a human lung model," in *Proceedings of the Spie Conference Medical Imaging*, San Francisco, CA, USA, 2002.
- [107] R. J. Clouthier, "Parallel disk arrays provide an architecture for high-performance acquisition and archival storage for medical imaging," in *Proceedings of SPIE-The International Society for Optical Engineering*, Newport Beach, CA, USA, 1992.
- [108] Q. Wang, Z. Zhang, L. Chai et al., "Femtosecond Nanophotonics and femtosecond laser technology," in *The 10th Chinese Symposium on Basic Optics and Optical Physics and the 11th Symposium on Laser Physics*, Xian, China, 2002.
- [109] H. B. Liu, H. Zhong, N. Karpowicz, Y. Chen, and X. C. Zhang, "Terahertz spectroscopy and imaging for defense and security applications," *Proceedings of the IEEE*, vol. 95, no. 8, pp. 1514-1527, 2007.
- [110] C. Narayan, A. Deshpande, S. Shrestha, T. Farrahi, and G. C. Giakos, "Future trends in nanophotonics: medical diagnostics and treatment," *Computational Nanophotonics*, CRC Press, Boca Raton, FL, USA, 2013.
- [111] T. H. Dou, Y. Min, J. Neylon, D. Thomas, and A. P. Santhanam, "Fast simulated annealing and adaptive Monte Carlo sampling based parameter optimization for dense optical-flow deformable image registration of 4DCT lung anatomy," in *SPIE Medical Imaging. Medical Imaging 2016: Image-Guided Procedures, Robotic Interventions, and Modeling*, San Diego, CA, USA, 2016.



## Review Article

# Chemical Constituents and Pharmacological Activities of Steroid Saponins Isolated from *Rhizoma Paridis*

Fen Liu , Luning Li , Xinchun Tian , Dengtian Zhang , Wenxue Sun ,  
and Shulong Jiang 

Cancer Institute, Jining First People's Hospital, Jining Medical University, Jining 272000, China

Correspondence should be addressed to Wenxue Sun; sunwenxue121@126.com and Shulong Jiang; jnslijang@163.com

Received 25 August 2021; Accepted 4 September 2021; Published 17 September 2021

Academic Editor: Weiguo Li

Copyright © 2021 Fen Liu et al. This is an open access article distributed under the Creative Commons Attribution License, which permits unrestricted use, distribution, and reproduction in any medium, provided the original work is properly cited.

*Rhizoma Paridis*, the rhizome of liliaceous plants *Paris polyphylla*, is one of the most commonly used herbal drugs in China. Phytochemical and pharmacological studies have shown that steroid saponins were the major effective ingredients of *Rhizoma Paridis* to exert antitumor, anti-inflammatory, hemostasis, and antifibrosis functions. In this review, we discussed the chemical structures of steroid saponins and their related biological activity and mechanisms in cellular and animal models, aiming to provide a reference for future comprehensive exploitation and development of saponins.

## 1. Introduction

*Rhizoma Paridis*, the dried rhizome of liliaceous plants *Paris polyphylla* Smith var. *yunnanensis* (Franch.) Hand.-Mazz or *Paris polyphylla* Smith var. *chinensis* (Franch.) Hara, is a commonly used herbal drug in China, which has a long clinical application history to treat multiple diseases including malignant boils, carbuncles, snake and insect bites, and injuries [1]. It is also one of the core ingredients of Yunnan Baiyao, a well-known haemostatics Chinese medicine. The *Rhizoma Paridis* family comprised 24 species discovered in the world, 22 of them was found in the Yunnan, Sichuan, Guizhou, and Guangxi provinces of China [2].

As an essential component of complementary and alternative therapies, medicinal plants have been accepted worldwide to improve health and prevent or cure diseases because of their rich sources and composition diversity. To understand their function and underlying mechanism, it is critical to analyze the major active substances within these plants. Recent phytochemical and pharmacological studies demonstrated that the extract of *Rhizoma Paridis* contains a large number of chemically active components, including steroid saponins, cholestanol, flavonoids, sterols, and triterpenoids [3–6]. The steroid saponins were shown to be the major effective ingredient exerting antitumor [7],

antibacterial [8], antivirus [9], anti-inflammatory [10], hemostasis [11], immune regulation [7], antiliver fibrosis [12], and other biological functions. In particular, the antitumor pharmacological activity of *Rhizoma Paridis* extracts has emerged a major focus of research. Recent several years, polyphylla saponins have been widely reported to inhibit tumor growth in cancer of the breast [13], liver [14], lung [15], ovary [16], and colon [17], as well as other types of malignancy. All these findings bring lights to the discovery of new drugs for cancer. In this review, we summarized the chemical constituents and pharmacological functions of *Rhizoma Paridis* extracts and discussed the chemical structures of Paris saponins (PSs), their related biological activity, and potential mechanism.

## 2. Chemical Structure of Paris Saponins Derived from *Rhizoma Paridis*

Approximately hundreds of steroid saponins, a family of glycosides with a chemical structure that contains either a steroid or a triterpenoid attached via C-3 and an ether bond to a sugar side chain, have been extracted from *Rhizoma Paridis*, which are considered as the major bioactive ingredients of *Paris* species [18]. According to the configuration of C-25 and the cyclized state of F ring in the

spirostanane structure, steroid saponins are divided into four types (Figure 1): (1) spirostanol, (2) isosprirostanol, (3) furostanol, and (4) pseudospirostanol [3]. Among them, isosprirostanol-type saponins are the main active substance basis of this genus. Moreover, most of the aglycones are diosgenin and pennogenin which generally have hydroxyl substituents at  $3\beta$ ,  $7\beta$ , and  $17\beta$  sites and D-glucose, L-rhamnose, and L-arabinose on the sugar groups. The representative active ingredients of isosprirostanol saponins include polyphyllin I, polyphyllin II, polyphyllin V, polyphyllin VII, parisyunnanoside G-I, and pariposides A-D. Furthermore, phytochemical investigation shows that pennogenyl saponins mainly exist in *Rhizoma Paridis*, whereas diosgenyl saponins are rich in *Rhizoma Dioscoreae nipponicae* [19]. Furostanol-type saponins, with a  $\beta$ -glucopyranosyl moiety at C-26 of the aglycone, are a class of F-ring cracking compounds. It is generally considered that the furostanol-type saponins are usually the precursor compounds of spirirostanol-type saponins [19]. The aglycones of pseudosprirostanol-type saponins are all nautigenin, which can be isolated from the stems and leaves of *P. diyunnanensis* and are also the special components of the upper part of *P. diyunnanensis*. Those nautigenin compounds commonly have hydroxyl substituents at positions 3, 7, 17, and 26. The representative active constituents of pseudosprirostanol-type saponins include chonglou SL-9 ~ SL-15 and abutiloside L.

### 3. Pharmacological Activities of Paris Saponins

As described above, PSs extracted from *Rhizoma Paridis* were capable of exerting antitumor [7], antibacterial [8], antiviral [9], anti-inflammatory [10], hemostasis [11], immune regulation [7], antiliver fibrosis [12], and other biological functions. The possible mechanisms are discussed as follows.

**3.1. Antitumor Activity.** Accumulating studies have shown various antitumor effects of PS in various tumor models. The underlying mechanisms were associated with inhibiting proliferation, inducing apoptosis, antiangiogenesis, inducing differentiation, blocking metastasis, and reversing multidrug resistance of cancer.

A few studies have investigated the cytotoxicity influence of PS in liver cancer. Pennogenin 3-O-Rha-(1 $\rightarrow$ 2)-[Glc-(1 $\rightarrow$ 3)]-Glc (Compound 1), polyphyllin D, pb/formosanin C, and polyphyllin VII isolated from *Rhizoma Paridis* were found to exhibit dose-dependent antitumor effect in HepG2 cells which are involved in a number of signaling pathways including the activation of the Fas and JNK pathways, deregulation of the MAPK pathway, and inhibition of the PI3K/Akt/mTOR pathway. Furthermore, polyphyllin VII was able to cause autophagic cell death and interfere with the metabolism in HepG2 cells [20–22]. Pennogenin 3-O-Rha-(1 $\rightarrow$ 2)-[Glc-(1 $\rightarrow$ 3)]-Glc (Compound 1) and polyphyllin VII showed significant antitumor activity in HepG2, MCF-7, and PC-3 cells by activation the mitochondrial apoptotic cascades, inhibition of the CDK1 and PI3K/Akt pathways, and modulation of MAPK pathway [23]. Polyphyllin D was

revealed to induce the expression of p21 and cyclin E1 leading to G2/M cell cycle arrest in HepG2 cells [21]. A proteomic study demonstrated that PS was capable of downregulation of dUTPase, hnRNP K, and GMP synthase, whereas upregulation of DNase- $\gamma$ , nucleoside diphosphate kinase A, and centrin-2 [24]. This study provided a deep insight into the antitumor mechanism of polyphyllin D and pb/formosanin C [24]. PS also inhibits the oxidation of fatty acids pathway and the gluconeogenesis cascade, two core metabolic pathways affecting energy metabolism, to block the tumor growth in the H22 mouse hepatocarcinoma model. Interestingly, the effects in the tumor mice appear to be very different from those in normal mice. In a normal animal group, polyphyllin D, pb/formosanin C, polyphyllin V, polyphyllin VI, polyphyllin VII, Paris saponin H, and gracillin significantly reduced the concentration of lipid and glycerate, but increased glucose level. However, these three compounds in H22 mice with hepatocarcinoma had opposite effects, i.e., increase in lipid and glycerate and decrease in glucose level [25]. In addition, the mixed compounds of polyphyllin D and pb/formosanin C exhibited more robust and powerful antitumor effects than either of them alone in HepG2 and Bel-7402 cells. The combinations significantly strengthened cycle arrest at G1 phase and promoted mitochondria-dependent apoptosis in hepatocarcinoma cell [26].

Polyphyllin D, pb/formosanin C, polyphyllin VI, and polyphyllin VII have potent proapoptotic effect on human ovarian cancer. A recent study showed that pb/formosanin C induced the expression levels of several proapoptotic proteins, including Bax, cytosolic cytochrome c, activated-caspase-3, and activated-caspase-9 in the SKOV3 cellular model [27]. Moreover, formosanin C was shown to suppress NF- $\kappa$ B signaling, resulting in inhibition of the expression of VEGF and angiogenesis [27]. In addition, reduction of ERK1/2 phosphorylation and Bcl-2 expression was observed upon the treatment of SKOV3 cells with formosanin C compound [28]. Polyphyllin VII treatment of ovarian cancer cells (A2780 and SKOV3) was found to trigger the mitochondrial location of dynamin-related protein 1 (DRP1) and inhibit the PP2A/AKT pathway, leading to mitochondrial dysfunction [29]. It was also demonstrated that polyphyllin D promoted apoptosis and hampered migration cells by reducing caspase-9 and Wnt5a levels and elevating c-Jun expression *in vitro* and *in vivo* [16]. In addition to cytotoxic effects, pb/formosanin C markedly compromised angiogenesis by reduction of VEGF and inhibition of VEGFR2 phosphorylation as well as inactivation of proangiogenic kinases Src, FAK, and Akt in xenograft models established with either SKOV3 or HOC7 cell line [30].

A number of studies have also examined the PS in lung cancer models. In DEN-induced mouse lung cancer, polyphyllin D, pb/formosanin C, dioscin, polyphyllin V, polyphyllin VI, polyphyllin VII, Paris saponin H, and gracillin displayed significant inhibitory effects on tumor development and growth, and the possible mechanism was due to reduction of the expression levels of TNF- $\alpha$ , IL-6, COX-2, PGE2, CK8, and CK18 and inactivation of the EGFR/PI3K/Akt, EGFR/Ras/Erk, and NF- $\kappa$ B pathways [15]. In the LA795

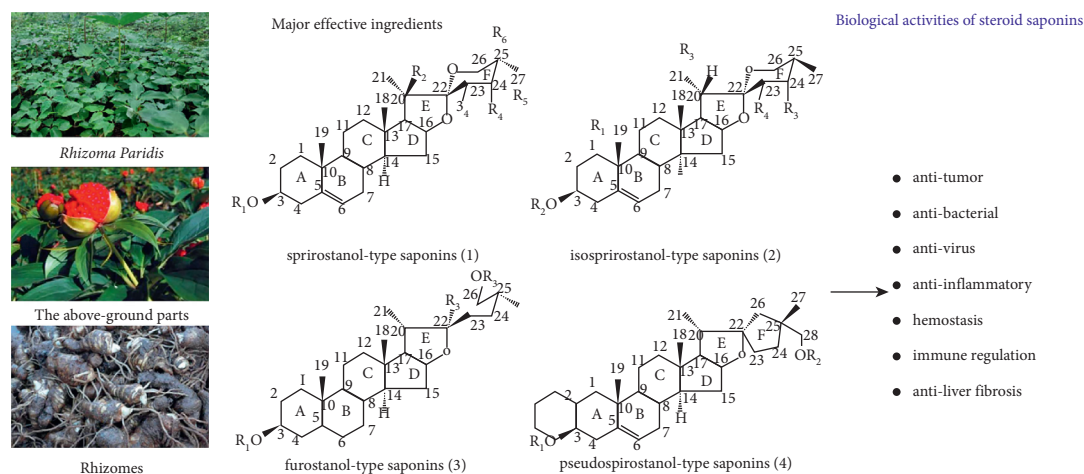


FIGURE 1: The major effective ingredients of *Rhizoma Paridis* and their biological activities.

cellular and xenograft model, polyphyllin D, pb/formosanin C, dioscin, Paris saponin H, and polyphyllin VII were also shown to have significant antitumor activity by inducing apoptosis and blocking the migration [31]. Moreover, pb/formosanin C was found to restrain the proliferation and induce the apoptosis, autophagy, and paraptosis by activation of the JNK pathway in NCI-H460 and NCI-H520 lung cancer cells [32]. In addition, pb/formosanin C was able to inhibit cell migration, invasion, and metastases by repression of MMP-2 and MMP-9 enzyme activity as well as MMP-1, -2, -3, -9, and -14 expression in LA795 cells and T739 mice with lung adenocarcinoma [33]. Combination of polyphyllin D with hyperthermia (43°C) potently induced apoptosis and G2/M cell cycle arrest via decrease of Bcl-2 expression and increase of Bax level [34]. Notably, polyphyllin D was shown to reverse gefitinib-resistance in non-small cell lung cancer by increasing Bax/Bcl-2 ratio and total caspase-3 level both *in vitro* and *in vivo* [35].

PSs were also evaluated for their antitumor properties in the cervical cancer model. A previous study showed that polyphyllin VII significantly induced apoptosis in HeLa cells, and the underlying mechanism involved in increasing the expression of caspase-3, caspase-9, and Bax and decreasing Bcl-2 level [36].

Except for the abovementioned effects, a recent study using UHPLC-qMS spectrum-effect analysis manifested that polyphyllin VII, dioscin, polyphyllin I, and progenin III were identified as the main antitumor chemical compositions in HT29 and MDA-MB-231 cell lines [37]. In addition, polyphyllin VI was shown to trigger S and G2/M cell cycle arrest and extrinsic apoptosis by activation of the p38/p53 and the caspase 3/8 pathways in tongue squamous carcinoma SCC-15 cells [38]. Furthermore, polyphyllin D, Paris saponin H, and polyphyllin VII also displayed notable antitumor and antimetastasis activity in B16 melanoma cells [39].

Interestingly, Paris saponin H was demonstrated to induce cell cycle arrest at G1 phase and accelerate cell apoptosis by blocking A1 adenosine receptor (ARA1) and ARA3 expression and suppressing the Akt and MAPK cascades in glioma U251 cells [40]. Polyphyllin D also

hampered vasculogenic mimicry (VM) formation, an indication of cancer metastasis, through inhibition of the PI3K-Akt-Twist1-VE-cadherin pathway in several HCC cell lines including SMMC7721, PLC, HepG2, Hep3B, and Bel-7402 [41].

According to the abovementioned compounds, the antitumor activities of steroid saponins *in vitro* and *in vivo* are summarized in Tables 1 and 2.

Recently, it has been widely used to study the interaction between drugs and proteins by simulating the docking of small-molecule drug ligands and protein receptor targets [42]. The interaction between ligand and receptor is a process of mutual recognition between molecules through hydrogen bond, electrostatic interaction, and van der Waals force [43]. The binding mode and affinity could be predicted by calculation. In this case, molecular docking is often used as an essential reference for designing targeted drugs and screening effective compounds [44]. Using bioinformatics analysis and molecular docking in hepatitis B virus-related liver cancer, polyphyllin I had been shown to have good affinity with various protein targets, including STAT3, PTP1B, IL2, BCL2L1, FIS1, MFN1, MFN2, and OPA1 [45, 46]. Computational docking also manifested that polyphyllin I has a high affinity with the allosteric drug and metabolite site of AMPK, which induces autophagy and inhibits NSCLC cell growth after activation. This finding was further supported by microscale thermophoresis (MST) and drug affinity responsive targeting stability (DARTS) assays [47].

**3.2. Anti-Inflammatory.** Polyphyllin D has been shown to inhibit LPS/IFN- $\gamma$ -stimulated inflammatory cytokine secretion from peritoneal elucidated macrophages (PEMs) and attenuate IKK $\alpha/\beta$  and p65 phosphorylation *in vitro*. Furthermore, polyphyllin I alleviated the bone erosion and synovitis and prevented M1-like macrophage and T-cell infiltration from ankle joint in the collagen-induced arthritis (CIA) mouse model [48]. Polyphyllin D has also been demonstrated to suppress the inflammation by inhibition of the activation of NF- $\kappa$ B pathway in acne. Accordingly, inflammatory cytokines, including interleukin (IL)-6, IL-8, and

TABLE 1: Efficacy of *Rhizoma Paridis*-derived steroid saponins against cancer *in vitro*.

Compound	Cell line and IC50	Targeting pathways	Ref.
Polyphyllin D	HepG2 (4.01 uM, 24 h)	Fas and JNK pathways; p53-Bax/Bcl-2 and p53-p21-cyclin E/	[21]
	Bel-7402 (4.74 uM, 24 h)	CDK2 pathways; NF-κB and MMP-9	[25,26]
	PC-9 (2.69 μg/ml, 48 h)	Bcl-2/Bax	[34]
	PC-9-ZD (2.51 μg/ml, 24 h; 2.07 μg/ml, 48 h; 1.53 μg/ml, 72 h)	Bax/Bcl-2-caspase-3	[35]
	Hela (2.62 μM, 24 h)	Bcl-2/Bax-caspase-3/9	[36]
Pb/formosanin C	HepG2 (13.62 ug/mL, 24 h; 3.29 ug/mL, 48 h)	NMR metabolic pathways	[22]
	Bel-7402 (4.36 uM, 24 h)	p53-Bax/Bcl-2 and p53-p21-cyclin E/CDK2 pathways; NF-κB and MMP-9	[25,26]
	SKOV3 (20.99 uM, 24 h; 10.44 uM, 48 h; 8.83 uM, 72 h)	NF-κB-VEGF and NF-κB-Bcl-2/Bcl-xL	[27]
	CaSki (5.7 μM), SiHa (3.7 μM), HEC-1A (2.1 μM), and A549 (4.0 μM)	Bax-caspase-3/9 and ERK/Bcl-2	[28]
	HOC-7 (6.44 uM, 48 h)	VEGF	[30]
Compound 1	NCI-H460 (2.0 μM, 48 h) and NCI-H520 (1.6 μM, 48 h)	JNK pathway	[32]
	HepG2 (2.35 uM, 48 h)	Mitochondrial apoptotic, CDK1, PI3K/Akt, and MAPK pathways	[23]
Polyphyllin VII	MCF-7 (2.59 uM, 48 h)		
	PC-3 (4.76 uM, 48 h)		
Polyphyllin VI	HepG2 (1.77 uM, 48 h), MCF-7 (2.71 uM, 48 h), PC-3 (4.67 uM, 48 h)	Mitochondrial apoptotic, CDK1, PI3K/Akt, and MAPK pathways	[23]
	A2780 (3.0 μM, 24 h) and SKOV3 (3.0 μM, 24 h)	PP2A/AKT/DRP1 signaling axis	[29]
Paris saponin H	SCC-15 (25.80 μM, 24 h; 21.22 μM, 48 h; 19.57 μM, 72 h)	p38/p53 and caspase 3/8 pathways	[38]
	U251 (100 μg/ml, 48 h)	ARA1/ARA3 and Akt/MAPK	[40]

TABLE 2: Summary of the anticancer activities of steroid saponins *in vivo*.

Animal models	Drug dose	Effects	Ref.
HepG2 xenografts in nude mice	Intraperitoneal injection with 1 or 3 mg/kg compound 1 and polyphyllin VII for 3 weeks	Compound 1 and polyphyllin VII significantly and dose-dependently inhibited the growth of HepG2 xenografts through regulation of MAPK and PI3K/Akt pathways	[20]
SKOV3 xenografts in nude mice	Intraperitoneal injection with 1, 2, and 3 mg/kg polyphyllin VII for 3 weeks	Polyphyllin VII markedly restrained tumor growth meanwhile increased the ratio of BAX/BCL-2 and cleaved caspase-3 expression	[29]
SKOV3 or HOC-7 xenografts in nude mice	Intraperitoneal injection with 1, 2, and 3 mg/kg pb/formosanin C for 4 weeks	Formosanin C remarkably compromised angiogenesis by reduction of VEGF and inhibition of VEGFR2 phosphorylation as well as inactivation of proangiogenic kinases Src, FAK, and Akt	[30]
PC-9-ZD xenografts in nude mice	2, 4, and 8 mg/kg polyphyllin D by gavage administration for 2 weeks	Polyphyllin D treatment robustly decreased 18F-FDG-uptake compared with the control group	[35]
PLC xenografts in nude mice	Intragastrical administration with 10 mg/kg polyphyllin D for 25 days	Polyphyllin D hampered vasculogenic mimicry (VM) formation, an indication of cancer metastasis, through inhibition of the PI3K-Akt-Twist1-VE-cadherin pathway	[41]

tumor necrosis factor (TNF)- $\alpha$  were decreased after Paris I treatment [49]. In addition, polyphyllin G was shown to be able to decrease the synthesis of NO and PGE<sub>2</sub> and reduce the expressions of cytokines (TNF- $\alpha$ , IL-1 $\beta$ , and IL-6) and enzymes (inducible NO synthase, cyclooxygenase-2, and matrix metalloproteinase-9) at both protein and mRNA levels [10].

**3.3. Antifibrosis.** Liver fibrosis is a pathological change in the structure and function of the liver, resulting from

excessive proliferation and abnormal deposition of extracellular matrix (ECM) components. Progression of liver fibrosis may lead to cirrhosis or hepatocellular carcinoma [50]. However, liver fibrosis is reversible and PS had been reported as one of the effective therapeutic agents. It has been demonstrated that polyphyllin G, polyphyllin VI, pb/formosanin C, and polyphyllin D were efficacious in improving CCl<sub>4</sub>-induced hepatic fibrosis and cirrhosis in Sprague Dawley rat models. These 4 compounds not only relieved the degeneration and

necrosis of liver tissue but also reduced the degree of fibroplastic proliferation via the suppression of VEGF, ERK1/2, RASAL1, PDGF, and  $\alpha$ -SMA [12,51,52]. Furthermore, polyphyllin G was also shown to induce the apoptosis of hypertrophic scar fibroblasts through the modulation of the ERK/JNK pathway [53]. Collectively, these results indicate that PS is a class of potential antifibrosis agents, which deserve future serious investigation.

**3.4. Hemostasis.** As described above, *Rhizoma Paridis* is a key ingredient of two Chinese hemostasis medicines, “Yunnan Baiyao” and “Gongxuening” [1]. Thus, it has been widely used as a hemostatic medicine in China. A recent study demonstrated that Paris saponin H significantly enhanced thrombin activity, thereby shortening the bleeding time in the mouse tail snipping model, suggesting that Paris saponins could interact with thrombin [54]. Polyphyllin VII was found to act directly on platelets and hemostasis and cause 62% platelet aggregation at 300 ug/ml concentration [11]. Another study showed that polyphyllin VII, polyphyllin II, dioscin, and polyphyllin I all could serve as favorable hemostatic agents [37]. These results indicate that PSs are promising candidates for development of hemostatic drugs.

**3.5. Other Effects.** Polyphyllin G has been shown to be a potential stimulator of interferon gene (STING) agonist, which initiates macrophages activation and accelerates cytotoxic T lymphocytes infiltration in tumor microenvironment. In the meantime, polyphyllin G treatment robustly increased the expression of PD-L1 on macrophages, suggesting that the combination polyphyllin G with anti-PD1/PD-L1 immunotherapy is beneficial for the cancer treatment [55]. In addition, predominant antibacterial activity against propionibacterium acnes was found in several PSs including chonglouoside SL-2, chonglouoside SL-3, chonglouoside SL-6, trillin, polyphyllin V, diosgenin 3-O-Rha-(1 $\rightarrow$ 4)-Glc, dioscin, pennogenin 3-O-Rha-(1 $\rightarrow$ 4)-Rha-(1 $\rightarrow$ 4)-Glc, polyphyllin VII, and methylprotodioscin [8].

## 4. Conclusions and Prospect

Active ingredients extracted from medicinal plants and metabolic products are the primary resources for developing medical drugs. The compounds isolated from *Rhizoma Paridis* have significant pharmacological activities, among which steroid saponins are the major active material components. Saponins have antitumor, antifibrosis, anti-inflammatory, hemostasis, and other properties. In particular, polyphyllin D, pb/formosanin C, polyphyllin VI, and polyphyllin VII displayed considerable antitumor activity in both *in vitro* and *in vivo* cancer models. The possible mechanisms include inducing cell apoptosis, hampering angiogenesis, inhibiting cell invasion and metastasis, regulating the tumor microenvironment, and reversing tumor drug resistance. Several signaling pathways were modulated by these compounds, including PI3K/Akt, Ras/Erk, mTOR, PP2A, and NF- $\kappa$ B cascades. Hepatic fibrosis and cirrhosis have been one of the most serious diseases to cure.

Polyphyllin D, pb/formosanin C, polyphyllin VI, and polyphyllin VII exhibited dramatic antifibrosis activities against liver fibrosis and cirrhosis.

In summary, the saponins have great potential for anticancer and antifibrosis drug discovery. The chemical constituents and biological activities of isolated sterol saponins need to be further studied.

## Abbreviations

PSs:	Paris saponins
Fas:	Factor-related apoptosis
JNK:	c-Jun N-terminal kinase
MAPK:	Mitogen-activated protein kinase
PI3K:	Phosphoinositide 3-kinase
mTOR:	Mammalian target of rapamycin
CDK1:	Cyclin-dependent kinase 1
Bax:	Bcl-2-associated X
Bcl-2:	B-cell leukemia/lymphoma 2
VEGF:	Vascular endothelial growth factor
NF- $\kappa$ B:	Nuclear factor kappa-B
Caspase-3:	Cysteine-aspartic acid specific protease 3
Caspase-9:	Cysteine-aspartic acid specific protease 9
ERK1/2:	Extracellular-regulated kinase 1/2
DRP1:	Dynamin-related protein 1
PP2A:	Protein phosphatase 2A
VEGFR2:	Vascular endothelial growth factor receptor 2
Src:	Sarcoma gene
FAK:	Focal adhesion kinase
TNF- $\alpha$ :	Tumor necrosis factor alpha
IL-6:	Interleukin-6
COX-2:	Cyclooxygenase-2
PGE2:	Prostaglandin E2
CK8:	Cytokeratin 8
CK18:	Cytokeratin 18
MMP-2:	Matrix metalloproteinase 2
MMP-9:	Matrix metalloproteinase 9
ARA1:	A1 adenosine receptor
ARA3:	A3 adenosine receptor
VM:	Vasculogenic mimicry
LPS:	Lipopolysaccharides
IFN- $\gamma$ :	Interferon $\gamma$
PEMs:	Peritoneal elucidated macrophages
IKK $\alpha/\beta$ :	Inhibitor of nuclear factor kappa-B kinase $\alpha/\beta$
CIA:	Collagen-induced arthritis
NO:	Nitric oxide
PGE2:	Prostaglandin E2
ECM:	Extracellular matrix
RASAL1:	Ras GTPase-activating-like protein 1
PDGF:	Platelet-derived growth factor
$\alpha$ -SMA:	$\alpha$ -Smooth muscle actin
STING:	Stimulator of interferon gene
PD-L1:	Programmed death ligand 1
PD-1:	Programmed cell death protein-1.

## Data Availability

All data included in this study are available upon request by contact with the corresponding author.

## Conflicts of Interest

The authors declare that they have no conflicts of interest.

## Authors' Contributions

Shulong Jiang and Wenxue Sun contributed to the conception of the review. Fen Liu wrote the manuscript with support from Shulong Jiang, Luning Li, and Wenxue Sun. Xinchun Tian and Dengtian Zhang collected the related literature. All authors have read and approved the final version of the manuscript.

## Acknowledgments

This work was supported in part by the National Natural Science Foundation of China (grant no. 81873249) and the Young Taishan Scholars Program of Shandong Province (grant no. tsqn201909200).

## References

- [1] C. P. Commission, *Pharmacopoeia of the People's republic of China*, China Medical Science Press, Beijing, China, 2015.
- [2] X. Wu, L. Wang, G.-C. Wang et al., "New steroidal saponins and sterol glycosides from Paris polyphylla var. yunnanensis," *Planta Medica*, vol. 78, no. 15, pp. 1667–1675, 2012.
- [3] J.-C. Wei, W.-Y. Gao, X.-D. Yan, Y. Wang, S.-S. Jing, and P.-G. Xiao, "Chemical constituents of plants from the Genus Paris," *Chemistry and Biodiversity*, vol. 11, no. 9, pp. 1277–1297, 2014.
- [4] Y. Ling, Z. Fu, Q. Zhang, L. Xu, and L. Liao, "Identification and structural elucidation of steroidal saponins from the root of Paris polyphylla by HPLC-ESI-QTOF-MS/MS," *Natural Product Research*, vol. 29, no. 19, pp. 1798–1803, 2015.
- [5] X. Wu, L. Wang, H. Wang, Y. Dai, W.-C. Ye, and Y.-L. Li, "Steroidal saponins from Paris polyphylla var. yunnanensis," *Phytochemistry*, vol. 81, pp. 133–143, 2012.
- [6] Y. Zhao, L. P. Kang, Y. X. Liu et al., "Steroidal saponins from the rhizome of Paris polyphylla and their cytotoxic activities," *Planta Medica*, vol. 75, no. 4, pp. 356–363, 2009.
- [7] Y. Tian, G. Y. Gong, L. L. Ma, Z. Q. Wang, D. Song, and M. Y. Fang, "Anti-cancer effects of Polyphyllin I: an update in 5 years," *Chemico-Biological Interactions*, vol. 316, Article ID 108936, 2020.
- [8] X.-J. Qin, D.-J. Sun, W. Ni et al., "Steroidal saponins with antimicrobial activity from stems and leaves of Paris polyphylla var. yunnanensis," *Steroids*, vol. 77, no. 12, pp. 1242–1248, 2012.
- [9] B. Joshi, S. K. Panda, R. S. Jouneghani et al., "Antibacterial, antifungal, antiviral, and anthelmintic activities of medicinal plants of Nepal selected based on ethnobotanical evidence," *Evidence-based Complementary and Alternative Medicine: eCAM*, vol. 2020, p. 1043471, Article ID 1043471, 2020.
- [10] C. Zhang, C. Li, X. Jia et al., "Vitro and in vivo anti-inflammatory effects of polyphyllin VII through down-regulating MAPK and NF-kappaB pathways," *Molecules*, vol. 24, no. 5, 2019.
- [11] C.-L. Sun, W. Ni, H. Yan et al., "Steroidal saponins with induced platelet aggregation activity from the aerial parts of Paris verticillata," *Steroids*, vol. 92, pp. 90–95, 2014.
- [12] S. Man, W. Fan, W. Gao et al., "Anti-fibrosis and anti-cirrhosis effects of Rhizoma paridis saponins on diethylnitrosamine induced rats," *Journal of Ethnopharmacology*, vol. 151, no. 1, pp. 407–412, 2014.
- [13] Z.-Z. Xie, M.-M. Li, P.-F. Deng et al., "Paris saponin-induced autophagy promotes breast cancer cell apoptosis via the Akt/mTOR signaling pathway," *Chemico-Biological Interactions*, vol. 264, pp. 1–9, 2017.
- [14] J. Liu, S. Man, J. Li, Y. Zhang, X. Meng, and W. Gao, "Inhibition of diethylnitrosamine-induced liver cancer in rats by Rhizoma paridis saponin," *Environmental Toxicology and Pharmacology*, vol. 46, pp. 103–109, 2016.
- [15] S. Man, J. Li, P. Qiu et al., "Inhibition of lung cancer in diethylnitrosamine-induced mice by Rhizomaparidis saponins," *Molecular Carcinogenesis*, vol. 56, no. 5, pp. 1405–1413, 2017.
- [16] L. Gu, J. Feng, Z. Zheng, H. Xu, and W. Yu, "Polyphyllin I inhibits the growth of ovarian cancer cells in nude mice," *Oncology letters*, vol. 12, no. 6, pp. 4969–4974, 2016.
- [17] W.-J. Teng, P. Chen, F.-Y. Zhu et al., "Effect of Rhizoma paridis total saponins on apoptosis of colorectal cancer cells and imbalance of the JAK/STAT3 molecular pathway induced by IL-6 suppression," *Genetics and Molecular Research*, vol. 14, no. 2, pp. 5793–5803, 2015.
- [18] T. Zhang, H. Liu, X.-T. Liu, D.-r. Xu, X.-q. Chen, and Q. Wang, "Qualitative and quantitative analysis of steroidal saponins in crude extracts from Paris polyphylla var. yunnanensis and P. polyphylla var. chinensis by high performance liquid chromatography coupled with mass spectrometry," *Journal of Pharmaceutical and Biomedical Analysis*, vol. 51, no. 1, pp. 114–124, 2010.
- [19] X. Huang, W. Gao, S. Man, G. Ying, and C. Liu, "Isolation and identification of compounds present in rhizomes of paris axialis H. Li and study of their cytotoxic effects," *Latin American Journal of Pharmacy*, vol. 30, no. 3, pp. 540–545, 2011.
- [20] Y.-S. Chen, Y. He, C. Chen et al., "Growth inhibition by pennogenyl saponins from Rhizoma paridis on hepatoma xenografts in nude mice," *Steroids*, vol. 83, pp. 39–44, 2014.
- [21] Y. Zeng, Z. Zhang, W. Wang et al., "Underlying mechanisms of apoptosis in HepG2 cells induced by polyphyllin I through Fas death and mitochondrial pathways," *Toxicology Mechanisms and Methods*, vol. 30, no. 6, pp. 397–406, 2020.
- [22] Y. Li, S. Man, J. Li et al., "The antitumor effect of formosanin C on HepG2 cell as revealed by 1H-NMR based metabolic profiling," *Chemico-Biological Interactions*, vol. 220, pp. 193–199, 2014.
- [23] F.-Y. Long, Y.-S. Chen, L. Zhang et al., "Pennogenyl saponins induce cell cycle arrest and apoptosis in human hepatocellular carcinoma HepG2 cells," *Journal of Ethnopharmacology*, vol. 162, pp. 112–120, 2015.
- [24] Z.-X. Cheng, B.-R. Liu, X.-P. Qian et al., "Proteomic analysis of anti-tumor effects by Rhizoma Paridis total saponin treatment in HepG2 cells," *Journal of Ethnopharmacology*, vol. 120, no. 2, pp. 129–137, 2008.
- [25] S. Man, W. Fan, Z. Liu et al., "Antitumor pathway of Rhizoma Paridis Saponins based on the metabolic regulatory network alterations in H22 hepatocarcinoma mice," *Steroids*, vol. 84, pp. 17–21, 2014.
- [26] J. Liu, S. Man, Z. Liu, L. Ma, and W. Gao, "A synergistic antitumor effect of polyphyllin I and formosanin C on hepatocarcinoma cells," *Bioorganic & Medicinal Chemistry Letters*, vol. 26, no. 20, pp. 4970–4975, 2016.
- [27] M. Yang, J. Zou, H. Zhu et al., "Paris saponin II inhibits human ovarian cancer cell-induced angiogenesis by

- modulating NF- $\kappa$ B signaling,” *Oncology Reports*, vol. 33, no. 5, pp. 2190–2198, 2015.
- [28] X. Xiao, J. Zou, T. M. Bui-Nguyen et al., “Paris Saponin II of *Rhizoma Paridis* - a novel inducer of apoptosis in human ovarian cancer cells,” *BioScience Trends*, vol. 6, no. 4, pp. 201–211, 2012.
- [29] L. Zhao, Z. Liu, X. Deng et al., “Polyphyllin VII induces mitochondrial apoptosis by regulating the PP2A/AKT/DRP1 signaling axis in human ovarian cancer,” *Oncology Reports*, vol. 45, 2020.
- [30] X. Xiao, M. Yang, J. Xiao et al., “Paris Saponin II suppresses the growth of human ovarian cancer xenografts via modulating VEGF-mediated angiogenesis and tumor cell migration,” *Cancer Chemotherapy and Pharmacology*, vol. 73, no. 4, pp. 807–818, 2014.
- [31] M. Shuli, G. Wenyan, Z. Yanjun, M. Chaoyi, Y. Liu, and L. Yiwen, “*Paridis saponins* inhibiting carcinoma growth and metastasis in vitro and in vivo,” *Archives of Pharmacal Research*, vol. 34, no. 1, pp. 43–50, 2011.
- [32] S. Man, P. Lv, J. Cui et al., “Paris saponin II-induced paraptosis-associated cell death increased the sensitivity of cisplatin,” *Toxicology and Applied Pharmacology*, vol. 406, Article ID 115206, 2020.
- [33] S. Man, W. Gao, Y. Zhang et al., “Formosanin C-inhibited pulmonary metastasis through repression of matrix metalloproteinases on mouse lung adenocarcinoma,” *Cancer Biology & Therapy*, vol. 11, no. 6, pp. 592–598, 2011.
- [34] P. Zhao, H. Jiang, D. Su, J. Feng, S. Ma, and X. Zhu, “Inhibition of cell proliferation by mild hyperthermia at 43°C with Paris Saponin I in the lung adenocarcinoma cell line PC-9,” *Molecular Medicine Reports*, vol. 11, no. 1, pp. 327–332, 2015.
- [35] H. Jiang, P.-J. Zhao, D. Su, J. Feng, and S.-L. Ma, “Paris saponin I induces apoptosis via increasing the Bax/Bcl-2 ratio and caspase-3 expression in gefitinib-resistant non-small cell lung cancer in vitro and in vivo,” *Molecular Medicine Reports*, vol. 9, no. 6, pp. 2265–2272, 2014.
- [36] W. Zhang, D. Zhang, X. Ma, Z. Liu, F. Li, and D. Wu, “Paris saponin VII suppressed the growth of human cervical cancer Hela cells,” *European Journal of Medical Research*, vol. 19, no. 1, p. 41, 2014.
- [37] X. Qiao, C. Qu, Q. Luo et al., “UHPLC-qMS spectrum-effect relationships for *Rhizoma Paridis* extracts,” *Journal of Pharmaceutical and Biomedical Analysis*, vol. 194, Article ID 113770, 2021.
- [38] J.-Y. Ke, W. Zhang, R.-S. Gong et al., “A monomer purified from Paris polyphylla (PP-22) triggers S and G2/M phase arrest and apoptosis in human tongue squamous cell carcinoma SCC-15 by activating the p38/cdc25/cdc2 and caspase 8/caspase 3 pathways,” *Tumor Biology*, vol. 37, no. 11, pp. 14863–14872, 2016.
- [39] S. Man, W. Gao, Y. Yan, Z. Liu, and C. Liu, “Inhibition of matrix metalloproteinases related to metastasis by diosgenyl and pennogenyl saponins,” *Journal of Ethnopharmacology*, vol. 137, no. 3, pp. 1221–1227, 2011.
- [40] L. Bi, Y. Liu, Q. Yang et al., “Paris saponin H inhibits the proliferation of glioma cells through the A1 and A3 adenosine receptor-mediated pathway,” *International Journal of Molecular Medicine*, vol. 47, no. 4, 2021.
- [41] T. Xiao, W. Zhong, J. Zhao et al., “Polyphyllin I suppresses the formation of vasculogenic mimicry via Twist1/VE-cadherin pathway,” *Cell Death & Disease*, vol. 9, no. 9, p. 906, 2018.
- [42] A. Khursheed, V. Jain, A. Rasool, M. A. Rather, N. A. Malik, and A. H. Shalla, “Molecular scaffolds from mother nature as possible lead compounds in drug design and discovery against coronaviruses: a landscape analysis of published literature and molecular docking studies,” *Microbial Pathogenesis*, vol. 157, Article ID 104933, 2021.
- [43] P. E. Hansen, “NMR of natural products as potential drugs,” *Molecules*, vol. 26, no. 12, 2021.
- [44] M. M. Salman, Z. Al-Obaidi, P. Kitchen, A. Loreto, R. M. Bill, and R. Wade-Martins, “Advances in applying computer-aided drug design for neurodegenerative diseases,” *International Journal of Molecular Sciences*, vol. 22, no. 9, 2021.
- [45] S. Yu, W. Gao, P. Zeng et al., “Exploring the effect of Polyphyllin I on hepatitis B virus-related liver cancer through network pharmacology and in vitro experiments,” *Combinatorial Chemistry and High Throughput Screening*, vol. 24, 2021.
- [46] S. Yu, W. Gao, P. Zeng et al., “Exploring the effect of Gupi Xiaoji Prescription on hepatitis B virus-related liver cancer through network pharmacology and in vitro experiments,” *Biomedicine and Pharmacotherapy*, vol. 139, Article ID 111612, 2021.
- [47] Y. Wu, Y. Si, Y. Xiang et al., “Polyphyllin I activates AMPK to suppress the growth of non-small-cell lung cancer via induction of autophagy,” *Archives of Biochemistry and Biophysics*, vol. 687, Article ID 108285, 2020.
- [48] Q. Wang, X. Zhou, Y. Zhao et al., “Polyphyllin I ameliorates collagen-induced arthritis by suppressing the inflammation response in macrophages through the NF- $\kappa$ B pathway,” *Frontiers in Immunology*, vol. 9, Article ID 2091, 2018.
- [49] T. Zhu, W. Wu, S. Yang, D. Li, D. Sun, and L. He, “Polyphyllin I inhibits propionibacterium acnes-induced inflammation in vitro,” *Inflammation*, vol. 42, no. 1, pp. 35–44, 2019.
- [50] E. L. Ellis and D. A. Mann, “Clinical evidence for the regression of liver fibrosis,” *Journal of Hepatology*, vol. 56, no. 5, pp. 1171–1180, 2012.
- [51] Y. Han, L. Pan, S. Ran et al., “*Rhizoma Paridis* saponins ameliorates hepatic fibrosis in rats by downregulating expression of angiogenesis-associated growth factors,” *Molecular Medicine Reports*, vol. 19, no. 5, pp. 3548–3554, 2019.
- [52] Y. Hong, Y.-Q. Han, Y.-Z. Wang et al., “*Paridis Rhizoma* Saponins attenuates liver fibrosis in rats by regulating the expression of RASAL1/ERK1/2 signal pathway,” *Journal of Ethnopharmacology*, vol. 192, pp. 114–122, 2016.
- [53] C. Zhong, Q. Nong, W. Feng et al., “Polyphyllin VII induces fibroblasts apoptosis via the ERK/JNK pathway,” *Burns*, vol. 47, no. 1, pp. 140–149, 2021.
- [54] F. Wen, T. Chen, H. Yin, J. Lin, and H. Zhang, “Vitro effects on thrombin of paris saponins and in vivo hemostatic activity evaluation of paris fargesii var. brevipetala,” *Molecules*, vol. 24, no. 7, 2019.
- [55] J. Yu, H. Deng, and Z. Xu, “Targeting macrophage priming by polyphyllin VII triggers anti-tumor immunity via STING-governed cytotoxic T-cell infiltration in lung cancer,” *Scientific Reports*, vol. 10, no. 1, Article ID 21360, 2020.